Topology of genes in mammalian cell nuclei with special emphasis on the *MLL* gene and its translocation partners

Andrea Eveline Murmann

Dissertation

submitted to the
Combined Faculties for the Natural Sciences and for Mathematics
of the Ruperto-Carola University of Heidelberg, Germany
for the degree of
Doctor of Natural Sciences

Presented by

Diplom Biologist: Andrea Eveline Murmann
born in: Kronach, Oberfranken, Germany

Oral examination: 21.12.2004:

Topology of genes in mammalian cell nuclei with special emphasis on the *MLL* gene and its translocation partners

Referees: Prof. Dr. Werner Buselmaier
Prof. Dr. Peter Lichter

This work was carried out at the German Cancer Research Center (DKFZ) in Heidelberg in the Division of Molecular Genetics (December 1998 to July 1999) and at the University of Chicago in the Department of Medicine, Section Hematology/Oncology (January 2000 to December 2004) under the scientific guidance of Prof. Dr. Peter Lichter and Prof. Dr. Janet D. Rowley.

Darwin said that Nature couldn't make any jumps, **natura non facit saltum.**

To Johannes and Julie, the two most wonderful presents of my live

Publications

Vogel R., R. Viereck, A. Murmann, T. Rausch. 1999. Cloning of a higher plant elongation factor 2 cDNA: Expression of eEF2 and a subunit of eEF1B in sugar beet cells during phosphate and carbohydrate starvation. J Plant Physiol. 154:192-196.

Algeciras-Schimnich ,A., L. Shen, B.C. Barnhart, A.E. Murmann, J.K. Burkhardt, M.E. Peter. 2002. Molecular ordering of the initial signaling events of CD95. Mol Cell Biol 22:207-20.

Scheuermann M.O., A.E. Murmann, K. Richter, S. Görisch, H. Herrmann, P. Lichter. Characterization of the ICD compartment in mammalian cells with distinctly different karyotype, in preparation.

Murmann A.E., A. Mincheva, M. Scheuermann, M. Gauthier, F. Yang, A. Fischer, E. Carpenter, J.D. Rowley, P. Lichter. Comparative mapping of bovine loci to Indian and Chinese muntjac chromosomes by FISH, in preparation.

Murmann A.E., J. Gao, M. Encinosa, M.E. Peter, R. Eils, P. Lichter, J.D. Rowley. Gene density within 2 Mbp of a locus determines its 3D position in the interphase nucleus of hematopoietic cells, in preparation.

Gao J, A.E. Murmann, J.D. Rowley, P. Lichter, R. Eils. Three-dimensional quantitative tools to analyze the spatial arrangement of translocation partner gene, in preparation.

Posters

Spatial organization of chromosomal domains in the interphase nucleus of *Muntiacus muntjak*-fibroblasts. Murmann A.E., P.L. Strissel, R. Strick, S. Lampel, P. Lichter, J.D. Rowley. Biological Science and Learning Center, 2001, University of Chicago, Chicago, IL.

The structure of the interchromosomal domain (ICD) compartment is similar in mammalian nuclei from species with very different chromosomal organization. Scheuermann M.O., A.E. Murmann, K. Richter, H. Herrmann, P. Lichter. Dynamic Organization of Nuclear Function, 2002, Cold Spring Harbor Laboratory, NY.

Talks

3-D organization of the genome in interphase nuclei of higher mammalian cells. SMSI (State Microscopical Society of Illinois) meeting, 2001, Chicago, IL.

New computational tools to analyze the spatial distribution of nuclear entities. FOM (Focus on Microscopy) meeting, 2004, Philadelphia, PA.

Acknowledgements

This work grew to a large part because I could benefit from quite a number of people who have helped and supported me over the course of the thesis, and everybody contributed in their own way to make it possible for me to complete it. I had the great fortune to find two outstanding and wonderful people as my supervisors during the time of my thesis, who I admire for their contribution to science as well as for their human spirit. I am deeply grateful for having had the opportunity to work with both of them, Prof. Dr. Janet D. Rowley and Prof. Dr. Peter Lichter. Thank you so much for your incredible trust in me during all this time, for your support and interest in my research and for the truly unique opportunity to work on a thesis in Heidelberg and in Chicago.

I wish to thank current and former members of the Rowley laboratory at the University of Chicago, for their friendship and support; Dr. Pamela Strissel and Dr. Reiner Strick for giving me the opportunity to work in the Rowley lab, and for their encouragement to follow my curiosity to investigate the whereabouts of *MLL* and Co.; Dr. Yanming Zhang for sharing his wealth of knowledge about leukemia and translocations; Dr. Sanggyu Lee and Dr. Run Shi for giving me insights into the SAGE-continuum and their never ending patience to listen to my ideas; Miao Sun for the computer SAGE tag searches; my students Emily Carpenter, Marissa Encinosa and Harshal Dave, who I tremendously enjoyed training over the summers; and my friends Dr. Yuri Kobzev, Susanne Borgers, Mary Beth Neilly, Nimanthi Jayathilaka, Neelmini (Nimmi) Emmanuel, Heidrun (Heidi) Gerr, Loretta Li and Michelle Nassin.

The Rowley lab is located in a great environment of other research groups with terrific people right next door, the Le Beau- and the Olopade-labs. I owe a large gratitude to many of the members of these labs for all their help I was fortunate to receive. I want to thank in particular Dr. James Fackenthal and Elizabeth (Liz) Davis. Both helped me with their wisdom and experience, always available, never tired to answer my thousands of questions throughout the years. Special thanks also to Aparna Palakodeti for sharing her expertise in cell synchronization, Yanwen Jiang for his math skills, and Dr. Katrin Carlson from the Cytogenetics lab for teaching me the identification of human chromosomes. I am also grateful to Dr. Tatyana Grushko, Dr. Gleb Baida, Dr. Lucy Godley, Dr. Isabelle Lucas, Anthony (Tony) Fernald, Lise Sveen, Fitsum Hagos, Johnnie Byrd and Gene Lee. Without them I would have had a less joyous time.

I want to thank Dr. Michelle Le Beau and Dr. Janis Burkhardt especially for their help to get me focused during the time my laboratory-supervisors left the University and their generosity and encouragement to seek skilled advice from members of their groups.

Thanks to Dr. Vytas Bindokas, Shirley Bond, and Julie Auger for their help to master many great machines in the Core Facilities of the University of Chicago; Rafael Espinosa and Ian Miller for support in computer and ftp-server related issues; Shanda Maaskant, Larry Hill and Tracie DeMack for helping in administrative aspects; Gloria Davis and Jade Giacobbe for all the food, coffee and clean labware that make the lab run. It was an enrichment to have contact with Dr. Antje Fischer, who provided material from Chinese muntjac, and Dr. Jörg Volkland, who helped me to obtain tissue from roedeer.

I want to thank the Lichter-lab at the DKFZ in Heidelberg so much for making me feel welcomed each time I came to give a progress report, to complete critical experiments or to learn new techniques. This was a very important part of my thesis. I am also grateful to Dr. Stefan Lampel for starting the muntjac project and teaching me the basics of 3D-FISH. Millions of thanks to Dr. Markus Scheuermann for his friendship, our collaboration and all the interest and excitement for my work, and Dr. Antoinetta Mincheva for her experience and skills in FISH.

Very special thanks to the miracle worker Juntao Gao from the Eils Group, without whom the 3D world of the interphase nucleus could not have been mapped so precisely. He played an important role in helping me complete the work.

I could not think of a better family, than mine, my parents, Marianne and Volkmar, and my three sisters, Annette, Sabine and Tanja, who are there for me, always, and especially my great children Johannes and Julie, and Marcus, my wonderful friend, partner and husband, for his encouragement, belief in me, computer support, and cheerful optimism, from which I benefit every day.

Thank you.

Table of Contents:

1. INTRODUCTION

1.1. The mammalian nucleus

When investigating eukaryotic cells with the light microscope, the nucleus is the most visible organelle. First described by Brown in 1831, the cell nucleus contains most of the cellular DNA in compacted form, RNA and protein components (Brown, 1831). The human haploid genome contains about 3 x 10^9 nucleotide pairs and is similar in size when compared to other mammalian genomes. The haploid human genome is organized as 22 different autosomes and 2 sex chromosomes, X and Y in males and 2 X in females; thus the diploid human genome consists of 46 different DNA molecules per normal diploid cell. The length of the uncoiled human DNA of one cell is estimated to measure 2 m demonstrating the efficiency of DNA packing in eukaryotic cells (Bradbury, 1998). Different levels of chromosome packing of the DNA molecule can be observed. The genome is packaged into a nucleoprotein structure known as chromatin. A chromatin subunit model was first proposed in 1974 by Olins and Olins (Olins and Olins, 1974). The basic repeating unit of the chromatin, the nucleosomes, comprises approximately two turns of DNA wrapped around an octamer of pairs of 4 histone proteins, H2A, H2B, H3 and H4, which are highly conserved among eukaryotic organisms (for review see (Olins and Olins, 2003), primary literature in (Luger et al., 1997; Tyler, 2002; White et al., 2001)). The nucleosomes are usually packed together, with the aid of histone H1 molecules, into higher order arrays to form a 30 nm fiber (Hamkalo and Rattner, 1980). At this level of compaction, the human genome would have an average length of 0.1 m and could still span the nucleus more than 100 times. There is nearly a 10,000-fold reduction in length in an interphase nucleus (Alberts et al., 1994). It is believed that the 30 nm fibers form loops, each of which attach to a central scaffold, and giant super coils and subdomains are formed. The mechanisms for this higher order compaction of the DNA are still not fully understood.

The nucleus is surrounded by the nuclear envelope that consists of two layers of double membranes. These membranes contain the nuclear pore complexes, which actively transport selected molecules to and from the cytosol. The envelope is directly connected to

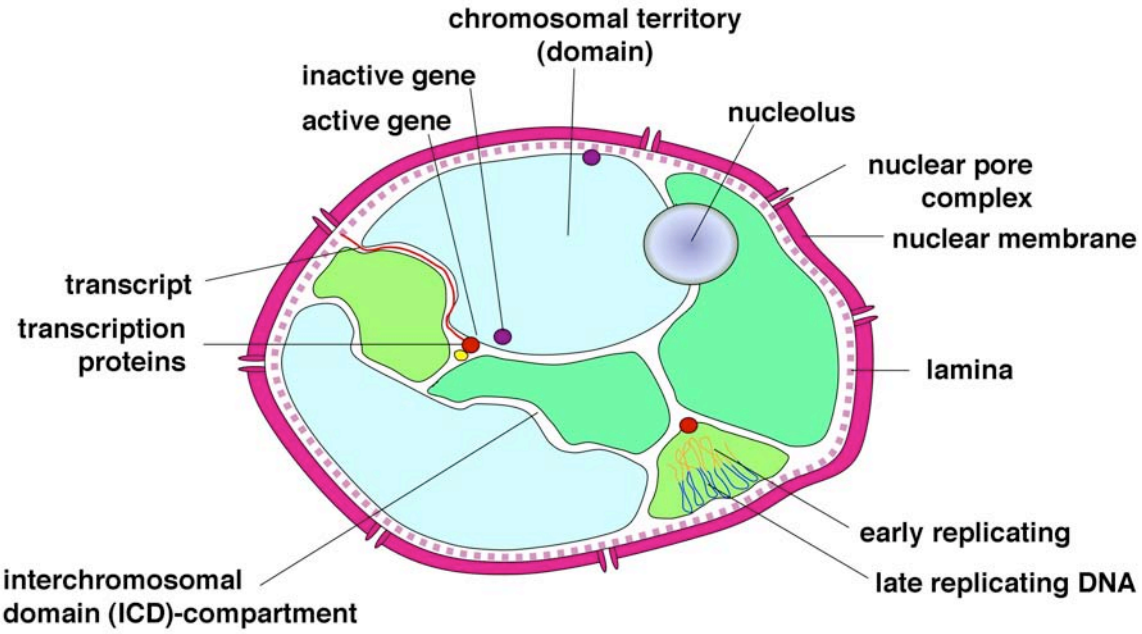

Figure 1: Model of a mammalian interphase nucleus.
One single nucleus is represented.

the extensive membranes of the endoplasmic reticulum, and it is supported by a network of intermediate filaments, the nuclear lamina.

Chromosomes are generally more decondensed during interphase as compared to metaphase where the DNA is at its most compacted stage. Nuclease sensitivity assays revealed that about 10% of the DNA in interphase vertebrate cells is in a relatively uncondensed conformation that correlates with DNA transcription in these regions. Such "active chromatin" is also called euchromatin and contains early replicating DNA, which is found more frequently in the interior of the nucleus and contains most of the active genes. Heterochromatin is more condensed, and therefore densely stained. It contains late replicating DNA found to be predominantly near the nuclear periphery or the nucleoli (for review see (Lamond and Earnshaw, 1998)) (**Figure 1**). Different genes are expressed at very different levels and many are expressed in specific cells and at precise times during development raising the question of how different levels of gene expression are maintained. For regulated expression of a gene both the chromatin status as well as the availability of

activating transcription factors are important to drive RNA synthesis. The role of chromatin structure is clearly important for the success of this process. It has been known for many years that active and inactive genes have very distinct chromatin states and that inert chromatin is able to spread and thereby down regulate previously active genes (Dillon and Festenstein, 2002; Kosak et al., 2002). It was also reported that the packing of chromatin can influence the activity of genes. One such example is Ikaros, a lymphoid specific transcription factor. Ikaros seems to transcriptionally inactivate genes by recruiting the gene to the centromeric heterochromatin (Brown et al., 1997).

1.1.1. Positions of chromosomes within the nucleus

The chromosomes in nuclei of lower species tend to retain the so-called Rabl orientation, first described by Rabl in 1885, throughout interphase, with their centromeres facing one pole of the nucleus and their telomeres pointing toward the opposite pole. In simpler eukaryotes, such as yeast, the telomeres of chromosomes have the propensity to cluster at the nuclear periphery and suppress subtelomeric genes (Hediger and Gasser, 2002). In mammalian cells a consensus on the predetermined localization of centromeres has not been reached. This is complicated by the observation of cell cycle, tissues and species specific effects. The localization of many chromosomes seems to be independent of other nuclear structures. However, clustering of chromosomes (e.g. chromosomes 17, 19 and 22) has been described (Boyle et al., 2001). It is also well established that specific genes from separate interphase chromosomes are brought together at a single site in the nucleus when the nucleolus forms. For example the DNA of the short arm and satellite region of 5 different human chromosomes (13, 14, 15, 21 and 22) interact to form nucleoli (for review see (Dundr and Misteli, 2001; Sullivan et al., 2001).

Initially it was shown that the spatial organization of centromeres is non-random and cell-type specific (Manuelidis, 1984). Later it was reported that neither the telomeres nor the centromeres are consistently located at the nuclear surface of human cells (Croft et al., 1999). A recent more detailed analysis of individual chromosomes demonstrated that in both human and murine resting lymphocytes, most centromeres were found in clusters at the

nuclear periphery. The distribution of telomere clusters, however, differed: in mouse nuclei, most clusters were detected at the nuclear periphery, while, in human nuclei, most clusters were located in the nuclear interior (Weierich et al., 2003). The behavior of centromeres seemed to be similar in all cell types studied and the localization seemed to change with the cell cycle (Ferguson and Ward, 1992; Solovei et al., 2004). The cell cycle is a sequence of steps in which a cell duplicates the chromosomes and divides into two, taking 10-20 h depending on the cell type and developmental state of the cell. In most higher and lower eukaryotes, the cell cycles can be divided into four phases: gap (G)1, synthesis (S), G2, and mitotic (M)-phase. The interphase comprises the G1, S, and G2 phases. DNA is synthesized in S-phase, and other cellular macromolecules are synthesized throughout interphase. During G2 the cell is preparing for the M phase, when the copies of the genetic material is distributed to the two newly formed daughter cells. Nondividing cells exit the normal cycle from G1, entering the quiescent G0 state. In cycling cells the localization of the centromeres changes. In the early G1 phase, centromeres were found in the nuclear interior, during late G1 and early S phase the centromeres shifted to the nuclear periphery and fused in clusters. At the late S and G2 phase, centromeres partially declustered and migrated towards the nuclear interior. In resting, non cycling and terminally differentiated monocytes a peripheral location and clustering of centromeres was most pronounced (Solovei et al., 2004).

1.1.2. Movements of chromosomes within the nucleus

Chubb et al. (2002) noted that the chromatin is constrained by association with nuclear compartments. Loci at the nucleoli or the nuclear periphery were found to be significantly less mobile than other, more interior loci, and disruption of the nucleoli increases the mobility of nucleolar-associated loci. These data suggest that the chromatin and nuclear compartments such as nucleoli are relatively immobile in the interphase nucleus (Chubb et al., 2002). Hence movement of chromosomes is restricted but does occur. One way to monitor movements of chromosomes is to track the location of their centromeres. The location of chromosome centromeres was analyzed *in situ* and *in vivo* by tracking the movement of GFP-fused human CENP-A (centromeric protein A) throughout the cell cycle.

Individual centromeres moved infrequently but could move over distances of 1 to 10 μm per hour (Sugimoto et al., 2000). Another study demonstrated by tracking a lac repressor GFP-fusion protein bound to an artificial array of thousands of lac operators (Robinett et al., 1996), that a late-replicating, heterochromatic region on a chromosome arm moved during interphase (Li et al., 1998). During the G1 phase, the stained domain moved from the periphery into the interior of the nucleus where it remained during S-phase and back to the periphery during G2. Another analysis using GFP labeled centromeres, however, demonstrated that during interphase, centromeres show very little movement in general, behaving as if they were embedded in a rigid matrix. Occasional movement was observed, suggesting that the chromosome position is changed during interphase (Sullivan and Shelby, 1999).

The localization of chromosomes within the nucleus also changes with cell aging. Bridger et al. demonstrated that the nuclear architecture is altered in cells that have become either quiescent or senescent. Upon cell cycle exit, the gene-poor human chromosome 18 moved from a location at the nuclear periphery to a more internal site in the nucleus, and changed its association with nuclear substructures. The authors therefore concluded that the sub-nuclear organization of chromosomes in quiescent or senescent mammalian somatic cells is fundamentally different from that in proliferating cells and that the spatial organization of the genome is plastic (Bridger et al., 2000).

1.2. Chromosomal territories

The idea of a territorial organization of chromosomes was first proposed at the turn of last century by Rabl (1885) and Boveri (1909). Rabl predicted that chromosomes retain structural integrity (Rabl, 1885). Boveri speculated on genetic identity throughout the cell cycle. He also postulated that each chromosomal territory would occupy a specific region of the nucleus, maintaining its own coherence and not mix with the other territories (Boveri, 1909). This idea was dismissed, after electron microscopic techniques during the 1960s and early 1970s failed to distinguish the hypothetical chromosome territories (Wischnitzer, 1973). At that time, the nucleus was still viewed by many scientists as a bag with chromatin

fibers from the different chromosomes intermingling in the nucleoplasm like "spaghetti in a soup". First evidence that a territorial organization of chromosomes does exist was produced after fluorescence *in situ* hybridization (FISH) technique was developed (Pinkel et al., 1986). Chromosomal paints for individual chromosomes revealed a cohesive territorial organization of chromosomal domains in interphase nuclei (Lichter et al., 1988; Pinkel et al., 1988). It is now assumed that chromosomes are organized in "territories" where only the material for one chromosome is located and not intermingled with the DNA of other chromosomes, with a functional channel-like compartment between them into which genes from the surface of chromosomes are transcribed and the resulting RNA is released, spliced, and transported to the nuclear envelope for export (Lampel et al., 1997; Zirbel et al., 1993). The term chromosome territory was coined to distinguish the area/space occupied by an individual chromosome from domains, which could be sub-chromosomal.

Chromosome territories are not compact lumps of chromatin. The chromosome fibers may be compact or locally unfolded to some degree (**Figure 1**). Genes are preferentially located at the periphery of chromosome territories independent of their transcriptional status, whereas nonexpressed sequences seem to be randomly located throughout territories or preferentially in the interior of the corresponding chromosome territory (Kurz et al., 1996).

The *ANT3* gene located on the X-chromosome, which escapes X-inactivation, showed a peripheral location in both, the active and inactive X chromosome territories. In contrast, the *ANT2* gene of the active X territory had a peripheral localization, whereas the silenced *ANT2* allele, subjected to X inactivation, showed a more interior localization (Dietzel et al., 1999).

Genes have also been shown to be located outside the compact region of their chromosomal territory. This "looping out" of genes seems to be dependent on the activity status of a region where the genes are expressed. In keratinocytes the genes of the epidermal differentiation complex at 1q21 are highly expressed and were frequently positioned external to the chromosome 1 territory (Williams et al., 2002). In contrast in lymphoblasts these genes are not expressed and their locations are more often peripheral or internal (Williams et al., 2002). Furthermore, activation of cells can also cause movement of genes to

a looped out position. This was demonstrated for the major histocompatibility class II complex genes on chromosome 6. Stimulation of MRC5 fibroblasts with interferon γ induced a looped out position of this gene locus (Volpi et al., 2000). In summary in the interphase nucleus, chromosomes occupy a discrete compact space. Genes are preferentially found in a peripheral location within these territories especially actively transcribed genes which can even be found outside the territory.

1.3. The interchromosomal domain (ICD) compartment model

Chai and Sandberg (1988) proposed an interchromosomal space, after detailed electron microscopic studies on the organization of chromosomes during the cell cycle (Chai et al., 1988). Concentrations of splicing components visualized by Sm-antigen were found to reside outside of chromosome territories (Zirbel et al., 1993). It was determined that single species of RNA are always located immediately outside of the chromosome from which the RNA originated (Clemson and Lawrence, 1996; Clemson et al., 1996; Zirbel et al., 1993) and further results supported the view that RNA processing and trafficking occurs in the ICD-compartment (Lampel et al., 1997) (**Figure 1**). Some of the most intriguing data supporting the existence of the ICD were obtained by using a temperature sensitive vimentin as a "nuclear space shuttle". The intermediate filament protein vimentin from *Xenopus laevis* has an interesting property. It exists as a monomer at 37˚C and polymerizes when the temperature is lowered to 28˚C (Herrmann et al., 1993). When cells are transfected with this protein fused to a nuclear localization sequence (NLS) it can be switched back and forth between a filamentous and a granular nuclear body type localization by changing the cell culture temperature. With this nuclear targeted vimentin in stably transfected human cells the interchromosomal compartment could be visualized at least in part upon polymerization of NLS-vimentin (Bridger et al., 1998). At 37°C the cells showed a distinct amount of internuclear speckles. Upon a temperature shift to 28°C NLS-vimentin progressed into intranuclear filamentous arrays. The filaments were located almost exclusively outside of chromosome territories. These filaments colocalized with specific nuclear RNA, coiled

bodies, and PML bodies, all situated outside of chromosome territories, thereby interlinking these structures. It is likely that all these components occupy the same space, the ICD compartment.

1.4. The position of genes in the nucleus affects their function

A comprehensive understanding of genomic sequence may require considering its arrangement in the nucleus. The form DNA takes in the nucleus reveals not only its high ordered structure, but it may contain information regarding its function. The localization of genes within the nucleus can affect their level of transcription. Alfred Sturtevant (Sturtevant, 1925) was the first to postulate the "position effect", in which the expression of a gene depends on its position in relation to other genes. Today 80 years later modern technology allows us to study this phenomenon directly and the idea that the actions of a gene may be influenced by its particular location in the nucleus is seriously considered (Parada and Misteli, 2002; Shannon, 2003).

Kosak and coworkers were able to correlate the relative position in the nucleus of the V_H gene array of the immunoglobulin heavy chain (IgH) locus with its transcriptional status. Active V_H locus in B-lymphocytes was centrally disposed, while inactive V_H locus in T lineage cells was localized to the nuclear periphery. However, as shown for the immunoglobulin kappa locus (Igκ) a more central position can also occur in the absence of transcriptional activation (Kosak et al., 2002).

1.5. 3 dimensional localization of chromosomes and their genes in the nucleus - the role of gene density

Since the location of genes in the nucleus affect their activity the mechanism of what determines the 3 dimensional (3D) localization of chromosomes and their genes in the nucleus are of considerable interest. Chromosomes are non-randomly positioned. It is assumed that chromosome positioning patterns are statistical representations of chromosome positions but do not provide information on the precise coordinates of a given chromosome

in a single nucleus (Parada et al., 2003). The chromosome position patterns are therefore probabilistic rather than absolute. The factors that determine the relative positions of chromosomes within the nucleus are not fully understood. There seems to be correlation between the estimated gene density (number of genes per Mbp) of each chromosome and its average position within the nucleus. The estimated gene density of each chromosome has been correlated with its average position within the nucleus. Chromosomes with few genes are often associated with the nuclear periphery, while gene rich chromosomes reside in a more internal nuclear position (Boyle et al., 2001; Croft et al., 1999). Chromosome size was not found to be a determining factor for the position of chromosomes within the nucleus (Boyle et al., 2001). The connection between gene density and localization was also evident in a comparison of the localization of human chromosome 18 and 19 and their derivatives generated by reciprocal translocation. While similar in size chromosome 19 is highly gene dense whereas chromosome 18 is relatively gene poor (Croft et al., 1999). In nuclei of all normal cells, the chromosome 19 territory had a more internal position than that of chromosome 18. The derivative chromosome 18 (der 18) seemed to be slightly less peripheral than the normal chromosome 18 suggesting that the chromatin composition of a given segment, by itself, is important for its nuclear location. Interestingly in 7 out of 8 tested tumor cell lines some of which had imbalances or rearrangements of these two chromosomes this localization was less pronounced suggesting that chromosome aberrations can influence the localization of chromosome territories (Cremer et al., 2003).

The trend of chromosomes having a preferred location according to their gene density was also supported by the work of (Saccone et al., 2002). This group produced paints containing DNA from different isochores. Isochores are DNA segments that are distinguished by GC content (Macaya et al., 1976) and were grouped into 5 families: two GC poor, and three GC rich families (Saccone and Bernardi, 2001). GC/gene rich regions were predominantly distributed in the interior of the nucleus, whereas the gene /GC poorest DNA regions were closer to the nuclear envelope (Saccone et al., 2002; Saccone et al., 1999). For large chromosomes a polar arrangement, with the region of the chromosome with high density located to the interior of the nucleus was evident. Chromosomal arms with GC

low isochores were oriented to the periphery. A comparison of the location of the GC-rich/gene-rich fractions with AT-rich/gene-poor fractions of human genomic DNA revealed that GC-rich sequences were localized in interior and exterior of the territories at similar frequency, whereas AT-rich DNA fragments were observed more to the interior of the same chromosome territories (Tajbakhsh et al., 2000). Little is known on what determines the position of individual genes in the nucleus. However, it was shown that external influences such as inducers of differentiation or exposure to gamma radiation can change positions of genes. After irradiation of cells *MYC* was repositioned closer to the nuclear center, and returned back to a more peripheral position 24 hours after radiation (Bartova et al., 2000). Taken together, it appears that gene density is one of the determining factor for the localization of chromosomes within the nucleus. However, prediction of the localization of individual genes and loci may have to consider not only the gene density of entire chromosomes, the gene density of chromosomal arms, or chromosomal subdomains, but may require analysis of the DNA composition in the immediate chromosomal neighborhood of genes or the local environment, which may be dynamic and changing depending on the cellular conditions.

1.6. The evolution of the mammalian genome - the genus Muntiacus

The genus Muntiacus is comprised of several species of Asiatic deers, and belongs to the order Artiodactyla, which groups them into the same phylogenetic classification with cattle, sheep and pigs. With roedeer (of the genus Capreolus) they share the same family Cervidae. The genus Muntiacus shows a large variability in the number of chromosomes. The Indian muntjac (*M. muntjak*) has a very low number of diploid chromosomes (female, 2n = 6 see **2A** lower panel; male 2n = 7 **see Figure 2A** upper panel) (Wurster and Benirschke, 1970). This makes the female *M. muntjak* the record holder among the mammals with the lowest diploid chromosome number found to date.

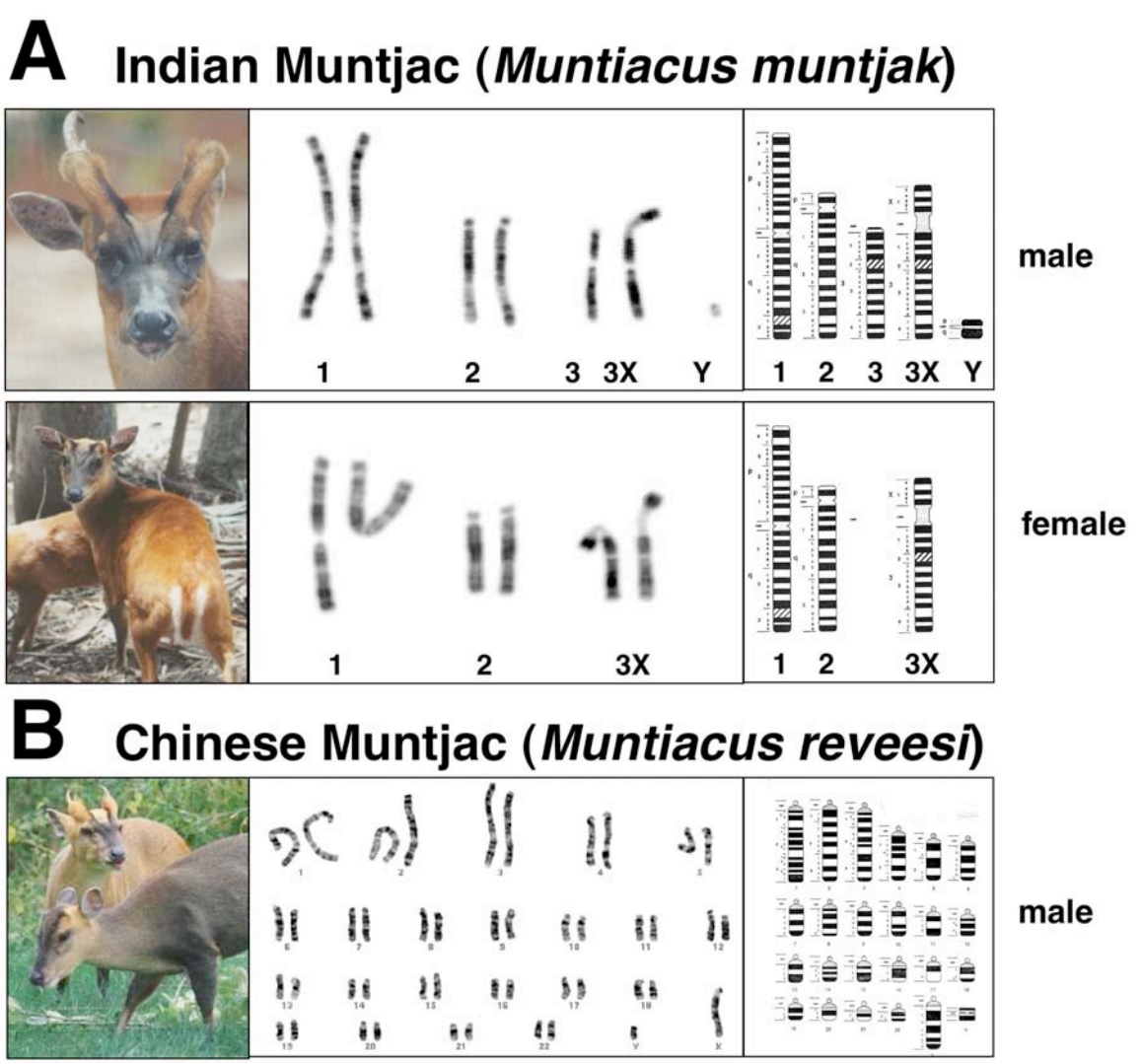

Figure 2: Karyotype and Ideogram of two muntjac species.

A: Karyotype of male and female Indian muntjac (*Muntiacus muntjak*).

Left: Pictures of an adult male (top) and an adult female (bottom) Indian muntjac. Photographs of both adult animals are displayed with permission of Brent Huffman (www.ultimateungulate.com)

Center: Enhanced DAPI banded metaphase chromosomes of the male Indian muntjac (top) with 2n = 7 chromosomes, and female muntjac (bottom) with 2n = 6 chromosomes from the cell lines ATCC157 and FIM, respectively.

Right: Ideogram of male (top) and female (bottom) Indian muntjac modified after Yang et al. (Yang et al., 1995).

B: Karyotype of the male Chinese muntjac (*Muntiacus reevesi*).

Left: Picture of male and female Chinese muntjac. Photograph was taken by Beryl Buckingham (www.deer-uk.com/muntjac_deer.htm).

Center: G-banded metaphase chromosome of Chinese muntjac with 2n = 46, courtesy of Dr. Fentang Yang, England.

Right: Ideogram of male Chinese muntjac modified after Yang et al. (Yang et al., 1995).

The chromosomes of the Indian muntjac (*M. muntjak*) are significantly larger, than the chromosomes of the Chinese muntjac (*Muntiacus reevesi* or Reeve's muntjac), indicating that similar genomes can come in different number of "packages" (differently sized chromosomes). The female *M. muntjak* karyotype (**Figure 2A**, bottom panel) consists of one pair of metacentric autosomes (chromosome 1), one pair of acrocentric autosomes (chromosome 2), and one pair of submetacentric chromosomes (chromosome 3X). These 3X chromosomes are actually compound elements, in which the "true" X has been translocated onto a third autosome and both are connected by a constricted heterochromatic region to which I will refer as the "neck" region of chromosome 3X. Males (**Figure 2A** upper panel) have the two pairs of autosomes, and three unique chromosomes.

In the literature these chromosomes were named inconsistently. Name combinations used are "X, Y1, and Y2" or "X, Y2, and Y1" or "X, 3, and Y". To be precise and avoid any confusion in this thesis, I will refer to these chromosomes as 3X, 3 and Y. Chromosome 3 is the telocentric homolog of the autosomal portion of the 3X, whereas Y is a small metacentric element, representing the "true" Y (Levy et al., 1993). Interestingly, the karyotype of *Muntiacus reevesi* (*M. reevesi)* is composed of 46 acrocentric chromosomes (Wurster and Benirschke, 1967). Phenotypically these two karyotypically different species are similar and are capable of producing viable (but sterile) hybrid offspring (Liming and Pathak, 1981).

1.7. The tandem fusion theory

How could a mammalian species have evolved with only 6 or 7 chromosomes? Comparison of the G-banding pattern between *M. muntjak* and *M. reevesi* revealed a large degree of homology (Liming et al., 1980) and it was suggested that the Indian muntjac was a result of multiple tandem and centromeric fusion events. The assumed ancestral karyotype of Cervidae may have been composed of 35 acrocentric pairs (2n = 70) (Fontana and Rubini, 1990). During the phyletic evolution of this family, different types of chromosome rearrangements took place. In the subfamily Muntiacinae (to which all species of the genus Muntiacus belong) centric and tandem fusions are assumed to have been the most common

chromosomal rearrangements (Fontana and Rubini, 1990). A large body of literature supports this theory: The highly conserved telomeric DNA sequence $(TTAGGG)_n$ were detected not only at the termini of *M. muntjak* metaphase chromosome but also in the arms of its chromosomes 1 and 2 (Lee et al., 1993), which was interpreted as former telomeres of the ancestral species. A centromeric satellite sequences from the *M. reevesi* localizes to the putative fusion points, which were determined by comparative chromosome painting and presumably represents the remnants of ancestral centromeric sequences (Lin et al., 1991). Different satellite sequences, which are in general terminally oriented on *M. reevesi* chromosomes were found throughout the *M. muntjak* chromosomes (Li et al., 2000). These data were used to define the fusion-associated breakpoints that might have let to the formation of *M. muntjak* chromosomes. And these findings were confirmed by colocalizing interstitial satellite DNA loci with the margins of conserved human/Indian muntjac syntenic segments (Fronicke and Scherthan, 1997). The 3X chromosome is believed to have evolved from a centric fusion of an evolutionarily older X-chromosome and an autosome (Green and Bahr, 1975). *M. muntjak* contains (2n = 6/7) chromosomes, raising the question, whether the DNA content of an individual *M. muntjak* cell remains the same when compared with that of similar organisms with a higher number of chromosomes. Several studies reported DNA content measurements of the Indian muntjac. The most convincing result was published by Levy et al. (Levy et al., 1993). Flow cytometric quantification of propidium iodide-stained cells was used, and the DNA content of muntjac cells calculated to be approximately 94% that of human cells. Previously published estimates a range from 61 - 72.4% when compared with human cells (Wurster and Atkin, 1972). This difference was likely caused by the variability of the applied methods (microdensitometric quantification of Feulgen-stained nuclei). In conclusion, there is only a reduction of about 6% of the DNA content in *M. muntjak* compared to that of human. In comparing *M. muntjak* and *M. reevesi* it was shown that *M. muntjak* shows a reduction of the middle repetitive DNA (Johnston et al., 1982).

Compared to human, only a few genes have been mapped in *M. muntjak* (Levy et al., 1992). Syntenic regions between muntjac, human and other species were identified by using the technique of Zoo-FISH (cross-species chromosome painting). Such analyses for human

and cattle, human and *M. muntjak* and *M. muntjak* as well as *M. reevesi* were reported (for human and *M. muntjak* (Fronicke and Scherthan, 1997), for *M. muntjak* and *M. reevesi*: (Yang et al., 1997b), for human and *M. muntjak*: (Yang et al., 1997a). Assumed homologue regions between cattle and *M. muntjak* were mentioned in Yang et al., 1997 (Yang et al., 1997a). Although syntenic regions between *M. muntjak* and *M. reevesi* as well as human and cattle were identified, little information is currently available on the localization of individual genes.

1.8. Differences and shared principles that determine gene localization among mammalian species

Early estimates of the number of genes in mammals ranged from 70,000 to 100,000 (O'Brien et al., 1999). Today, after the genomes of human (Venter et al., 2001), rat (Gibbs et al., 2004) and mouse (Waterston et al., 2002) have been sequenced, the number was considerably reduced to less than 30,000. All these genes are arranged in linear order along their chromosomes, with a total length of about 3 billion nucleotide pairs (Gibbs et al., 2004; Venter et al., 2001; Waterston et al., 2002). Chromosome numbers in mammalians range from as low as three pairs (2n = 6 in the female Indian muntjac) to as high as 67 pairs (2n = 134 in the black rhinoceros, *Diceros bicornis*) (O'Brien et al., 1999). Today gene maps of human, mouse and about 30 other mammal species were constructed or are in the progress of construction. 3 different categories of markers are used: Type I markers (coding genes, that allow identification of gene orthologs based on their conserved sequences), Type II markers (hypervariable microsatellites, also called short tandem repeats) and Type III markers (single nucleotide polymorphisms) (O'Brien, 1991). A small number of translocation events were necessary to discriminate the hypothetical primate ancestor (estimated to have existed over 60 million years ago) from the human genome organization (O'Brien et al., 1999). In primates, e.g., only a handful of differences are apparent between the genomes of humans and the great apes. A minimum of 13 rearrangements separate human and cat, and 27 separate human and cattle (reviewed in (O'Brien et al., 1999) Throughout the mammalian species a large number of conserved synthetic segments are

found. All these findings are an indication that the mammalian genome is dictated by "a high degree of genomic conservation" (O'Brien et al., 1999). The physical clustering of gene families has been observed (such as the major histocompatibility complex, immune globulin genes, *Hox* genes, the T cell receptor cluster, and chemokine receptors). It is not clear, whether they are the result of adaptive combinations of coordinate *cis* regulation, gene editing, or selective retention. It is also poorly understood, whether longer linkage associations preserved for tens of millions of years through billions of individuals in thousands of species are merely “frozen accidents” or were selectively retained by developmental or functional dependence (O'Brien et al., 1999; Ohno, 1973).

Despite of the large number of changes during evolution, many of the observations on localization of genes and chromosomal subregions in different vertebrates suggest a number of underlying principles/rules that determine 3D structure. Tanabe et al. (2002) tested the radial distribution pattern of human chromosome 18- and 19-homologous chromatin by three-dimensional FISH in seven different primate species (Tanabe et al., 2002). The data demonstrated that gene-density-correlated radial chromatin arrangements were conserved during higher-primate genome evolution, irrespective of the major karyotypic rearrangements that occurred in different phylogenetic lineages. Chromosome 19-homologous chromatin was found toward the nuclear interior. This radial distribution pattern was thus maintained over a period of at least 30 million of years, irrespective of the extensive chromosomal rearrangements that occurred during the evolution of higher primates. It fits the hypothesis that radial chromatin arrangements reflect differences in gene density (Boyle et al., 2001). In general the evolutionarily conserved positioning of homologous chromosomes or chromosome segments in related species provides support for a model in which functionally relevant higher-order chromatin arrangement is correlated with gene-density.

An analysis of chicken chromosomes provided further evidence for an evolutionary conserved effect of gene density on chromosomal localization (Habermann et al., 2001). An analysis of chromosome territories in nuclei of chicken fibroblasts and neurons (chicken has 9 pairs of macrochromosomes, and 30 pairs of microchromosomes, which represent only

23% of the genome but contain 50% of its genes) revealed that microchromosomes cluster in the nuclear interior, macrochromosomes at the periphery. These data suggest an evolutionary conservation of several features of higher-order chromatin organization between mammals and birds (chicken and human have a common ancestor about 300-350 million years ago according to (Hedges et al., 1996) despite their differences in their karyotypes.

1.9. Chromosomal translocations

Chromosomal aberrations are found in all types of human cancer. Specific recurring chromosome aberrations, such as certain translocations, are often associated with a particular type of leukemia, lymphoma or sarcoma and may be a cause of cellular transformation. However, is generally unknown, how translocation actually occur. Most chromosomal translocations are the result of reciprocal exchange of large-chromosomal segments, typically between two different chromosomes.

(Graeves, 2003) summarized a number of criteria, which probably have to be met for a functional, leukemogenic chromosome translocation to happen: "Simultaneous double-strand breaks (DSBs) have to occur in two chromosomes in a single cell and spatial proximity of broken chromosome regions is required. Breaks have to occur in 'relevant' introns of 'relevant' genes to generate a functional chimeric gene product. Chromosome recombination has to be in frame to generate a functional chimeric gene product. Breakage and recombination have to occur in a stem cell with progeny that is permissive for the expression and function of the translocation product. Finally, the DNA DSBs that initiate the translocation cannot be lethal to the cell in which they occur".

Chromosomal translocations can have different outcomes. Translocations of breakpoint junctions by fusion of two chromosomes may result in direct exchange of material between these chromosomes, leading to a fusion gene. The first example of gene fusion was discovered through the cloning of the breakpoint of the Philadelphia chromosome in chronic myelogenous leukemia (CML) (Groffen et al., 1984). A reciprocal translocation between chromosomes 9 and 22 results in a t(9;22)(q34;q11) where *ABL*

normally located at 9q34, fuses with the *BCR* gene at 22q11 (Shtivelman et al., 1985). The resulting fusion or hybrid gene, *BCR-ABL* created on the der(22) chromosome, encodes a chimeric protein with the tyrosine kinase function of ABL being inappropriately and constitutively activated and it is believed to be involved in malignant transformation (Lugo et al., 1990).

Alternatively translocation events can bring genes under control of a strong promotor resulting in their inappropriate high expression. An example is the t(8;14)(q24;q32) translocation found in Burkitt's lymphoma. In this chromosomal rearrangement, the *MYC* gene, located at chromosome band 8q24, is placed under the control of regulatory elements from the immunoglobulin heavy chain locus located at 14q32 (Siebert et al., 1998). The transcription factor MYC is overexpressed, and leads to uncontrolled cellular proliferation (Yamamoto et al., 1998).

Translocations may also result in either duplication or deletion of DNA sequences at the junction. Duplications and deletions observed in hematopoietic malignancies may be rather small (van der Feltz et al., 1989; Zhang et al., 2004). Microduplication may occur because of staggered cleavage in the DNA duplex followed by ligation and gap repair of the single stranded region. Alternatively, a 5' protrusion may be filled in prior to joining to the other chromosome in a translocation (Roth and Wilson, 1986). Tandem duplications of several kilobases can also be mediated by Alu-Alu recombination. This was observed for the *MLL* gene (Strout et al., 1998).

A number of theories exist to explain the occurrence of chromosomal translocations. Qumsiyeh (1995) speculated that the physical proximity of different chromosomes in interphase, may be important in determining the likelihood of any two chromosomes meeting and exchanging material in a translocation (Qumsiyeh, 1995). Croft et al. (1999) supported this view after analyzing the position of chromosome 18 and 19, which are preferentially located in extreme positions in interphase nuclei. Due to the difference in their location it was assumed, that translocation between these chromosomes occurs rarely, since chromatin movement in living interphase cells is constrained (Marshall et al., 1997). Marshall et al. (1997) observed that chromatin movement in *Saccharomyces cerevisiae* is

constrained but is free to undergo substantial Brownian motion, and proposed that a given chromatin segment is confined to a subregion of the nucleus. Chubb (2002) also observed constrained chromatin movement in mammalian cells, and speculated that these constraints are actually a reflection of the physical attachment of chromatin to the nucleolus and nuclear periphery, suggesting a role of these nuclear compartments in maintaining the three-dimensional organization of chromatin in the human nucleus (Chubb et al., 2002).

Database searches for balanced t(18;19) translocations in humans confirmed that this translocation is very rare in the human population when compared with other translocations among small chromosomes (Croft et al., 1999). A number of data support a model in which the size of the chromosomes is a major risk factor for translocations. Data base analyses of cytogenetic abnormalities in γ-irradiated lymphocytes or in atomic bomb survivors suggested that more translocation events are found on larger chromosomes (Bickmore and Teague, 2002; Cafourkova et al., 2001). In summary large chromosomes may be more frequently involved in translocation events than smaller ones because a larger size of a chromosome presents a larger target size for the initial DSBs. Although chromosome size is considered to be a contributing factor for translocation events found in the human population, there are definitely other factors that influence the translocation frequency.

Spatial proximity may influence the occurrence of acquired chromosome translocations associated with cancers and leukemias. For example, Kozubek and coworkers suggested that the spatial proximity of *ABL* and *BCR* genes on chromosomes 9 and 22 may account for the high incidence of the Philadelphia chromosome t(9;22) in human leukemias (Kozubek et al. 1999).

Conforth et al. reported a predominantly random localization of chromosomes with respect to each other in the interphase nucleus (Cornforth et al., 2002). The only increased incidence of exchanges between chromosomes they found was among chromosomes 1, 16, 17, 19 and 22 after irradiation of lymphocytes providing evidence in support of spatial clustering of these 5 chromosomes in the nucleus. In another report more than 60% of the breakpoints were localized in R bands, which are gene rich (Martinez-Lopez et al., 1998).

Bickmore and Teague did not find a correlation between the gene density and the number of translocations (Bickmore and Teague, 2002). However, since in their analysis only the gene densities of whole chromosomes were considered, it does not rule out that subchromosomal regions with high gene density might be involved in translocations more frequently.

The propensity of the *MLL* gene to rearrange and the diversity of the partner genes that fuse to *MLL* have made it difficult to postulate a common mechanism to explain the biological basis for leukemogenesis of the fusion transcript. Biological evidence for the leukemogenic role of the *MLL*/*AF9* fusion has been described (Corral et al., 1996). It was suggested that the N-terminus of *MLL* in the chimeric proteins after translocation plays a significant role in leukemogenesis (Joh et al., 1996).

1.10. Double strand breaks are involved in translocation events

One of the requirements for a translocation event is the occurrence of DSBs. In fact DSBs can induce frequent chromosomal rearrangements, translocations between nonhomologous chromosomes, deletions or chromosome loss. It was demonstrated that two DSBs, each on a different chromosome are sufficient to promote frequent reciprocal translocations in mammalian cells (Richardson and Jasin, 2000).

Three inducers of DNA breaks were proposed to be associated with translocation events leading to leukemia: V(D)J recombination, topoisomerase II and apoptotic endonucleases. All breaks that are created by these enzymes, occur mostly in introns and might have DNA-sequence requirements (for V(D)J recombination and topoisomerase II) or structural requirements (for apoptotic endonucleases).

1.10.1. V(D)J recombination as a contributor to DSBs

Two alternative repair pathways have been evolved during evolution to insure the proper repair of DSBs. Homologous recombination is a major DNA repair pathway in mammalian cells (Thompson and Schild, 2001). Nonhomologous end joining is another repair mechanism to repair DSBs (Tsukamoto and Ikeda, 1998). When a DSB is formed, the cell is capable of searching the genome and finding homologous sequences suitable for

repair, even when these sequences reside on otherwise non homologous chromosomes (Richardson et al., 1998). However, crossover events that would result in genome rearrangements are suppressed. Therefore, Richardson et al. favored the model, in which translocation is coupled to replication (Richardson et al., 1998). That DNA repair programs are involved in the generation of translocations is evidenced by the observation of accidental oncogenic translocations in mature B-cell lymphomas and in T-cell ALL. It is commonly believed that this is caused by a deregulated activity of the repair machinery, which regulates the V(D)J recombination of the T- and B-cell receptor genes which is important in establishing the immunological repertoire (Greaves and Wiemels, 2003).

1.10.2. Topoisomerase II as contributor to DSBs

MLL is also involved in 11q23 translocations in treatment-related leukemia, which develops as secondary acute leukemia, usually treatment-related AML (t-AML) after chemotherapy for a primary tumor. The general treatment of such tumors is usually radiation and/or various types of chemotherapy, particularly treatment with alkylating agents (e.g. cisplatin). These agents damage DNA and cause leukemias with losses of chromosomes 5 and/or 7 or of their arms (unbalanced chromosome aberrations with partial deletions or with loss of whole chromosomes). New drugs, which target topoisomerase II, were developed, (reviewed in (Rowley and Olney, 2002). The normal function of this enzyme is to untangle chromosomes. Different topoisomerase II inhibitor drugs like epipodophyllotoxins (e.g. VP16 = etoposide or VM26 = teniposid) and androchinones (e.g. doxorubicin) were used for treatment, but they led to high numbers of secondary leukemias that involved 11q23 translocations (Super et al., 1993). These balanced chromosome aberrations may be the result of illegitimate recombinations related to the activity of DNA-topoisomerase II resulting from DSBs, because the religation function of topoisomerase II was inhibited (Strick et al., 2000). Natural substances in food have also been suspected to contribute to DSBs. It was shown that dietary bioflavonoids, natural inhibitors of topoisomerase II, induce cleavage in the *MLL* gene and may contribute to infant leukemia (Strick et al., 2000) (for commentary see (Ross, 2000)).

1.10.3. The role of apoptosis in leukemogenesis

Apoptosis, also called "programmed cell death", is a self-destruction mechanism in multi cellular organisms, that has developed to eliminate damaged (and potentially harmful) cells or cells that are no longer needed by the organism. The suicide program is activated by various stimuli (such as DNA-damage) and leads to a fixed sequence of events (Hengartner, 2000; Kerr et al., 1972; Wyllie et al., 1980). Early events during apoptosis include a series of cytoplasm changes, including a drop in mitochondrial transmembrane potential and a phosphatidylserine flip from the inner to the outer leaflet of the plasma membrane. The activity of these "engines of self-destruction" triggers a sequential cascade of proteolysis events that activate caspases, cysteine proteases, that cleave several key cellular components (Earnshaw et al., 1999). At this stage, effects on a single chromosome territory have not yet been described, however, early cytoplasmic changes occur, which are followed by the progression of morphological changes in the nucleus. Dense chromosome condensation occurs along the nuclear periphery. The cell body shrinks although most organelles remain intact. Later events dramatically affect the integrity of the cell. Chromosomal DNA is fragmented, organelle structures are disrupted and the usual cell shape is lost after cleavage of actin and other cytoskeletal proteins. In the final stages of this suicide program, cells break up into apoptotic bodies (small membranes surrounded cell fragments) that are then phagocytosed by other cells. Khodarev and coworkers hypothesized that the initial stages of apoptotic DNA fragmentation is reversible and connected with the initiation of recombinatorial events and certain chromosomal translocations (Khodarev et al., 1999). These early events are connected with the introduction of limited amounts of DSBs into genomic DNA, some of which may subsequently rejoined. It has been shown that early stages of p53-induced apoptosis are indeed reversible. By removing the apoptotic stimulus, cells with externalized phosphatidylserine can be rescued, and it was observed that unscheduled DNA synthesis and general DNA repair activity increases in p53-induced early apoptotic cells (Geske et al., 2001), which is a possible explanation for this reversibility. A commitment phase to apoptosis was defined, which was (among different events) characterized by partial chromatin condensation during which the apoptogenic events are

reversible, if the strength of the stimulus is low and of short duration (Dumont et al., 2000). The activation of the main effector caspase 3 was suggested as the point of no return (Geske et al., 2000). More recently, however, it has become clear that the release of proapoptotic factors from the mitochondria such as cytochrome c more likely represents the point of no return (Green and Kroemer, 1998; Green and Kroemer, 2004) since cells can survive (or may even require) a certain level of active caspase 3 (Algeciras-Schimnich et al., 2002). It is conceivable, that with the reversal of early apoptotic events (also called "abortive apoptosis", (Khodarev et al., 1999)), translocations happen more frequently due to missrepair. That raises the question, whether this mechanism might be responsible for the re-occurring translocation events in leukemias. Investigating chromosome domains in hematopoietic stem cells (HSC) at the reversible early apoptotic stage could help to unravel the mechanisms responsible for these reoccurring events. Etoposide treatment, which frequently results in induction of apoptosis, was shown to cause segmentation of chromosome territories before any nuclear apoptotic bodies were found (Bartova et al., 2003). Interestingly, it was recently shown that fragmentation of the nuclear DNA during apoptosis does not occur completely randomly. Telomeric regions are excluded from nucleosomal fragmentation during apoptosis (Schliephacke et al., 2004). A contribution of apoptosis induced DNA fragmentation in translocation events came from studies of the gene *MLL*. It was observed that in the initial stages of apoptosis, DNA cleavage within the *MLL* breakpoint cluster region (bcr) is a specific event (Betti et al., 2001; Betti et al., 2003). After apoptotic DNA cleavage induced by treating cells with an antibody against the apoptosis-inducing death receptor CD95 (APO-1/Fas), a *MLL-AF9* translocation was initiated in the cells surviving this selection. This is consistent with the idea that the apoptotic program can have a pathogenic role in leukemogenesis (Brady, 2003). Interestingly it was even suggested that a fusion protein resulting from a translocation itself may render cells more resistant to apoptosis. Lavau and coworkers showed that by introduction of a t(11;19) fusion product *MLL*/*ELL* or *MLL*/*ENL* using a retrovirus, murine haematopoietic precursor cells are immortalized *in vitro* (Lavau et al., 2000a; Lavau et al., 2000b).

Within the *MLL* bcr a site was identified (Stanulla et al., 1997; Strissel et al., 1998) that is uniquely susceptible to DNA double strand cleavage, both *in vitro* (Stanulla et al., 1997) and *in vivo* (Aplan et al., 1996; Strick et al., 2000; Strissel et al., 2000) in response to topoisomerase II inhibition, DNAse I or apoptosis. It was also demonstrated that these site-specific DNA cleavage events within the *MLL* gene was independent of the chromosomal context. The same specific DNA cleavage event was observed in the *MLL* bcr region when located on an episomal vector, or when integrated into a different location of the genome (Stanulla et al., 2001).

1.11. The *MLL* gene

The *MLL* (for mixed-lineage leukemia or myeloid-lymphoid leukemia) gene was initially identified and cloned in 1991 from translocations that involved chromosome band 11q23 (Ziemin-van der Poel et al., 1991). The *MLL* gene spans 120 kb and contains at least 34-37 exons. The cDNA is 11.7 kb long and encodes a large protein with 3,968 amino acids with a predicted size of 431 kDa. *MLL* is also referred to as *HRX* (Tkachuk et al., 1992), *ALL-1* (Gu et al., 1992b), or *HTRX1* (Parry et al., 1993). Several regions of the protein have homologies to the product of Drosophila developmental gene trithorax (*trx*; (Mazo et al., 1990)). In Drosophila, *trx* is involved in the transcriptional maintenance of homeotic genes during Drosophila embryogenesis, (such as those of the Bithorax and Antennapedia complexes) and is assumed to indirectly activate transcription (Kennison et al., 1993).

MLL contains a region similar to the AT hooks of high-motility-group (HMG)-I/Y proteins (Domer et al., 1993; Zeleznik-Le et al., 1994), which binds to AT rich regions of the minor groove of the DNA double helix (Grosschedl et al., 1994; Reeves et al., 1990). Data to date suggest that *MLL* is also a transcription regulating factor, that possesses at least two DNA binding domains (Zeleznik-Le et al., 1994). The gene is expressed in a variety of tissues and exhibits alternative splicing. By analogy to *trx*, its activity could vary in different tissues (Bernard et al., 1995a). Data obtained from *MLL*-deficient mice support the hypothesis that *MLL* is the functional homologue of the trithorax gene in mammals. In *MLL*-/+ mice, sternal and axial skeletal malformations, and bi-directional homeotic

transformations were observed. Homozygous deletion of *MLL* resulted in an embryonic lethal phenotype (Yu et al., 1995). MLL is bound to metaphase chromosomes, with a preference for G-bands. A punctuate staining pattern for the MLL protein was observed in interphase nuclei, whereas its distribution on metaphase chromosomes followed a banding pattern, suggesting a close association with chromatin in general (Pam Strissel and Reiner Strick, personal communication).

1.12. Leukemias that involve the translocation of the *MLL* gene locus

Most of the translocations identified in myeloid leukemias, both acute and chronic, and in many of the B- and T-cell leukemias, are caused by DNA-breaks in introns or rarely in exons of two independent genes, that are involved in this translocation, resulting in the formation of a new chimeric gene with an in-frame fusion. This leads to the expression of a unique fusion or chimeric protein found only in these malignant cells (Rowley, 1998a). Chromosomal abnormalities involving the 11q23 band occur frequently in various hematopoietic malignant disorders. They are common in acute leukemia, both lymphoid (lymphocytic, lymphoblastic) and myeloid (myeloblastic) leukemia (ALL stands for acute lymphoblastic (lymphocytic/lymphoid), AML for acute myeloid (myeloblastic/ myelomonocytic/monocytic) leukemia). They are less common in lymphoma (solid tumors of lymphoid glands). Furthermore, chromosomal abnormalities are frequent in treatment-related leukemias. Deletions of 11q were also reported in AML, ALL, malignant lymphoma, and myelodysplastic syndromes (MDS) (Mitelman, 1991). The translocations are reciprocal between *MLL* and a partner gene, so two fusion genes and, therefore, two potential transcripts can be formed. However, more commonly a single fusion transcript is observed derived from the der(11) chromosome due to deletion of 3'*MLL* with disruption of one fusion protein (Bernard et al., 1995b).

Translocations involving 11q23 are seen in about 5% of patients with AML and in up to 10% of patients with ALL (Kaneko et al., 1986). *MLL* is involved in 95% of all 11q23 translocations including AML and ALL (Bernard et al., 1995a). 11q23 translocations are

found in the majority of infant leukemia (children under 1 year of age) usually of the ALL or AML type (Chen et al., 2000). All of the most important chromosome aberrations found in de novo AML were also found in t-AML. It was therefore suggested that t-AML may serve as a model in the search for mechanisms leading to the development of AML (Pedersen-Bjergaard and Rowley, 1994).

Sequencing the breakpoints of *MLL* showed that these breakpoints of de novo or secondary leukemias occur in the same bcr-region (Bernard et al., 1995b; Strissel et al., 2000). Although there are general models, attempting to explain how *MLL* recombines molecularly with its translocation partner genes (Marschalek et al., 1997), it is virtually unknown how recombination occurs at the level of chromosome domains and at which cell cycle or differentiation stage.

In all cases studied so far, the chromosome 11 breakpoints clustered within a 8.3 kb region, which has been fully sequenced (Park et al., 2000). This region spans exons 5-11 of the *MLL*-gene (Bernard et al., 1995a). The sequence was analyzed for motifs that might explain, why breaks occur preferentially in this particular region (Strissel et al., 1998). Translocations result in an in-frame *5'MLL*/3' partner gene transcript. In all fusion proteins, *MLL* provides the amino-terminus joined in-frame to the carboxy portion of the partner product, creating fusion proteins that are critical for leukemogenesis (Johansson et al., 1998).

1.13. Translocations involving *MLL* may occur in differentiating cells during hematopoiesis

The different types of blood cells develop from pluripotent hematopoietic stem cells (HSCs; see **Figure 3**) (Alberts et al., 1994). In the adult, HSCs are found mainly in the bone marrow, where they normally divide infrequently to produce more stem cells for self-renewal and various committed progenitor cells to give rise to the myeloid or lymphoid lineage that lead to the differentiated cell types, such as T- or B-cells, monocytes, eosinophils etc. (**Figure 3**).

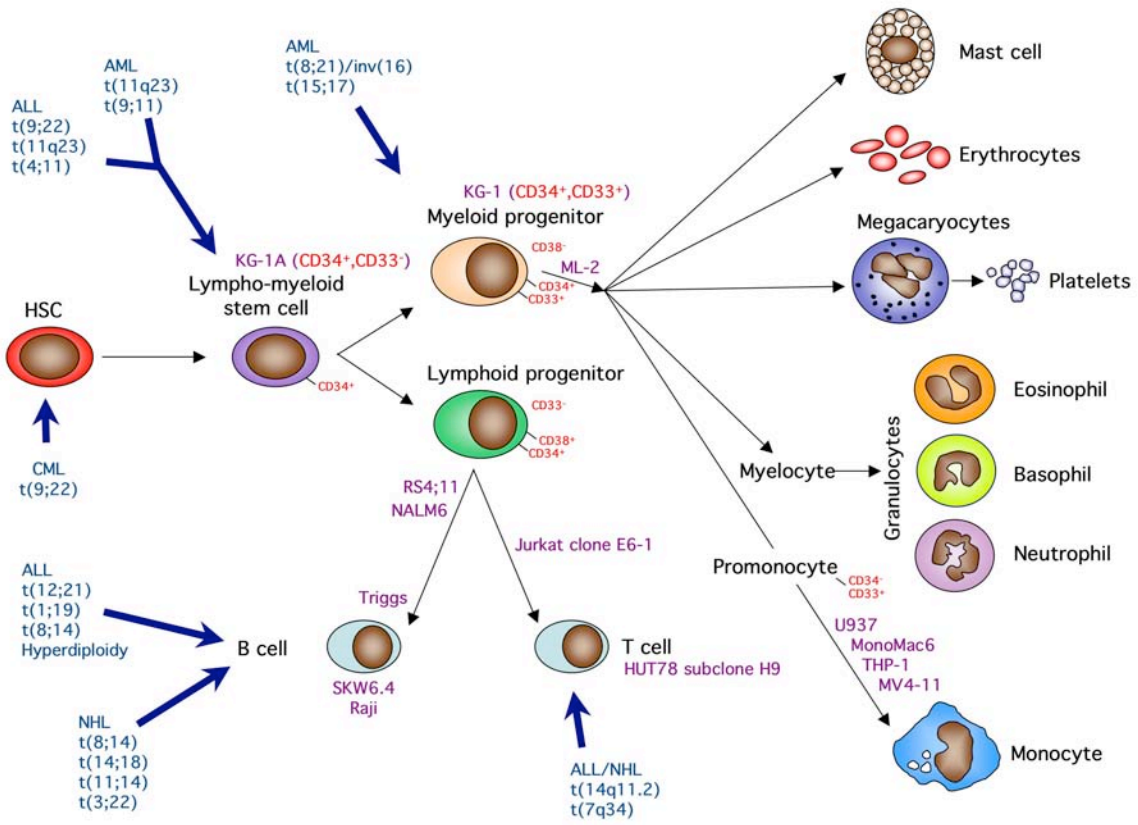

Figure 3: Model of human hematopoiesis.
The scheme shows the path of the development from pluripotent hematopoietic stem cells to terminally differentiated blood cells. The overview was modified after a slide received from Dr. Michelle LeBeau, University of Chicago, which was based on information taken from a review by Graeves (Graeves, 2003).
Purple: Various cell lines, used in this thesis, placed into the scheme according to their described characteristics.
Red: Surface antigens that characterize cells or cell lines used in the thesis.
Blue: Frequently observed translocations associated with leukemia. Blue arrows point to their assumed target cells.
Information on the characteristics of cell lines was taken from publications (Drexler, 2003; Drexler et al., 2004; Mrozek et al., 2003) and electronic sources (www.dsmz.de and www.atcc.com).

The committed progenitor cells divide abundantly under the influence of various cytokines, such as colony-stimulating factors (CSFs) and then differentiate into mature blood cells, which usually die after several days or weeks. Cell death, controlled by the

availability of cytokines, also plays an important part in regulating the numbers of mature differentiated peripheral blood cells.

The differentiation status of hematopoietic cells can be characterized by their expressed surface antigens. Primitive human haematopoietic progenitor cells express CD34 and AC133 (de Wynter et al., 1998). In malignant haematopoiesis AC133 is expressed in 60-80% of CD34+ cells of patients with acute leukemias (Waller et al., 1999). **Figure 3** provides a rough overview on where translocations actually occur. Translocations happen at various stages of hematopoiesis (Passegue et al., 2003). For instance Davi et al. (1996) showed that the B-lineage ALL arises from a lymphocytic progenitor and that a transformation event does not preclude further maturation (Davi et al., 1996). Studying the 3D localization of *MLL* and its translocation partners in nuclei of hematopoietic cells

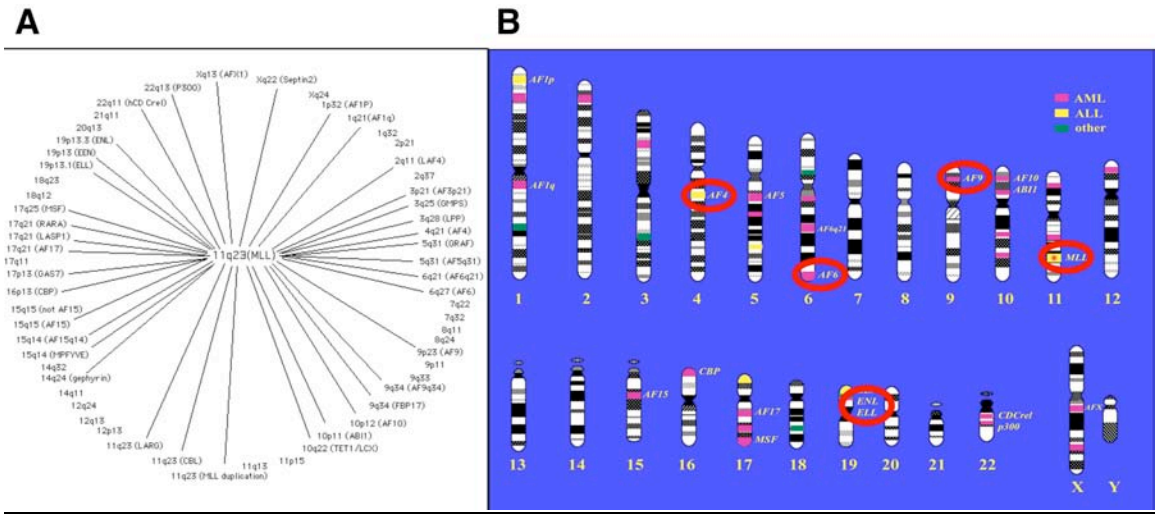

Figure 4: Chromosomal location of *MLL* translocation partners.

A: Summary of 60 described regions in the human genome to translocate with *MLL* (Huret, 2003).

B: Ideograms of the human chromosomes. The chromosomal location of *MLL* and its most frequent translocation partners are circled in red. The image was received from Rafael Espinosa at the Laboratory of Dr. Michelle LeBeau, University of Chicago, and was based on the information obtained from Mitelman (Mitelman et al., 2001).

Recurring 11q23 translocations involve the following chromosomal bands: 1p32, 1q21, 2p21, 4q21, 6p27, 9p22, 10p11, 11q25, 17q21, 17q25, 19p13.1, 19p13.3, Xq13. The following chromosomes or chromosome arms have not or only in selected cases been found to rearrange with *MLL*: 7, 8, 13, 14, 20, 21, Y, 2q, 4p, 5p, 9q, 12q, 16q, 18p, Xp.

representing different stages of development might provide new insights into the mechanisms that underlie translocations events leading to leukemogenesis.

1.14. The most frequent translocations involving the *MLL* gene

The four most common translocations involving *MLL* seen in human leukemia are t(4;11), t(6;11), t(9;11) and t(11;19) (Rowley, 1990) (**Figure 4** and **Table 1**). t(4;11) and t(11;19)(q23;p13.3) translocations are found in acute lymphoblastic leukemia and t(6;11), t(9;11), and t(11;19)(q23;p13.1) translocations in acute myeloblastic leukemia.

Chr	Chromosomal Band	Symbol	Name	Locus-link ID	Tumour Types (Somatic Mutations)	Translocation Partner
1	1p32	*EPS15*	epidermal growth factor receptor pathway substrate 15 (AF1p)	2060	ALL	*MLL*
1	1q21	*AF1Q*	ALL1-fused gene from chromosome 1q	10962	ALL	*MLL*
2	2q11.2-q12	*LAF4*	lymphoid nuclear protein related to AF4	3899	ALL	*MLL*
3	3p21	*AF3p21*	SH3 protein interacting with Nck, 90 kDa (ALL1 fused gene from 3p21)	51517	ALL	*MLL*
3	3q24	*GMPS*	guanine monphosphate synthetase	8833	AML	*MLL*
3	3q28	*LPP*	LIM domain containing preferred translocation partner in lipoma	4026	leukemia	*HMGA2, MLL*
4	4q21	*MLLT2*	myeloid/lymphoid or mixed-lineage leukemia (trithorax homolog, Drosophila); translocated to, 2 (*AF4*)	4299	AL	*MLL*
5	5q31	*AF5q31*	ALL1 fused gene from 5q31	27125	ALL	*MLL*
5	5q31	*GRAF*	GTPase regulator associated with focal adhesion kinase pp125(FAK)	23092	AML, MDS	*MLL*
6	6q21	*FOXO3A*	forkhead box O3A	2309	AL	*MLL*
6	6q27	*MLLT4*	myeloid/lymphoid or mixed-lineage leukemia (trithorax homolog, Drosophila); translocated to, 4 (*AF6*)	4301	AL	*MLL*
8	8q22	*CBFA2T1*	core-binding factor, runt domain, alpha subunit 2;translocated to, 1 (ETO)	862	AML	*MLL, RUNX1*
9	9p22	*MLLT3*	myeloid/lymphoid or mixed-lineage leukemia (trithorax homolog, Drosophila); translocated to, 3 (*AF9*)	4300	ALL	*MLL*
9	9q23	*FNBP1*	formin binding protein 1 (FBP17)	23048	AML	*MLL*
10	10p11.2	*SSH3BP1*	spectrin SH3 domain binding protein 1 (*ABI1*)	10006	AML	*MLL*
10	10p12	*MLLT10*	myeloid/lymphoid or mixed-lineage leukemia (trithorax homolog, Drosophila); translocated to, 10 (AF10)	8028	AL	*MLL, PICALM*
10	10q21	*LCX*	leukemia-associated protein with a CXXC domain	80312	AML	*MLL*
11	11q23	*MLL*	myeloid/lymphoid or mixed-lineage leukemia (trithorax homolog, Drosophila)	4297	AML, ALL	*MLL, MLLT1, MLLT2, MLLT3, MLLT4, MLLT7, MLLT10, MLLT6, ELL, EPS15, AF1Q, CREBBP, SH3GL1, FNBP1, PNUTL1, MSF, GPHN, GMPS, SSH3BP1, ARHGEF12, GAS7, FOXO3A, LAF4, LCX, SEPT6, LPP, CBFA2T1, GRAF, EP300, PICALM*
11	11q14	*PICALM*	phosphatidylinositol binding clathrin assembly protein (CALM)	8301	TALL, AML	*MLLT10, MLL*
11	11q23.3	*CBL*	Cas-Br-M (murine) ecotropic retroviral transforming	867	AML	*MLL*
11	11q23.3	*ARHGEF12*	RHO guanine nucleotide exchange factor (GEF) 12 (LARG)	23365	AML	*MLL*
14	14q24	*GPHN*	gephyrin (GPH)	10243	AL	*MLL*
15	15q14	*AF15Q14*	AF15q14 protein, *(MPFYVE, ZFYVE19*)	57082	AML	*MLL*
16	16p13.3	*CREBBP*	CREB binding protein (CBP)	1387	AL, AML	*MLL, MORF, RUNXBP2*
17	17p	*GAS7*	growth arrest-specific 7	8522	AML*	*MLL*
17	17q11-q21.3	*LASP1*	LIM and SH3 protein 1	3927	AML	*MLL*
17	17q21	*MLLT6*	myeloid/lymphoid or mixed-lineage leukemia (trithorax homolog, Drosophila); translocated to, 6 (AF17)	4302	AL	*MLL*
17	17q25	*MSF*	MLL septin-like fusion	10801	AML*	*MLL*
19	19p13.1	*ELL*	*ELL* gene (11-19 lysine-rich leukemia gene)	8178	AL	*MLL*
19	19p13.3	*SH3GL1*	SH3-domain GRB2-like 1 (EEN)	6455	AL	*MLL*
19	19p13.3	*MLLT1*	myeloid/lymphoid or mixed-lineage leukemia (trithorax homolog, Drosophila); translocated to, 1 (*ENL*)	4298	AL	*MLL*
22	22q11.2	*PNUTL1*	peanut-like 1 (Drosophila), (hCD Crel)	5413	AML	*MLL*
22	22q13	*EP300*	300 kd E1A-Binding protein gene	2033	AML	*MLL, RUNXBP2*
X	Xq13.1	*MLLT7*	myeloid/lymphoid or mixed-lineage leukemia (trithorax homolog, Drosophila); translocated to, 7 (AFX1)	4303	AL	*MLL*
X	Xq24	*SEPT6*	septin 6	23157	AML	*MLL*

Table 1: List of all translocation partners of *MLL* that have be confirmed by sequence analysis (Table was adapted from (Futreal et al., 2004)).
Only the genes that translocate with *MLL* are listed.
AL = acute leukemia, ALL = acute lymphocytic leukemia , AML = acute myelogenous leukemia, MDS = myelodysplastic syndrome, TALL = T-cell acute lymphoblastic leukemia, * = other germline mutation was found.

t(4;11) translocations

The t(4;11) translocation is often seen in ALL (Rowley, 1998b). The majority of the t(4;11) translocations occur in infancy and childhood and have a poor prognosis (Pui et al., 1991a; Pui et al., 1991b). The translocation partner of *MLL* during this translocation is *AF4*/*FEL* located on chromosome 4q21. *AF4* is normally transcribed in various tissues and exhibits alternative splicing at the 5'-end (Nakamura et al., 1993). Due to sequence similarities Hiwatari et al. suggested that *AF4* together with *LAF4*, and *AF5q31* might define a new family particularly involved in the pathogenesis of 11q23-associated ALL (Hiwatari et al., 2003).

t(6;11) translocations

The human *AF6* gene was identified as another common translocation partner gene of *MLL* in the t(6;11)(q27;q23). This translocation is associated with AML and more rarely t-AML patients (Mitterbauer et al., 2000). *AF6* codes for a Ras-binding protein (Joh et al., 1997) and contains 32 exons spanning 140 kb (Saito et al., 1998). A number of analyzed breakpoints in *AF6* was localize in the largest intron 1 (Saito et al., 1998).

t(9;11) translocations

The t(9;11)(p22;q23) is the most common of the 11q23 translocation in both de novo AML and t-AML, but rarely in ALL, with the result of a fusion of parts of *MLL* and the *AF9*/*LTG9* gene at 9p22 (Iida et al., 1993a; Iida et al., 1993b). It was suggested that the fusion point within the *AF9* gene (and thus the amount of *AF9* material included in the *MLL-AF9* fusion gene product), may influence the phenotype of the resulting leukemia (Strissel et al., 2000). *AF9* carries two major breakpoint positions, site A and site B (Yamamoto et al., 1994). It was shown that site A fusions correlate with AML and the more rare site B fusions coincide with ALL (Super et al., 1997). The cell line MonoMac6 (derived from an AML-patient) is characterized by a *MLL-AF9* fusion (Super et al., 1997).

t(11;19) translocations

The t(11;19)(q23;p13) chromosomal abnormality is found in different types of acute leukemia. Rearrangement with t(11;19)(q23;p13.3) leads to ALL, and rearrangement with t(11;19)(q23;p13.1) leads to AML (Rowley, 1998b). Different partner genes in this region were identified as translocation partners for *MLL*. The most frequent translocation on chromosome 19 involve *ENL* (eleven-nineteen leukemia) at 19p13.3 (Tkachuk et al., 1992). The second most common at 19p13.1 is *ELL/MEN* (Eleven nineteen lysine-rich leukemia) (Thirman et al., 1994). A third gene, *EEN* (Extra Eleven Nineteen) located at 19q3.3, was found to be a translocation partner in a case of AML (So et al., 1997a).

In summary, translocations involving 11q23 in leukemia result in the translocation of *MLL* with other genes on chromosomes 4, 6, 9, or 19. Interestingly the fusion partners of *MLL* on these chromosomes (e.g. *ENL* and *AF9*) show high homology to each other. They all contain nuclear targeting sequences as well as serine-rich and proline-rich regions (Nakamura et al., 1993). *MLL* can also rearrange with itself. Partial duplication of *MLL* has been observed in cases of AML with normal karyotype or trisomy 11 (So et al., 1997b).

MLL rearranges with more then 50 other loci. Such a variety of rearrangements involving the same band is not too common among chromosome abnormalities found in human malignancies. Some other examples, where a chromosome band has multiple fusion partners were described (a summary can be found in the supplemental information of (Futreal et al., 2004)). Two other examples are the transcription factor *TEL*/*ETV6* gene located at 12p12.1 to 12p13.3, which was shown to be involved in more than 41 different translocations (Odero et al., 2002) and *AML1* on chromosome 21q22 which has more then 30 translocation partners (Richkind et al., 2000) http://www.infobiogen.fr/services/chromcancer/Genes/AML1.html.

Studying the mechanisms underlying chromosomal translocations involving *MLL* may lead to a better understanding of the mechanisms that underlie disease causing chromosomal translocations. In addition, *MLL* and its various translocation partners provide a unique and naturally occurring system to study the effects of a change in local gene density caused by the translocation on the 3D position of a locus within the nucleus.

1.15. Aim of the thesis

The aim of this thesis was to investigate the topology of mammalian cell nuclei, and to identify principles that determine the 3D position of genes in the nucleus. Suitable cell material and genomic clones for FISH probes had to be gathered; methods and computational tools had to be established to allow 3D analysis of interphase nuclei.

MLL, which has the propensity to translocate with a vast number of other genes, five of its translocation partners, *AF4*, *AF6*, *AF9*, *ENL* and *ELL*, and 4 control loci, 2q33, 2q35, 7q22 and 8q34, that had not been described previously to translocate with the 11q23 locus in hematopoietic cells, were chosen as a model system to determine the relation between the immediate environment of a gene and its intranuclear localization. Probes to detect *MLL*, the various translocation partners, and the control loci, had to be obtained or generated. Using these tools, the position of genes should be determined in 3D interphase nuclei and characterized in different species with a minimal amount of perturbance of the nuclear structure. To address the question whether a difference in chromosomal numbers has an effect on the localization of genes and whether the findings could be generalized to different mammalian species, three different species were chosen: two relatively closely related species of deer, *Muntiacus reevesi* and *Muntiacus muntjak*, with a great difference in chromosome number, and the well characterized human species. To investigate the two muntjac species, materials had to be produced and gene loci had to be mapped.

To elucidate the possible mechanism, which might be responsible for the positioning of specific DNA sequences within the 3D volume of the interphase nucleus, the position of *MLL* and some of its translocation partners, had to be analyzed in various cell lines and primary cells under various conditions. The effect of translocations on gene position should be studied in cells carrying well defined translocations involving *MLL* and some of its translocation partners. A set of locus specific probes had to be designed to allow simultaneous detection of the genes on normal and derivative chromosomes. These studies were expected to shed light on the mechanisms that determine the position of genes in the 3D space of the nucleus and provide further insights into positional changes of genes caused by chromosomal translocations.

2. ABBREVIATIONS

2n	diploid chromosome number
2 x	two fold
2D	two dimensional
3D	three dimensional
22-mer	primer sequence with 22 nucleotides
7-AAD	7-amino-actinomycin D
A	adenosine
A_{280}	absorbion at 280 nm
A_{260}	absorbion at 260 nm
AF4	*ALL1* fused gene from chromosome 4
AF6	*ALL1* fused gene from chromosome 6
AF9	*ALL1* fused gene from chromosome 9
AL	acute leukemia
ALL	acute lymphoblastic (lymphocytic/lymphoid) leukemia
AML	myeloid (myeloblastic) leukemia
BAC	bacterial artificial chromosome
bcr	breakpoint cluster region
B-cell	B lymphocytes\
bp	base pair
BPB	bromophenol blue buffer
BSA	bovine serum albumin
BTA	chromosome from *Bos taurus* (cattle)
C	cytidine
˚C	degree Celcius
CBL	chronic myelogenous leukemia
CCD	cold coupled device
CD	cluster of differentiation
cDNA	complementary deoxyribonucleic acid
chr	normal chromosome
cm	centimeter
dATP	2'-deoxyadenosine-5'-triphosphate
DAPI	4’,6-diamidin-2’-phenylindol-dihydrochloride

dCTP	2'-deoxycytidine-5'-triphosphate
del	chromosome with deletion
der	derivative chromosome
dGTP	2'-deoxyguanosine triphosphate
dH_2O	destilled water
ddH_2O	double destilled water
DIC	differential interference contrast
DMEM	Dulbeccos modified Eagle medium
DMSO	dimethyl sulfoxide
dNTP	nucleotide triphosphate mix with dATP, dCTP, dGTP and dTTP
DNP	dinitrophenol
DNA	deoxyribonucleic acid
DNase	deoxyribonuclease
dNTP	2'-deoxyribonucleoside (5‘- triphosphate; see dATP, dCTP, dGTP, dTTP)
DOP	degenerated oligonucleotide primer
DSB	double strand breaks
dUTP	2'-deoxyuracil-5'-triphosphate
EBV	Epstein-Barr virus
E. coli	*Escherichia coli*
EDTA	ethylendiaminotetraacetate
ELL	eleven nineteen lysine-rich gene on chromosome 19
ENL	eleven-nineteen leukemia gene on chromosome 19
FACS	fluorescence activated cell sorter
FBS	fetal bovine serum
FISH	fluorescence *in situ* hybridization
FITC	fluorescein isothiocyanate form
G	guanosine
g	gram
g	centrifugal force
G0	Gap 0 phase, resting phase of the cell cycle
G1	Gap 1 phase of the cell cycle
G2	Gap 2 phase of the cell cycle
G-banding	Giemsa-banding

GFP	green fluorescent protein
h	hour(s)
HSA	chromosomes from *Homo sapiens* (human)
HSC	hematopoietic stem cells
Hz	Herz
ICD	interchromosomal domain compartment
IMEM	Iscoves modified Dulbecco's medium
IV-file	file in Inventor format
kb	kilo base
kDa	kilo dalton
LB	„Luria-Bertani“, full medium for bacteria
lb/sq.in	pounds per square inch (pressure)
m	meter
M	molar
M-phase	mitotic phase of the cell cycle
M. muntjak	*Muntiacus muntjak*
M. reevesi	*Muntiacus reevesi*
mA	milliampere
MAA	methanol/acetic acid
Mbp	mega base pairs (one million base pairs)
MDS	myelodysplastic syndrome
min	minutes
ml	milliliter
mg	milligram
MLL	myeloid/lymphoid or mixed lineage leukemia
mm	millimeter
mM	milimolar
MMV	*Muntiacus muntjak* chromosome
MRE	*Muntiacus reevesi* chromosome
mRNA	messenger ribonucleic acid
n	number
NCBI	National Center of Biotechnology Information
ng	nanogram

nm	nanometer
NLS	nuclear localization sequence
NTP	ribonucleoside (5‘- triphosphate; see ATP,CTP, GTP, UTP)
OD	optical density
PAC	P1-derived artificial chromosome
PAGE	polyacrylamide gel electrophoresis
PBS	phosphate buffered saline
PCR	polymerase chain reaction
PE	phycoerithrin
PFA	paraformaldehyde
R	nuclear radius
rDNA	ribosomal DNA
RGB	red/green/blue
RNA	ribonucleic acid
RNase	ribonuclease
rpm	revolution per minute
RT	room temperature
SAGE	sequence analyzed gene expression
S-phase	synthesis phase of the cell cycle
SDS	sodiumdodecylsulfate
sec	seconds
ssDNA	single stranded DNA
T	thymidine
t(18;19)	translocation between chromosomes 18 and 19
t-AML	treatment-related AML
T-cell	T lymphocyte
TBE	tris HCl-boric acid-EDTA buffer
Tris	N,N,N-tris[hydroxymethyl]aminomethan
U	units
UTP	uridine-5'-triphosphate
UV	ultraviolet light
v/v	volume per volume
w/v	weight per volume

Zoo-FISH	cross-species chromosome painting
λ	wave length
µg	microgram
µl	microliter
µm	micrometer
µM	micromolar
%	percent

3. MATERIAL

For details and addresses of companies, materials were purchase from, see Appendix I.

3.1. Cells

Cells were received from various collaborating laboratories as listed in **Table 2**. Their karyotypes are listed in **Table 3**. Primary human cells from fresh bone marrow (CD34+ and

Cell name	Cell type	Species	Sources, cells were received from	Medium composition	Split density (cell/ml) or split ratio	Recommend et maintaining cell density (cell/ml)	Max. cell density (cell/ml)	Fluit renewal
HUT-78 subclone H9	Mature T-cell line; TCR alpha beta+ T, cell line (recommended reference cell line)	*Homo sapiens*	ATCC: HTB-176, Dr. Peter, University of Chicago	90%RPMI1640, 10%FBS, 1% penicillin-streptomycin	$1x10^5$		$1x10^6$	2-3 days
Jurkat, clone E6-1	Immature T-cell line (recommended reference cell line)	*Homo sapiens*	ATCC: TIB-152, Dr. Peter , University of Chicago	90%RPMI1640, 10%FBS, 1% penicillin-streptomycin	$1x10^6$	0.5-1.5 x 10^6	$1x10^6$	2-3 days
SKW 6.4	EBV transformed lymphoblastoid mature B-lymphocyte	*Homo sapiens*	ATCC: TIB-215, Dr. Peter, University of Chicago	90%RPMI1640, 10%FBS, 1% penicillin-streptomycin	$0.5x10^6$		$2x10^6$	2-3 days
Nalm6	Precursor B-cell line; human B cell precursor leukemia	*Homo sapiens*	Dr. Janis Burkhardt, former University of Chicago, now University of Philadelphia)	90%RPMI1640, 10%FBS, 1% penicillin-streptomycin	$0.5x10^6$	1.0-2.0 x 106	$6x10^6$	2-3 days
Triggs	EBV-transormed B-cell type	*Homo sapiens,* female	Dr. Michelle LeBeau, University of Chicago	90%RPMI1640, 10%FBS, 1% penicillin-streptomycin	$0.5x10^6$		$2x10^6$	2-3 days
Raji	EBV positive, Burkitt's lymphoma cell line; B lymphocyte; Burkitt's lymphoma	*Homo sapiens*	ATCC: CCL-86, Dr. Peter, University of Chicago	90%RPMI1640, 10%FBS, 1% penicillin-streptomycin	$0.5x10^6$		$1x10^6$	2-3 days
KG-1	Myelocytic cell line (Reference cell line) Myelocytic cell line; lymphmyeloid stem cell-like	*Homo sapiens*	ATCC: CCL-246, Dr. Janet D. Rowley, University of Chicago	90%RPMI1640, 10%FBS, 1% penicillin-streptomycin	$1x10^6$	0.2-1.0 x 10^6	$1.5x10^6$	2-3 days
KG-1A	Less mature daughter cell line from KG-1	*Homo sapiens*	ATCC: CCL-246-1; Dr. Janet D. Rowley, University of Chicago	90%RPMI1640, 10%FBS, 1% penicillin-streptomycin	$1x10^6$	0.5-1.5 x 10^6	$2.5x10^6$	2-3 days
U-937	Monocytic cell line	*Homo sapiens*	ATCC: CRL-2367, Cytogenetics laboratory, University of Chicago, cytogenetics case #15534)	90%RPMI1640, 10%FBS, 1% penicillin-streptomycin	$0.5x10^6$	0.1-1.0 x 10^6	$2x10^6$	3-4 days
Mono Mac 6	Monocytic cell line (recommended reference cell line)	*Homo sapiens*	Cytogenetics laboratory, University of Chicago, cytogenetics case #, originaly from Germany	90%RPMI1640, 10%FBS, 1% penicillin-streptomycin	$0.3x10^6$	0.3-1.0 x 10^6	$1x10^6$	2-3 days
THP-1	Monocytic	*Homo sapiens*	ATCC: TIB 202, Dr. Janet D. Rowley, University of Chicago)	90%RPMI1640, 10%FBS, 1% penicillin-streptomycin	$0.5x10^6$	0.1-1.0 x 10^6	$1x10^6$	3-4 days
Rs4;11	B cell precursor leukemia	*Homo sapiens*	DSMZ: ACC 508, Dr. Janet D. Rowley, University of Chicago)	90% Iscove's modified Dulbecco's medium, 10% FBS, 1% penicillin-streptomycin, 0.5% gentamycin, 1% sodium pyruvate, and 1 mm l-glutamine.	$0.5x10^6$	0.5-1.0 x 10^6	$4x10^6$	3-4 days
MV4-11	Monocytic	*Homo sapiens*	Dr. Janet D. Rowley, University of Chicago	90%RPMI1640, 20%FBS, 1% penicillin-streptomycin	$0.6x10^6$	0.2-1.0 x 10^6	$1.5x10^6$	3-4 days or longer
ML-2	Acute myelomonocytic leukemia	*Homo sapiens*	Dr. Janet D. Rowley, University of Chicago	90%RPMI1640, 10%FBS, 1% penicillin-streptomycin	$0.5x10^6$	0.5-1.0 x 10^6	$1x10^6$	2-3 days
PB	Peripheral blood from normal female donor	*Homo sapiens, female*	normal female donor	90%RPMI1640, 10%FBS, 1% penicillin-streptomycin				n.a.
HDF	Primary dermal fibroblast from foreskin	*Homo sapiens, male*	Dr. Peter Lichter, DKFZ Heidelberg, Germany	90%RPMI1640, 10%FBS, 1% penicillin-streptomycin	1:3 - 1:5		90%	2-3 days
CCL-157	Fibroblast	*Muntiacus muntjak,* male	ATCC: CCL-157	90% DMEM, 10% FBS, 1% l-Glut, 1% penicillin-streptomycin	1:3 - 1:5		90%	2-3 days
FIM	Primary female Indian muntjac fibroblast	*Muntiacus muntjak,* female	Dr. Roger A. Schultz, UT Southwestern Medical Center, Dallas	90% DMEM, 10% FBS, 1% l-Glut, 1% penicillin-streptomycin	1:3 - 1:5		90%	2-3 days
PCF	Primary male Chinese muntjac fibroblast	*Muntiacus reevesi,* male	Dr. Anja Fisher; University of Bielefeld	90% DMEM, 10% FBS, 1% l-Glut, 1% penicillin-streptomycin	1:3 - 1:5		90%	2-3 days
CCL-44 = EBTr (NBL-4)	adherent, trachea; normal	*Bos taurus,* male, embryonic	ATCC: CCL-44	90% DMEM, 10% FBS, 1% l-Glut, 1% penicillin-streptomycin	1:3 - 1:5		90%	2-3 days

Table 2: Characteristics of cell lines used in this thesis.
Sources, cells were received from, and growth conditions.
ATCC = American Type Culture Collection, Manassas, VA.
DSMZ = Deutsche Sammlung von Mikroorganismen und Zellkulturen GmbH, Braunschweig, Germany.

CD33+) were isolated by and purchased from AllCells Inc. (Berkeley, CA).

Cell name	Karyotype description	Source of information source
HUT-78 subclone H9	Near triploid cell line (modal number = 69; range = 58 to 74). Higher ploidies is 2.5%. Complex karyotype with nearly 60% of the chromosomes in each cell being structurally altered marker chromosomes. Among the markers are t(3p4q), t(5q6q), t(5p6p), i(18q), i(18p); t(4q7p), and del(7)(q32). The first four of these are usually paired. Normal N4, N5, N6, N7, N10, N13, N18, N19, N20 an X are absent.	www.atcc.org
Jurkat, clone E6-1	Pseudodiploid; modal chromosome number is 46, occurring in 74% with polyploidy at 5.3%. The karyotype is 46,XY,-2,-18,del(2) (p21p23),del(18) (p11.2). Most cells had normal X and Y chromosomes.	www.atcc.org
SKW 6.4	n.d.	no karyotype decription found
Nalm6	Near diploid karyotype; 46(43-47)<2n>XY, t(5;12)(q33.2;p13.2)	www.dsmz.de
Triggs	Diploid. With increasing passages tendency to triploidy and tetraploidy	Dr. Michelle LeBeau
Raji	t(8;14)(q24;q32); Karyotype 100% stable within male diploid stemline of 46. Cells with 47 chromosomes frequently contained an extra "E" group chromosome.; 6% polyploidy and occasional disparity in the size of the homologs of the number 1 chromosome and the number 4 chromosome.	www.atcc.org
KG-1	Hypodiploid, 4.5% polyploid; 45(42-47) <2n> X/XY, -4, +, +8, -12, -17, -20, +2mar, der(5;17)(q10;q10) del(5)(q?11q?13), dup(7)(q12q33), del7(q22q35), i(8q)2x, der(8)t(6;8)(p11;q22), der(8)t(8;12)(p11;q13), der(11)t(1;11)(q13-21;p11-q13), der(16)t(?12;16)(?p113;q13/21)	Mrozek et. al (2003)
KG-1A	The stemline chromosome number is 46 (pseudodiploid), with the 2S component occurring at 5.8%. Seven markers, including five ATCC CCL-246-specific markers, were found in most, if not all metaphases analyzed. Another marker ? del (7) was found only in about 50% of the metaphases. Normal chromosomes 5, 7, 8, 12, 17 and 22 were monosomic. The Y chromosome is detected in the Q-banded preparations.	Mrozek et. al (2003)
U-937	Flat-moded, hypotriploid; 63(58-69) <3n> XXY, -2, -4, -6, +7, -9, -20, -21, +3mar, t(1;2)(q21;p13), der(5)t(1;5)(p22;q35, add(9)(p22), t(10,11)(p14;q23), i(11q), i(12p), add(16)(q22), add(19)(q13), unique tranlocation t(10;11)(p13;q14) -> CALM-AF10 fusion gene	www.dsmz.de
Mono Mac 6	Hypotetraploid, flat-moded, near dipliod (8%), poliploid (17%) sidelines; 84-90 <4n> XX/XXX, -Y, +6, +7, -12, -13, -13, -16, -16, +2mar, t(9;11)(p22;q23)x2, add(10)(p11)x2, add(12)(q21), del(13)(q13q14)der(13)t(13;14)(p11;q21)x2, der(17)t(13;17)(q21;p11)x2. unique translocation: t(9;11)(p22;q23) -> *MLL -AF9* fusion gene	www.dsmz.de, own obervation confirmed for chromosomes 9 and 11
THP-1	Human near-tetraploid karyotype; 94(88-96)<4n>XY/XXY, -Y, +1, +3, +6, +6, - 8, -13, -19, -22, -22, +2mar, add(1)(p11), del(1)(q42.2), i(2q), del(6)(p21)x2-4,i(7p), der(9)t(9;11)(p22;q23)i(9)(p10)x2, der(11)t(9;11)(p22;q23)x2, add(12)(q24)x1-2, der(13)t(8;13)(p11;p12), add(?18)(q21); carries t(9;11) involving genes *MLL* and *AF9*	Odero et al. (2002) www.dsmz.de, own obervation confirmed for chromosomes 9 and 11
Rs4;11	Human hyperdiploid karyotype; 47/48<2n>X/XX, +8, +18, t(4;11)(q21;q23), i(7q); sideline without +8/18; carries *MLL - AF4* fusion gene	www.dsmz.de, own obervation confirmed for chromosomes 4 and 11
MV4-11	Human hyperdiploid karyotype; 48(46-48)<2n>XY, +8, +18, +19, -21, t(4;11)(q21;q23) involving genes *MLL* and *AF4*	www.dsmz.de, own obervation confirmed for chromosomes 4 and 11
ML-2	Tetraploid karyotype; 92(84-94)<4n>XX, -Y, -Y, -7, -9, -10, -10, +11, +12, +12, +13, +13, -15, -16, -17, -17, +18, +18, -20, -20, +4mar, der(1)t(1;?)(p21;?)x2, del(6)(q23)x2, der(6)t(6;11)(q27;?q23)x2, ?der(11)t(6;11)(q27;?q23)/del(11)(q23)x2, der(11)t(11;?)(?->11p11->11q23:)x2, der(11)t(11;?)(q11-13;?), dup(13)(q32->qter) x2, der(18)t(5;?;18)(q21;?;q11) x2; ML-2 may carry rare t(6;11) involving genes *MLL* and *AF6*	www.dsmz.de, own obervation confirmed for chromosomes 6 and 11
HDF	Diploid, less then 10% of poliploid metaphases were observed	Own observation
PB	Diploid	Own observation
CCL-157	Diploid, less then 10% tri- and tetraploid metaphases were observed	www.atcc.org
FIM	Diploid, less then 5% abnormal metaphases	Own observation
PCF	Diploid	Own observation
CCL-44	Assumed diploid	www.atcc.org

Table 3: Karyotypes of cell lines used in this thesis.

72 h peripheral blood cultures were received from the Cytogenetics Laboratory of the University of Chicago, and used for the preparation of metaphase chromosomes. For details and addresses of the collaborating laboratories see Appendix II. For details about the core facilities of the University of Chicago, that were used, see Appendix III.

3.2. Primers

Primers were purchase from Integrated DNA Technologies (Inc. Coralville, IA) with PAGE purification for the DOP-PCR 6MW primer, with standard desalting for all other primers. These primers were used to verify the received genomic clones.

Primer name	Size of primer	Sequence 5'__3'	Orientation of primer	Product size [bp]	Temp used for PCR	For species	Chrom. locus	Designed for gene
DOP-PCR 6MW	22-mer	CCGACTCGAGNNNNNNATGTGG	both	variable	see DOP PCR prodocoll	any	any	n.a.
MLLT2F	20-mer	ATGCCTTGGGCACTATTTTG	forward	200	50°C	HSA	4	*AF4*
MLLT2R	20-mer	AGGCAAGAGCATCTCTCAGG	reverse		50°C	HSA	4	*AF4*
MLLT3F	25-mer	GGACACTTTCTTATCACAAACACAA	forward	100	50°C	HSA	9	*AF9*
MLLT3R	22-mer	CAAGATGTTCCAGATGTTTCCA	reverse		50°C	HSA	9	*AF9*
M12R1	19-mer	TAGCCTGATGTTGCCTTCT	forward	120	50°C	HSA	11	*MLL* mRNA
M11H	18-mer	GGACAAACCAGACCTTAC	reverse		50°C	HSA	11	*MLL* mRNA
MLLF	20-mer	TGCTGGCACATCTTCTTCAG	forward	200	50°C	HSA	11	*MLL*
MLLR	20-mer	AGGCACTAGTGGCAAGAGGA	reverse		50°C	HSA	11	*MLL*
forw-sod1	24-mer	GTTTGGCCTGTGGTGTAATTGGAA	forward	275	55°C	BTA	1q12-q14	*SOD1*
rev-sod1	24-mer	GGCCAAAATACAGAGATGAATGAA	reverse		55°C	BTA	1q12-q14	*SOD1*
forw-vil1ms	24-mer	GAGTTGGGGAGAAAATCAAGGTTG	forward	~300	55°C	BTA	2q43	*VIL1MS*
rev-vil1ms	24-mer	ACACTCACACACACACAAAGCCTC	reverse		55°C	BTA	2q43	*VIL1MS*
forw-HSD3B1	21-mer	AAGACGGCCGTGAAGAAGAGC	forward	334	55°C	BTA	3q12	*HSD3B1*
rev-HSD3B1	22-mer	TGGATGTTTGGGACCTTTTTGG	reverse		55°C	BTA	3q12	*HSD3B1*
forw-INHBA	25-mer	AGTCACCATCCGTCTCTTTCAACAG	forward	289	55°C	BTA	4q26	*INHBA*
rev-INHBA	23-mer	CCCTTCCCCCTCCTCTTCTTTCT	reverse		55°C	BTA	4q26	*INHBA*
forw-IFNG	25-mer	AGTAACTAGGCAAGTCTATGGGATT	forward	278	55°C	BTA	5q22-q24	*IFNG*
rev-IFNG	22-mer	GAGATGCTATGTTTTTGTCAGG	reverse		55°C	BTA	5q22-q24	*IFNG*
F3_exon4_CSN3	21-mer	AAATACTGTGCCTGCCAAGTC	forward	305	50°C	BTA	6q31	*CSN10*
R4_exon4_CSN3	22-mer	CTGCGTTGTCTTCTTTGATGTC	reverse		50°C	BTA	6q31	*CSN10*
forw-RASA1	24-mer	GGGCCACAGCCCAGGATCGGGAGC	forward	187	55°C	BTA	7q24-qter	*RASA1*
rev-RASA1	23-mer	CCCTTCCGCTTTAGTGCAGCCAG	reverse		55°C	BTA	7q24-qter	*RASA1*
F-BTA7-IL4	22-mer	ACATTCAGGTCTGTGATCCATG	forward	100	50°C	BTA	7q	*IL4*
R-BTA7-IL4	20-mer	GTGAGGAAAAGGAAGAACTGT	reverse		50°C	BTA	7q	*IL4*
F-BTA7-PAM	21-mer	GTGAGGAAAAGGAAGAACTGT	forward	280	50°C	BTA	7q	*PAM*
R-BTA7-PAM	23-mer	CATGTCTTCCTGTACTAAGAAGT	reverse		50°C	BTA	7q	*PAM*
forw-IFN1@	23-mer	CATCTCTGTGCTCCACGAGGTGA	forward	294	55°C	BTA	8q15	*IFN1@*
rev-IFN1@	25-mer	GGCTCTCATGACTTCTGCTCTGACA	reverse		55°C	BTA	8q15	*IFN1@*
forw-IGF2R	21-mer	CTCCGACCAAATCCGATGGGA	forward	191	58°C	BTA	9q27-q28	*IGF2R*
rev-IGF2R	19-mer	CACGCTCAAGGTGAGGGCA	reverse		58°C	BTA	9q27-q28	*IGF2R*
forw-CYP19	24-mer	GCCATGGTGATGATGAAGGTCGTC	forward	183	55°C	BTA	10q26	*CYP19*
rev-CYP19	24-mer	TAGCGCTCGAGGCACTTGTCTGAAT	reverse		55°C	BTA	10q26	*CYP19*
forw-LGB	24-mer	TGTGCTGGACACCGACTACAAAAA	forward	300	55°C	BTA	11q28	*LGB*
rev-LGB	24-mer	GCTCCCGGTATATGACCACCCTCT	reverse		55°C	BTA	11q28	*LGB*
forw-RB1	17-mer	GAATGAGGAAGTGAGAT	forward	137	50°C	BTA	12q13	*RB1*
forw-RB1F	24-mer	CTTGTGTGATTAACTTATTTAGAG	reverse			BTA	12q13	*RB1*
forw-IL2RA	25-mer	GGATTGCTATAAATGATGCTCCACA	forward	133	55°C	BTA	13q13-q14	*IL2RA*
rev-IL2RA	25-mer	ACATTAGATGTACTGCTCCCTTATC	reverse		55°C	BTA	13q13-q14	*IL2RA*
forw-TG	19-mer	GGCCCTGGCCCTATGGGTC	forward	63	55°C	BTA	14q12-q15	*TG*
rev-TG	19-mer	AAAGATGTTGGCGGATGCC	reverse		55°C	BTA	14q12-q15	*TG*
forw-FSHB	21-mer	TCAAGGAGCTGGTCTACGAGA	forward	188	55°C	BTA	15q25-qter	*FSHB*
rev-FSHB	22-mer	CCGCTGCTCTTTATTCTTTGAT	reverse		55°C	BTA	15q25-qter	*FSHB*
forw-PIGR	25-mer	GACCGGATTTCAATCAGGAGCTACC	forward	100	55°C	BTA	16q13	*PIGR*
rev-PIGR	25-mer	TCTGGAGAGGCTCCCATGTTGTCAC	reverse		55°C	BTA	16q13	*PIGR*
forw-FGG	22-mer	GGTCGGAGTAGAACATCACGTT	forward	192	55°C	BTA	17q12-q13	*FGG*
rev-FGG	22-mer	GGGAATACAGTCCAAAGTGAGT	reverse		55°C	BTA	17q12-q13	*FGG*
forw-GPI	18-mer	GGCCGCTACTCGCTGTGG	forward	92	58°C	BTA	18q22-q24	*GPI*
rev-GPI	22-mer	CCAGTGAGCTCCTGAGAGCAGC	reverse		58°C	BTA	18q22-q24	*GPI*
forw-GH1	21-mer	TATGAGAAGCTGAAGGACCTG	forward	337	55°C	BTA	19q22	*GH1*
rev-GH1	20-mer	GTGCCATCTTCCAGCTCCTG	reverse		55°C	BTA	19q22	*GH1*
forw-MAP1B	25-mer	TTTCTCCACCAGACTTCTCCCCTAA	forward	178	60°C	BTA	20q14-q15	*MAP1B*
rev-MAP1B	22-mer	AGTGGGCCCGTTTTCAGTGATA	reverse		60°C	BTA	20q14-q15	*MAP1B*
forw-IGH@	23-mer	GGACTGGTGAAGGCTTCGGAGAC	forward	227	50°C	BTA	21q23-q24	*IGH@*
rev-IGH@	25-mer	ACAGAGCTCAGCCTCAGGGAGAACT	reverse		50°C	BTA	21q23-q24	*IGH@*
forw-LTF	20-mer	GATTCAAGCTGAGGCATTCC	forward	164	55°C	BTA	22q24	*LTF*
rev-LTV	19-mer	CCAAAGTGGCCAATTTGAC	reverse		55°C	BTA	22q24	*LTF*
forw-BOLADYA	24-mer	TCCCTGAAGTGGCTGTGTTTCC	forward	167	55°C	BTA	23q12-q13	*BOLADYA*
rev-BOLADYA	25-mer	ACTCTTGGGGTAGAAGGTGGTCTCA	reverse		55°C	BTA	23q12-q13	*BOLADYA*
forw-DSC@	18-mer	CAGTGACTGGCACAACTT	forward	811	58°C	BTA	24q21-q22	*DSC@*
rev-DSC@	20-mer	AGTGTGTCCTCTAATGGATT	reverse		58°C	BTA	24q21-q22	*DSC@*
forw-ELN	19-mer	CGGGAACAGGGCCAGCAGC	forward	161	55°C	BTA	25	*ELN*
rev-ELN	21-mer	CTGGGTCTGACTGGACTGGAC	reverse		55°C	BTA	25	*ELN*
forw-TNFRSF6	27-mer	GGGCTAAAATGGCAAATATTAGGTAAG	forward	200	55°C	BTA	26q13	*TNFRSF6*
rev-TNFRSF6	27-mer	TATCTTTGCAACTTTTCTGTAAGTCGA	reverse		55°C	BTA	26q13	*TNFRSF6*
forw-DEFB1	21-mer	CATTTCCTTCTGCATAGAAAA	forward	912	56°C	BTA	27q13-q14	*DEFB1*
rev-DEFB1	18-mer	AAGCCCATGCTTGGCCTG	reverse		56°C	BTA	27q13-q14	*DEFB1*
forw-CGN1	18-mer	CTGCTCCTGCTCACACAG	forward	143	55°C	BTA	28q18	*CGN1*
rev-CGN1	20-mer	TCTCCCATCTTGTCCATCAT	reverse		55°C	BTA	28q18	*CGN1*
forw-LDHA	20-mer	ATGAGGTGATCAAACTGAAA	forward	119	55°C	BTA	29qter	*LDHA*
rev-LDHA	20-mer	CCTTAATCATGGTGGAAATC	forward		55°C	BTA	29qter	*LDHA*
forw-IGF2	19-mer	GACCATCCAGCCGCATAAA	reverse	100	55°C	BTA	29qter	*IGF2*
rev-IGF2	20-mer	GGGGGTGGCACAGTAAGTCT	reverse		55°C	BTA	29qter	*IGF2*
forw-PGK1	20-mer	GGATGTTCTGTTCTTGAAGG	forward	177	55°C	BTA	Xq21-q22	*PGK1*
rev-PGK1	20-mer	CTTGTTCCCAGAAGCATCTT	reverse		55°C	BTA	Xq21-q22	*PGK1*
forw-ZFY	20-mer	GGTTATTAAATCGCCACCTT	forward	198	55°C	BTA	Yp13	*ZFY*
rev-ZFY	19-mer	GTTTTCACATGCGTCTTCA	reverse		55°C	BTA	Yp13	*ZFY*

3.3. Nucleotides

A deoxynucleoside-triphosphate set, PCR grade (Roche, Indianapolis, IN) or TAKARA dNTP mix (Fisher Scientific, Chicago, IL) was used for PCR reactions. Labeled nucleotides were purchased from Roche (biotin-16-dUTP, digoxigenin-11dUTP, estradiol-15-dUTP) or PerkinElmer (Boston, MA) (DNP-11-dUTP). The production of estradiol-15-dUTP has been discontinued.

3.4. Sources for genomic DNA

3.4.1. Animal tissue

Roe deer spleen tissue for DNA-extraction was received from forest official Volkland (Staatliches Forstamt Schwetzingen). The animal was a road kill. Chinese muntjac tissue for DNA-extraction was obtained from a stillbirth from a fawn after a 12 h period, stored at 4°C provided by Antje Fischer (Department of Animal Behaviour, University of Bielefeld). The DNA-preparation on this material was performed by Dr. Markus Scheuermann (Dr. Peter Lichter's laboratory, DKFZ, Heidelberg), which was then received for this work. For details of his preparation, see his thesis ((Scheuermann, 2004). The methods he applied were from (Ausubel et al., 1998)).

3.4.2. Genomic DNA

Genomic DNA from various species were purchased from Sigma (St. Louis, MO), Invitrogen (Carlsbad, CA) or Applied Genetics Labs (Foster City, CA): sonified Salmon testes-DNA, human Cot-1 DNA, cattle Cot-1 DNA were used for FISH-experiments, human placental DNA and calf thymus DNA were used for PCR and to prepare Cot-1 DNA.

3.4.3. Bacterial clones

3.4.3.1. Bacterial clones for syntenic analysis of both muntjac species

55 clones for the syntenic analysis of both muntjac species were received from different sources. Clone identification number, name of the contained genes and assignment of the chromosomal locus are listed in **Table 4**. 3 clones containing genomic sequences from

Clone ID	Gene name	Gene location on BTA (unigene or inra webpage)	Gene location on HSA (unigene webpage)	Gene location on MMV	Location matches BTA/HSA-MMV prediction ?	BTA synteny predicted for this MMV locus (expected)	Gene location on MRE	Location matches MMV-MRE prediction ?	MRE synteny predicted for this MMV locus (expected)	Note	Source
426H12	*SOD1*	1q12-q14	21q22.1	3q11	+		18	+			MG
406B01	*VIL1MS*	2q43	2q25-q36	2q12	-	(8; 9)	16 or 19	-	(11)	n.v.	MG
219F9	*HSD3B1*	3q12	1p13.1	1q25-q26	+		1q21-q24	+			MG
453B12	*INHBA*	4q26	7p15-p13	3q14-q15	+		not		(6)	n.v.	MG
945H5	*IFNG*	5q22-q24	12q14	1q24-q25	+		4q22-q23	+		n.v.	MG
505F4	*CSN10*	6q31	4q21	3q39-q41	+		18, 20 or 21	(+)	(21)		MG
531H12	*PAM*	7q	5q14-q21	1q34-tel.	+		1q36-q37	+			MG
512F12	*IL4*	7q15-q21	5q31.1	1q31-q32	+		1q31-q33	+			MG
143F11	*RASA1*	7q24-qter	5q13.3	2q38-q39	-	(11)	9?		(10)		MG
982C11	*RASA1*	7q24-qter	5q13.3	1q34	+		1q33-q36	+			MG
344C12	*IFNA*	8q15	9p22	1p12-p13	+		19	+		n.v.	MG
70B4	*IFNA*	8q15	9p22	1p12-p13	+		19	+		n.v.	MG
293G9	*IGF2R*	9q27-q28	6q26	1p15-p16	+		3	+		n.v.	MG
0963H01	*CYP19*	10q26	15q21.1?	2q32-q33	-	(7;16)	not		(2).	n.v.	MG
cattle 27A	*TCR-A*	10q15, (pers.com. JB)	14	3q41	+		not		(8; 21).	n.v.	JB
286F8	*LGB*	11q28	n.n.	1p43-tel.	+	no human equivalent	3q-tel	+			MG
783G1	*RB1*	12q13	13q14.2	3q33-q34	+		9q- centr.	+			MG
283G8	*IL2RA*	13q13-q14	10p15-p14	2q34-q35	+		2q1.1	+			MG
1004F08	*TG*	14q12-q15	8q24.2-q24.3	1p31	+		12	+			MG
462D8	*FSHB*	15q25-qter	11p13	2q38-q39	+		10 or 13	(+)	(10)	n.v.	MG
349E11.	*PIGR*	16q13	1q31-q41	3q21-q31	+		5q21	+			MG
111B07	*FGG*	17q12-q13	4q28	1p16-p17	n.n.	no pred. for MMV	9?		(3;17)		MG
651C8	*GPI*	18q22-q24	19q13.1	2q34	+		2q35	+			MG
393G12	*GH1*	19q22	17q24.2	1p17-p21	+		17	+		n.v.	MG
cattle 36H	*TCR*	19q17, (pers.com. JB)	17 ?	1p17-p21	+		not		(3;17)	n.v.	JB
713A1	*MAP1B*	20q14-q15	5q13	2q21	+		13	+			MG
355H4	*IGH-cluster*	21q23-q24	14 ?	2q15-q16	+		not		(13;15)		MG
336B8	*LTF*	22q24	3q21-q23	1q21-q22	+		4q15-q21	+			MG
712H8	*BOLA-DYA*	23q12-q13	6p21.3 ?	1p22-p23	+	no human equivalent	22	+			MG
531B11	*BOLA-DYA*	23q12-q13	6p21.3 ?	1p22-p23	+	no human equivalent	22	+			MG
cattle20K	*MHC-1*	23q22, (pers.com. JB)	6p21.3 ?	1p24	+		not		(22)	n.v.	JB
810H10	*DSC* -cluster	24q21-q22	18q12	1p22-p23	+		4q1	+			MG
513H8	*ELN*	25	7q11.23	2q31-q34	+		2q26-q31	+			MG
839E10.	*TNFRSF6*	26q13	10q24.1	2q24-q26	+		2q21-q22	+			MG
312A6	*DEFB1*	27q13-q14	8p23.2-p23.1	2q12-q13	+		11	+			MG
601B8	*CGN1*	28q18	10 ?	2q25	+		2q21-q23	+			MG
196G04	*CGN1*	28q18	10 ?	2q25	+		2q21-q22	+		n.v.	MG
953A11	*IGF2*	29qter	11p15.5	1p11-p12	+		5q11-q21	+			MG
39CF	*IGF2 & LDHA*	29qter	11p15.4 (LDHA)	1p11-p12	+		5q11	+			MG
834C6	*XIST*	X	Xq1	3Xp13-p14	+		Xq4	+		n.v.	MG
327D2	*PGK1*	Xq21-q22	Xq13	3Xp13-p14	+		Xq4	+			MG
0809B10	*MLL*		11q23	2q37-q38	+		10	+			MG
0494F04	*AF4*		4q21	3q39	+		21	+			MG
1086D03	*AF9*		9p22	1p12-p13	+		19	+			MG
455E12.	not listed,	n.n.	n.n.	2q25-q26	no gene ID	(10;16)	2q25-q26	+		n.n.	MG
259D9	not listed, IGF2R?	n.n. (9q27?)	n.n. (6q26?)	1p14-p16	(+?), no gene ID		not		(3;19)	n.n.	MG
18S-rDNA	*18s* -rDNA, Mouse	n.n.	13, 14, 15, 21 and 22	1q31 and 3q21	n.n.	no pred. for MMV	1q28-q31 and 6q7	+ and +		n.v.	JE
982C12	*RASA1*	7q24-qter	5q13.3	not			not				MG
330C11	*ZFY*	Yp13	Yp11.3	not			not				MG
325C2	*ZFY*	Yp13	Yp11.3	not			not				MG
852D12	*ZFY*	Yp13	Yp11.3	not			not				MG
787C6	*SRY*	Y	Y?	not			not			n.v.	MG
0430B09	*MLL*		11q23	not			not				MG
0889E10.	*AF4*		4q21	not			not				MG
1022D02	*AF9*		9p22	not			not			n.v.	MG

Table 4: List of localized genes on Indian and Chinese muntjac using cattle clones.
Information for the locations of cattle genes were taken from:
http://www.ncbi.nlm.nih.gov/entrez/query.fcgi?db=unigene&cmd=search&term
http://locus.jouy.inra.fr/cgi-bin/lgbc/mapping/common/gene.operl?BASE=cattle
Identity of cattle clones from Munich were personal communication with Dr. J. Buitkamp.
Source of clones: MG = Dr. Mathieu Gautier, JE = Dr. Jens Eilbracht, JB = Dr. J. Buitkamp.
n.n. = not known.
n.v. = clones were not verified by PCR.
no gene ID = no information of containing gene was available.
no human equivalent = no human equivalent was found (Gautier et al., 2001).
no pred. for MMV = no prediction for syntenty between *M. muntjak* and human was available by Zoo-FISH according to (Fronicke and Scherthan, 1997; Yang et al., 1997a).
not = no signal was observed.
+ = location of gene matches the predicted location for synteny of human and/or cattle.
(+) = location has been narrowed down and is most likely correct.
(+?) = if gene location on HSA is correct, the signal location meets expectation.
- = location of gene is not according to prediction from known syntenic regions of human or cattle.

Name of clone	Chr	Chr. band	Gene contained	Genebank accession	Length [bp]	Start in chr.	End in chr.	Type of clone	Source	Clone Library	Lit.
CTD-2505N20	4	4q21.3 - 4q22.1	*AF4*	BAC-ends: AQ261037, AQ260436	226665	88378826	88605490	BAC	ResGen	CalTech D	
CTD-2574C18	4	4q21.3 - 4q22.1	*AF4*	BAC-ends: AQ425688, AQ425691	150868	88382458	88533325	BAC	ResGen	CalTech D	
P1-24	4	4q21	part of *AF4*					PAC	PD		
RP3-431P23	6	6q27	5'part of *AF6*	AL009178.4	147962	167849762	167997724	PAC	BPRC	RPCI-3	
RP3-470B24	6	6q27	3'end of *AF6*	AL049698.3	87779	168048666	168136445	PAC	BPRC	RPCI-3	
RPCI-11-207M15	6	*(not 6q27)* see **		BAC-ends: AQ414980, AQ414977	175209	167971409	168146617	BAC	BPRC	RPCI-11	
CTD-2177K11	9	9p21.3	*AF9*	BAC-ends: AQ104578, AQ126854	132251	20345653	20477903	BAC	ResGen	CalTech D	
CTD-3005E18	9	9p21.3	*AF9*	BAC-ends: AQ092954, AQ092697	183419	20408435	20591853	BAC	ResGen	CalTech D	
RP11-652L8	11	11q23.3	5' of *MLL*	AP002962	160222	117293371	117453592	BAC	BPRC	RPCI -11	
RP11-832A4	11	11q23.3	5' of *MLL*	AP002800	215441	117485768	117701208	BAC	BPRC	RPCI -11	
RP11-215H18	11	11q23.3	5' of *MLL*	AP001582	90256	117485768	117785612	BAC	BPRC	RPCI -11	
RP11-770J1	11	11q23.3	entire *MLL*	AP001267	194310	117782930	117977248	BAC	ResGen	RPCI -11	
RP11-158I9	11	11q23.3	3' of *MLL*	AP004609	195409	118191354	119386762	BAC	BPRC	RPCI -11	
RP11-45N4	11	11q23.3	3' of *MLL*	BAC-ends: AQ202198, AQ202195	191928	118010991	118202920	BAC	BPRC	RPCI -11	
RP11-861M13	11	11q23.3	3' of *MLL*	AP000941	199321	117933138	118125584	BAC	BPRC	RPCI -11	
RP1-217A21	11	11q23.3	5' part of *MLL*		~160000			PAC	ES	RPCI-1	1
RP1-167K13	11	11q23.3	3' part of *MLL*		~130000			PAC	ES	RPCI-1	1
31471	19	19p13.3	*ENL*					BAC	MT	CITB	
RP11-819E16	19	19p13.3	*ENL*	BAC-ends: AQ664641, AQ756419	194133	6068907	6263040	BAC	BPRC	RPCI -11	
19468	19	19p13.11	*ELL*	AC005253	39760	18,517,547	18557306	PAC	MT	LLNL-R	
29473	19	19p13.11	*ELL*	AC005387	46213	18479945	18,526,157	PAC	MT	LLNL-R	
BAC cl.43	2	2q33-q24	*Caspase-8* and *-10*					BAC	JL		2
RP3-470B24	2	new: 2q35 **	n.n.					PAC	BPRC	RPCI-3	
RP11-53G6	2	2q35	no genes contained		221000	220994811	n.n.	BAC	PL	RPCI -11	
CTB-152G17	7	7q22	*SRPK2, MLL5*	AC005070	113032	104301840	104414872	BAC	MLB	CITB	
RP1-80K22	8	8q24.3	*MYC*	AF315312	149172	128,623,028	128772199	PAC	PL	RPCI -11	

Table 5: List of genes probes used in this thesis.
References: 1 = (von Bergh et al., 2001), 2 = (Inohara et al., 1997).
JL = Dr. Jill Lathi, St Jude's Hospital Hospital, Memphis, TN, USA; MLB = Dr. Michelle LeBeau, University of Chicago, IL, USA; PL = Dr. Peter Lichter, DKFZ-Heidelberg, Germany; ES = Dr. Ed Schuuring, University Hospital Groningen, The Netherlands; PD = Dr. Peter Domer; University of Chicago, IL, USA; PBRC = BACPAC Resources Center, Oakland, CA, USA; ResGen = Invitrogen Corporation, Carlsbad, CA, USA; MT = Dr. Mike Thriman, University of Chicago, IL, USA; n.n. = not known; ** = clone was reassigned.

Bos taurus (cattle) were received from Dr. J. Buitkamp (Technische Universität München). DNA was isolated by Dr. Stefan Lampel (DKFZ, Heidelberg; now Ingenium Pharmaceuticals, Munich) and was available for this work. A total of 52 BAC-clones containing additional genomic cattle sequences were received from Drs. André Eggen and Mathieu Gautier (INRA, France) in the form of isolated DNA or bacterial agar stabs. 31 genes were marker genes, referred to in the literature as the Texas markers, which were used

earlier to definitively assign the 31 bovine syntenic groups to cattle chromosomes (Gautier et al., 2001; Hayes et al., 2000). More than one clone was tested for 8 loci. Two clones contained unidentified BTA sequences. Additional cattle BAC-clones containing sequences homologous to human *MLL*, *AF4*, and *AF9* were screened by Dr. Gautier. Isolated DNA of the mouse clone BT-18S was received from Dr. Jens Eilbracht (DKFZ, Heidelberg). The clone contained part of the 18S rDNA sequence (Grummt et al., 1979).

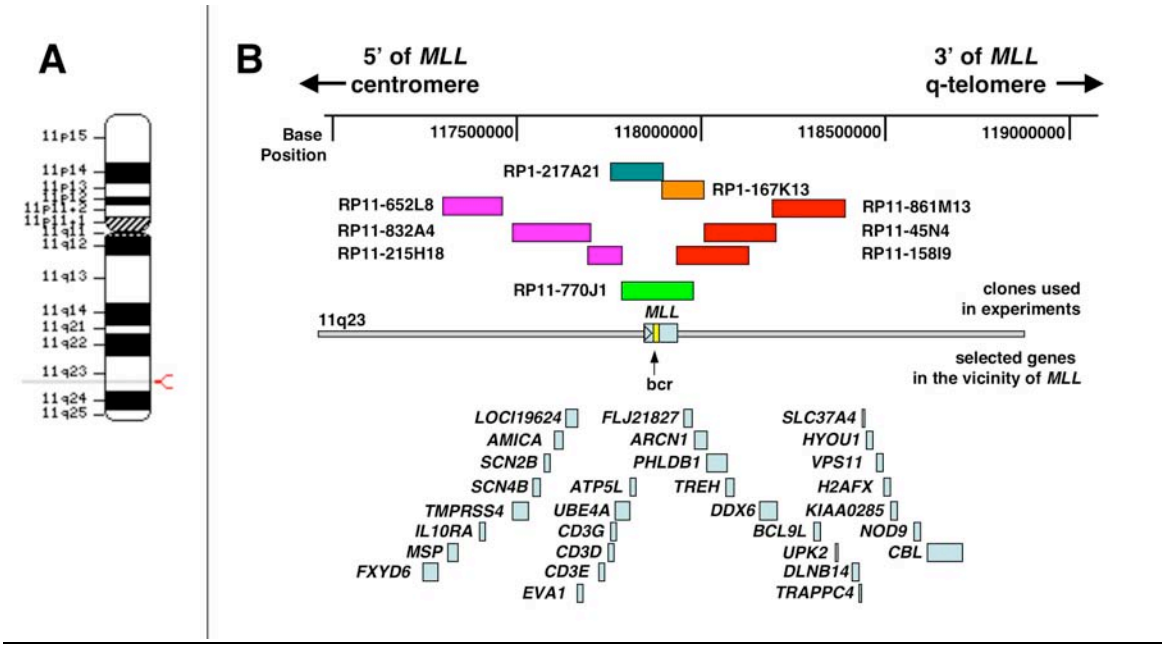

Figure 5: Localization of probes used to label chromosome 11q23 (*MLL*).

A: Ideogram of chromosome 11. A red marking indicates the position of the gene *MLL*. The ideogram was used as displayed on the website www.ncbi.nlm.nih.gov/mapview.

B: Alignment of the *MLL* gene, selected genes in its vicinity, and the genomic clones used in experiments in this thesis. The alignment was redrawn from a window display of the website http://genome.ucsc.edu//cgi-bin/hgTracks?position=chr11. Information on the location of the genes and clones was received from the Human Genome Browser Gateway freeze July 2003 (for details of the positions of the clones see Table 5).
Light blue boxes: Position of genes with their names next to the bars. The arrow head within the box of *MLL* indicates the transcriptional orientation of the gene.
Yellow box: Break point cluster region within the *MLL* gene.
Other colored boxes: Genomic clones used in various experiments. The color of a box reflects the color the clones as detected in FISH experiments and displayed in this thesis.

3.4.3.2. Bacterial clones for analysis of nuclear architecture in human cells

Human genomic BAC, PAC or cosmid clones were received from collaborating laboratories or purchased from BACPAC Resources Center (Children's Hospital, Oakland, CA) or Invitrogen. (for complete list of clones see **Table 5**, for the alignment of the clones see **Figures 5, 6, 7** and **8**).

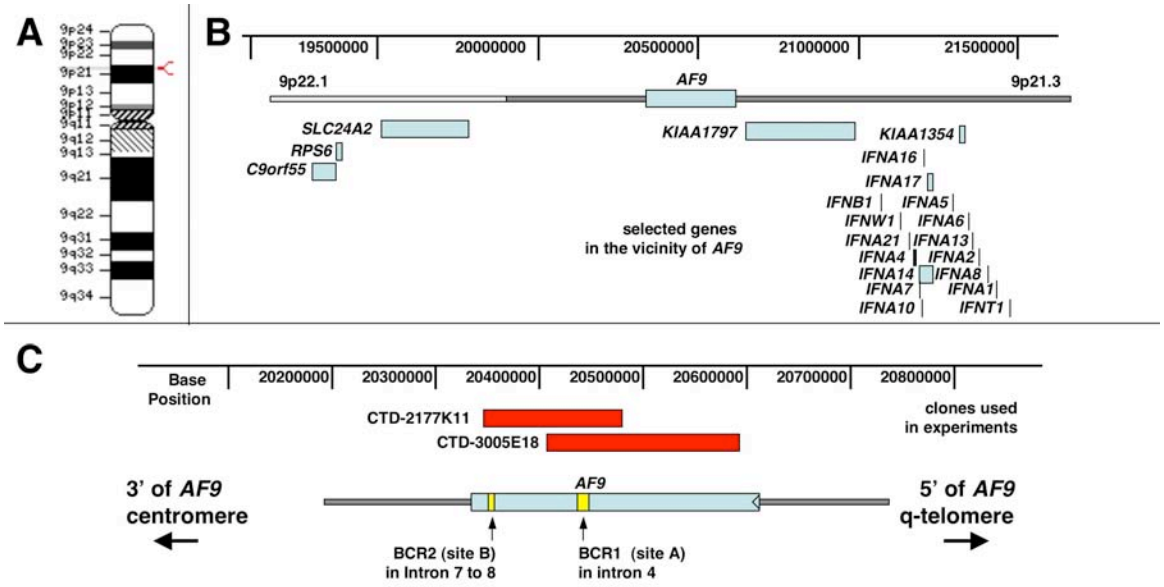

Figure 6: Localization of probes used to label chromosome 9p21.3 (*AF9*).

A: Ideogram of chromosome 9. A red marking indicates the position of the gene *AF9*. The ideogram was used as displayed on the website www.ncbi.nlm.nih.gov/mapview.

B: Alignment of the *AF9* gene and selected genes in the vicinity of chromosome 9p22.1 and 9p21.3.

C: Close up of the vicinity of *AF9* with the position of clones used in FISH experiments. The alignments in B and C were redrawn from window displays on the website http://genome.ucsc.edu//cgi-bin/hgTracks?position=chr9. Information on the location of the genes and clones was received from the Human Genome Browser Gateway freeze July 2003 (for details of the positions of the clones see Table 5).

Light blue boxes: Position of genes with their names next to the boxes. The arrow head within the bar of *AF9* indicates the transcriptional orientation of the gene.

Yellow box: Two break point cluster regions within the *AF9* gene.

Other colored boxes: Genomic clones used in various experiments. The color of a box reflects the color the clones as detected in FISH experiments and displayed in this thesis.

3.4.4. DNA material for production of whole chromosome painting probes

3.4.4.1 DOP-PCR products from flow sorted chromosomes for Chinese muntjac

Primary DOP-PCR products from flow sorted chromosomes of the Chinese muntjac were obtained from Dr. Fengtang Yang (Department of Clinical Veterinary Medicine, University of Cambridge, UK) and were used for the production of whole chromosome painting probes for Chinese muntjac.

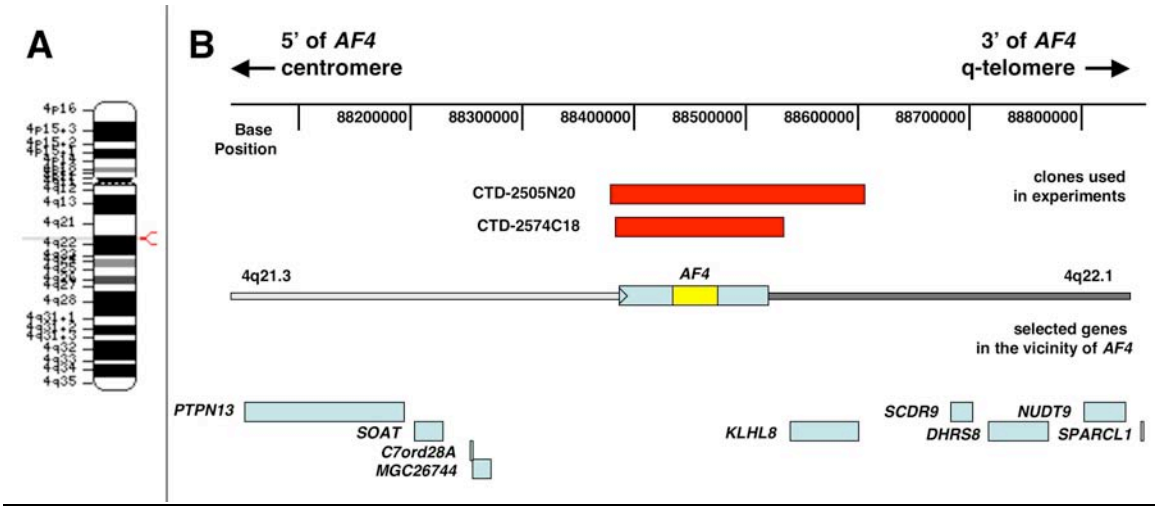

Figure 7: Localization of probes used to label chromosome 4q21.3-4q22.1 (*AF4*).

A: Ideogram of chromosome 4. A red marking indicates the position of the gene *AF4*. The ideogram was used as displayed on the website www.ncbi.nlm.nih.gov/mapview.

B: Alignment of the *AF4* gene, selected genes in its vicinity, and the genomic clones used in experiments of this thesis. The alignment was redrawn from a window display of the website http://genome.ucsc.edu//cgi-bin/hgTracks?position=chr4. Information on the location of the genes and clones was received from the Human Genome Browser Gateway freeze July 2003 (for details of the positions of the clones see Table 5).
Light blue boxes: Position of genes with their names next to the boxes. The arrow head within the box of *AF4* indicates the transcriptional orientation of the gene.
Yellow box: Break point cluster region within the *AF4* gene.
Other colored boxes: Genomic clones used in various experiments. The color of the box reflects the color the clones as detected in FISH experiments and displayed in this thesis.

3.4.4.2. Flow sorted chromosomes from male Indian muntjac

Flow sorted chromosomes of the male Indian muntjac were kindly provided by Dr. Nigel Carter (Wellcome Trust Sanger Institute, Molecular Genetics, Cambridge, UK). Flow sorting was done with a FACStar Plus (Becton Dickinson Immunocytometry Systems, UK) according to Carter et al (1990) (Carter et al., 1990). 500 chromosomes were collected per peak in 30 µl sterile ddH_2O in a PCR reaction tube. The tubes were shipped on dry ice. Upon receipt, the tubes were stored at -80°C until use.

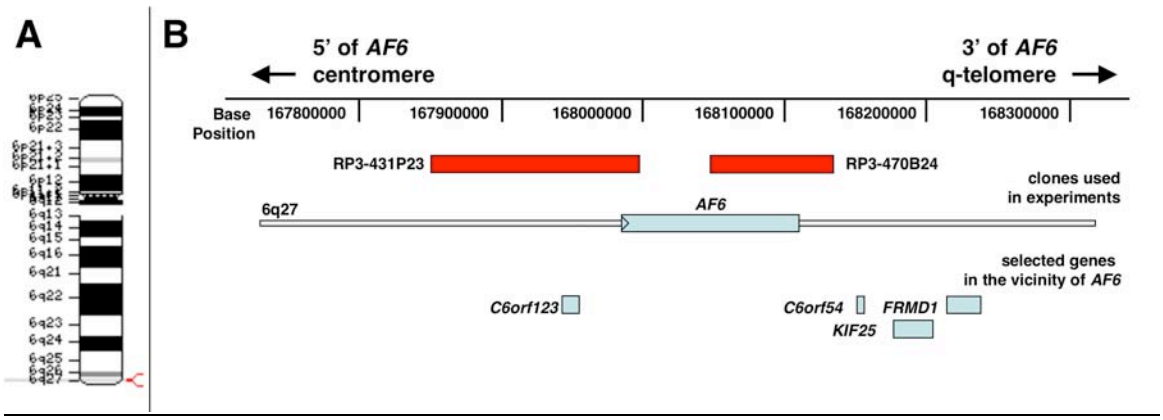

Figure 8: Localization of probes used to label chromosome 6q27 (*AF6*).

A: Ideogram of chromosome 6. A red marking indicates the position of the gene *AF6*. The ideogram was used as displayed on the website www.ncbi.nlm.nih.gov/mapview.

B: Alignment of the *AF4* gene, selected genes in its vicinity, and the genomic clones used in experiments of this thesis. The alignment was redrawn from a window display of the website http://genome.ucsc.edu//cgi-bin/hgTracks?position=chr6. Information on the location of the genes and clones was received from the Human Genome Browser Gateway freeze July 2003 (for details of the positions of the clones see Table 5).
Light blue boxes: Position of genes with their names next to the boxes. The arrow head with in the box of *AF6* indicates the transcriptional orientation of the gene.
Other colored boxes: Genomic clones used in various experiments. The color of the bar reflects the color the clones as detected in FISH experiments and displayed in this thesis.

3.5. Primary antibodies and conjugated reagents

Antibodies were used for immunofluorescence to visualize surface antigens or in FISH experiments for the detection of labelled nucleotides.

Primary antibodies	Antigen	Type	Origin	Used dilution	Received from	Stock conz
Streptavidin-FITC	biotin			1:100 (m-FISH), 1:300 (3D-FISH)	Vector labs	0.4 mg/ml
Streptavidin-Cy3	biotin			1:100 (m-FISH), 1:300 (3D-FISH)	Jackson	1.8 mg.ml
Streptavidin-Cy5	biotin			1:100 (m-FISH), 1:300 (3D-FISH)	Jackson	1.7 mg/ml
Mouse-anti-digoxigenin-fitc	digoxigenin	monoclonal	mouse	1:100	Jackson	1.7mg/ml
Mouse-anti-digoxigenin-Cy3	digoxigenin	monoclonal	mouse	1:100	Jackson	1.7mg/ml
Mouse-anti-digoxigenin-Cy5	digoxigenin	monoclonal	mouse	1:100	Jackson	1.7mg/ml
sheep-anti-digoxigenin-FITC	digoxigenin	IgG F(ab')2	sheep	1:100	Roche	0.4 mg/ml
Rabbit-anti-dinitrophenyl	dinitrophenol	whole antiser.	rabbit	1:200	Sigma	1.2 mg/ml
Rabbit-anti-estradiol rhodamine	estradiol	IgG	rabbit	1:200	Roche *	400 µg/ml
Rabbit-anti-Estradiol	estradiol	IgG	rabbit	1:200	Roche *	400 µg/ml
mouse IgG1	unspecific	FITC	mouse	20 ul per test	Bec.Dikins.	50µg/ml
anti CD33	human CD33	PE	mouse	20 ul per test	Bec.Dikins.	20µl/test
anti CD34	human CD34	FITC	mouse	20 ul per test	Bec.Dikins.	20µl/test

3.5.2. Secondary antibodies

Secondary antibodies	Antigen	Type	Origin	Used dilution	Received from	Stock conz
Goat-anti-rabbit-FITC	rabbit	IgG F(ab')2	goat	1:200	Jackson	1 mg/ml
Goat-anti-rabbit-cy3	rabbit	IgG F(ab')2	goat	1:200	Jackson	1 mg/ml
Goat-anti-rabbit-cy3	rabbit	IgG (H+L)	goat	1:200	Amersham	1 mg/ml
Goat-anti-rabbit-cy5	rabbit	IgG F(ab')2	goat	1:200	Jackson	1.5 mg/ml
Biotinylated goat-anti-streptavidin	streptavidin		goat	1:1000	Vector labs	1 mg/ml
Donkey-anti-rabbit-cy3	rabbit	IgG F(ab')2	donkey	1:500	Jackson	1.5 mg/ml
Donkey-anti-rabbit-fitc	rabbit	IgG F(ab')2	doneky	1:500	Jackson	1.5 mg/ml
Donkey-anti-mouse-cy3	mouse	IgG (H+L)	donkey	1:500	Jackson	1.4 mg/ml
Donkey-anti-goat-cy5	goat	IgG F(ab')2	donkey	1:500	Jackson	0.3 mg
Donkey-anti-sheep-fitc	sheep	IgG F(ab')2	rabbit	1:500	Jackson	0.3 mg

3.6. Chemicals and enzymes

Chemicals, if not specifically listed, were purchased from Sigma and Fisher Scientific in ACS grade quality. Additional material that was not specifically listed was purchased from Fisher Scientific.

3.6.1. Antibiotics

Antibiotics were purchased from Sigma or Invitrogen. Ampicillin, kanamycin and chloramphenicol were used to grow bacterial clones selectively. Penicilin/streptamycin solution was used for tissue culture.

3.6.2. Enzymes

Enzymes used in different techniques in this thesis:

Technique	Enzyme	Supplier
PCR	Takara Taq	Fisher Scientific
DOP-PCR, PCR	AmpliTaq DNA polymerase	Roche
Nick translation	DNase I, RNase-free	Roche
Nick translation	DNA Polymerase I	New England BioLabs
Cot-1 preparation	Nuclease S1 (1400 U/μl)	Roche

3.6.3. DNA size and concentration markers

1-Kb DNA Ladder (Invitrogen) was used as a DNA size marker to determine the size of a nick-translation reaction of a PCR product. This DNA ladder yields the following discrete fragments (sizes in base pairs): 12216, 11198, 10180, 9161, 8144, 7126, 6108, 5090, 4072, 3052, 2036, 1636, 1018, 517, 506, 396, 344, 298, 220, 201, 154, 134, 75. Alternatively 1-Kb Plus DNA Ladder (Invitrogen) was used. The DNA ladder consists of 12 bands: 12000, 5000, 2000, 1650, 1000, 850, 650, 500, 400, 300, 200, 100 bp. Other ladders were used, when small DNA fragments between 10 and 500 bp were expected in a PCR reaction: 10 bp DNA Ladder (Invitrogen). This DNA ladder consists of 33 ten-base pair repeats between 10 to 330 bp. 25 bp DNA Ladder (Invitrogen). The DNA ladder consists of 19 twenty five-base pair repeats between 25 to 500 bp. Usually 1 volume of the ladder was mixed with 1 volume of 6x loading buffer and 1 volume of water. MassRuler DNA Ladder-mix, ready-to-use (Fermentas Inc**.,** Hanover, MD) with following 20 discrete fragments: 10000, 8000, 6000, 5000, 4000, 3000, 2500, 2000, 1500, 1031, 900, 800, 700, 600, 500, 400, 300, 200, 100, 80 bp. By loading 10 μl, these bands contains the following amount of DNA (in ng): 100, 80, 60, 50, 40, 30, 25, 20, 16, 100, 90, 80, 70, 60, 100, 40, 30, 20, 10, 8.

3.6.4. Cell culture material

The following components for tissue culture work were purchased from Invitrogen:

RPMI 1640

DMEM

Iscoves modified Dulbecco's medium = IMEM

Fetal bovine serum = FBS

Penicillin/Streptomycin

Sodium pyruvate

Trypsin EDTA

KaryoMAX colcemid in PBS

For the cattle cell line, CCL44, complete growth medium and FBS tested for this cell line was purchased from ATCC (Manassas, VA).

Plastic ware for tissue culture work was purchase from Fisher Laboratories or Continental Laboratory Products (San Diego, CA): Aerosol barrier tips for 10, 20, 200 and 1000 µl. 1, 2, 5, 10, 25 and 50 ml Falcon-pipettes as well as Corning Tissue culture vented flasks small (T-25), and large (T-75) or Petri dishes (100 mm x 20 mm) suitable for tissue culture.

3.6.5. Other chemicals and materials

1.5 ml and 2.0 Eppendorf tubes (Fisher Scientific)

1.5 Nunc CryoTube*TM* vials for bacterial glycerol stocks (Nalge Nunc International, Rochester, NY)

15 ml and 50 Falcon tubes (Fisher Scientific)

Bio Gard Hook (Baker Company Inc. through DAI Scientific Equipment, Inc. Libertyville, IL)

Buffer saturated phenol pH 7.5 = phenol/TE (Invitrogen)

Chloroform (Fisher Scientific)

DMSO = Dimethyl sulfoxide (Sigma)

Ethanol, 200 and 100 proof (AAPER Alcohol and Chemical Co., Shelbyville, KY 40066-0339)

Formamide, ultra grade deionized (Midwest Scientific, St. Louis, MO)

Fyrite to monitor CO_2 content of tissue culture incubator (Bacharach Inc., Pittsburgh, PA)

Glycerol (Sigma)

Glycogen (Sigma)

Isopropanol (Sigma)

Latex gloves (Kimberly-Clark Corporation, Neenah, WI)

Liquid nitrogen and CO_2 (BOC Group Inc., Murray Hill, NJ)

Marabu Fixogum Rubbercement (Marabuwerke GmbH & Co., Tamm)

Metal block to hold Eppendorf tubes cold on ice (Marsh Biomedical Products Inc., Rochester, NY)

Mineral oil (Applied Biosystems, Foster City, CA)

Nalgene filter unit 150-250 ml, 500 – 1000 ml (Nalgene Nunc International)

Nocodazole =Methyl[5-(2-thienylcarbonyl)-1H-benzimidazol-2-yl]carbamate (Sigma)

Paraformaldehyde (Sigma)

Press to seal silicon isolator, one well 20 mm diameter, 1.0 mm deep (Molecular Probes)

Racks to hold Eppendorf tubes, 15 or 50-ml Falcon tubes (Fisher Scientific)

Round bottom tubes for bacterial growth (Fisher Scientific)

Sephadex G-50 raisin (Amersham Biosciences, New Jersey, NJ)

Scalpel

Superfrost slides in various colors (Fisher Scientific)

Slides coated with poly-L-lysine (Sigma)

Triton X-100 (Sigma)

Tween-20 (Bio-Rad Laboratories)

Vectarshield® mounting medium for fluorescence microscopy with or without DAPI (Vector laboratories, Burlingame, CA)

Water tissue culture grade (Biofluids Inc., Rockville MD)

Whole serum from donkey or goat (Vector laboratories)

Wooden toothpicks (PGC Scientific)

3.7. Kits

QIAGEN Plasmid purification midi and maxi kit (Qiagen, Valencia, CA)
QIAquick PCR purification kit (Qiagen)

3.8. Instruments

3.8.1. Flow sorting instruments

Flow sorting was performed at the flow cytometry facility of the University of Chicago, Flow sorting to analyze the cell cycle or the fragmentation of the nuclei was performed on a BD FACScan, Excitation source: 488 nm Argon-Ion laser. Software to run the machine: Cell Quest Software. Flow sorting to analyze dual labelled cells was performed on a BD LSR-II flow sorter (3 excitation sources: 325 HeCd Laser, 488 Sapphire OPSL, 633 nm HeNe, powered by FACSDiVa software). Flow sorting of chromosomes was performed on a DakoCytomation MoFlo-HTS instrument, which had 3 excitation sources available (coherent I90-5 tuned to 457,488 or 513, coherent I90-5K tuned to UV or violet, 633 nm HeNe laser).

3.8.2. Microscopes, Objectives and related instruments

3.8.2.1. Light microscopes

Light microscope to inspect cells in tissue culture flasks:
Axiovert 25 from Zeiss with the following Zeiss-objectives:
CP-Achromat 5x /0.12, °°/-, CP-Achromat 10x /0.25, °°/-, LD-Achrostigmat 20x /0.30, °°/0-2, and LD-Achrostigmat 32x /0.44, °°/0.5-1.5.

Light microscope to count cells in the tissue culture:
Merz Optical Instrument with a 1.25x ocular and following Zeiss objectives:
Neofluar 10x /0.30, 160/-, Neofluar 16x /0.40, 160/-, Neofluar 25x /0.45, 160/0.17, Neofluar 40x /0.65, 160/0.17, and Neofluar 63x /0.80, 160/0.17.

Light microscope to inspect metaphase cells:

Upright Zeiss microscope with following Zeiss objectives:

Neofluar 25x /0.60, 160/0.17, and Neofluar 40x /0.75, 160/0.17.

3.8.2.2. Fluorescence microscope and material for evaluation of regular 2D-FISH

Fluorescence microscope Axioplan from Zeiss was used with the following Zeiss-objectives and filter blocks: Plan Apochromat 100x, 1.4 oil, Plan Neofluar 63x, 1.25 oil, Plan Neofluar 40x, 1.30 oil, Plan Neofluar, 25x, 0.80 imm corr °°/-, Plan Neofluar, 16x, 0.50 imm with filter blocks specific for DAPI, FITC, FITC/Red-dualcolor, CY3, CY5 were purchased from Sullivan and Kelly (Darien, IL). Results of the FISH analysis were documented by photographs, using the CCD camera system Model SenSys Series 200 from Photometrics LTD (Tucson, AZ), and IPLab software, to capture the images, and to export them in tiff format.

3.8.2.3. Fluorescence microscope and material for 2D-FISH during analysis of position of genes relative to chromosome territory surface

The Zeiss Axovert 200M Inverted microscope was used when the position of the genes relative to the territory surface was analyzed, providing the advantage of motor controlled filter movement to avoid shift between the different channels. For the other microscope, the filters had to be moved manually resulting in potential shifts between the channels, which were manually corrected for within the computer program Adobe Photoshop 6.0.1. The following objectives and optical filters were used: 100x Plan Apochromat 1.4na oil, 63x Plan Apochromat 1.4na oil, 40x Plan Neofluar 1.3na oil, 20x Neofluar 0.5na, and Filter blocks for DAPI (360nm X/ 400nm BS /460nm M), FITC (480/505/535), Cy5 (620/660/700), and Texas Red (560/595/645). The results of the FISH analysis were documented by photographs, using the CCD camera system Hammatsu Orca ER, which was operated by the software Improvision's Openlab version 3.17. The program was also used for image processing (deconvolution).

3.8.3. Additional instruments

Centrifuges:

Eppendorf table top centrifuge 5415 D and 54952 C (Brinkmann Instruments Inc., Westbury, NY)

Sorvall RC50 Plus with rotors SLA1500 (VWR International, Batavia, IL)

Sorvall RT6000B refrigerated centrifuge (VWR International)

Sorvall GLC – 2B general laboratory centrifuge (with no cooling capability), (VWR International)

Sorvall GLC-4 General Laboratory centrifuge (VWR International)

Gel electrophoresis chamber:

Power supplies BioRad Power PAC 300 (Bio-Rad laboratories, Hercules, CA)

Gel electrophoresis chamber (Bio-Rad)

Crosslinker UV-Stratalinker 2400 (Stratagene, La Jolla, CA)

Fridges and freezers:

Cryostorage System K Series with liquid nitrogen (Taylor-Wharton-Cryogenics, Theodore, AL)

Freezer -80°C (Midwest Laboratory Services)

Traulsen 4°C (Pierce Equimpent Company, Countryside, IL)

Ice machine (Cornelius commercial ice system)

PCR-machines:

For the primary DOP-PCR reaction: GeneAmp PCR System 9600 from PerkinElmer.

For all other PCR reactions: Gene Amp PCR system 9700 from PerkinElmer.

Additional Instruments

Autoclave AMSCO 2021 Eagle Series

Beckman Φ40 pH Meter (Beckman Coulter, Inc., Fullerton, CA)

CO_2 incubator for tissue culture Model 6300 (NAPCO)

Cooled water bath Microcooler Model 260011 (Broekel Industries, Inc. through Fisher Scientific)

Dual-Intensity UV-transilluminator (UVP Inc., Upland, CA)

Drummond pipettor (for tissue culture) from Drummond Scientific Co.

Dry type bacteriological incubator (Lindberg/Blue M, Asheville, NC)

Gilson pipettors for 10, 20, 200, and 1000 µl volumes

Heating block Model 111002F (Fisher Scientific)

Hood for tissue culture work Model Hoodgard (Lab Safety Corporation, Chicago, IL)

Incubator Fisher Isotemp Oven 100 Series Model 106G (Fisher Scientific)

Kodak digital Sciences: Electrophoresis documentation and analysis system 120. with Software Kodak 1D3.0 (NEN™ Life Science Products, Inc. Boston, MA)

Lab-Line L-C incubator (Barnstead/Thermolyne, Dubuque, IA)

Laboratory counter (Clay-Adams Inc., New York, NY)

Labquake Shaker/Rotisserie Model No 400110 (Branstead/Thermolyne)

Mettler Balance Model PC2200 (Mettler Instrument Corp., Hightstown, NJ)

Model A160 Denver Instrument company (C&M Scale Company, Forest Park, IL)

Orbital Shaker (Forma Scientific Inc., Marietta, OH)

Slide warmer (Lab-Line Instruments Inc.)

Sonicator Model # 2000 (B. Brown Biotech, Inc., Dubuque, Iowa)

Spectrophotometer DU530 UV/Vis with single cell module and 50 µl volume quarzcuvette (Beckman Coulter, Inc. Fullerton, CA)

Thermo Savant DNA Speed Vac DNA120 (Savant Instruments, Holbrook, NY)

Oncor Template Tamer with White & UV Light (Oncor)

Fisher Vortex Genie (Fisher Scientific)

Vortexer Maxi Mix II (Branstead/Thermolyne)

Water bath (Lindberg/Blue M)

3.9. Computer programs

3.9.1. Macintosh compatible programs:

AngleX (created by Johannes M. Peter and Andrea Murmann for angle presentation)

Adobe Acrobat 5.0

Adobe Photoshop 7.0 (image processing)

CA-Cricket Graph III (Graphical presentation)

Fetch 4.0.3 (Transfer of data files between University of Chicago and DKFZ Heidelberg)

IPlab 3.6.4 (for FISH-experiment documentation)

Kodak 1D3.0 (Gel photography)

Laser Gene 3.0 (Primer design)

LCS 2.5v1347 (Confocal microscopy)

MacVector 6.5.3 (Primer design)

Microsoft Excel (Calculation and statistics)

Microsoft PowerPoint

Microsoft Word

Openlab (for 4 color FISH documentation and processing)

3.9.2. PC compatible programs:

Amira 3.1 (processing of confocal image stacks and 3D rendering)

3D computational tools (created by Juntao Gao, in part during the collaboration with Andrea Murmann. For more details, see Results).

3.10. Electronic sources

3.10.1. Photographs and images from online sources

Photographs of the muntjacs in Figure 2 were downloaded from the internet:

Indian muntjac: http://www.ultimateungulate.com/, webmaster@ultimateungulate.com

Permission to use these images in the thesis was received from Brent Huffman.

Chinese muntjac: www.bds.org.uk/species/ muntjacdeer.html -or-

http://www.chantec5.co.uk/animaluk/articles/deer/deer1.html. The image was taken by BeryI Buckingham. The left image in Figure 3 giving an overview on the translocation partners of the gene *MLL* was taken from the online source Atlas of Genetics and Cytogenetics in Oncology and Haematology. URL http://www.infobiogen.fr/services/chromcancer.

3.10.2. Database searched for DNA clones and sequences

BAC clones were searched, using the UCSC Genome Browser (http://genome.ucsc.edu/cgi-bin/hgGateway). Sequences for genes or BAC clones were obtained, using NCBI Web pages (http://www.ncbi.nlm.nih.gov/).

3.10.3. Database used for gene density analysis

The NCBI MapViewer (http://www.ncbi.nlm.nih.gov/mapview/map_search.cgi) was used for the analysis of the gene density of chromosomes and sub chromosomal regions.

3.10.4. Online-source with information about signal enhancement techniques and definition of median filter

http://rkb.home.cern.ch/rkb/AN16pp/node168.html
http://www.cee.hw.ac.uk/hipr/html/median.html

3.11. Buffers and solutions

Analytical quality chemicals used for the production of the buffers and solutions were purchases from Sigma or Gibco, unless otherwise noted (see material list for companies). For the preparation for all solutions, deionized and triple-distilled water was used. All glass- and plastic-ware was sterilized prior to preparation of all the components.

1 x PBS (pH 7.4): 2.7 mM KCl, 1.7 mM KH_2PO_4, 137 mM NaCl, 10 mM Na_2HPO_4

DNA extraction buffer (10 mM Tris-HCl pH 8.0 / 100 mM Na_2EDTA / 20 µg/ml RNase from pancreas (DNase free), 0.5% SDS)

Proteinase K-stock solution (20 mg/ml, stored in aliquots at -20°C)

3M NaAcetate, pH 5.2

TE-buffer (10 mM Tris pH8, 0.1mM EDTA pH8.0)

1/10 TE was prepared by diluting 1 part of TE-buffer with 9 parts of sterile water 1:10

Lysis buffer (20 mM Tris-HCl pH 8.0 / 1% SDS)

0.5M EDTA, pH 7.0

7.5M NH_4Acetate

Chloroform / isoamyl alcohol (24 / 1)

24 parts of chloroform were mixed with 1 part of isoamyl alcohol

Phenol / chloroform / isoamyl alcohol (25 / 24 / 1)

25 parts of phenol were mixed with 24 parts of chloroform and one part of isoamyl alcohol

Chloroform / isoamyl alcohol (24 / 1)

24 parts of phenol were mixed with 1 part of isoamyl alcohol

70%, 80% and 90% ethanol

Diluted ethanol solutions were prepared by diluting 100 proof ethanol (= 95% concentrated ethanol) with appropriate amount of sterilized water.

5M NaCl

10 X TBE electrophoresis buffer

108 g Tris Base, 55g Boric Acid, 20 ml 0.5M EDTA were diluted in 1 liter of deionized water. After autoclaving, the solution was stored at room temperature. 1 x TBE was diluted 10-fold with water and was used as running buffer for agarose-gel electrophoresis.

6 x loading dye solution (0.09% bromophenol blue, 60% glycerol and 60 mM EDTA)

LB-medium for bacterial growth

1% of bacto-tryptone, 0.5% of bacto-yeast extract, and 1% of NaCl were added to one litre of deionized water. The solution was autoclaved for 20 min at 15 lb per square inch

on the liquid cycle setting. The pH adjustment with NaOH was omitted, because it remained between pH 7.0 and 7.2.

LB-plates for bacterial growth

For the preparation of 10 LB-plates, 4.5 g of bacteriological agar (Sigma, A-5306) were added to 300 ml LB-medium, autoclaved for 20 min at 15 lb/sq.in. on liquid cycle and cooled down to 50°C in a water bath. At this temperature, components that were not thermo stable (e.g. antibiotics) were added and mixed. After cooling down to hand warm (~40°C), Petri dishes were filled with the still liquid solution, on a level surface that was wiped down with 70% ethanol. The lids of the filled Petri dishes were put on to cover only part of the plate to allow evaporation of excess liquid. After solidifying and cooling down, the plates were stored at 4°C until they were used.

P1 = resuspension buffer (filter sterilized, stored at room temperature*): 50 mM Tris, pH 8.0, 10 mM EDTA.

*After adding 100 µg/ml RNase A, the solution was kept on ice.

P2 = lysis buffer (filter sterilized, stored at room temperature): 0.2N NaOH, 1% SDS. This buffer was mixed freshly before every preparation for the best results.

P3 = neutralization buffer (autoclaved, stored at 4°C): 3M KOAc, pH 5.5.

Antibiotics

The antibiotics were added to LB-medium or plates to selectively grow various bacterial clones received for this work. Ampicillin was solved in water for a 50 mg/ml stock concentration. For kanamycin, a 25 mg/ml stock solution in water was produced. Chloramphenicol was solved in 100% ethanol to a concentration of 34 mg/ml. All stock solutions were aliquotted in 1.5 ml Eppendorf tubes and stored at –20°C. Ampicillin and kanamycin were used for cosmid and PAC-clones at a working concentration of 50 µg/ml, Chlorampenicol for BAC-clones at a working concentration of 12.5 or 20 µg/ml.

Freezing medium: 10% sterile DMSO, 20% FBS, 70% complete medium (specific for each cell line) mixed freshly and put on ice prior to use.

1M Thymidine stock solution (stored in aliquots at -20°C)

Solution A EGTA (stored at 4°C)

3.8 g EGTA (anhydrous, MW 380.4, Sigma #E-4378) was dissolved in 2 liters of water. While the solution was stirring pellet of NaOH were added to dissolve the EGTA. When the EGTA was not in solution after 15 min, one pellet of NaOH was added every 5-10 min until EGTA was finally dissolved.

Solution B EDTA (stored at 4°C)

119.28 g KCl, 47.28 g Tris-HCl, anhydrous, MW 157.6 Sigma #T-3253, 23.38 g NaCl and 15.21 g EDTA, (anhydrous, MW 380.2, Sigma #ED4SS) were dissolve in 1 liter water.

Spermine stock solution : 13.93 g spermine tetrahydrochloride was dissolved in 100 ml water (Behring Diagnostics Inc.). Aliquots of 2 ml were stored at -20°C.

Spermidine stock solution: 25.46 g spermidine trihydrochloride was dissolved in 100 ml water (Behring Diagnostics Inc.). Aliquots of 2 ml were stored at -20°C.

Polyamine sheath suffer for flow sorting chromosomes (according to (Fawcett et al., 1994)). 4 liters of polyamine sheath buffer was required for each flow sorting session. To make 4 liters of sheath solution 400 ml solution A (EGTA) and 200 ml solution B (EDTA) were added to 3.4 liters of water. The pH was adjusted 7.2, using concentrated solutions of HCl or NaOH. The sheath buffer was filter sterilized, and finally 2 ml each of spermine and spermidine stock solutions were added. The sheath buffer had to be degassed prior to the cooling down, and using in the MoFlow flow sorter. The degasation was done with a water vapour pump. Omitting the degasation resulted into air bubbles clogging the tubes and preventing the flow sorting procedure.

Nocodazole stock solution

Nocodazole was dissolved in DMSO to a stock solution 1 mg/ml = 3.319 mM stock solution, which was store at -20°C. Before use, the stock solution was thawed and diluted 1:20 with sterile DMSO to an end concentration of 0.2 µM.

Colcemid

KaryoMax colcemid solution 10 µg/ml was diluted with sterile water to 5 µg/ml and stored at 4°C. Used end concentration 0.01 to 0.5 µg/ml.

Hypotonic buffer for chromosome isolation for flow sorting:

75 mM KCl, 0.2 mM Serine, 0.5mM spermidine

Various ethanol concentrations (100% ethanol, 90%, 70%)

Diluted Ethanol prepared with ddH_2O

Polyamine buffer for chromosome isolation for flow sorting:

15 mM Tris(hydroxymethyl)methylamine, pH 7.4, 0.2 mM spermine, 0.5mM spermidine, 2 mM EDTA, 0.5 mM EGTA, 80 mM KCl, 20 mM NaCl, 14 mM β-mercaptoethanol, 0.25% Triton X-100

1 M $MgSO_4$ the solution was filter sterilized.

1 M Chromomycin A3 staining solution

Chromomycin A3 powder was dissolved in a few drops of methanol to facilitate solubility. Then it was diluted with Mac Ilvaine's working solution to a concentration of 1M. The chromosomes were stained with an end concentration of 40 µg/ml Chromomycin A3.

Mac Ilvaine's buffer

Mac Ilvaine's buffer was prepared from two stock solutions 164.7 ml 0.2 M Na_2HPO_4 (Sigma S-3397) and 35.2 ml 0.2 mM sodium citrate were mixed. The pH was adjusted to 7.0 with HCl or NaOH.

Hoechst 33258-staining solution (2 mg/ml Hoechst 33258 (bis-benzimide))

The powder was dissolved in sterilized water.

1M NaSulphite (the solution was filter sterilized)

1 M NaCitrate (the solution was filter sterilized)

50 mM Etoposide - VP16 (Sigma E-1383, 25 mg, stored at RT)

The powder was solubilized in sterile DMSO. Aliquots were stored at –20°C.

Fixative for 2D or metaphase spread preparation (MAA = methanol / acetic acid = 3) :

3 parts of methanol were mixed with 1 part of acetic acid the same day it was used.

Hypotonic KCl solution for metaphase chromosomes:

0.075 M KCl was prepared freshly every week.

PI-staining solution

(500 μg/ml propidium iodide in 3.8 x 10^{-2} M sodium citrate, pH 7.0)

RNase stock solution

RNase powder was resuspended in 10 mM Tris-HCl, pH7.5 to a concentration of 10 mg/ml, incubated for 30 minutes in boiling water, aliquotted, and stored at -20°C.

Hypotonic fluorochrome solution for the analysis of DNA fragmentation

(50 μg/ml propidium iodide in 0.1% sodium citrate, 0.1% (v/v) Trion X-100)

4% PFA 1 x PBS

4 g paraformaldehyde was mixed with 100 ml 1 x PBS. It was placed into 60°C water bath, since und occasional shaking until the solution was clear. The solution was used either directly after cooling down, or it was frozen in 50 ml aliquots and stored at -20°C. The addition of NaOH, and later readjusting of the pH to 7.0 was only necessary if the solution did not clear up on its own, after approximately 3 h in the water bath.

0.5% (w/v) Saponin, 0.5% (v/v) Triton X-100, 1 x PBS-solution:

1 g of Saponin and 1 ml of Triton X-100 were added to 100 ml PBS. The solution was mixed until the substances dissolved and the solution looked clear.

20% glycerol, 1 x PBS: 20 ml Glycerol were mixed with 80 ml 1 x PBS.

10 x deoxynucleotide-mix

0.5 mM dATP, 0.5 mM dCTP, 0.5 mM dGTP and a mix of 0.5 mM nucleotide mix of the hapten-conjugated dUTP and dTTP. The ratio varied with the labeled:

0.4 mM biotin-16-dUTP / 0.1 mM dTTP

0.4 mM DNP-11-dUTP / 0.1 mM dTTP

0.125 mM digoxigenin-11-dUTP / 0.375 mM dTTP

DNase I stock solution (3 mg/ml in 0.6 M NaCl and 50% glycerol)

The stock solution was stored at -20°C. The DNase-working solution for nick translation was mixed with ice cold ddH_2O.

0.1 M 2-mercaptoethanol solution

10% SDS (10 g of SDS powder was mixed in 100 ml of sterile ddH_2O)

Gel filtration buffer (10 mM Tris/HCl (pH 8.0), 1mM EDTA und 0.1% w/v SDS)

Sephadex G-50 raisin as matrix for the gel filtration columns:

30 g Sephadex G-50 medium™ (Pharmacia Biotech) were added to 300 ml gel filtration buffer and autoclaved.

Sheared salmon sperm-DNA

After DNA was dissolved in water to 1 mg/ml and sheared with a 1 ml syringe and 18gauge needle (Becton Dickinson), it was aliquotted and stored at -20°C.

Hybridization buffer

4 x SSC, 20% dextransulfat-disodium salt

After mixing components, the solution was heated up on a heating block to 50°C and stirred, aliquotted and store at -20°C.

20 x SSC-stock solution

175.3 g of NaCl and 88.2 g of sodium citrate were dissolved in a final volume of 1 liter ddH_2O. The pH was adjusted to 7.0 with a few drops of 1M HCl. The solution was sterilized by autoclaving. To produce less concentrated SSC solutions (such as 1 x, 2 x, 4 x SSC) the stock solution was diluted with ddH_2O.

Denaturation buffer A: 70% formamide, 2 x SSC, pH 7.0

The buffer was prepared freshly with deionized formamide. The solution was heated up to 73°C.

Equilibrations buffer for 3D fixation of cells

70% formamide, 2 x SSC, pH 7.0

The buffer was prepared freshly with deionized formamide. The solution was heated up to 73°C.

Washing buffer A (50% (v/v) formamide in 2 x SSC (pH 7.0).

The solution was heated up to 42°C prior to use.

Washing buffer B

The concentration of the buffer depended on the needed stringency. A range of 2 x SSC to 4 x SSC (pH 7.0) was used. Usually 4 x SSC was used when signals on muntjac and 1 x SSC when human probes were detected. The solution was heated up to 42°C prior to use.

Blocking solution for FISH (4% (w/v) BSA in 4 x SSC)

Blocking solution for 3D (4% (w/v) BSA in 4 x SSC + 10% whole serum

Detection solution (1% (w/v) BSA, 0.1% (v/v) Tween 20 in 4 x SSC)

Washing buffer C (0.1% (v/v) Tween 20 in 4 x SSC)

The solution was heated up to 42°C prior to use.

DAPI-solution (200 µg/ml stock)

5 mg were solved in 25 ml of 2 x SSC and mixed well, aliquotted and stored at -20°C. To prepare the staining solution the 40 µl of the stock solution diluted in 50 ml 2 x SSC and filtered twice over a 0.2 µm filter into a Coplin jar and store 4°C in the dark. The staining solution was good for about a month.

4. METHODS

4.1. DNA techniques

Genomic DNA was isolated, using a modified protocol from Current Protocols in Molecular Biology (1998), unit 2.2.1-2.2.3.

4.1.1. Isolation of genomic DNA from animal tissue

10 g of freshly isolated roe deer spleen, was cut in small pieces and transferred into a 50 ml Falcon tube. 30 ml DNA extraction buffer was added. The mixture was incubated for 1 h at 37°C. Proteinase K was added to a final concentration of 0.1 mg/ml. The solution was incubated for 1 day at 45°C under constant shaking. An equal volume of buffer saturated phenol (phenol/TE) was added and incubated for 1 h while rotating followed by centrifugation at 2000 g for 45 min at 10 °C. The upper phase was transferred to a new tube. The phenol/TE step was repeated twice. The phenol phase was properly disposed, and the supernatant from all 3 rounds was combined. An equal volume of chloroform/isoamyl alcohol (24:1) was added. The mixture was rotated for 30 min, centrifuged for 5 min at 2000 g. The upper phase was transferred to a new tube. This step was repeated once. After centrifugation, both upper phases were combined. The contained DNA was precipitated by adding 1/10 of volume 3M NaAcetate and 1 volume of isopropanol to reduce the precipitation of salt. The DNA precipitated immediately after addition of isopropanol. The formed DNA-cloud was transferred with a pipette tip into an Eppendorf tube. After air drying, the DNA was resolved in TE-buffer, and stored at –20°C.

4.1.2. Isolation of genomic DNA from cells grown in tissue culture

Since no animal tissue was available for the Indian muntjac, all genomic DNA had to be isolated from the fibroblast tissue culture. Usually cells from 3 Petri dishes (or multiples of that) were isolated and processed simultaneously in a 15 ml-Falcon tube. Near confluent fibroblast tissue cultures were harvested after a trypsin-EDTA digest (see methods for tissue culture techniques). The cells were collected by centrifuging the tube at 300 g, 10 min at RT. The supernatant was removed, and cells were resuspended in the remaining drops of liquid.

The resuspension prior to adding the lysis buffer made it easier to break all cells open. 9 ml of lysis buffer was added and mixed with the cells gently to avoid breakage of DNA. The tube was incubated for 10 min. Then 270 µl 0.5M EDTA, pH 8.0 (end concentration 15 mM) and 180 µl 20 mg/ml Proteinase K (end concentration 400 µg/ml) was added, and the entire solution was mixed by gentle agitation. The tube was incubated overnight at 37°C. The next day 120 µl 7.5M NH_4Acetate (100 mM final concentration) and 6 µl 20 mg/ml glycogen were added to the solution to allow an optimal DNA recovery, then 9 ml of phenol were added. The tube was rotated for 15 min, left on ice for 15 min. and centrifuged at RT for 15 min at 7000 rpm. The upper phase was removed and kept on ice. The lower phase was incubated a second time with 150 µl TE-buffer. After rotation for 15 min at RT, 15 min on ice, it was centrifuged 15 min centrifugation at RT with maximum speed. The upper phase was removed and combined with the first upper phase. The phenol phase was properly discarded. 1 volume of phenol/chloroform/isoamyl alcohol was added to the combined upper phases, left for 15 min at RT on the rotator, 15 min on ice, and then centrifuged for 15 min at RT with maximum speed. The upper phase was transferred into a new tube, where 1 volume of 1:1 chloroform/isoamyl alcohol (24/1) was added. After rotating the tube for 15 min at RT and 15 min on ice, it was centrifuged for 15 min at RT with maximum speed. The DNA containing upper phase was removed into a glass corex tube and precipitated with one volume of isopopanol and 0.6M NH_4Acetate end concentration. The DNA was precipitated overnight at –20°C. Corex tubes with precipitated DNA were centrifuged in an SS34 rotor for 1h at 4°C and 10,000 rpm. After the centrifugation, the supernatant was carefully removed and the DNA pellet washed with 70% ethanol and centrifuged again for 30 min at 4°C and 10,000 rpm. After removing the liquid, the DNA was allowed to air dry at RT. The DNA was dissolved in 200 µl TE or aqua bidest., for 1 h at 37°C in a water bath. The DNA was transferred with a cut pipette tip into a 1.5 ml Eppendorf tube for storage at –20°C. The DNA concentration was determined by spectrophotometry (see method section 4.1.6.1.) and the quality was monitored, using gel electrophoresis (see method section 4.1.6.2.).

4.1.3. Preparation of Cot-1 DNA from genomic DNA

25 mg of genomic DNA were dissolved in 5 ml TE-buffer in the original bottle, overnight at 37˚C, under slow rotation. The solution was diluted to a final concentration of 1 mg/ml by adding additional TE-buffer. 10 ml of DNA solution sonicated in 50 ml Falcon tubes while incubated on ice. The sonication was done in 2 min intervals with the volume setting on 2/3, interrupted by 2 min of cooling periods to avoid overheating. When necessary, additional cooling time was added. After each 4 min of sonication time, an aliquot was taken and analyzed on a 1% agarose gel (see method section 4.1.4.). The sonication was stopped when the required size range for the "bulk" of the DNA was 300-600 bp with an average of 400-450 bp. The sonicated DNA was placed in a 50 ml tube in a boiling water bath for 6 min, then transferred to a 65°C water bath to equilibrate to this temperature for 4 min. NaCl solution was prewarmed to 65°C and was added right after the equilibration to a final concentration of 0.3 M. The DNA was allowed to anneal for 6 min, the time needed for the Cot-1 fraction of the DNA to form double stranded DNA. Subsequently, an equal volume of ice cold 2x S1 nuclease buffer (Roche) and S1 nuclease was added to a final concentration of 400 U/µl. The mixture was incubated at 37°C for 30 min so that the remaining single stranded DNA could be digested. After cooling down to RT, the DNA was extracted, using 3 extraction steps, as described in the protocol of genomic DNA extraction (1. phenol, 2. phenol:chloroform:isoamyl alcohol 24:24:1, and 3. chloroform: isoamyl alcohol 24:1). By adding 1/10 of volume 3M NaAcetate and 2 volumes of 100% ethanol, the DNA was precipitated. It was stored at -80°C for 1 h, or at -20°C overnight before the centrifugation. The DNA was precipitated by centrifugation at 4˚C, for 20 min at 10,000 rpm in 30 ml glass corex tubes. The DNA precipitate was washed once with 70% ethanol, air dried, resuspended in 1 ml TE-buffer. The DNA was dissolved at 4°C overnight before it was transferred in an Eppendorf tube for long term storage at -20°C/. The DNA was quantified by spectrophotometry and diluted to the concentration of 1 µg/µl.

4.1.4. Gel electrophoresis

Agarose gel electrophoresis was used to separate DNA-fragments in an electric field. The smaller the fragments are, the faster they migrate in the gel. The concentration of agarose used was dependent on the size of the DNA fragments separated. Agarose powder was mixed with 1 x TBE buffer, heated to boiling in a microwave oven and poured into a gel sled with a comb. After solidifying, the gel was transferred into a gel chamber and covered with 1 x TBE buffer. The samples, mixed with a 6 x loading buffer, were loaded onto the gel. An appropriate DNA size marker (see 4.4.3) was also loaded. In general 8 µl of DOP-PCR reactions and nick translations were analyzed on a 1% agarose gels and run at 120V, 500 mA for 30 - 45 min. 10 µl of regular PCR products were separated on 1 - 2.5%, depending on the expected product size, and run at 70 V, 500 mA for 2 - 4 h. The quality and quantity of isolated genomic DNA or plasmid isolation was controlled on a 1% agarose gel, run at 70 V, 500 mA for 1 - 2 h. To estimate the DNA concentration of an isolated plasmid, the MassRuler DNA Ladder was loaded at 2 different concentrations. After the run, the gel was stained for 5 min 1 µg/ml ethidium bromide at RT. The banding was made visible with UV-illumination. Images were taken with the Electrophoresis Documentation and Analysis System 120 from Kodak.

4.1.5. Polymerase chain reactions and purification of PCR products

4.1.5.1. DOP-PCR

The protocol for the DOP-PCR was a modification of the method described by Telenius et al. and Yang et al. (Telenius et al., 1992; Yang et al., 1995). The design of the DOP-PCR primers allows a relatively sequence nonspecific amplification at low annealing temperatures with the random part of the primer. With a higher amplification temperature, the sequence specific part of the primer allows a specific amplification of a previously created DOP-PCR product. For the generation of chromosome specific painting probes from flow sorted Indian muntjac chromosomes, 2 different DOP-PCR reactions were needed: The primary DOP-PCR, to initially amplify the original flow sorted chromosomes, by using a

low annealing temperature; the secondary DOP-PCR, in which the products of the primary DOP-PCR were amplified for the production of a large quantity of products, that could be used for labeling reactions after their purification.

4.1.5.1.1. Primary DOP-PCR amplification of the flow sorted chromosome fractions

Master mix for 50 µl final reaction volume:

30 µl	sterile ddH_2O containing 500 flow sorted chromosomes
5 µl	10 x Gene Amp PCR-buffer
5 µl	dNTP-mix (200 µM final concentration)
5 µl	6-MW DOP-primer (2 µM final concentration)
0.25 µl	AmpliTaq® DNA polymerase (final concentration: 1.25 U/ in 50 µl)

add 50 µl sterile ddH_2O

PCR program:

Denaturation:	94°C 10 min
9 cycles of low stringency:	94°C 1 min
	30°C 1 min 30

with a transition time of 3 min to 72°C 3 min

30 high stringency cycles:	94°C 1 min
	62°C 1 min
	72°C 3 min + 1 second per cycle
Final extension:	72°C 10 min,
	4°C

4.1.5.1.2. Secondary DOP-PCR amplification

The PCR products of the primary DOP-PCR were reamplified in a high stringent second DOP-PCR. In a 50 µl reaction 2 µl template of the primary DOP-PCR product were used:

Master mix for 50 µl final reaction volume:

2 µl	primary DOP-PCR product
5 µl	10x GeneAmp PCR-buffer
5 µl	dNTP-mix (200 µM final concentration)
5 µl	6-MW DOP-primer (2 µM final concentration)
0.25 µl	AmpliTaq® DNA polymerase (final concentration: 1.25 U/ in 50 µl)

add 50 µl sterile ddH2O

PCR program:

Denaturation:	94°C 10 min
30 cycles of high stringency:	94°C 1 min
	62°C 1 min
	72°C 3 min
Final extension:	72°C 10 min
	4°C

The DOP-PCR products (5-7 µl) were analyzed on a 1% agarose gel. A DNA smear ranging from 100 to 2000 bp was visible. The DOP-PCR products were purified with the PCR-purification kit from Qiagen to prepare them for nick translation and labeling as DNA probes for FISH analysis.

4.1.5.2. Gene specific PCR

In general the identity of obtained gene specific clones was tested before their use in FISH-analysis. With the help of gene specific PCR and the use of gene specific primers (see Table of primers in section 2.2.) the clones were evaluated as being verified when the amplification product matched the expected product size. A clone was scored as not being verified when the amplification product differed from the expected size or no amplification could be observed on genomic cattle DNA.

PCR-volume 25 µl

DNA	1 µl
Primer 1 (20 pmol/µl)	1 µl
Primer 2 (20 pmol/µl)	1 µl
dNTP (2.5 mM each)	1 µl
10x PCR buffer	2.5 µl
ddH_2O	15 µl
TaKaRa-Taq	0.5 µl

PCR program on PerkinElmer PCR-machine:

Denaturation	94°C	2min
30 cycles	94°C	30 sec

	72°C	1 min
1 cycle	72°C	7 min
	4°C	

To determine, if the PCR reaction was successful, 10 µl of the reaction volume was analyzed by gel electrophoresis.

4.1.5.3. Purification of DOP-PCR product

Purification of DOP-PCR products prior to nick translation and subsequent FISH analysis was done with the PCR purification kit (Qiagen). All centrifugation steps were performed at 10,000 g in a conventional table top micro centrifuge. 5 volumes of buffer PB was mixed with 1 volume of the PCR sample. A QIAquick spin column was placed in a 2 ml collection tube. The mixture was applied to the QIAquick column and centrifuged for 1 min. The flow through was discarded. 0.75 ml wash buffer PE was added to the QIAquick column and centrifuged for 1 min. Again the flow-through was discarded. The QIAquick column was centrifuged for an additional minute at maximum speed to completely remove the residual buffer. The QIAquick column was transferred in a clean 1.5 ml micro centrifuge tube and the DNA was eluted. To increase the efficiency of the DNA elution, the sterile H_2O was prewarmed to 70°C. 50 µl water were placed directly on the filter and left on the column for 3 min. Then the column was centrifuged for 1 min. The eluate was stored at -20°C. DNA concentration was analyzed, using spectrophotometry.

4.1.6. Determination of DNA concentration

4.1.6.1. Spectrophotometry to determine the DNA concentration

The concentration of genomic DNA, PCR products (from RT-PCR, regular PCR, or DOP-PCR for FISH probes) or isolated plasmid DNA was determined spectrophotometrically, using a spectrophotometer. The absorbance of the nucleic acid solution was measured at a wave length of 260 nm. Usually, 1:20 and 1:100 dilutions were measured. Contamination with proteins or phenol could be detected by calculating the ratio

of A_{260}/A_{280}, as protein or phenol influence the A_{280}. A ratio of 1.8 to 2.0 indicated low protein contamination of the DNA. In general, the higher the ratio, the purer the nucleic acids. A ratio < 1.6 indicated the presence of residual amounts of protein or phenol, a ratio > 2 occurred when the sample is too diluted. An absorbance unit of the optical density of 1 at $\lambda = 260$ nm ($OD_{260} = 1$) corresponds to a concentration of 50 µg/ml DNA.

4.1.6.2. Gel electrophoresis to determine the DNA concentration

The concentration of DNA isolated with minipreps was estimated with the help of gel electrophoresis. The concentration of plasmids was estimated by comparing the band density staining to the intensity of the bands of the MassRuler DNA Ladder, after ethidium bromide staining. 1 to 5 µl of the isolated plasmid was loaded on a 1% Agarose in TBE gel. The gel was run for about 1 h at 60 volts and then stained with ethidium bromide. Photographs of the gel were taken with an electronic camera to document the band intensities; images was saved on a computer and printed. On the printout, the DNA concentration of the probe was estimated.

4.2. Growing bacteria

4.2.1. Culturing of bacterial clones

Before the beginning of any work with bacteria, all manipulation was done in a semi sterile environment. All material used was sterilized by autoclaving or flaming prior to their use. Bacteria containing genomic clones were received from various commercial sources or from collaborating laboratories (see Tables 4 and 5) in agar stabs, on selective LB-plates, or as glycerol stocks. Each bacterial clone, when received, was streaked out onto a selective LB-plate containing the appropriate antibiotics and grown overnight at 37°C. Five single colonies were picked with sterile wooden toothpicks, and were used to inoculate 5 ml of selective LB media in 14 ml round bottom tubes. The bacterial culture was grown under vigorous shaking for not more than 16 h at 37°C. This 5 ml bacteria culture was used to prepare either a glycerol stock (see method section 4.2.2.) for storage or as a miniprep (see

method 4.2.3.1.) to isolate the genomic plasmid. To inoculate a selective LB medium of 100 ml for maxiprep (see method section 4.2.3.2.), the 5 ml culture was only grown for 6-8 h. Once the clones were verified by PCR or FISH signal location, the frozen glycerol-stocks were used to inoculate new LB-medium by transferring bacteria from the glycerol stock to the medium with a sterile wooden toothpick.

4.2.2. Glycerol stock for long term storage of bacterial clones

800 µl of an overnight culture was mixed with 200 µl sterile glycerol, and stored in color-coded 1.8 ml cryotubes at –80°C.

4.2.3. Plasmid preparation from growing bacteria

The solutions P1, P2 and P3 needed for plasmid preparation were used either from Qiagen, or were mixed in the laboratory. The buffers PE, PB and QBT, QC, QF buffers were used as supplied by Qiagen.

4.2.3.1. Isolation of BACs on a small scale (miniprep)

DNA material obtained with this extraction method was used in PCR reactions to verify the identy of the clones or for FISH analysis. The protocol of the QIAprep miniprep handbook from Qiagen was followed. The grown bacteria containing the plasmid of interest were centrifuged at 3000 rpm in a conventionall table top centrifuge for 10 min. The resulting pellet was resuspended in 250 µl ice-cold buffer P1 + RNase and transferred into an Eppendorf tube. 250 µl buffer P2 were added at RT. The reaction tube was carefully inverted 4 - 6 times and incubated for 5 min at RT. Then 300 µl of ice cold buffer P3 was added and the reaction tube was gently inverted again and incubated on ice for 5 min. After centrifuging for 10 min at 13.000 rpm, the DNA-containing supernatant was decanted onto the QIAprep spin column. The column was in a collection tube and centrifuged for 1 min. The flow-through was discarded. The column was washed with 0.5 ml of buffer PB in a second centrifugation step of 1 min. The flow-through was discarded. A second wash of the

column was performed with 0.75 ml buffer PE and the column was centrifuged for 1 min. The flow-through was discarded again. To remove residual wash buffer the filter unit was centrifuged an additional 1 min. The DNA was eluted by placing 40 µl of 60°C warm water or 1/10 TE onto the filter, letting it sit for 5 min and centrifuging for 1 min. The eluted DNA was stored on ice or at –20°C until used.

4.2.3.2. Isolation of BACs on a larger scale (maxiprep)

DNA material obtained with this extraction method could be used for PCR and for FISH analysis. The protocol of the QIAprep plasmid purification handbook from Qiagen was used. After growing for not more than 16 h, the bacterial culture was centrifuged at 6000 *g* in a GS3 rotor for 15 min. The resulting pellet was carefully resuspended in 10 ml of ice-cold buffer P1 + RNase and transferred into an 50 ml centrifuge tube. 10 ml of buffer P2 were added at RT. The reaction tube was carefully inverted 4 - 6 times and incubated for 5 min at RT. Then 10 ml of ice cold buffer P3 was added and the reaction tube was gently inverted again and incubated on ice for 20 min. After centrifuging for 30 min at 20,000 rpm in a Sorvall SS-34 rotor, the depris separated out as a white pellet. The recommended re-centrifugation step was avoided by filtering the DNA containing supernatant over (with water) wet filter paper (Cat. No. 5802-185, Whatman, Inc, Dlifton, NJ USA). The Qiagen-tip 100 was equilibrated with 4 ml of buffer QTB. The pre-filtered supernatant was applied to the equilibrated Qiagen-tip 100 and allowed to enter the column matrix by gravity flow. The Qiagen-tip was washed twice with 10 ml of buffer QC to remove impurities. To elute the DNA from the column, 60°C warm buffer QF was added and collected in a new 30 ml tube. The DNA was precipitated by adding 0.7 volume of isopropanol kept at RT. The solution was mixed and centrifuged immediatelly at 15,000 *g* at 4°C for 30 min. The DNA precipitate was washed with 2 ml 70% Ethanol and re-centrifuged at 15,000 *g* for 10 min. The supernatant was air dried and redissolved with 500 µl of 1/10 of TE buffer, pH 8.0 or water. The redissolved DNA was stored on ice or at –20°C until used. To increase the concentration of the solution, the volume sample was reduced in a Speed Vac concentrator.

4.2.3.3. Miniprep according to the method collection of the laboratory of Dr. M. Le Beau, University of Chicago ("dirty miniprep")

This method is a faster variant of the regular miniprep isolation. By omitting the column purification step, and using hand mixed buffers P1, P2 and P3, time and money was saved. Plasmid DNA obtained with this extraction method was used for FISH analysis only. Other enzymatic reactions were inhibited due to the impurity of the DNA. In general, two to four 5 ml cultures in LB-medium + antibiotics were grown simultaneously, and isolated separately. At the end, the dissolved plasmid DNA of different preparations was combined to obtain enough material for multiple labeling reactions. The volumes during the isolation in this protocol were optimized so that the isolation could be done entirely in 1.5 ml Eppendorf tubes but yet allow optimal extraction of the plasmid DNA. After the bacterial culture was grown no longer than 16 h, the tube was centrifuged at 6000 *g*. The supernatant was discarded and the bacterial pellet kept on ice. The pellet was resuspended in 0.3 ml P1-buffer + RNase and transfer into 1.5 ml Eppendorf tube. 0.3 ml of P2-buffer was added and the content gently mixed. After exactly 5 min at RT, 0.3 ml of chilled P3-buffer was added, mixed quickly and left on ice for 5 min. Debris was separated from the DNA fraction by centrifugation at 10,000 rpm at 4°C for 10 min. The supernatant was transferred into a labeled 1.5 ml Eppendorf tube containing pre-aliquotted -20°C cold 0.8 ml isopropanol. The mixture was inverted a few times and left on ice for at least 5 min (or they were left at –20°C for longer if the schedule required it). The precipitate was pelleted by centrifugation at 4°C for 15 min. The supernatant was removed carefully and the pellet washed with 0.8 ml 70% Ethanol (RT). The final centrifugation step was done for 10 min. Ethanol was removed, and the pellet allowed to dry at RT, or until all the residue of ethanol had evaporated. When the pellet was dry, it was resuspended in 40 µl of 1/10 TE-buffer for a minimum of 30 min with occasional tapping, or overnight at 4°C.

4.3. Cell culture techniques

Standard methods for cell culture were based on techniques described in a laboratory manual (Spector et al., 1998).

4.3.1. Isolation and culture of cell lines and primary cells

The CD33+ and CD34+ subsets from fresh bone marrow were isolated with magnetic bead separations. The cells were harvested from normal human donors, and received the following day on ice overnight. These cells were not maintained but used immediately for fixation purposes. Isolation of the primary fibroblasts from a dead Chinese muntjac fawn was performed by Dr. Markus Scheuermann. For details of the isolation procedure, see his thesis (Scheuermann, 2004) who applied the method as described in (Ausubel et al., 1998). All cells were grown in vented tissue culture flasks (Corning, purchased through Fisher) of two different sizes (small, T-25 Cat. No. 10-126-37, or large, T-75, Cat. No. 10-126-28) at a 95% relative air humidity, 37°C, and 5% CO_2 enriched atmosphere. Generally flasks with adherent cells were incubated laying flat, flasks with suspension cell lines were incubated upright. For details of the medium composition for the various cell lines, see Table 2. When adherent cells reached about 90% confluency, they were split. The old medium was removed, the cells washed with sterile PBS. Prewarmed 1 or 2.5 ml (depending on the flask size) of Trypsin EDTA solution (Invitrogen) was added for several minutes or until cells detached. The progress of detaching was monitored under the light microscope and was sped up by tapping on the flask to keep the trypsin exposure time to a minimum. The cells were transferred to a conical 15 ml Falcon tube and centrifuged for 8 min at 1000 rpm. The supernatant was disposed, the cell pellet was gently resuspended with 9 ml of fresh medium. The cell suspension was distributed into 3 to 5 new flasks of the same size which contained an additional 10 ml fresh medium for T75 bottles, 5 ml for T-25). The adherent cells were fed every 2 to 3 days. Three quarter of the old medium was removed and replaced with fresh medium. An experiment on fibroblasts was usually performed on cultures of 70 - 80% confluency, which were usually fed the day prior to an experiment. For maintenance, suspension cell lines were split when the cell density approached the maximum cell density

to a cell density that ranged for each cell line from 0.3 to 1 x 10^6 cells/ml (for details for each cell line see Table 2). Suspension cells were usually split the day earlier prior of an experiment to a concentration around the recommended maintained cell density (see Table 2).

4.3.2. Freezing of cells

After trypsination of adherent cells, cells were centrifuged in conical Falcon tubes (15 or 50 ml) at 300 x g, for 8 min, the supernatant was discarded. The cells were gently resuspended with fresh, ice cold freezing medium to a cell density of 3 to 6 x 10^6 cells per ml and aliquotted in prechilled cryovials. DMSO is toxic to cells, but it prevents the formation of ice crystals within the cells during the freezing process. Therefore the freezing process was done slowly. The cryovials were transferred into a freezing box placed at RT (alcohol in the box slowed down the cooling rate to an optimal profile) and transferred immediately to -80°C. The following day the frozen vials were transferred into liquid nitrogen for long term storage.

4.3.3. Thawing of cells

The thawing process was done quickly to avoid both damaging effects of ice crystal formation and the toxic effect of DMSO. The cryovials were thawed in a 37°C water bath with constant monitoring. As soon as the cell aliquot was almost thawed, the tube exterior was sterilized with 70% ethanol. The tube content was quickly transferred into a 15 ml conical Falcon tube containing 10 ml of pre-warmed complete medium. The tube was centrifuged for 8 min and the supernatant discarded. The cells were gently resuspended with warm medium and transferred into a culture flask. For attached cell lines, the medium was exchanged the next day, to remove dead cells and cell debris. For suspension cell lines, the dead cell count was monitored the next day with a Neubauer counting chamber. If the dead cell count was very high, the cells were pelleted by centrifugation and resuspended in fresh medium. If the cell count was much lower than the recommended maintenance cell density, the cells were resuspended in a smaller volume of medium.

4.3.4. Growth manipulation of cells

4.3.4.1. Synchronization of cells with double thymidine block

Synchronization of Triggs cells with a double thymidine block was based on a protocol described in (Spector et al., 1998). The time of cell-incubation was optimized by Aparna Parlacodetti (a member of Dr. LeBeau's laboratory, University of Chicago, Chicago, IL). 24 h after splitting, the cells were treated with 2 mM thymidine for 17-18 h, released from the arrest for 9 h and arrested a second time with thymidine. After 18 h, the cells were released and followed for 0 to 8 h depending on the experiment. To monitor the cell cycle progression aliquots for 0, 2, 4 and 8 h after release were collected. For 3D FISH analysis to determine gene positions at specific cell cycle stages, aliquots were collected 0, 4 and 8 h after release.

4.3.4.2. Synchronization of cells to harvest metaphase chromosomes for the production of whole chromosome painting probes

The method used was a variation of two different protocols (Fawcett et al., 1994; Yang et al., 1995). All solutions prepared for the experiment were filter sterilized or autoclaved. Cells of the female Indian muntjac were used to isolate chromosomes by flow sorting. For better manageability of large quantities of culture, the cells were grown in Petri dishes suited for tissue culture (Corning treated 10 cm polystyrene dishes with, purchased from Fisher). In general, 10 to 30 dishes were treated for one experiment. The cells were grown to a confluency of 80%. To increase the number of mitotic cells for the next step, the cells were treated overnight with a final concentration of 0.2 μM nocodazole. The cells were arrested at the end of the G2 phase of the cell cycle and were visible as rounded cells in suspension. The block was released after washing the cells with warm PBS and adding new medium (half fresh medium, half one day conditioned medium of the same culture) with 0.1 μm/ml colcemid for 5 h. Mitotic cells were shaken off and centrifuged ad 300 *g* for 8 min. The cell pellet was resuspended in hypotonic buffer. Cells were allowed to swell for 15 min at RT and centrifuged again, at 300 *g* (~1000 rpm) for 5 min. The cell pellet was resuspended in

500 µl of polyamine buffer and incubated on ice for 10 min to break open the cells to release the mitotic chromosomes. To avoid disintegration of the native isolated chromosomes, the following steps were all performed on ice whenever possible. The suspension was vortexed 10 to 15 seconds and centrifuged briefly at 100 *g* for 1 min to remove large cell debris. The isolated native chromosomes were differentially stained with two DNA staining dyes. Chromomycin A3 stains preferentially GC rich regions and Hoechst 33258 AT rich regions. The chromosomes were stained on ice with 40 µg/ml Chromomycin A3, 400 µg/ml $MgSO_4$ and 2 mM Hoechst 33258. Chromomycin A3 and $MgSO_4$ were added first for 16 h, the Hoechst 33258 dye was added second for a total of 2 h. 10 min before the flow sorting was started, to enhance the brightness of the chromosomal dyes, 10 mM sodium sulphite and 25 mM sodium citrate were added to the stained chromosomal suspension and the solution was gently mixed. 300 to 500 chromosomes were sorted directly into separate sterile 0.5 ml PCR-tubes containing 30 µl of sterile distilled water and then stored at –80°C. The flow sorting was performed with a MoFlow sorter. 300 to 500 chromosomes were sorted into a 0.5 ml Eppendorf tube containing 30 µl of sterilized water.

4.3.4.3. Induction of double strand breaks with the topoisomerase II inhibitor VP16

The method applied was a variation of Strick et al. (Strick et al., 2000). Triggs cell line were diluted to 0.5 x 10^6 cells the day prior to the experiment. On the day of the experiment, the cells were distributed into different bottles (one for each inhibitor concentration). Aliquots from each "stock" culture were removed for each time point for FACS analysis or for the fixation of the cells for 3D FISH analysis. VP16 was added to the cultures at concentrations of 0, 25, 50, 100, 200 and 400 µM. After incubation for 6 h, cultures were washed and resuspended in prewarmed complete medium without inhibitors. The culture was incubated for an additional 19 h. All concentrations were analyzed for DNA fragmentation after 3 h, 6 h with VP16 and 12 h and 19 h after release. The concentrations 0, 25 and 100 µM at the time points 6 h with VP16, and 12 h and 19 h after release were fixed for 3D FISH analysis.

4.4. Fixation of cell material

The different fixation methods were based on protocols described in the laboratory manual published by (Spector et al., 1998).

4.4.1. Fixation for metaphase chromosome preparation

The fixative (methanol/acetic acid 3:1) was prepared freshly for each experiment. Cell cultures in logarithmic growth were used to prepare cells in metaphase for chromosome analysis using mitotic arrest and a hypotonic solution. The mitotic index of adherent cells was monitored, using light microscopy. Cells in mitosis were rounded up and were easily detached from the surface by tapping the culture flask. The cell suspension derived from up to 10 bottles was centrifuged and placed into two culture bottles. For both, adherent and suspension cultures, 0.05 μg/ml colcemid was added to the medium for 20 min to 1 and 1/2 h. The time points were chosen to increase the number of mitotic cells in the cultures but to have a preparation with chromosomes that were not too highly condensed to show a clear banding pattern after DAPI staining. Up to 8 different cultures were processed simultaneously. After colcemid incubation, the cells were harvested from the culture flask and transferred to a 15 ml conical Falcon tube. Cells were pelleted by centrifugation for 8 min and the supernatant was discarded. The cells were carefully resuspended in the remaining liquid of the tube by gently tapping and swirling. 10 ml of the hypotonic buffer was added to the resuspended cells. Cells were mixed by inverting the tube. Remaining cells in the bottom of the tube were resuspended with the help of a long thin glass pipette. The cells were incubated for 16 min for suspension cell lines, and 25 min for fibroblast cell lines at 37°C. After incubation, the tube was immediately centrifuged at 300 *g* for 8 min. Most of the hypotonic buffer was removed, and the cell pellet was again resuspended in the remaining liquid (ca. 250 μl) by gently tapping and swirling. Under constant gentle shaking the freshly mixed and cold fixative (methanol/acetic acid-fixation solution) was added drop wise to one tube until a volume of 6 ml was reached. Then the tube was placed at 4°C for 30-60 min before centrifuging the cells at 300 *g* for 8 min. The fixative was removed, the

cell pellet was resuspended in the remaining liquid of the tube by gently tapping and swirling. Then 6 ml of new fixative was added. The fixative exchange was repeated 5 to 10 times. The fixed cells remained at -20°C overnight or until used. The next day, the fixative exchange was repeated 3 times before the metaphase preparation. Glass slides were soaked in 95% ethanol at -20°C at least overnight. The slides were wiped with lint-free Kim wipe tissue, dipped in fixative, and the excess liquid was drained on a tissue. One to two drops of fixed cell suspension was placed on the middle of the slide. The slide was immediately placed over the vapour of a water bath with a temperature not higher then 48°C. The slide remained over the water bath until the fixative was evaporated. Large droplets on the slides were removed with compressed air to avoid background spots. The slides were aged for a minimum of one day, and were stored at RT for up to two months. For long-term storage, slides were sealed within a mailer and desiccant, and stored at -80°C until used (up to one year).

4.4.2. Ethanol fixation for flow sorting to analyze the cell cycle status of the cell culture

2.5×10^6 cells were transferred from the culture flasks to a 15 ml tube and washed twice with 1 x PBS by centrifugation at 300 *g*. The cells were resuspended in a volume of 500 µl PBS. The cells were resuspended carefully, which was important to avoid fixation of clumps. 5 ml of cold 100% ethanol was added drop wise while vortexing to prevent clumping. The cells were fixed overnight at 4°C (cells could remain in this fixative for up to 3 weeks before staining). The ethanol was removed after centrifuging at 1000 *g*. The pellet was vortexed and washed two times with 5 ml of PBS with 1% BSA. The pelleted cells were resuspended in 400 µl of PBS containing 1% BSA. 50 µl of PI-staining solution (500 µg/ml propidium iodide in 3.8×10^{-2} M sodium citrate, pH 7.0) and 50 µl of RNase A stock solution was added and the sample was incubated at 37°C for 30 min. Then the sample was stored at 4°C until the flow sorting was performed; 10,000 events were recorded for each sample.

4.4.3. Analysis of CD antigens of cells by flow sorting and immunofluorescence

An analysis of surface antigens, CD33 and CD34, of the cell lines KG-1 and KG-1A was performed. For each sample, 500,000 cells were used. The cells were centrifuged and resuspended in 100 µl of PBS. 20 µl of goat serum for blocking was added and the cells were incubated for 10 min. 10 µl of the two CD-antibody solutions were added. Control samples with only one, isotype control antibody or no antibody were prepared at the same time. The cells were incubated for 2 h at 4°C. Then the cells were washed one time with PBS. The supernatant was discarded. The cells were resuspended by gentle flicking of the tube, and 200 µl PBS was added. If analysis was not done the same day, the cells were fixed. To the 200 µl volume, 50 µl of a 10% paraformaldehyde stock was added to each tube and vortexed. The cells were stored at 4°C in the dark until analysis was performed on a flow sorter. An aliquot of the same cells was taken and mixed with an antifade (Vectarshield + DAPI). The suspension was mounted on a glass slide and images of the cells were analyzed with a fluorescence microscope.

To quantify the DNA content of nuclei, nuclei of cell cycle synchronized and of apoptotic cells were stained with propidium iodide. The nuclei are stained according to their DNA content. Propidium iodide was excited at 488 nm by an argon laser. To stain cells for specific surface markers dual color FACS analysis for FITC and PE was performed.

4.4.4. Analysis of the DNA fragmentation of stressed cells

The method used was described by (Nicoletti et al., 1991). Flow cytometry reveals apoptotic nuclei as a sub-G1 accumulation of DNA in the cell cycle histogram. 10^6 cells were resuspended in 100 µl of PBS. The cells were lysed with 250 µl of a hypotonic fluorochrome solution (50 µg/ml propidium iodide in 0.1% sodium citrate, 0.1% (v/v) Triton X-100). The solution was mixed well with a pipette. The sample was transferred into a round bottom FACS microtube, it was vortexed well, and incubated at least 4 h on ice. The samples could also be kept overnight at 4°C in the dark. The fluorescence of the propidium

iodide was read in a flow cytometer and plotted on a logarithmic scale. The results were presented as a percentage of DNA fragmentation.

4.4.5. Paraformaldehyde fixation for FISH experiments preserving the 3D morphology of cells

The paraformaldeyde (PFA) fixation method was based on previous descriptions (Kurz et al., 1996; Spector et al., 1998).

Adherent cells were grown on poly-L-lysine coated slides (Sigma) in Petri dishes after a regular splitting. The cells were grown overnight or until the desired density was reached. To limit the amount of suspension cells needed, a silicon rubber gasket with a diameter of 22 um was placed onto each slide. The volume of a cell suspension needed for one slide was reduced to 0.3 ml. All suspension cells, including the CD34+ and CD33+ cells, were resuspended in warm PBS and plated onto poly-L-lysine coated slides, that were marked with a glass cutter on either side of the silicon rubber gasket. Depending on cell size 0.3 to 1 x 10^6 cells per slide were plated. After the cells had attached to the slide (usually 5 to 20 min), the silicon rubber casket was carefully removed and the slide was dipped in fresh PBS before placing it in a 4% PFA /1 x PBS solution for 15 min to fix the cells. 3 short washes with PBS followed. To permeabilize the cells, the slides were then placed into a 0.5% (w/v) Saponin, 0.5% (v/v) Triton X-100, 1 x PBS-solution. 3 short washes with PBS followed. The cells were incubated in a 0.1 N HCl solution for 5 min for suspension cells, and for 15 min for fibroblasts. Fibroblasts were placed into the 20% glycerol, 1 x PBS solution immediately. Suspension cells were first washed 3 times in PBS. After freeze-thawing (up to 7 times for fibroblasts, and 1 to 3 times for suspension cells), the slides were placed into plastic mailers, and stored at -80°C until they were used. Primary cells were frozen only once, to minimize the loss of cells.

4.5. Fluorescence *in situ* hybridization (FISH)

General methods needed for the material preparation and detection were based on a description of various protocols (Kurz et al., 1996; Spector et al., 1998).

4.5.1. Preparation of labeled FISH-probes

4.5.1.1. Nick translation

In general, the reaction volume for a nick translation was 100 µl. When large quantities of probes were needed the volume was scaled-up to 300 µl.

2 µg DNA solution of the probe DNA
10 µl 10 x NT-buffer
10 µl 10 x deoxynucleotide-mix
10 µl 0.1 M 2-mercaptoethanol
2-5 µl diluted DNase I (5 µl of 1:250 for DNA clones, 3 µl 1:1000 for DOP-PCR products)
3 µl DNA polymerase A
---
add 100 µl ddH_2O

Using nick translation, genomic DNA (BAC, PAC, and cosmid clones) or purified DOP-PCR products were labeled with nucleotides bound to reporter molecules. The reaction mix was pipetted into 1.5 ml Eppendorf tubes on ice. The tubes were transferred to a 15°C water bath after gentle mixing and a short centrifugation step in a table top centrifuge, to insure that the entire reaction mix is well mixed and at the bottom of the tube. The reaction mix was incubated for 2 h when genomic DNA was labeled, and for 1 h 30 min when DOP-PCR products were labeled. The tube was placed on ice, to slow down the enzymatic reaction. A 5-10 µl aliquot was removed, to analyze the fragment size, incubated in a 95°C heating block for 5 min, and then placed back on ice. The sample was loaded on a 1% agarose TBE-gel (see methods on gel electrophoresis). The probe DNA was visible as a smear under the UV light. If the optimal probe size of 200 to 500 bp was not reached, an additional volume of 2 µl diluted DNase I and DNA-polymerase I were added and the digestion continued for one more h. When the optimal fragment size was reached, the enzymatic reaction was stopped by adding 1 µl of 10% SDS solution and 3 µl of 0.5 M EDTA solution (pH 8.0). The tubes were incubated for 15 min on a heating block at 68°C to inactivate the enzymatic reaction. Unincorporated nucleotides were removed with gel filtration (for details see methods on removal of unincorporated nucleotides.

4.5.1.2. Removal of unincorporated nucleotides

The removal of unincorporated nucleotides from labeled DNA was performed, using a Sephadex G-50 column. In this purification step, salts like SDS and EDTA, unincorporated nucleotides, and very short DNA fragments (<100 bp) were removed, which potentially cause a higher background in a FISH experiment. The purification was performed with the commercially available ProbeQuant G-50 micro columns as well as with self made columns. Chromosome painting probes purified with both methods gave high quality signals in FISH experiments. With the commercially available columns up to 100 µl per column, with the self-made columns up to 300 µl per column could be purified.

4.5.1.3. Production of Sephadex G50 columns (gel matrix spin column) in 1 ml syringes

For each labeling reaction one gel matrix spin column was prepared from a 1 ml syringe in the following way: The stamp of a 1 ml syringe was removed and a plug of silanized glass wool (2-3 mm high) put at the bottom of the syringe to create a barrier. The syringe was packed with the buffered Sephadex G-50 resin up to the 1 ml mark. The resin filled column was put in a 15 ml tube (polystyrol) and centrifuged at 1600 *g* for 5 min. The matrix was packed after the centrifugation step. When necessary, additional Sephadex G-50 resin was added and centrifuged again at the same speed and time. The end volume of the packed resin was approximately 0.8 - 0.9 ml. To equilibrate the column, 100 µl column buffer were loaded onto the column and centrifuged again. This step was repeated two more times. The DNA sample was applied and centrifuged with the same settings (1600 *g* for 5 min). The flow through contained the labeled DNA (the actual FISH- or painting probe). The painting probe was transferred in a labeled tube and stored at –20°C until it was used for a FISH-experiment.

4.5.2. Preparation of DNA-FISH-probe cocktail

Combination of painting probes

The painting probe preparation for 2D FISH or 3D FISH was in general the same except that for a 3D FISH experiment three times more precipitated DNA was used in the cocktail than for a 2D FISH analysis. The volumes given below were used to perform a metaphase- or 2D FISH analysis. For an experiment on human cell material, a typical probe combination was the following:

10 µl of FISH painting probe for gene A
10 µl of FISH painting probe for gene B
10 µl of FISH painting probe for gene C
5 µl of human Cot-1 DNA
5 µl of sonicated salmon sperm DNA
3 different labels for gene A, B and C, e.g. biotin, digoxigenin, dinitrophenol, were used.

For the localization of the cattle BAC on Indian and Chinese muntjac chromosomes, the following typical probe combination was used:

20 µl of FISH painting probe for gene A
20 µl of FISH painting probe for gene B
5 µl of cattle Cot-1 DNA
5 µl of sonicated salmon sperm DNA
20 µl of sonicated genomic cattle DNA or roedeer DNA (1 µg/µl)
2 different labels for gene A and gene B, e.g. biotin and digoxigenin.

For the hybridization of gene specific and whole chromosome painting probes on the muntjac specimens the following typical probe combination was used (the identification of the small Chinese muntjac chromosomes by FISH was confirmed by Dr. Antoinetta Mincheva, DKFZ, Heidelberg):

20 µl FISH painting probe for chromosome A
20 µl FISH painting probe for gene B
3 µl cattle Cot-1 DNA
3 µl Chinese muntjac Cot-1 DNA
10 µl sonified salmon sperm DNA
20 µl sonified genomic Indian or Chinese muntjac DNA (1 µg/µl)
2 different labels were used for chromosome A and gene B, e.g. biotin and digoxigenin.

The DNA was precipitated in a 1.5 ml-Eppendorf tube by adding 1/20 volume of 3 M NaAcetate, pH 5.2, and 2 volumes of 100% Ethanol, at –80°C for 1 h or at –20°C overnight. The DNA was precipitated by centrifugation for 30 min at full peed, washed with 70% ethanol, air dried and resuspended in a hybridization cocktail of 10 – 12 μl. Directly labeled probes were usually purchased from commercial sources such as Vysis and ALTechnologies. To receive the best signals for these probes in combination with other labeled probes, they were added to the cocktail after the precipitation step. In case a direct labeled Vysis FISH-probe was used, the DNA was resuspended in 7/10 volume of the Vysis-hybridization buffer, 2/10 of water and 1/10 of the direct labeled probe was added one full volume. In 3D-FISH the DNA was resuspended also in 10 – 12 μl, except when used in combination with commercial probes. Then no water and 3/10 volume of the direct labeled probe was added. FISH-probes from ALTechnologies were supplied in a less concentrated form. When these probes were used in a 3D-FISH experiment, the volume was reduced to a third in a Speed Vac concentrator, and added as 3/10 volume to the 7/10 volume of Vysis-hybridization buffer. The DNA in the hybridization buffer was resuspended on a vortex shaker for a minimum of 1 h under constant shaking. Then the tube was placed at 75°C for 5 min on a heating block to denature the DNA. For preannealing, the sample was transferred to a 37°C heating block until the probe was applied to the slide. The preannealing time was usually 30 min for human and cattle FISH probes. When whole chromosome painting probes from both muntjacs were used, the annealing time was extended to 1 – 2 h. The annealing times were identical for 2D or 3D FISH experiments.

4.5.3. Denaturation and hybridization of slides for 2D-FISH

Denaturation solution was prepared freshly at the same day the hybridization procedure was started. The solution was heated in a Coplin jar up to 68-69°C (the Coplin jar with the solution was placed in the water bath prior to the water heating up to avoid cracking of the glass). Aged slides with metaphase cells (see methods for details on metaphase cells) were marked with a glass cutter to indicate the side of hybridization. The slides were pre-

warmed on a heating plate to 42°C to reduce the temperature drop of the denaturation solution after putting them into the solution. Up to 3 slides were denatured simultaneously. The metaphase slides were denatured for exactly 2 min at 68°C. Time and temperature was very critical. Longer time or higher temperature resulted in "fuzzy" chromosomes, and made it more difficult to identify the chromosomes accurately. Immediately after the denaturation, the slides were transferred in Coplin jars containing 70% ethanol that was chilled to –20°C. After 5 min, the slides were transferred to 90% and then 100% ethanol. Then the slides were air-dried and placed on a slide warmer at 37 - 42°C. The preannealed DNA-FISH probe cocktail was pipetted onto the hybridization area of the slide, covered with a 18 x 18 mm cover slip and sealed with Fixogum glue (Marabu, Germany) to prevent evaporation of the hybridization cocktail. The hybridization was placed in a humid chamber at 37°C. The hybridization time was overnight for all human 2D FISH experiments, and 2 nights for 2D FISH experiment involving muntjac.

4.5.4. Preparation, denaturation and hybridization of slides for 3D-FISH

Slides with cells that were preserved for three-dimensional analysis were removed from the mailer at –80°C and thawed. During all the steps until the actual scanning, the fixed cells on the slide were never allowed to dry out. This was very important for the preservation of their 3D structure. Upon thawing the slides were placed in PBS and washed 3 times for 2 min. If the HCl step was omitted during the fixation procedure (see methods 3D fixation), the cells were incubated in 0.1 M HCl (7-15 min, depending on the cell type) as a final permeabilization step to facilitate the access of the FISH-probe into the nucleus. The slides were washed again 3 times for 3 min with PBS. For an RNA digestion, the slide were dipped in 2 x SSC and then incubated in a 2 x SSC with 100 μg/ml RNA for 30 min at 37°C. The slides were washed 2 times in 2 x SSC for 3 min and stored in 2 x SSC until the denaturation. Both the denaturation and the equilibration solution were freshly mixed. The solutions were put into Coplin jars and were warmed up to 75°C in a water bath. The denaturation of the chromatin was performed at 73°C in the denaturation solution for 3 min,

followed by exactly 1 min incubation in equilibration solution at the same temperature. The denatured and preannealed DNA probe was pre-pipetted onto a 18 x 18 mm pre-warmed cover slip, while the slide was still in the equilibration buffer. The equilibration solution was quickley drained from the slide and DNA probe on the cover slip was placed on the marked area of the slide. The hybridization area covered by the cover slip was sealed with Fixogum glue, to prevent the drying out of the hybridization area. The slide was placed in a humid chamber for 48 h at 37°C.

4.5.5. Detection of the FISH probes

After hybridization at 37°C, the cover slips were removed from the slides and the specimen placed in a pre-warmed (water bath 42°C) Coplin jar and washed in washing buffer A three times for 5 min at 42°C. Subsequently, three stringent washes for 5 min with washing buffer B (pre-warmed to 60°C) were performed in the 42°C water bath. The slides were then blocked for 30 min in a humid chamber with the blocking solution at 37°C. A detection step followed with the primary antibody or fluorochrome-conjugated substances (for concentrations see Table antibodies, sections 2.5.1 and 2.5.2) for 30 to 60 min. DNP was detected with two antibodies. In the first round DNP was detected with rabbit anti DNP antibody; in the second round the rabbit antibody was visualized with a goat anti rabbit-FITC antibody. Biotin and digoxigenin were detected in the second round. When signals were too weak, a third amplification round with the appropriate antibodies was performed. Different dye combinations were used that allowed optimal visualization of different probes used in an experiment. When 3 color FISH was used, the common color combination was Cy5 for biotinylated probes, Cy3 for digoxigenin labeled, and FITC for DNP-labeled FISH probes. After each round of detection, slides were washed three times for 5 min with washing buffer C in a 42°C water bath, to remove nonspecific bound antibodies. Then the slides were mounted with Vectashield® with DAPI and stored at 4°C until ready for microscopic analysis. When the banding of the chromosomes was important, the slides were stained in a DAPI-staining solution for 5 min. Excess DAPI-solution was washed away by

dipping the slide in fresh 2 x SSC and the slides were mounted with Vectarshield with no DNA stain. The banding of the chromosomes was much more pronounced.

4.6. Conventional light microscopy

The results of FISH or immunofluorescence experiments were analyzed preliminarily with an epifluorescence microscope. Images were acquired with a cooled CCD (charged coupled device) camera mounted on an epifluorescence microscope with immersion oil suitable objectives. The different fluorochromes were visualized and separated with the appropriate filter sets, e.g. FITC (450 - 490nm). The light source was a 100 Watt mercury lamp (HBO 100W, Osram). The image analysis was done with the Adobe® Photoshop 7.0 (Adobe, San Jose, CA).

Filter blocks for the Zeiss-Axioplan microscope used for fluorescence microscopy:

Fluorochrome	Absorption maximum	Emission maximum	Excitation filter	Beam splitter	Emission filter
DAPI	358	461	BP 365/12	FT 395	LP 397
FITC	490	520	BP 450 - 490	FT 510	BP 515 - 565
Cy3	554	568	BP 335 - 385	LP 565	BP 610 - 685
Cy5	652	672	BP 620 - 680	LP 660	LP 750

4.7. Confocal laser scanning microscopy

Filters used: Beam splitter of the Leica confocal microscope, RSP (= reflection short pass filter), TDC (= triple dichroic filter), DD (= double dichroic filter).

Filter	Excitation wave length
DAPI	405 nm
RSP465	≤ 465 nm

RSP500	≤ 500 nm
RSP525	≤ 525 nm
DD458/514	458, 514 nm ± 3 nm
TDC488/514/633	488, 514, 633 nm ± 3 nm

For the acquisition of confocal image stacks a Leica SP2 AOBS spectral laser scanning confocal microscope was used operated with the software LCS 2.5v1347. The body of the Leica DMIRE2 (inverted) microscope was equipped with conventional fluorescence (50W Hg) and DIC optics. The following objectives were available: 40x NA 1.2 oil, 63x NA 1.4 oil and 100x NA 1.4 oil plan apo and the matching DIC prisms for each objective. Wide DAPI, GFP and "rhodamine" filter sets for locating cells by wide-field fluorescence were used. For the acquisition of the confocal image stack, only the 64x objective was used. From the 5 lasers and the 9 possible laser lines the following were used do detect the respective fluorophores:

Laser type	Nominal power (mW)	Wave length (nm)	Fluorochromes and corresponding excitation (nm)
diode laser	20	405	DAPI (405)
argon laser	65	458, 476, 488, 514	FITC (488)
helium neon laser	1,2	543	Cy3 (543)
helium neon laser	10	633	Cy5 (633)

The fluorophores used were excited, using the appropriate laser in combination with the beam splitter of the corresponding wave length. The fluorescence signal was detected, using a photomultiplier tube (PMT). In contrast to conventional fluorescence microscopy, which uses glass filters to define the detected emission, the Leica SP-lines allow the user to adjust the detection band interactively by setting a spectrometer, which essentially combines

an optical position with a slit-diaphragm. Image processing was not done with the Leica software. Exported images were modified with Adobe Photoshop. Confocal image stacks for 3D measurements were modified exclusively with the Amira 3.1 program (for details see image processing). The pinhole for all scans was kept constant at 1 Airy. All 3D image stacks of fixed cells were acquired with steps between 0.2 µm and 0.5 µm in Z-directions. For each series, preferably the same step increments were used. The image resolution was 512 x 512 pixels. The scan speed was used in a maximum setting of 1000 Hz; for a zoom setting of 4 and above, 800 or 400 Hz were used, when a larger area was scanned. If two or more fluorochromes were imaged, the modus "sequential scan" was used. In the majority of the scans, the color order during acquisition was the following: Cy3, FITC, Cy5, DAPI + DIC. The detection range of the fluorochromes was adjusted to have as little overlap as possible. To improve the signal to noise ratio, all images were averaged 6 or 8 times. To delineate the shape of the nucleus and the cell, a differential interference contrast (DIC) image was acquired.

4.8. Analytical methods

4.8.1. Software

Primers were designed, using the programs MacVector 6.5.3 and LaserGene 3.0.

4.8.2. Image processing

2D metaphase images were enhanced in contrast and in signal intensity, using Adobe Photoshop. Obvious background spots were removed from the image. Total projections from confocal images were exported as tiff files and enhanced with Adobe Photoshop. Deconvolution of 4 color 2D-images was performed, using Improvision's Openlab version 3.17, prior to the analysis of the position of a gene relative to the territory surface. For the processing of confocal image stacks in Amira 3.1, see Results section 5.2.

4.8.3. Steps required from confocal image to 3D measurements

For the processing of confocal image stacks in Amira 3.1 see Results section 5.2. The confocal images were acquired with the Leica confocal scanning microscope. Each channel of a confocal image stack contains the signals for one detected fluorophore. Usually one gene was detected with one, but in selected cases, a gene was detected with 2 fluorophores.

Processing of confocal image stacks

The image stacks were imported unchanged into Amira 3.1. Figure 16A1 displays a stack with selected scan levels displayed for a better overview. The modifications within Amira 3.1 were reduced to a minimum. That way, the highest accuracy and reproducibility of the data remained. Out of various filter options, the median filter was chosen as a non-linear signal enhancement technique, because it was described to smooth signals, to suppress impulse noise, and to preserve edges. (online sources: http://rkb.home.cern.ch/rkb/AN16pp/ node168.html, and http://www.cee.hw.ac.uk/hipr/html/ median.html). Due to the lack of other reference points, the center and the periphery of a nucleus was chosen. Erosions of the nuclear surface could translate to an underestimation of the edge of the DAPI stainable nucleus. Then the error of the calculated distance between gene signal and surface would increase. The accurate description of the gene within the nucleus could also be jeopardized. The median filter applied in the Amira 3.1 program used a 3 x 3 kernel.

Threshold setting

Prior to the threshold setting, a total projection of all channels was created to gain an overview of the entire scan, and the positions of the signals (Figure 16A3 and 4). Cells of a known karyotype displaying the expected amounts of signals per channel were analyzed. A threshold was set for each channel. During the threshold determination, the image stack was scrolled back and forth; at the same time, the threshold setting was modified. By carefully comparing the grayscale images of each color with the outline of its rendered surface on all scan levels, a threshold was chosen that best covered the edge of the signals on all levels (Figure 16B1-2) to minimize the possibility of over or under sampling. The displayed

isosurfaces were adjusted in their display color, so that the different signals from the various channels could be distinguished more easily (Figure 16A5).

Creating files containing all surface points e.g. for a gene

After the threshold was set in a channel, an isosurface was visible (Figure16B3). A surface was created, matching the outline of the isosurface (Figure16B4). On this surface, possible background spots or second signals could be deleted (Figure16B5), leaving only the surface for e.g. one single gene homolog. By making the isosurface invisible (Figure16B), the remaining surface could be investigated in detail, to determine, if any background spots remained. The removal of any small background surfaces was important later for the accurate calculation of the center of gravity of a surface. The surface was then exported in IV-file format. The IV-file contained all X, Y and Z coordinates of the created surface. To be able to evaluate the position of two genes in one nucleus, 5 IV-files were created. One for the nucleus and 2 for each gene (Figure 16C1). To be able to describe the position of a gene within the 3D volume of a nucleus and relative to other genes, different calculations had to be performed. The program capable of all these calculations was created by Juntao Gao, a Ph.D. student of Dr. Roland Eils, in part prior to our collaboration. The first step was to determine the position of a gene in the 3D space. The decision was made to reduce the position of a gene to the X, Y, Z coordinates of its center of gravity. This way, the thresholding for the genes was less critical. Assuming the gene signal is spherical, different threshold settings would not notably change the center of gravity and therefore the 3D position of that signal within the nucleus. An algorithm was designed to calculate the X,Y, Z coordinates of its center of gravity for the IV-file (Figure16C2, and Figure17A). To be able to determine the distance of a gene to the nuclear surface an additional subprogram was written that allowed identification of the surface point closest to the center of gravity of a gene (Figure 17C).

Distances between two genes (Figure 16C4, red, green and yellow lines), between gene and nuclear center (Figure16C3, blue lines), gene to nuclear surface (Figure16C3, orange lines) therefore could be calculated by a simple vector calculation. The distance of

two signals in this scoring method might be slightly overestimated, e.g. signal edges that might be touching each other will not be scored differently, only the distance between both centers of gravity counted, but that was consistent within the system. An additional surface, which was identical with the visible isosurface was created and was exported in IV-file format. This file contained all X, Y, Z coordinates of all surface points, allowing the programs created by Juntao Gao to calculate the center of gravity of that particular surface or the search of the closest surface point of the nuclear periphery to a center of gravity of a gene signal.

When the signals of a gene were detected in two colors, using the same clone with two different labels, the surfaces were rendered for both colors and it was confirmed, that both colors identified the gene without bias. For further measurements and analysis, only the rendered surfaces of the Cy3-staining were used. When one gene locus was stained with a combination of two different clones, detected in two different colors (e.g. dual color probe of *MLL* with a green label for *5'MLL* and a red label for *3'MLL*), both surfaces were rendered and evaluated independently.

4.8.4. Analysis of SAGE data

To describe, if MLL and its translocation partners are low or highly transcribed genes in different hematopoietic cells, SAGE libraries of different cell types were analyzed. The

Name of SAGE-library	Total number of tags in SAGE-library	Number of Unique tags in SAGE-library	Percent of unique tags in SAGE-library
CD15	105006	38871	37.0
CD34	99954	42399	42.4
pre-B	110008	16189	14.7
pre-T	19882	15652	78.7

Table 6: Characteristics of the SAGE libraries used in Table 8.
SAGE libraries analyzed were produced in the Laboratory of Janet D. Rowley, Chicago, IL.

SAGE libraries had already been produced by the Rowley laboratory and were available for the analysis for this work (**Table 6**). SAGE tags specific for *MLL* and translocation partners (as listed in Table 1) were identified with the help of the NCBI-website. The occurrence of each of these SAGE tag sequences were looked up in the SAGE libraries and their frequency noted. SAGE-tags that had multiple designations were also looked up. For the final production of Table 6, these tags were not included. Finally the sum of all SAGE tags unique to a gene was listed in Table 8 and normalized by the total number of tags of the SAGE-library to describe the transcription frequency of each gene.

5. RESULTS

The main goal of this work was to determine the 3D localization of genes in mammalian interphase nuclei and to identify the underlying principles that determine gene localization. The generality of these principles should then be tested by analyzing the behavior of the human *MLL* gene and some of its translocation partners. It was interesting to compare various mammalian species with very different chromosome numbers. I chose to analyze the situation in humans and two closely related species of deer, *Muntiacus muntjak* and *Muntiacus reevesi* for the following reasons: Indian muntjac has the lowest number of chromosomes known in mammals, and Chinese muntjac has 46 chromosomes, the same number as found in humans. The two muntjac species were distant enough from humans but closely related to each other, allowing to determine the generality in the findings.

5.1. Identification of various gene loci on muntjac chromosomes and interphase nuclei

Many of the tools needed to study the two muntjac species were not available. At the beginning of this work the localization of only 5 loci had been determined for both muntjac species (Fronicke et al., 1997). An additional 4 loci were known for *M. muntjak* (Krawetz et al., 1990; Pardue and Hsu, 1975) using *in situ* hybridization. With other techniques, 5 genes were assigned to entire chromsomes of *M. muntjak* (Levy et al., 1992; Shows et al., 1976). The localization of the genes, which are in the focus of this thesis (*MLL*, and its translocation partners *AF4* and *AF9*), were unknown. The generation and characterization of a number of tools to study *M. muntjak* are described in this thesis.

5.1.1. Fine mapping of syntenic regions of *M. muntjak* and *M. reevesi* using specific DNA probes of cattle and mouse

In order to map known genes to specific chromosomal regions in *M. muntjak* and *M. reevesi*, a set of 55 clones containing known genes was used to perform FISH analysis on metaphase chromosomes. The probes used were either from cattle or mouse. A variety of clones from human and horse were tested, but they never produced identifiable FISH-signals on the chromosomes, and therefore were not listed.

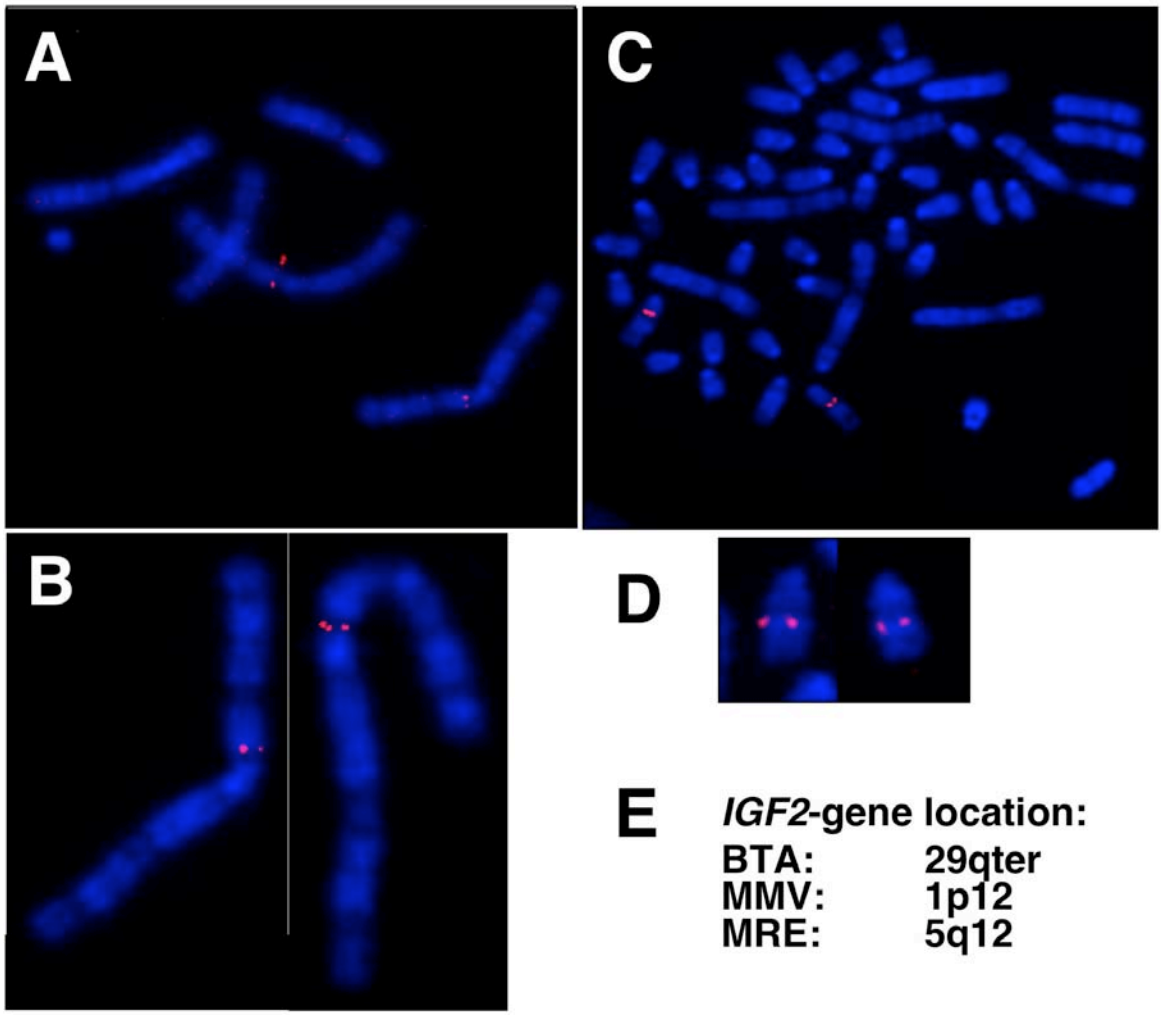

Figure 9: Identification of syntenic regions between Indian and Chinese muntjac using cattle BAC clones and FISH-analysis.

FISH on metaphase spreads with cattle clone 953A11 containing cattle gene *IGF2* from cattle chromosome 29qter, labeled with biotin and detected with streptavidin-Cy3.

A,B: Indian muntjac.

C,D: Chinese muntjac.

E: Summary of the chromosomal localization of *IGF2* in the three species. BTA (= cattle), MMV (= Indian muntjac), MRE (= Chinese muntjac).

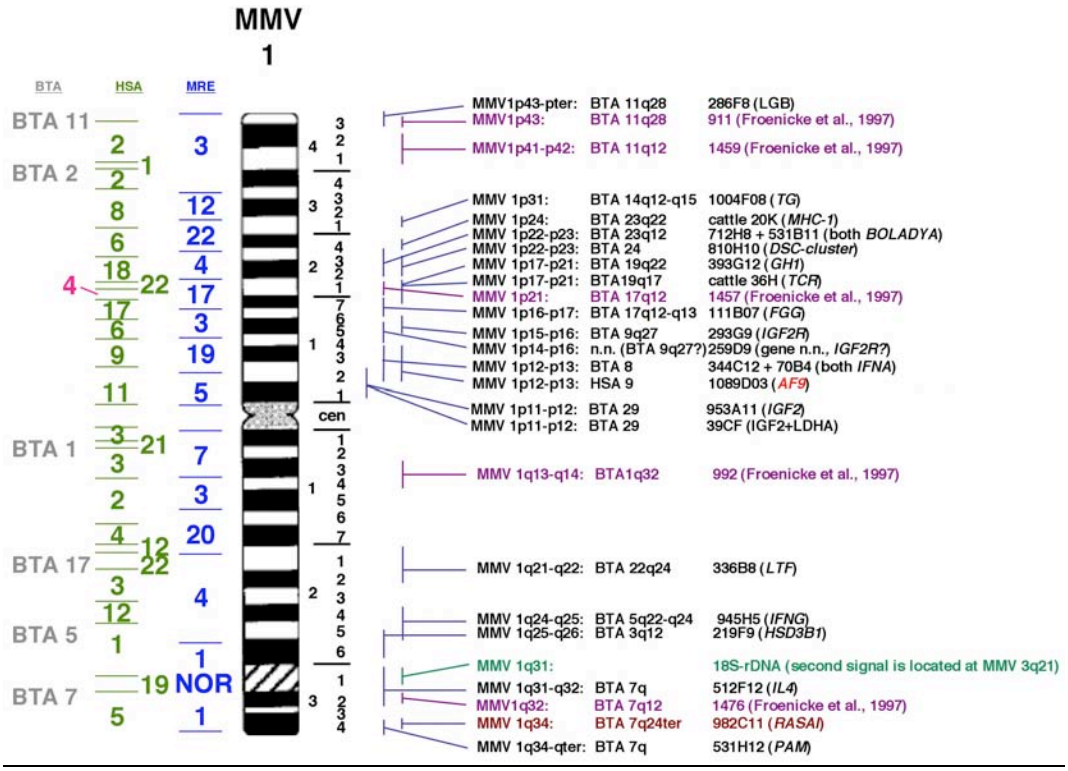

Figure 10: Summary of all localized genes on chromosome 1 of Indian muntjac.
Previously published data on chromosomal syntenic regions based on Zoo-FISH data are displayed to the left of the ideogram. To the right all clones are listed, which were localized on chromosomes of *M. muntjak* using FISH-analysis (see Table 5 for a complete list) including earlier published results.

Color coding to the left of the ideogram:

Grey: Assumed syntenic regions between *M. muntjak* and *Bos taurus* (= cattle) (Yang et al., 1997a).

Light green: Summary of syntenic regions between *M. muntjak* and *Homo sapiens* as published by Yang et al. (Yang et al., 1997a) and Fronicke and Scherthan (Fronicke and Scherthan, 1997).

Blue: Summary of syntenic regions between *M. muntjak* and *M. reevesi* as published by Yang et al. (Yang et al., 1997b).

Pink: Assignment of the previously unassigned small region located at 1q17-q21 to be syntenic to human chromosome 4. The assignment was based on data produced in this thesis and a report by Fronicke et al. (Fronicke et al., 1997).

Color coding to the right of the ideogram:

Purple: Published locations of genomic cattle BAC clones without gene identification (Fronicke et al., 1997).

Dark green: Position of 18S rDNA (2 signals in both muntjac species) verifying the data on Indian muntjac observed by (Pardue and Hsu, 1975) using radioactive in situ hybridization. The locations are MMV 1q31 and MMV 3q21 (MRE chromosomes 1q28-q31 and 6q7).

Brown: Contradictory result for 2 cattle clones. Both were described to contain the gene *RASAI (Gautier et al., 2001)*. Both observed hybridization locations are MMV 1q34 and MMV 2q38-q39.

Red: Genes *AF4*, *AF9* and *MLL* (MMV 3q39, MMV 1q12-q13 and MMV 2q38-q39) which are further discussed in the thesis.

BTA = chromosomes from *B. taurus* (= cattle); HSA = chromosomes from *H. sapiens;* MMV = chromosomes from *M. muntjak*; MRE = chromosomes from *M. reevesi,* NOR = nuclear organizer region, rDNA = ribosomal DNA.

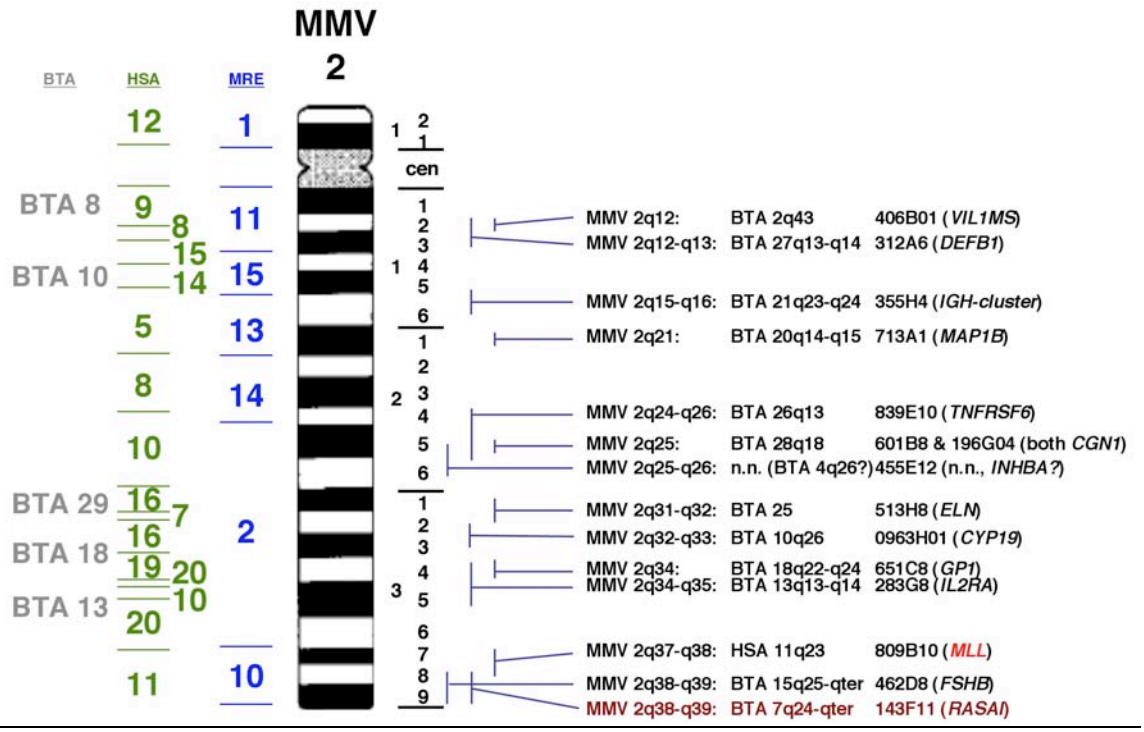

Figure 11: Summary of all localized genes on chromosome 2 of Indian muntjac.
For detailed description see Figure 10.

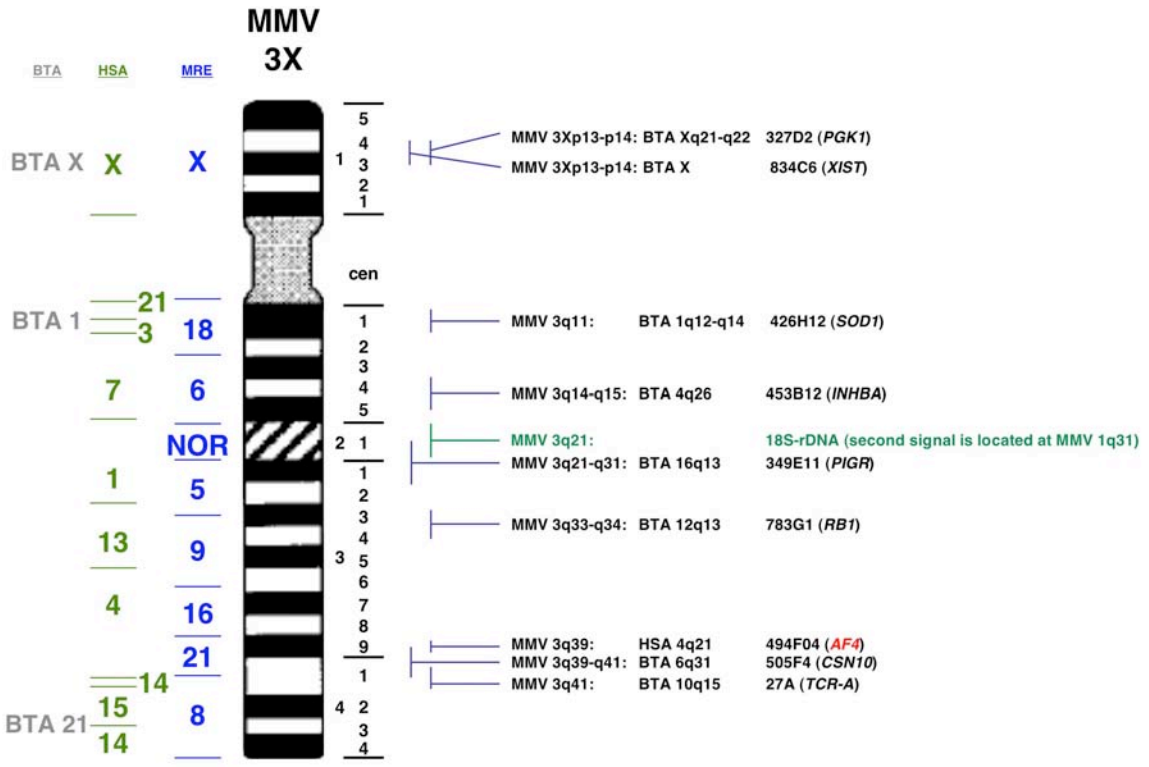

Figure 12: Summary of all localized genes on chromosome 3X of Indian muntjac.
For detailed description see Figure 10.

An example of the localization of a gene in both muntjac species is shown in **Figure 9**. To localize the *IGF2* gene, a cattle BAC-probe was used. This gene, which is located in cattle on the q-telomere of chromosome 29, was identified on chromosome band 1p12 in *M. muntjak* (**Figure 9A** and **B**) and on chromosome band 5q12 in *M. reevesi* (**Figure 9C** and **D**). A summary of all localized genes on both muntjac species is presented in Table 4. In total 40 gene loci were assigned to unique loci on *M. muntjak* and 28 on *M. reevesi*. The 18S rDNA was assigned to 2 loci on different chromosomes in both species. The location for the gene *RASA1* could not be assigned due to inconsistent results received from 2 clones containing this gene (in both clones the correctly sized PCR product could be amplified). Interestingly, none of the Y-specific genes could be mapped in either muntjac species. Identification of syntenic regions between human, cattle, and *M. muntjak*, and between *M. muntjak* and *M. reevesi* were reported (Chowdhary et al., 1998; Fronicke et al., 1997; Fronicke and Scherthan, 1997; Yang et al., 1997a; Yang et al., 1997c). These analyses were all based on using whole chromosome painting probes and not individual genes. This information helped to predict the possible location of certain genes in the *M. muntjak* genome (Chowdhary et al., 1998), and with the reduction of the chromatin content mainly found in the low repetitive sequences (Schmidtke et al., 1981), it is likely that most human or cattle genes are also found in *M. muntjak*. The results of an analysis of individual gene probes are summarized in **Figures 10-12**. 23 clones were localized on *M. muntjak* chromosome 1 (**Figure 10**), 14 clones on chromosome 2 (**Figure 11**), and 10 clones on chromosome 3X (**Figure 12**).

The genes for *MLL* and two of its translocation partners *AF4* and *AF9*, which were studied in detail as part of this thesis, were also localized and all were found to be on different chromosomes. *MLL* localized to *M. muntjak* chromosome 2q37 (**Figure 11**), *AF4* on 3Xq39 (**Figure 12**) and *AF9* on chromosome 1p12-p13 (**Figure 10**). The localization was also determined on *M. reevesi* chromosomes (see Table 4). This section presents the analysis of the 3D localization of *MLL*, *AF4* and *AF9* between human and a species, which has a vastly different number of chromosome, *M. muntjak*.

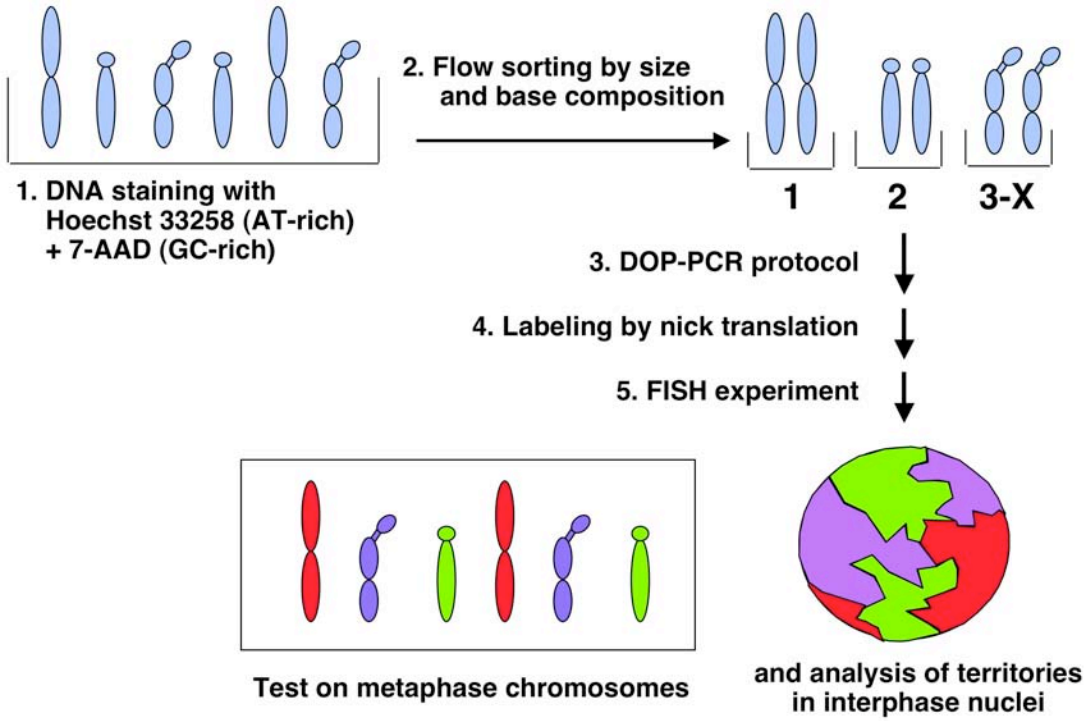

Figure 13: Overview of methods involved in the generation of whole chromosome painting probes for the Indian muntjac using flow sorting. For details see text.

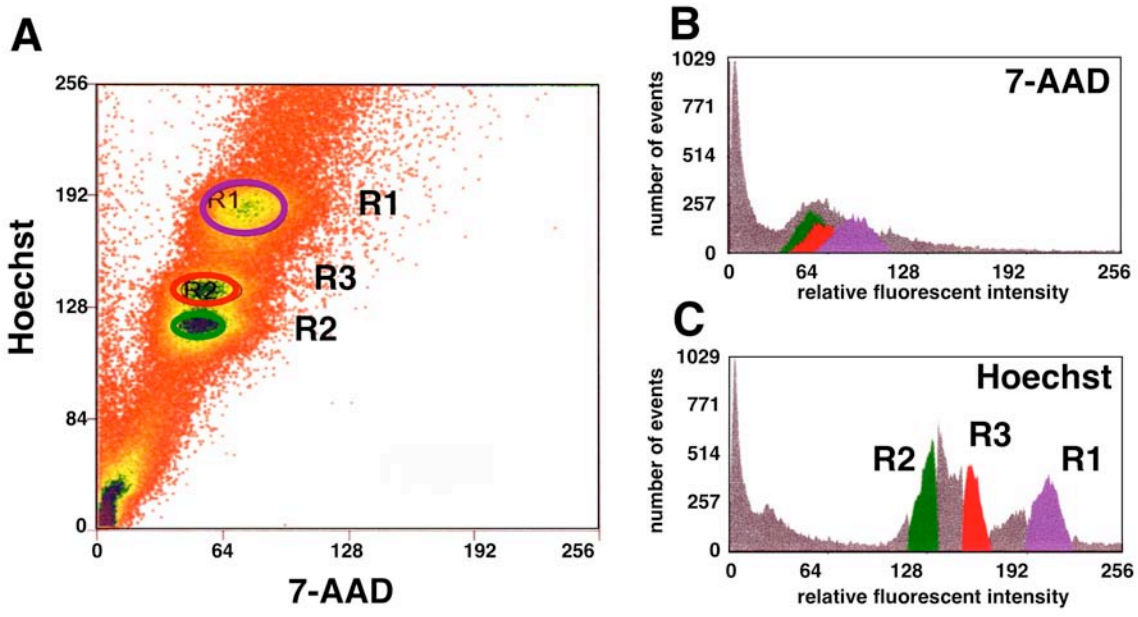

Figure 14: Flow sorting profile of chromosomes from female *M. muntjak*.
A: Flow sorting profile.
Purple: R1 region specific for *M. muntjak* chromosome 1.
Green: R2 region specific for *M. muntjak* chromosome 3.
Red: R3 region specific for *M. muntjak* chromosome 2.
B: Fluorescence intensity for 7-AAD.
C: Fluorescence intensity for Hoechst 33258.

Because potential differences could be due to the difference in species and not chromosome number, *M. reveesi* serves as a control for a species with the same chromosome number as the human.

5.1.2. Generation of whole chromosome painting probes from *M. muntjak* to visualize all individual *M. muntjak* chromosomes simultaneously

To have the ability to determine the 3D localization of *M. muntjak* genes within chromosome territories, whole chromosome painting probes for the 3 *M. muntjak* chromosomes were generated. The general strategy for isolation of chromosome specific DNA to generate chromosome specific painting probes is shown schematically in **Figure 13**. Chromosome specific DNA was obtained by separating individual chromosomes by flow-sorting according to their DNA content and base composition (**Figure 13**, step 1 and 2). Subsequently, chromosome specific DNA was amplified by DOP-PCR (degenerated oligo-primer polymerase chain-reaction) (**Figure 13**, step 3) using the two step protocol according to Telenius (1992) (Telenius et al., 1992), which allows a general and sequence independent amplification of any DNA template. PCR-products of the second PCR-reaction were labeled by nick-translation (**Figure 13**, step 4) with nucleotides bound to reporter molecules, such as digoxigenin, biotin, estradiol, or dinitrophenol, which allowed detection by antibodies bound to fluorophores. In a FISH-experiment (**Figure 13**, step 5) these paints were hybridized to the unique sequences of each chromosome in methanol acetic acid fixed metaphase cells for specificity control. These probes could then be used to stain PFA-fixed interphases nuclei using laser scanning confocal microscopy and 3D reconstruction of the territories.

To obtain the chromosome specific DNA, primary fibroblasts from female *M. muntjak* were used as described (Levy et al., 1991). Metaphase chromosomes of female *M. muntjak* were flow-sorted according to their relative size and their differential uptake of two dyes, Chromomycin A and Hoechst 33256 to stain GC- and AT-rich regions, respectively. **Figure 14** shows the result of a typical flow-sorting experiment of *M. muntjak* chromosomes. After counting about 10,000 events, three clearly defined populations with different staining intensities became visible. Chromosome 1 was identified in gate R1 (**Figure 14**, purple)

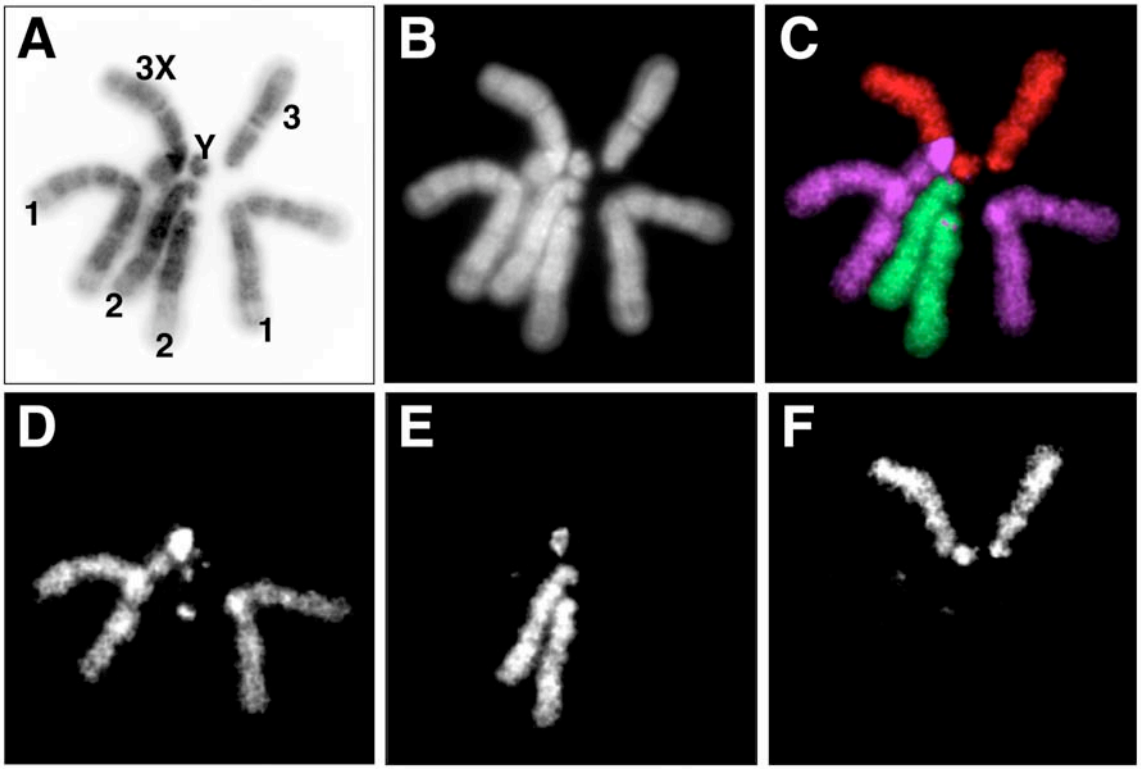

Figure 15: Three-color FISH on metaphase chromosomes of male *M. muntjak*.
A: Assignment of chromosome numbers.
B: DNA counterstain with DAPI.
C: Pseudocolored overlay of D, E, and F.
D: Chromosome 1 labeled with biotin, detected with streptavidin-Cy5.
E: Chromosome 2 labeled with digoxigenin, detected with goat anti-digoxigenin-FITC.
F. Chromosome 3X labeled with extradiol, detected with anti extradiol-rhodamine.

chromosomes 2 in gate 3 (**Figure 14**, red) and 3X in R2 (**Figure 14**, green). The flow-sorted chromosomes were amplified by a set of two DOP-PCR reactions, the material labeled and used as probe in a 2D-FISH experiment. In **Figure 15** paints from male *M. muntjak* cells for chromosomes 1 (biotin-labeled), 2 (digoxigenin-labeled) and 3X (estradiol-labeled) were hybridized to metaphase cells of male *M. muntjak* fibroblasts. The paints were detected with streptavidin-Cy5, anti-digoxigenin-FITC and anti-estradiol-rhodamine, a true 3-color FISH. This combination of three different labels (FITC, Rhodamine, and Cy5) to distinguish the

three individual whole chromosome paints for *M. munjtak* chromosomes 1, 2 and 3X is now available to analyze chromosomal territories in 3D fixed interphase nuclei.

5.2. Development of computational tools to determine 3D gene positions in interphase nuclei

5.2.1. Steps involved to convert a stack confocal of images into a reconstructed volume rendered nucleus

Most of the analyses of genes in the nuclear space, their distances to each other, their territory, or to the nuclear surface, were performed by using 2D imaging (Bartova et al., 2002; Bartova et al., 2000; Croft et al., 1999; Kozubek et al., 2001; Taslerova et al., 2003; Volpi et al., 2000). To obtain more accurate data, majority of the analyses in this work were performed using 3D imaging. The focus was on *MLL* and its translocation partners, which are highly relevant for hematopoietic cells. Since the geometry of nuclei of these cells is mostly spherical, methods had to be developed to accurately describe positions of genes in the 3D space of a sphere. Reference points chosen were the center of gravity of a nucleus and the nuclear surface.

Figure 16A illustrates the procedure to generate 3D rendered nuclei. Raw data of the image stacks obtained by confocal laser scanning microscopy containing between 20 and 35 individual scans were imported into the computer program Amira 3.1. The confocal images were created with a Leica confocal scanning microscope. Each channel of a confocal image stack contained the signals for one detected fluorophore. Usually one gene was detected with one, in selected cases, with two fluorophores. **Figure 16A1** shows a stack with only 6 scan levels for simplicity. To reduce the number of modifications of the images in the Amira 3.1 program, the median filter (3 x 3 kernel) was applied as a non-linear signal enhancement technique (not shown), because it smoothes signals, suppresses impulse noise, and preserves edges (see: http://rkb.home.cern.ch/rkb/AN16pp/node168.html, and http://www.cee.hw.ac.uk/hipr/html/median.html). Edge preservation was a requirement for the subsequent volume rendering of all detected signals to yield well defined and reproducible surfaces such

as the nuclear surfaces (as shown in **Figure 16A2**). Erosions of the nuclear surface could translate into an underestimation of the edge of the DAPI stainable nucleus.

A threshold was set for each channel (**Figure 16A2**). During the threshold determination the image stack was scrolled back and forth, at the same time the threshold

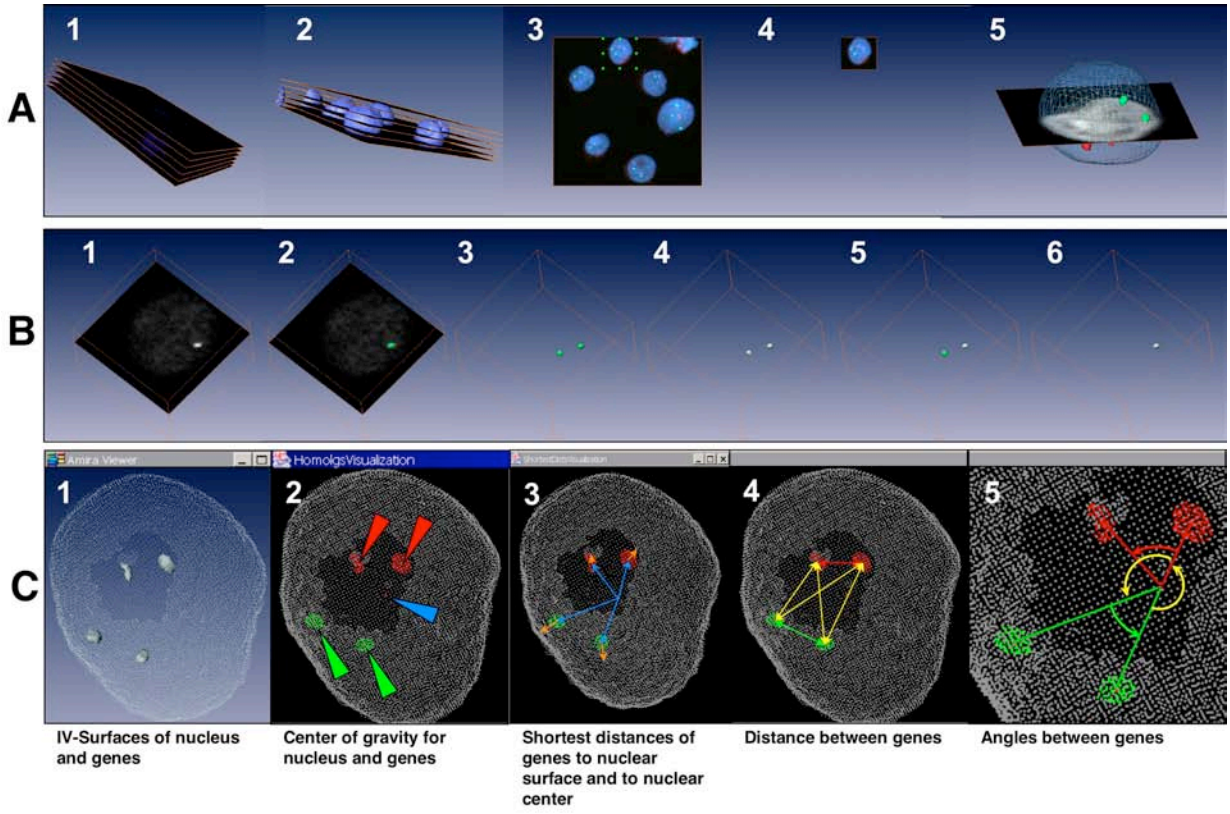

Figure 16: Development of computational tools to determine 3D gene positions in interphase nuclei.

A: Generation of a surface rendered nucleus in 5 steps. Beginning with the Z-section acquired with confocal microscopy. For simplicity a stack with only 6 sections is displayed.

B: Steps necessary to generate a file containing all surface points (IV-file) for one single gene signal within a 3D rendered nucleus.

C: Graphical representation of the 4 computational tools (2-5) used in this thesis. For details see text.

All pictures are actual images taken from the Amira 3.1 program (A and B) and the program developed by Juntao Gao, a Ph.D. student in Dr. R. Eil's laboratory (C). Most of these computational tools were developed by him prior to our collaboration. The tool to find the shortest distance of a gene to the nuclear surface (Figure 16C3, orange lines) was developed specifically for this work.

setting was modified. Prior to the threshold setting a total projection of all channels was created to gain overview of the entire scan, and the rough localization of the signals (**Figure 16A3**). Individual nuclei were selected by cropping (**Figure 16A4**). By carefully comparing the grayscale images of each color with the outline of its rendered surface on all scan levels, a threshold was chosen that best covered the edge of the signals on such an isolated nucleus. The displayed isosurfaces were adjusted in their display color, so that the different signals from the various channels could be easier distinguished (**Figure 16A5**).

5.2.2. Creation of a file containing all surface points for a single gene signal

In all FISH experiments gene labeling was combined with DAPI staining allowing rendering of the nucleus in addition to the gene signals. **Figure 16B1** shows a grey scale image of a single scan of a nucleus with a single labeled gene. After setting the threshold (**Figure 16B2**), a rendered volume was created for this signal (two genes) and their isosurface became visible (green structure in **Figure 16B2**) (Note: creating an isosurface is a technique used in three-dimensional data visualization where a surface is drawn around points in three-dimensional space that represent the same data value). To be able to inspect the created surface in detail, the visible confocal scan plane was removed (**Figure 16B3**). In the Amira 3.1 software, this first isosurface cannot be manipulated, therefore a second identical surface had to be generated (**Figure 16B4**). On this surface, possible background spots or second signals could be deleted (**Figure 16B5**), leaving only the surface of the signal of interest (white structure in **Figure 16B5**). By making the isosurface invisible (**Figure 16B6**), the remaining surface could be investigated in detail. The removal of any small background surface points at this stage was important to ensure accuracy of the subsequent calculation of the center of gravity of a structure. The surface was then exported in the IV-file format. The IV-file contained all X, Y and Z coordinates of the created surface. To be able to evaluate the position of two genes in one nucleus, 5 IV-files were created, one for the nucleus and two for each gene. A visualization of the resulting surfaces is shown in **Figure 16C1**.

5.2.3. Methods to determine positions of genes in nuclei using mathematical algorithms

To be able to describe the position of a gene within the 3D volume of a nucleus and relative to other genes, different calculations had to be performed. Programs capable of all these calculations were created by Juntao Gao, Ph.D. student in Dr. Roland Eils' group, DKFZ, Heidelberg, in part prior to our collaboration. As a basis for all these methods the positions of signals had to be defined in the 3D space. The position of a gene in the 3D space was sufficiently described by the position of its center of gravity. An algorithm was designed to calculate the X,Y,Z coordinate of its center of gravity for the IV-file (**Figure 16C2**, and **Figure 17A**). The center of gravity of the nucleus was chosen as a reference point. The surface point closest to a center of gravity of the gene was searched for in an additional program. Establishing these coordinates allowed various kinds of distance measurements using simple vector calculations: 1. The distance of genes to the nuclear center and to the closest nuclear surface point (**Figure 16C3**, blue lines and orange lines, respectively) and 2. the distance between genes (**Figure 16C4**, red, green and yellow lines). Using a different algorithm, angles between the genes could be determined (**Figure 16C5**).

Figure 17A-D shows the formulas the methods in **Figure 16C2-5** are based on. **Figure 17E** shows the calculations involved in the description of a gene position relative to the nuclear surface. After the nuclear radius R was calculated as a sum of the distances between nuclear center to gene and between gene to nuclear periphery, the distance of the gene to the nuclear periphery was expressed as percent of the nuclear radius. In this way, the gene position was defined in relation to both reference points, the nuclear center and the nuclear periphery (for more detailed explanation see section 3.2). This calculation was usually used when hematopoietic cells were analyzed. A different method of analysis was used for fibroblasts due to their different nuclear geometry, which is flat and oval in shape. With fibroblasts only the distance of genes to the nuclear center was analyzed.

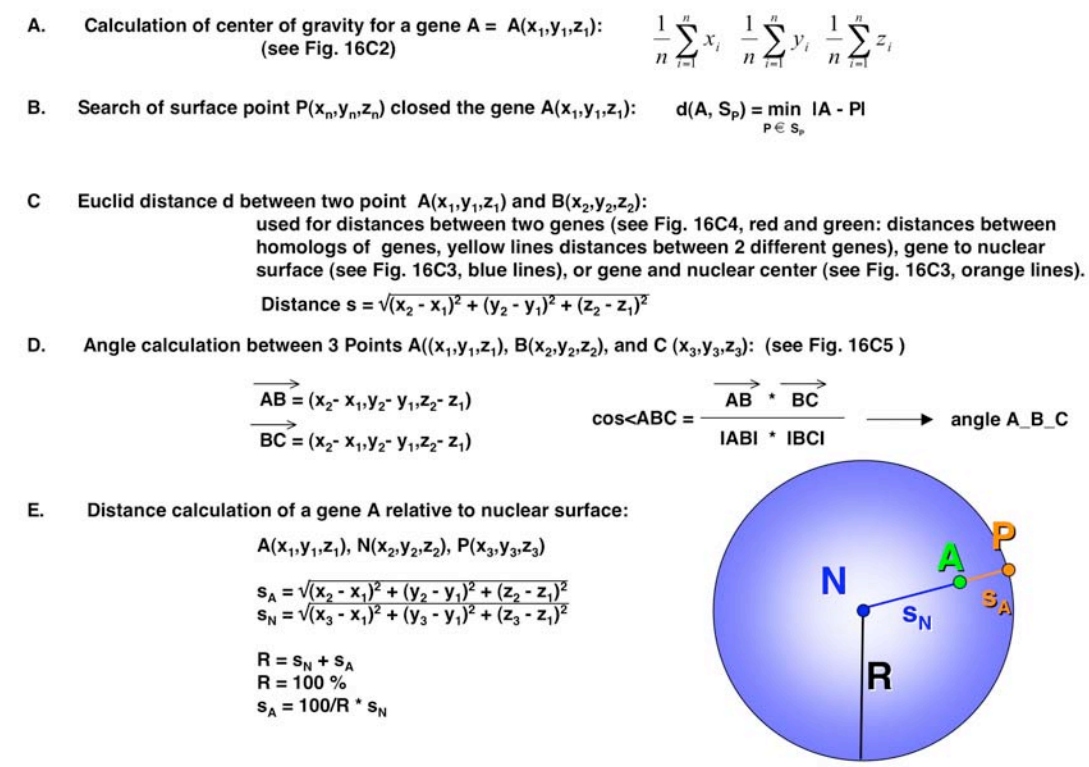

Figure 17: Mathematical formulas underlying the techniques used in this study.
A: Calculation of center of gravity for a gene as visualized in Figure 16C2.
B: Formula to search for a surface point that is closest to a gene.
C: Formula to calculate the Euclid distance between two points.
D: Formula to calculate the angle between 3 points.
E: Calculations to determine the distance of a gene relative to the nuclear surface. The distance of the gene to the nuclear surface is expressed as distance of the gene to the nuclear surface in % of R.
N = center of gravity for nuclear center.
A = center of gravity for gene A.
P = closest surface point to gene A.
S_A = distance between A and P.
S_N = distance between N and A.
S_P = point set (nuclear surface) that contains point P
R = total radius of the nuclear sphere as the sum of S_N and S_A.

5.2.4. Development of a computational tool to determine 3D gene positions in interphase nuclei

One of the tasks of the thesis was to determine the position of genes in the 3D space of the nucleus. Due to the lack of reference points in hematopoietic nuclei, which have a more or less spherical geometry, the only reference points that could be used are the nuclear center and the nuclear surface.

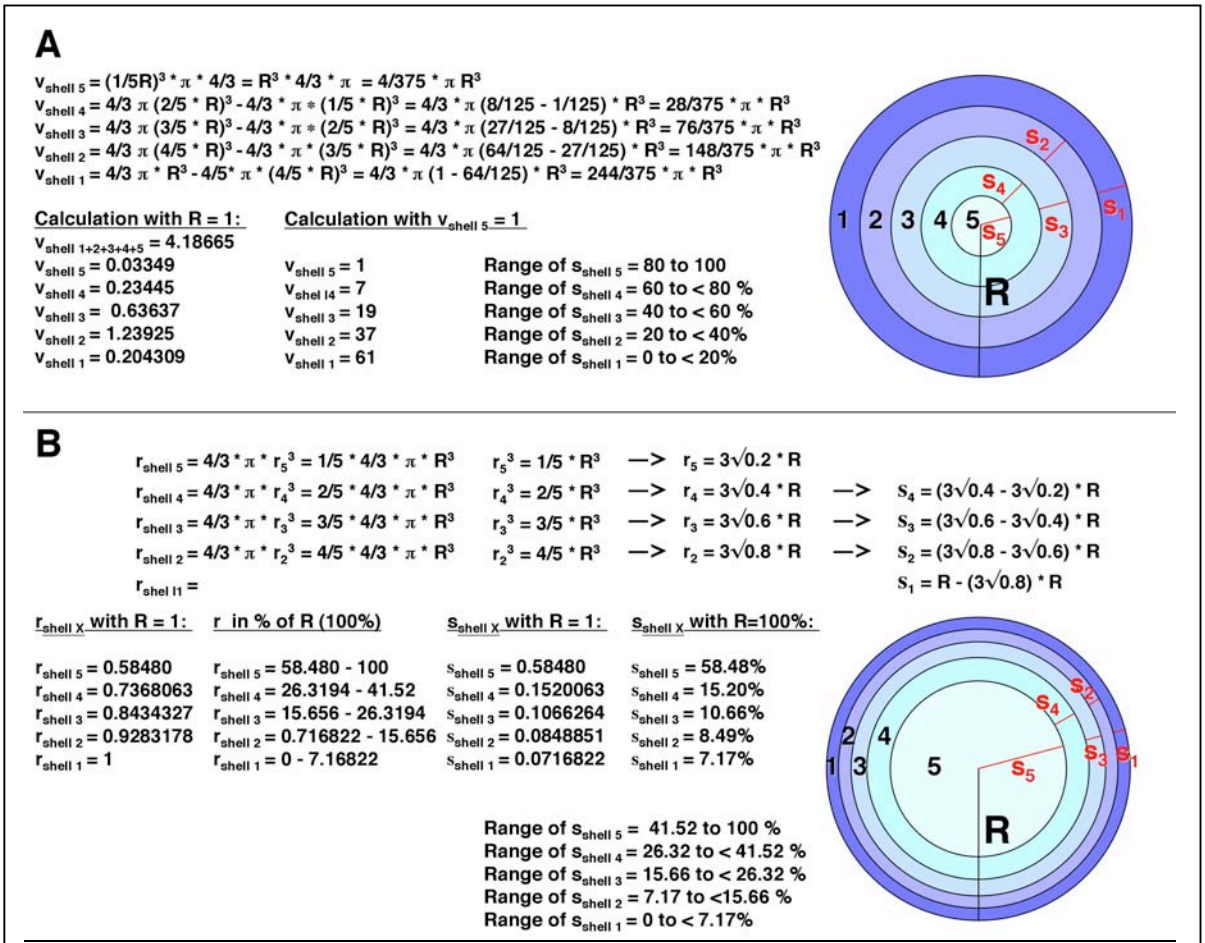

Figure 18: Two different approaches to subdivide the nucleus into 5 concentric shells.

A: Calculations of the volume of 5 concentric shells of equal thickness ($s_{shell\ X}$ = 1/5 of R) = method I.

B: Calculations of the radius of 5 concentric shells with equal volume ($v_{shell\ X}$ = 1/5 of V) = method II.

R = total radius of sphere;

V = total volume of sphere; $r_{shell\ X}$= radius of shell X.

$v_{shell\ X}$ = volume of shell X.

Shell 1 is the most outer, shell 5 the most inner shell.

I therefore developed a mathematically defined system which allowed me to determine the position of genes in the nucleus relative to the nuclear periphery and the nuclear center by dividing the nucleus into five concentrical shells. I had two options. I subdivide the nuclear radius into 5 equal parts resulting in 5 shells of identical depth but highly different volumes

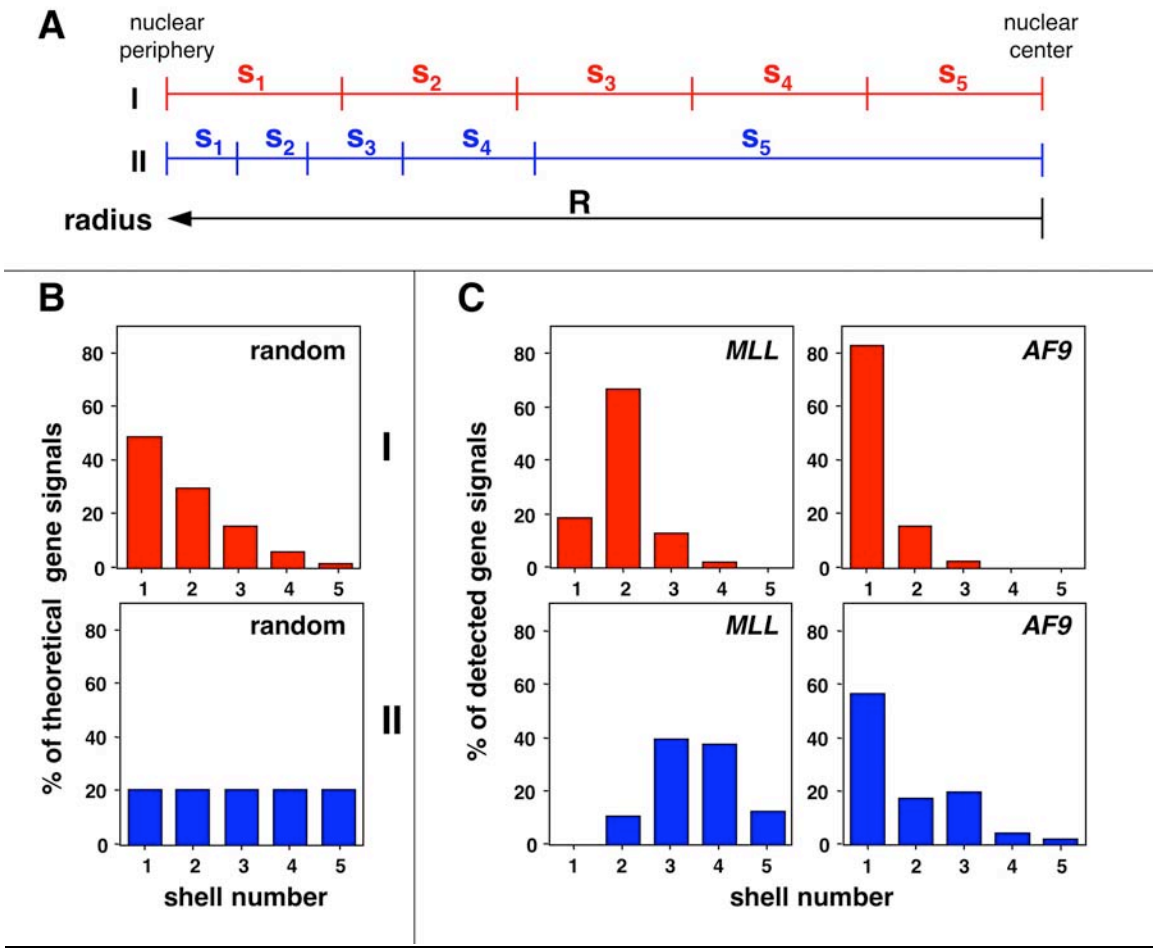

Figure 19: Comparison of the 3D localization of *MLL* and *AF9* in Triggs cells analyzed with the two methods presented in Figure 18.

A: Alignment of the shell thicknesses calculated using methods I and II as shown in Figure 18A and B.

B: Theoretical random distribution of a gene signal within the shells as calculated using method I or II.

C: Comparison of the distribution of *MLL* and *AF9* genes in Triggs cells within the shells as calculated by using method I or II.

(method I) or alternatively I could subdivide the nucleus into 5 shells of identical volume but different depths (method II). A color coded two dimensional representation of these two methods is shown in **Figure 18** including the formulas required to calculate the volumes and the depths of the shells in each model. The radius of each shell was drawn to scale. It is clear that changes of genes localized close to the nuclear surface are better represented using method II (**Figure 18B**). In contrast, changes of genes close to the nuclear center are more apparent using method I (**Figure 18A**). Depending on the type of question, I decided to use both methods to visualize better significant changes in the localization of genes. The difference between using method I and method II to analyze gene localizations is illustrated in **Figure 19** with the genes *MLL* and *AF9* localized in Triggs cells, a EBV-transformed B-cell type, as an example. As shown further down in hematopoietic cells, *AF9* was generally found to be much closer to the nuclear surface than *MLL*. In **Figure 19A** the shell depths obtained by performing an analysis using method I or II are compared. **Figure 19B** shows the theoretical random distribution of a gene in the five shells calculated using method I or II. Regardless of which method was used for the analysis, the localization of *MLL* and *AF9* was very different (**Figure 19C**). *AF9* was positioned much closer to the nuclear surface than *MLL*. With both methods *AF9* was predominantly found in shell #1. In contrast, *MLL*, which was in shell #2 using method I, was localized to shells #3 and 4 when method II was applied. Method II was, therefore, better suited to visualize the differences in the localization of these particular genes.

5.3. The 3-dimensional position of *MLL* and its translocation partners in interphase nuclei of haematopoietic cells

In order to define the localizations of *MLL* and its translocation partners in 3D fixed nuclei, *MLL* and various translocation partners had to be visualized using FISH analysis in different cells. Primarily cells of the lymphoid and myeloid lineages were chosen, in hopes of finding differences or similarities in the gene localization of genes involved in chromosomal translocations, that could provide a basis to explain the occurrence of translocations, which are believed to take place at certain stages of hematopoietic

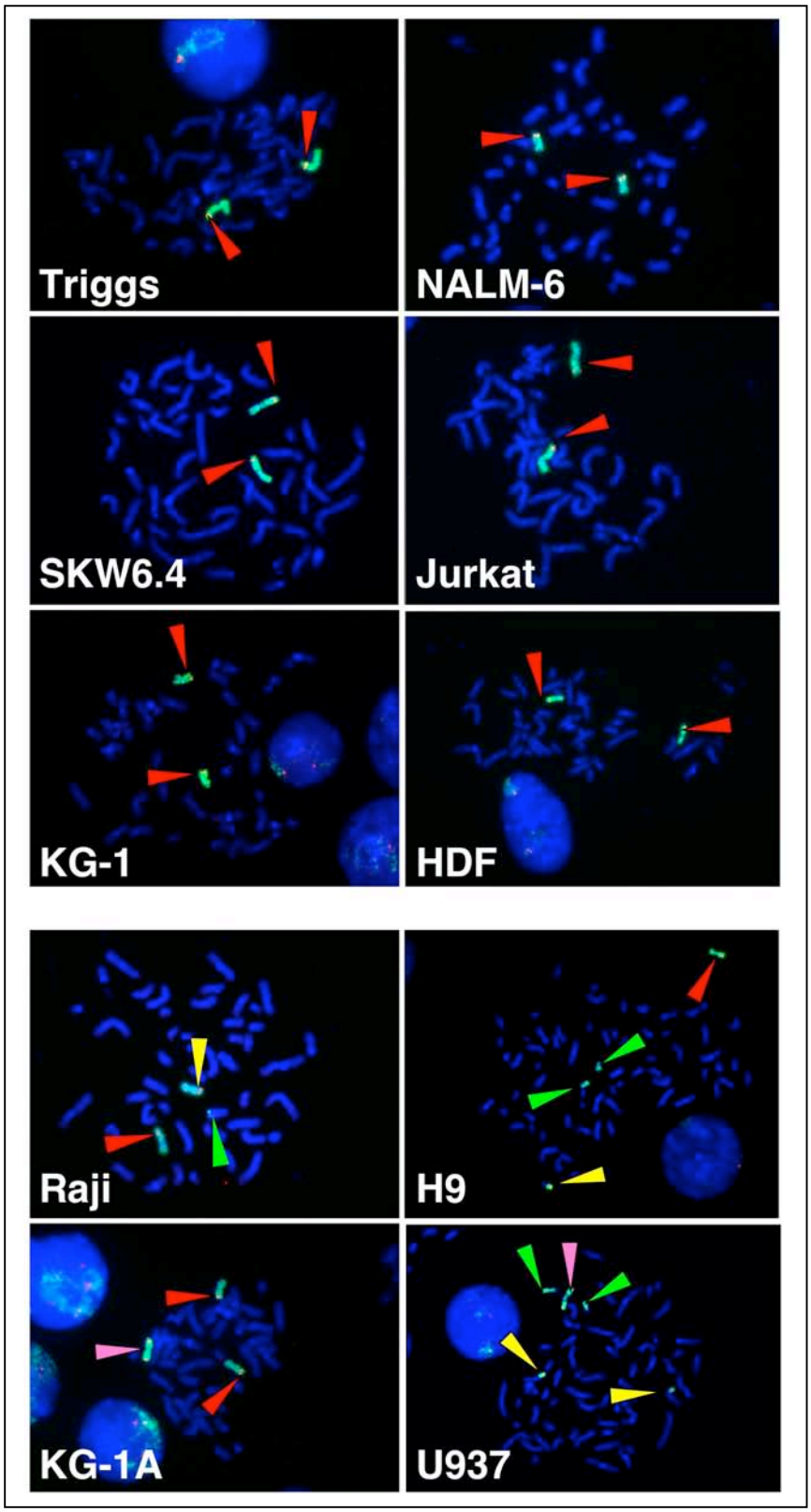

Figure 20: Detection of *MLL* and chromosome 11 on metaphase spreads of 10 different cells.

The upper 5 cell lines (Triggs, Nalm-6, SKW6.4, Jurkat, KG-1) and human dermal fibroblasts (HDF) are normal with respect to chromosome 11 and *MLL*. The bottom 4 cell lines (Raji, H9, KG-1A, U937) have a complex karyotype with translocations involving chromosome 11. Red arrow heads: chromosome 11 with *MLL*. Yellow arrow heads: derivative chromosome carrying t(?;11) including *MLL*. Pink arrow heads: inv(11) carrying 2 *MLL* signals. Green arrow heads: del(11) or t(?;11) without *MLL*.

development (Greaves and Wiemels, 2003). In addition, leukemic cell lines were analyzed, since they are frequently used as an *in vitro* models for the study of hematopoietic differentiation (Drexler and MacLeod, 2003; Pirruccello et al., 1994).

5.3.1. The position of *MLL* in different hematopoietic cells

The localization of genes could be altered by translocation events or by aneuploidy found in tumor cells. One of the objectives was to identify cell lines that either have *MLL* on a normal chromosome 11 or on a derivative chromosome 11 (der(11)). A FISH analysis of *MLL* in combination with a whole chromosome paint for chromosome 11 in various cells

Cell line name	Total of chr 11 signals	Total of *MLL* signals	Detailed description of chr 11 signals and the number of *MLL* signals found with them	
KG-1A	3	4	2 chr 11 1 inv(11q)	2x 1 *MLL* 1x 2 *MLL*
KG-1	2	2	2 chr 11	2x 1 *MLL*
U-937	5	4	2 del(11) 1 inv(11q) 2 t(10;11)(p13;q14) -> *CALM - AF10* fusion gene	none 1x 2 *MLL* 2x 1 *MLL*
HUT-78 subclone H9	4	2	1 chr 11 2 del(11q) 1 t(?;11)(?;q)	1x 1 *MLL* none 1x 1 *MLL*
Jurkat, clone E6-1	2	2	2 chr 11	2x 1 *MLL*
SKW 6.4	2	2	2 chr 11	2x 1 *MLL*
Nalm6	2	2	2 chr 11	2x 1 *MLL*
triggs	2	2	2 chr 11	2x 1 *MLL*
Raji	3	2	1 chr 11 1 del(11) 1 t(?;11qter)	1x 1 *MLL* 1x 1 *MLL* none
HDF	2	2	2 chr 11	2x 1 MLL

Table 7: Summary of the *MLL*-signals and chromosome 11 detected in different cell lines.
chr = chromosome**,** chr 11 = normal chromosome 11, del = chromosome with deletion, der = derivative chromosome, inv(11q) = 2 pieces of chr 11q are fused together inverted to each other, t() = translocation of chromosomes.

and cell lines identified 6 cell types with two normal chromosomes 11 (**Figure 20A**) and 4 cell lines with abnormal chromosomes 11 (**Figure 20B**). A summary of this analysis is shown in **Table 7**. These characterized cells were used to determine the position of *MLL* relative to the nuclear surface (**Figure 21)**. Triggs cells and primary $CD34^+$ and $CD33^+$ cells, isolated from human bone marrow obtained from normal individuals, represent cells with a normal karyotype, whereas Nalm-6, SKW6.4, Jurkat and KG-1 cells were analyzed, all containing an abnormal karyotype but a normal chromosome 11. In contrast, Raji, KG-1A and U937 cells have various abnormalities with either deletion or inversions of chromosome 11.

The analyses using method I (**Figure 21A**) and method II (**Figure 21B**) are shown for comparison. Method I demonstrates that *MLL* is generally located in the second shell. The distribution pattern of the *MLL* gene was therefore remarkably similar in all cells regardless of their karyotype. The localization of *MLL* to the second shell was most pronounced in the Raji cells. This cell line carries a translocation involving chromosome 11, where the q terminal end of one chromosome 11 is translocated to another chromosome. The *MLL* signal remains on the der(11). The localization of the *MLL* signal in shell #2 in the Raji cell line may be dependent on that translocation.

The cell lines KG-1A and U937 both carry 4 copies of *MLL*. The different *MLL* signals in these cells, whether located on normal chromosome 11, der(?;11) or inv(11), seemed to be unaffected and followed the pattern found in cells with just normal chromosome 11. The same undisturbed pattern of *MLL* in the nuclear space was found on a small data set in tri- and tetraploid Triggs cells (**Figure 22**). This analysis suggested that the 3D position of a gene depends mostly on its microenvironment provided by the chromosome it is located on and/or the gene composition of this chromosome and not so much on other chromosomes present in the nucleus.

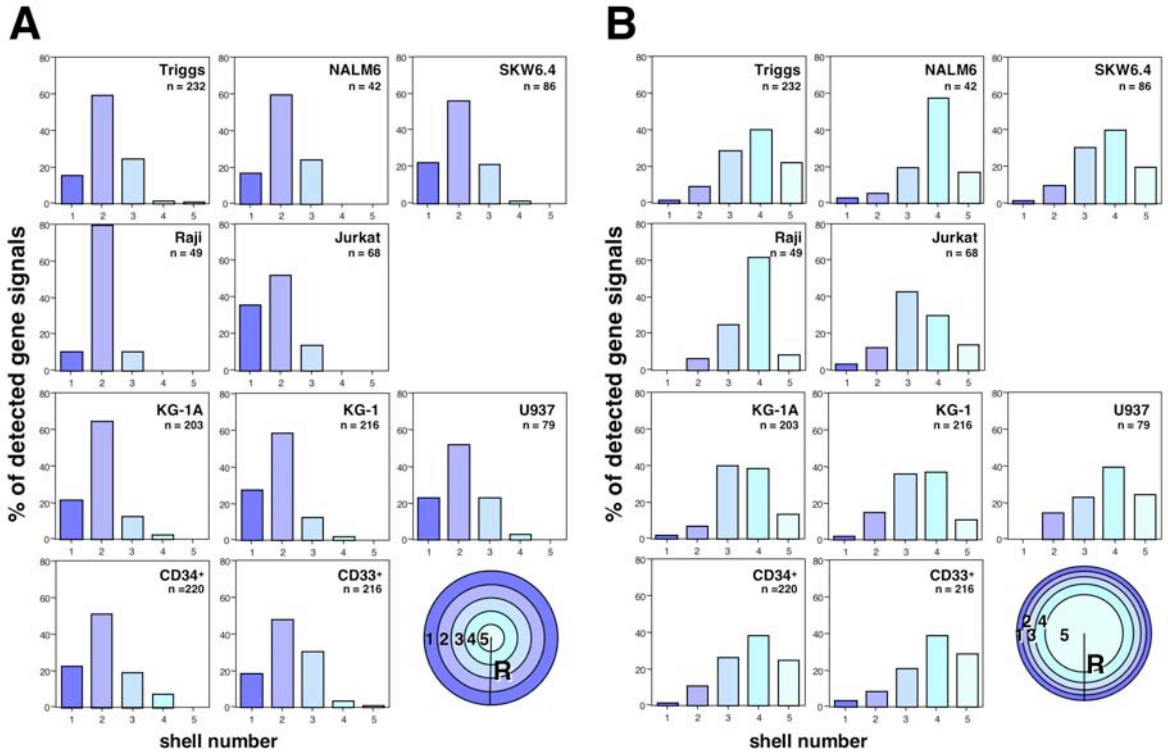

Figure 21: *MLL* has a defined 3D localization in various hematopoietic cells.

A: Analysis of the 3D position of *MLL* using method I: shells of equal radius division as shown in Figure 18A.

B: Analysis of the 3D position of *MLL* using method II: shells of equal volume as shown in Figure 18B.

n = number of analyzed genes.

Triggs, Nalm-6, SKW6.4, Raji, Jurkat, KG-1A, KG-1 and U937 are cell lines. $CD34^+$ and $CD33^+$ cells were primary hematopoietic stem cells and myeloid cells, respectively, (purchased from AllCells, LLC., CA) isolated from bone marrow with a MACS kit, purity of > 90%.

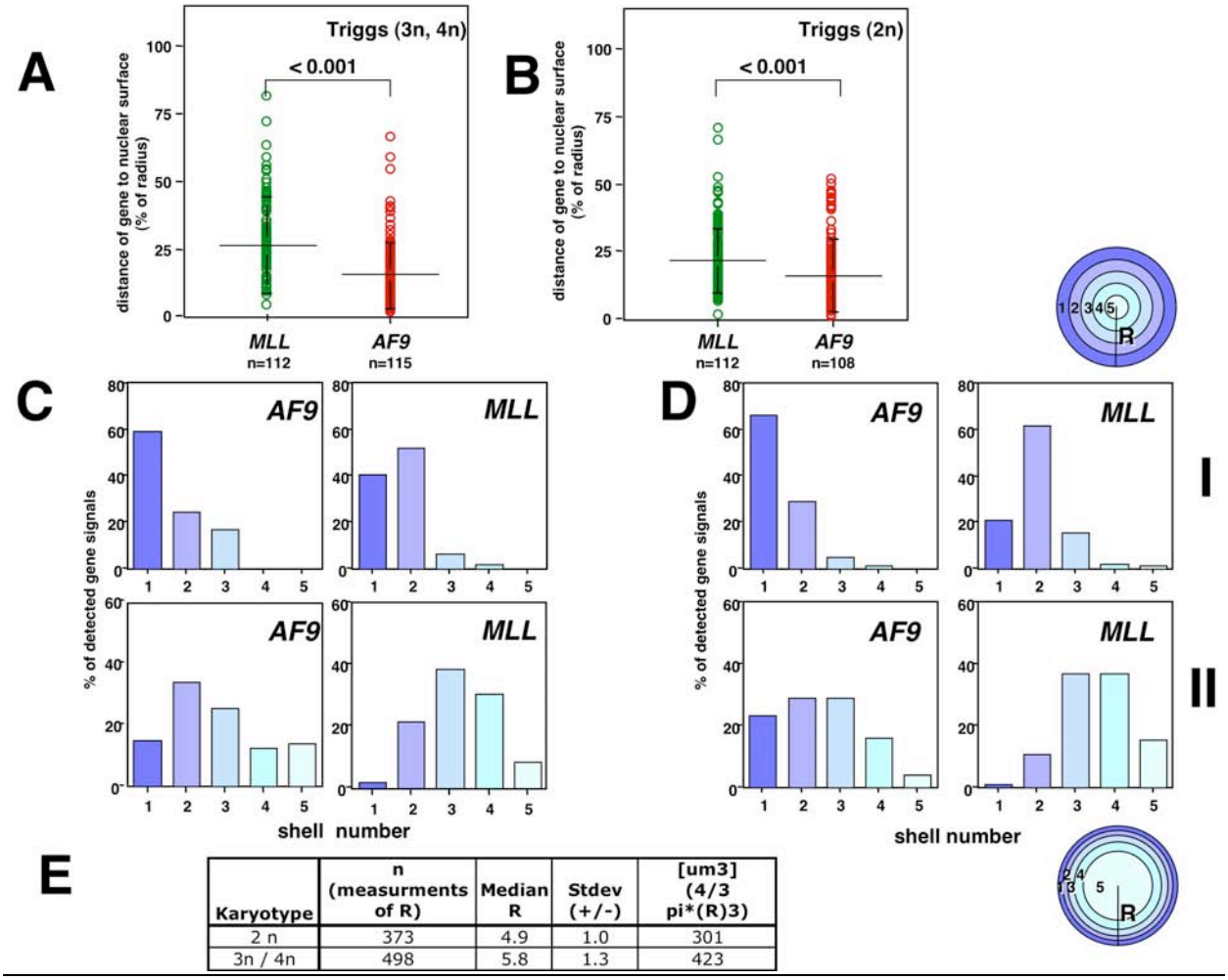

Karyotype	n (measurments of R)	Median R	Stdev (+/-)	[um3] (4/3 pi*(R)3)
2 n	373	4.9	1.0	301
3n / 4n	498	5.8	1.3	423

Figure 22: Chromosome duplications do not affect the localization of their containing genes.

A: Scatter blots representing distance measurements of *MLL* and *AF9* to the nuclear surface in polyploid Triggs cells.

B: Scatter blots representing distance measurements of *MLL* and *AF9* to the nuclear surface in diploid Triggs cells.

C, D: Analysis of the 3D position of *MLL* and *AF9* in polyploid (C) and diploid (D) Triggs nuclei method II described in Figure 18B.

E: R and volume size increase with the polyploidy.

A

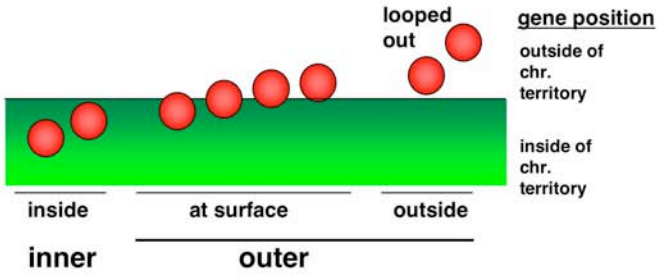

B

Cell type	FISH Probes GSP	WCP	Gene position inner	outer	n
PB	MLL	11	31.15	68.85	122
PB	5' of MLL	11	23.39	76.61	124
PB	3' of MLL	11	27.42	72.57	124
kg1-mll	MLL	11	45.51	54.49	156
kg1-5	3' of MLL	11	38.13	61.88	160
Jurkat	MLL	11	53.45	46.54	58
Jurkat	3' of MLL	11	60.34	39.66	58
SKW64	MLL	11	46.34	53.66	41
SKW64	3' of MLL	11	52.38	47.61	42
Nalm6	MLL	11	44.34	55.66	106
Nalm6	3' of MLL	11	47.22	52.78	108
Triggs	MLL	11	44.32	55.68	185
Triggs	3' of MLL	11	43.33	56.67	180
Raji	MLL	11	44.44	55.55	45
Raji	3' of MLL	11	42.22	57.77	45
HUT-78	MLL	11	55.06	44.95	89
HUT-78	3' of MLL	11	50	50	108
PB	AF9	9	61.5	38.5	52
KG1	AF9	9	59.8	40.2	92
Triggs	AF9	9	54.3	45.7	35

C

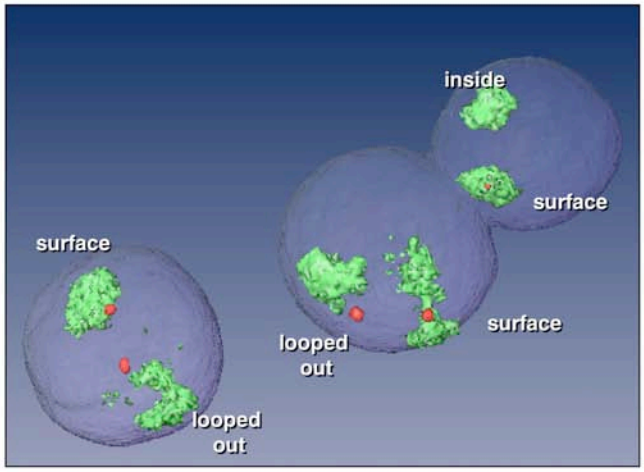

D

Cell type	FISH Probes GSP	WCP	Gene positi on inner	outer	n
CD34+	MLL	11	**22.4**	**77.6**	58
Jurkat	MLL	11	**22.2**	**77.8**	90
SKW64	MLL	11	**29.5**	**70.5**	95
Nalm6	MLL	11	**21.5**	**78.5**	79
Raji	MLL	11	**34.1**	**65.9**	41
U937	MLL	11	**13.6**	**86.4**	81

Figure 23: *MLL* is often found at the surface or outside the chromosome 11 territory.

A: Schematics to illustrate the system used to analyze the localization of *MLL* signal (red spheres) relative to its chromosomal territory (green).

B: Summary of a 2D FISH analysis of the localization of *MLL* in MAA fixed interphase nuclei of various cell lines stained with the listed painting probes. Percent of *MLL* located on the surface or outside the territory (outer) is shown and compared to *MLL* inside the territory (inner).

C: Example of 3D rendered Jurkat nuclei with stained *MLL* (red) and chromosome 11 (green) with scoring example in white letters. The cells were 3D PFA fixed.

D: Summary of the localization of *MLL* in various 3D fixed cells. Position of *MLL* was scored as in B. n = number of genes evaluated.

5.3.2. The *MLL* gene is weakly transcribed and localizes to the surface of the chromosome 11 territory

The gene for *MLL* has a certain probability of localization relative to the nuclear surface. In addition, during FISH analysis it also appeared to often be at the surface or even outside of the stainable territory of chromosome 11. This could be relevant for *MLL*'s propensity to be a major translocation hotspot (Drexler et al., 2004; Futreal et al., 2004). To analyze this systematically, various cells were stained for *MLL* and chromosome 11. In a 2D analysis using a fluorescence microscope, all signals, which clearly located inside the chromosome 11 territory, were scored to have an interior gene position (**Figure 23A**), whereas, all signals either at the surface or outside the territory were scored as having an outer gene position (**Figure 23A**). Analysis of peripheral blood and 7 hematopoietic cell lines confirmed this impression (**Figure 23B**). This localization seems to be characteristic of *MLL*, since a control gene, *AF9*, had a more internal localization. The analysis indicated that in the majority of the hematopoietic cells, *MLL* including the 3' chromosomal regions adjacent to *MLL* is located at the surface or outside of the stainable chromosome 11 territory. Finally, this was confirmed by 3D-analysis of these cell lines, which is shown in **Figure 23D**.

According to the literature, actively transcribed genes are often found at the surface of chromosome territories or in the interchromosomal space (Kurz et al., 1996; Mahy et al., 2002b; Volpi et al., 2000). Given *MLL*'s specific localization, it was therefore interesting to determine whether *MLL* is such a highly transcribed gene. One way to asses the level of transcription of a given gene is to utilize the SAGE (Sequence Analyzed Gene Expression) data. Comprehensive analyses have been accumulated in relevant cells in the Rowley laboratory. I therefore determined the expression levels in the libraries of CD34+, CD15+ cells, Pre-B-cells and Pre-T-cells with the help of Miao Sun (Rowley laboratory). The SAGE libraries used were shown in Table 6. In **Table 8** the level of transcription (expressed as numbers of SAGE tags) of all the translocation partners of *MLL* in these cells is shown. The total number of SAGE tags found per gene was normalized and expressed as tags found in 100,000 tags of each library. The results suggest that none of the *MLL* translocation

partners are highly transcribed genes, at least not according to SAGE-libraries examined derived from different tissues.

Chr	Chromosomal Band	Name of SAGE libary -- Name of gene (alphabetic order)	CD34	CD15	pre-B	pre-T	Number of SAGE tags found for gene
1	1p32	*AF1P*	2	3.81	2.73	10.1	*3*
1	1q21	*AF1q*	0	0	0	0	*0*
2	2q11.2-q12	*LAF4*	0	1.9	0.91	5.03	*3*
3	3p21	*AF3P21*	0	0	0	5.03	*1*
3	3q24	*GMPS*	2.001	2.857	0	0	*1*
3	3q28	*LPP*	1	2.857	1.818	10.06	*3*
4	4q21	*AF4*	4.002	1.905	0	5.03	*2*
5	5q31	*AF5q31*	0	0	0	0	*0*
5	5q31	*GRAF*	2.001	4.762	1.818	5.03	*4*
6	6q27	*AF6*	0	0.952	0	0	*1*
6	6q21	*AF6q21*	0	0	0	0	*0*
8	8q22	*CBFA2T1*	0	0	0	0	*0*
9	9p22	*AF9*	0	0	0	0	*0*
9	9q23	*FBP17*	0	0	0	0	*0*
10	10p11.2	*ABI1*	3.001	2.857	4.545	5.03	*3*
10	10p12	*AF10*	0	0	0	0	*0*
10	10q21	*LCX*	0	0	0	0	*0*
11	11q23.3	*CBL*	4.002	1.9	1.818	0	*2*
11	11q23.3	*LARG*	0	0	0.909	5.03	*1*
11	11q23	*MLL*	9.004	5.714	1.818	10.06	*6*
11	11q14	*PICALM*	3.001	8.571	6.363	15.09	*3*
14	14q24	*GPHN*	0	0	0	0	*0*
15	15q14	*AF15Q14*	3.001	0.952	0	0	*1*
16	16p13.3	*CBP*	1	2.857	0	0	*2*
17	17q21	*AF17*	3.0	1.0	4.545	5.03	*1*
17	17p	*GAS7*	0	1.905	3.636	5.03	*2*
17	17q11-q21.3	*LASP1*	0	0	0	0	*0*
17	17q25	*MSF*	2.001	9.523	1.818	5.03	*1*
19	19p13.3	*EEN*	1	1.9	2.73	0	*1*
19	19p13.1	*ELL*	0	0	0	0	*0*
19	19p13.3	*ENL*	0	0.95	0	0	*1*
22	22q13	*EP300*	1	0.952	0	5.03	*2*
22	22q11.2	*hCD Crel*	0	2.857	1.818	0	*1*
X	Xq13.1	*AFX1*	0	1.9	2.73	0	*1*
X	Xq24	*SEPT6.*	3.001	2.857	1.818	5.03	*3*
2	2q33	*caspase 10*	0	0	0	0	***0***
2	2q33	*caspase 8*	0	0	0	0	***0***
8	8q34	*MYC*	3.001	0.952	2.727	0	***1***

color code #
0
1
2
3
4
5
6
7
8
9
10
11
12
13
14
15
16
17
18
19
20
21
22
23
24
25-50
>50

Table 8: Expression of *MLL* and 38 sequenced translocation partners in hematopoietic SAGE-libraries.
Displayed are the sum of all SAGE-tags found that were unique to each gene and normalized "per 50,000 tags".
The numbers in the color code give the upper limit for each color. The color indicates the number of tags found per gene in each SAGE-library.

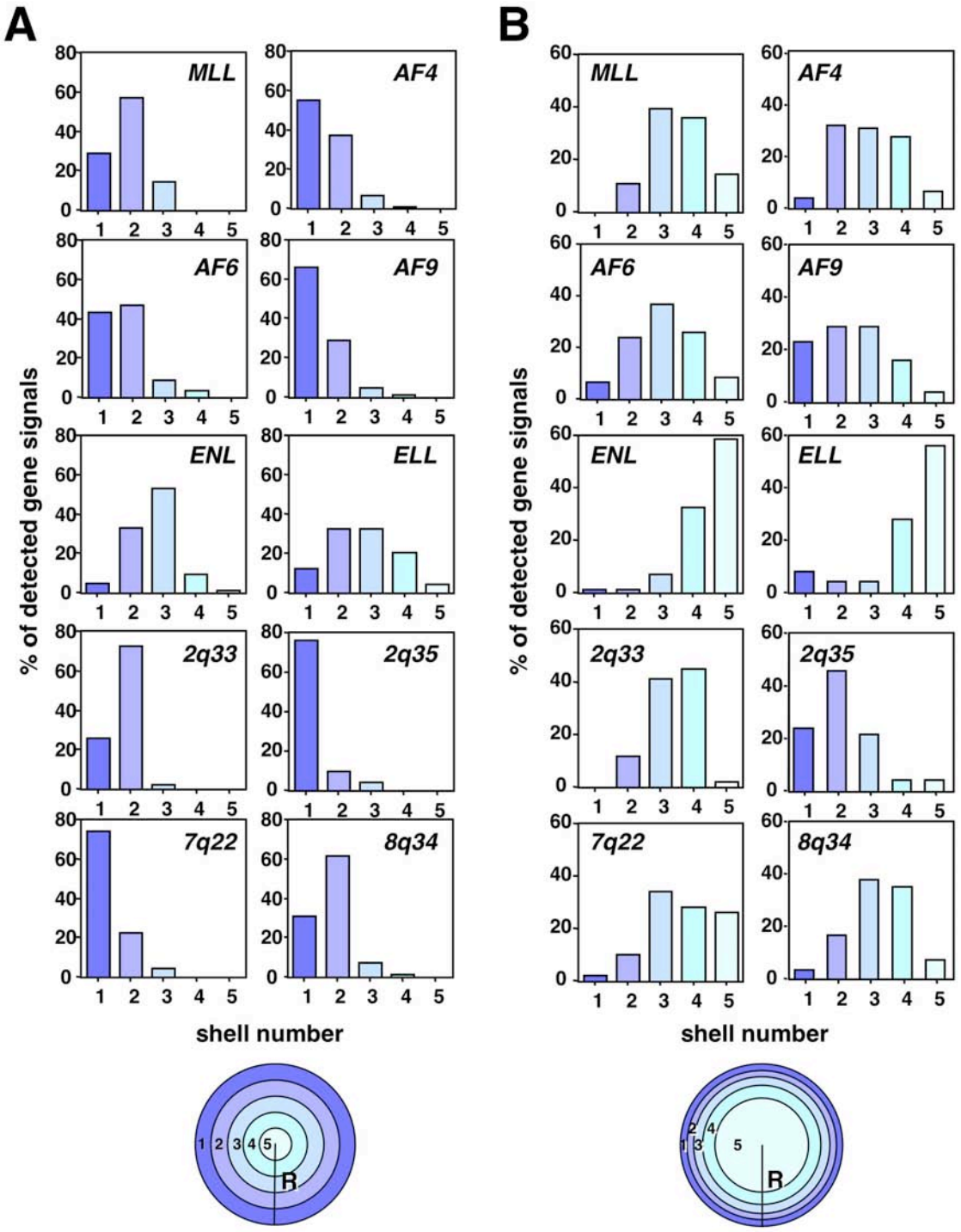

Figure 24: Comparison of the position of various genes in 3D fixed nuclei of Triggs cells.

A: Analysis of the 3D position of genes using method I: shells of equal radius division as shown in Figure 18A.

B: Analysis of the 3D position of genes using method II: shells of equal volume as shown in Figure 18B.

All cells were PFA fixed and 3D-FISH was performed. The combination of FISH-probes was performed with the *MLL* clone as a reference. For gene location and position of the clones used for detections, refer to Figures 5-8 and Tables 1 and 4.

5.3.3. *MLL* and its translocation partners have characteristic distances to the nuclear surface in hematopoietic cells

After establishing a consistent localization of *MLL* in hematopoietic cells, the localization of *MLL* was compared to five of its translocation partners. Triggs cells were chosen for this analysis, since they have a normal karyotype for all chromosomes. The analysis of *MLL* and *AF9* already established that they localize to different shells. In addition to *MLL* and *AF9*, the positions of the *MLL* translocation partners, *AF4*, *AF6*, *ENL*, *ELL*, and a set of control loci (2q33, 2q35, 7q22, and 8q34) were analyzed (**Figure 24**). The control loci were chosen from chromosome regions that have not been reported to

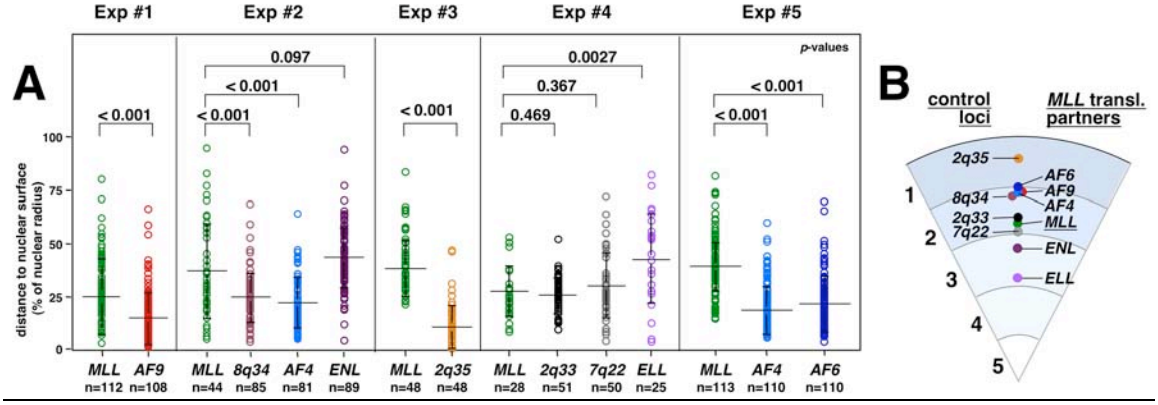

Figure 25: Genes have a characteristic localizations relative to the nuclear surface.
A: Scatter blots representing 5 experiments on the Triggs cells of distance measurements of various genes to the nuclear surface: *MLL*, 5 of its frequent translocation partners (*AF4*, *AF6*, *AF9*, *ENL* and *ELL*) and 4 control loci (2q33, 2q35, 7q22, 8q44). Each circle represents one measurement. The median values with error bars and the *p*-values are displayed. n = number of measurements.
B: Summary of the shell localization of all genes shown in A, after normalizing the distances to the position to *MLL* in each experiment.

translocate with *MLL* or 11q23 at the time of the experiments. Analyzed again by both methods, it is evident that each gene and chromosomal locus shows a characteristic distribution pattern in the interphase nucleus, with the extremes being 2q35 with the most exterior position, and the genes *ENL* and *ELL* on 19p13 at the most interior nuclear position. As predicted, the differences in 3D localization of a gene relatively close to the nuclear

center, such as *ENL* and *ELL*, was most obvious in the analysis using method II (**Figure 24B**). In contrast, a locus with a peripheral localization such as 2q35 was best separated from *MLL* in the analysis using method I (**Figure 24A**). **Figure 25** shows the defined localizations of all these genes in Triggs cells in scatter plots as determined in 5 different experiments, which were the basis for the summary shown in **Figure 25B**. The mean positions of all genes were normalized to the position of *MLL* in each experiment and plotted accordingly using method I. Interestingly, the distribution of the 3 most common translocation partners *AF6*, *AF9* and *AF4* was found to be remarkably similar. While they

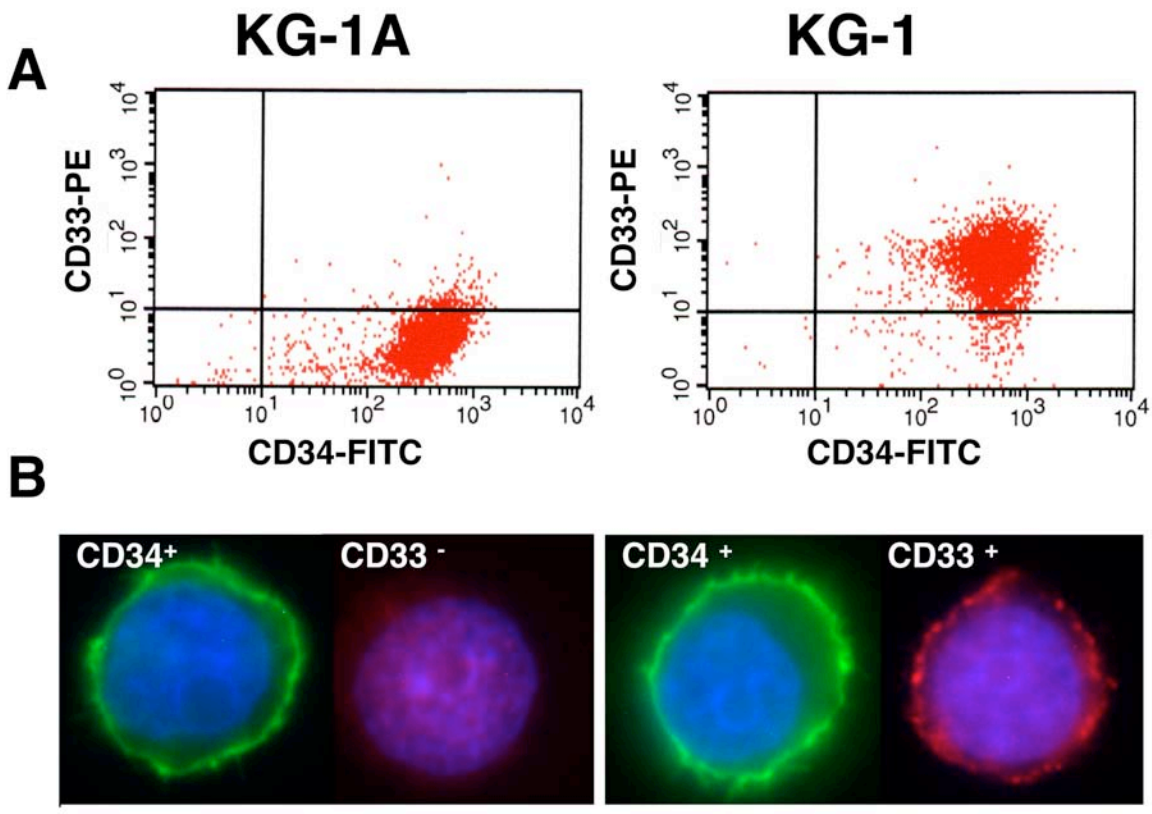

Figure 26: Expression of CD33 and CD34 on the lymphomyeloid stem cell lines KG-1 and KG-1A.
A: Dot blot of double staining for CD33 and CD34 derived from flow cytometry.
B: Immunofluorescence microscopy of KG-1 (left) and KG-1A (right) cells stained for CD34 and CD33.

As translocations are believed to occur at certain stages of hematopoietic development the analysis was extended to include both primary HSCs as well as a pair of cell lines representing such different stages of development. The cell line KG-1 and its less differentiated daughter cell line KG-1A represent an early stage of differentiation. KG-1 is assumed to have been derived from a common myeloid-lymphoid progenitor and KG-1A is a dedifferentiated variant of KG-1 (Bailly et al., 1995). According to one analysis both cell lines express CD34, but not CD33 (Bailly et al., 1995). However, the German collection of microorganisms and cell culture (www.dsmz.de) described both cell lines to express both CD34 and CD33. In contrast to both these descriptions the two cell lines used in this work showed a differential surface expression of the surface marker CD33 (**Figure 26**). The CD33 surface antigen could not be detected for the KG-1A cell line, but it was expressed on the more differentiated KG-1 cell line. These two cell lines were initially described in 1980 (Koeffler et al., 1980). It is possible that both cell lines show a variability regarding the CD33 antigen. To exclude any mix-up of these cells (obtained from the ATCC), their described karyotype regarding chromosome 11 (Mrozek et al., 2003) was confirming by FISH analysis (see Figure 20). The 3D localizations of *MLL*, *AF9*, *ENL* and 2q35 were determined in both cell lines (**Figure 27**). In general, 4 signals for *MLL*, 3 signals for *ENL*, and 2 signals for both *AF9* and 2q35 were observed in KG-1A, whereas 2 signals for each region were found in KG-1. Despite these differences all genes in both these cell lines again showed the same general distribution pattern.

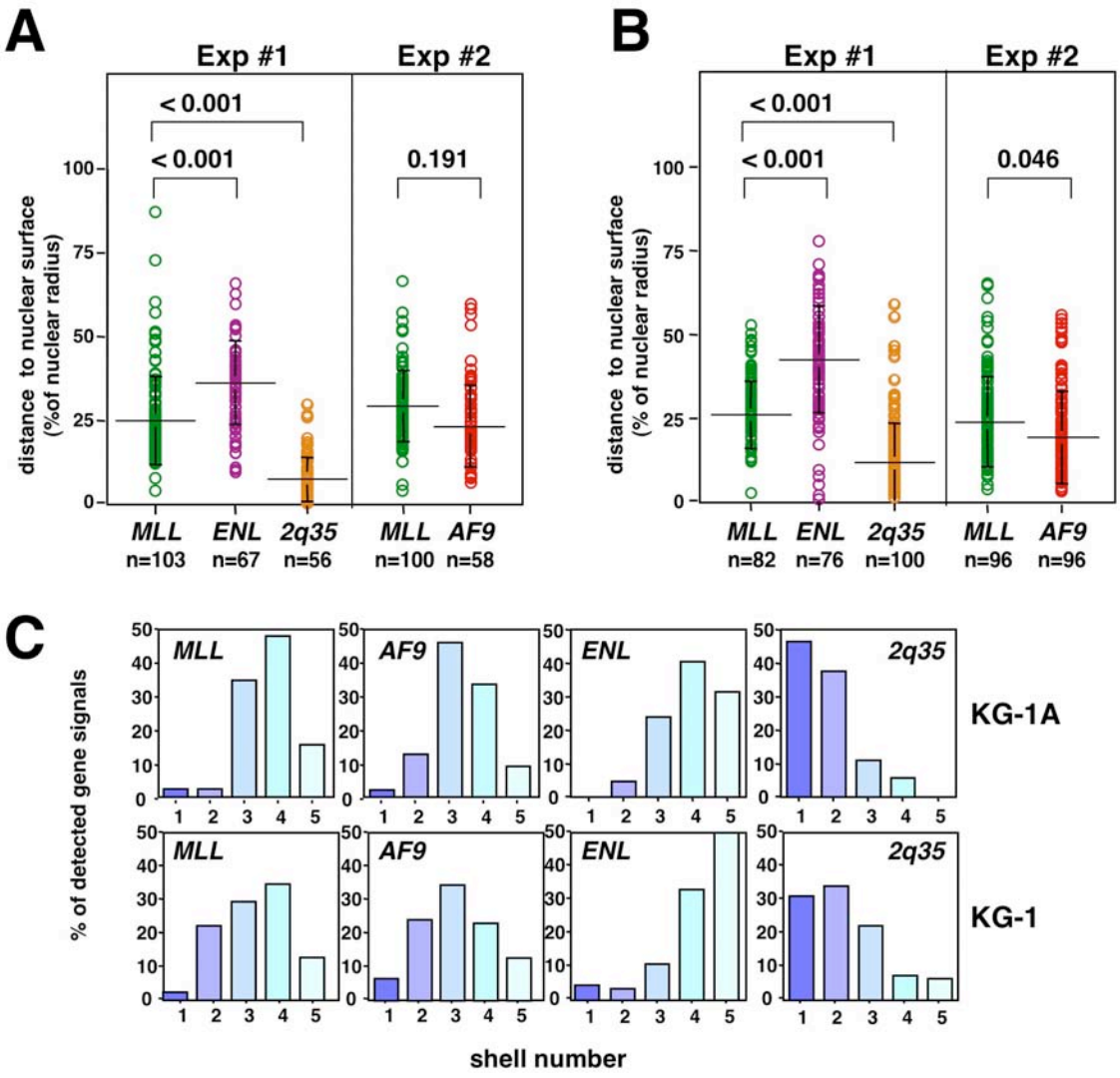

Figure 27: Chromosome duplications do not affect the localization of their containing genes.

A: Scatter blots representing 2 experiments of distance measurements of *MLL*, *ENL*, *AF9* and one control gene to the nuclear surface in KG-1A cells.

B: Scatter blots representing 2 experiments of distance measurements of *MLL*, *ENL*, *AF9* and one control gene to the nuclear surface in KG-1 cells.

C: Analysis of the 3D position of *MLL*, *ENL*, *AF9* and a control gene in KG-1A and KG-1 cells using method II described in Figure 18B.

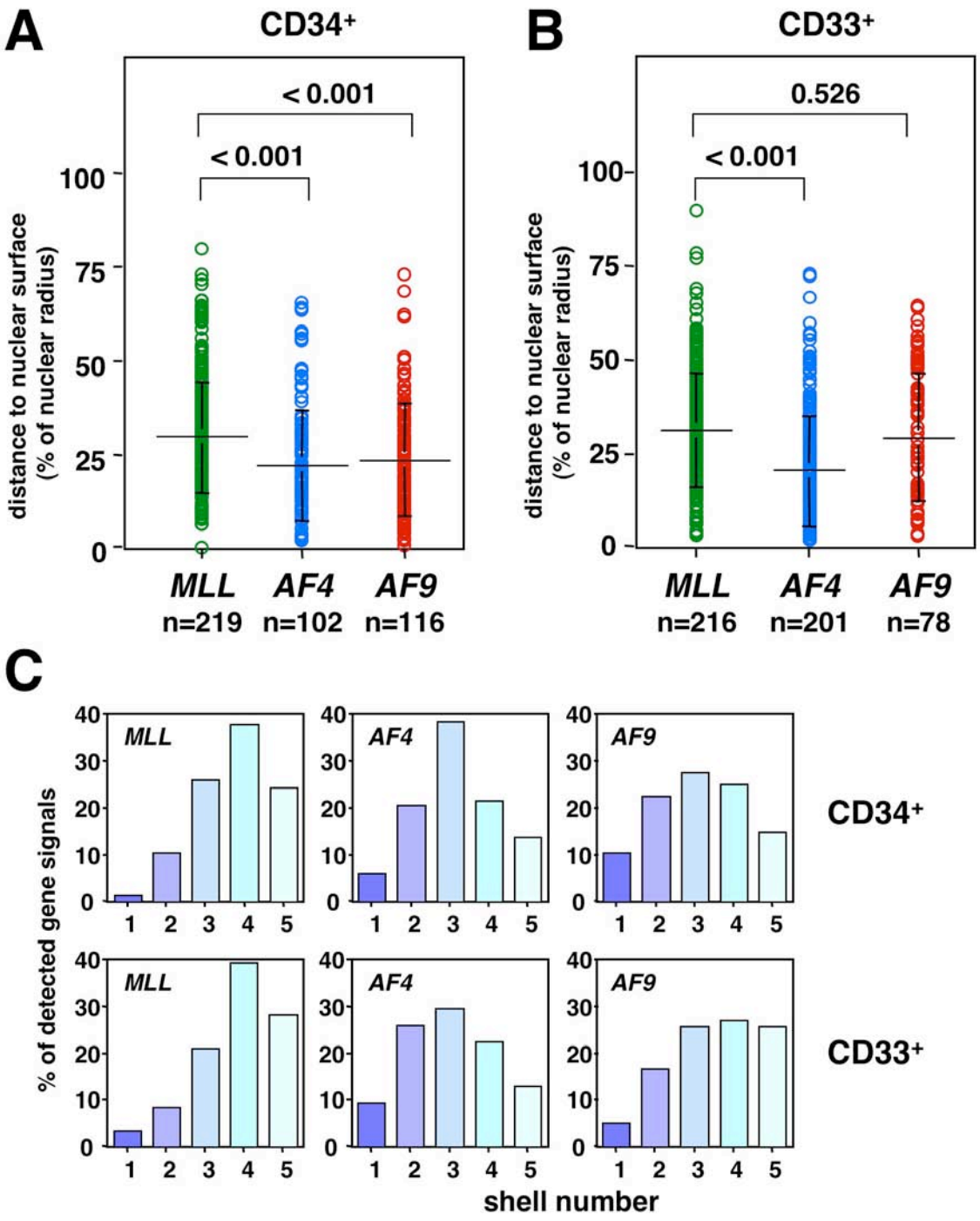

Figure 28: No difference in the 3D localization of *MLL*, *AF4* and *AF9* between primary CD33+ and CD34+ cells.

A: Scatter blots representing distances of *MLL*, *AF4*, *AF9* to the nuclear surface in CD34+ cells.

B: Scatter blots representing distances of *MLL*, *AF4*, *AF9* to the nuclear surface in CD33+ cells.

C: Analysis of the 3D position of *MLL*, *AF4*, *AF9* in CD34+ and CD33+ cells using the method II described in Figure 18B.

Finally, primary cell material of normal donors was analyzed. The data represented in **Figure 28** are the result of multiple experiments on slides with cells of the same isolation, fixed at the same time. The distribution pattern of all genes was again very similar to the one observed in the cell lines (see Triggs in Figure 24, KG-1 and KG-1A in Figure 27). In summary, a predictable distribution of individual genes seems to be a general finding for all hematopoietic cells. Interestingly, chromosome duplications do not seem to affect the localization of their containing genes. This can be concluded from the analysis of the KG-1 and KG-1A cells, since only KG-1A cells have an additional inv(11) chromosome and therefore carry 4 *MLL* genes and from the analysis of polyploid Triggs cells (see Figure 22).

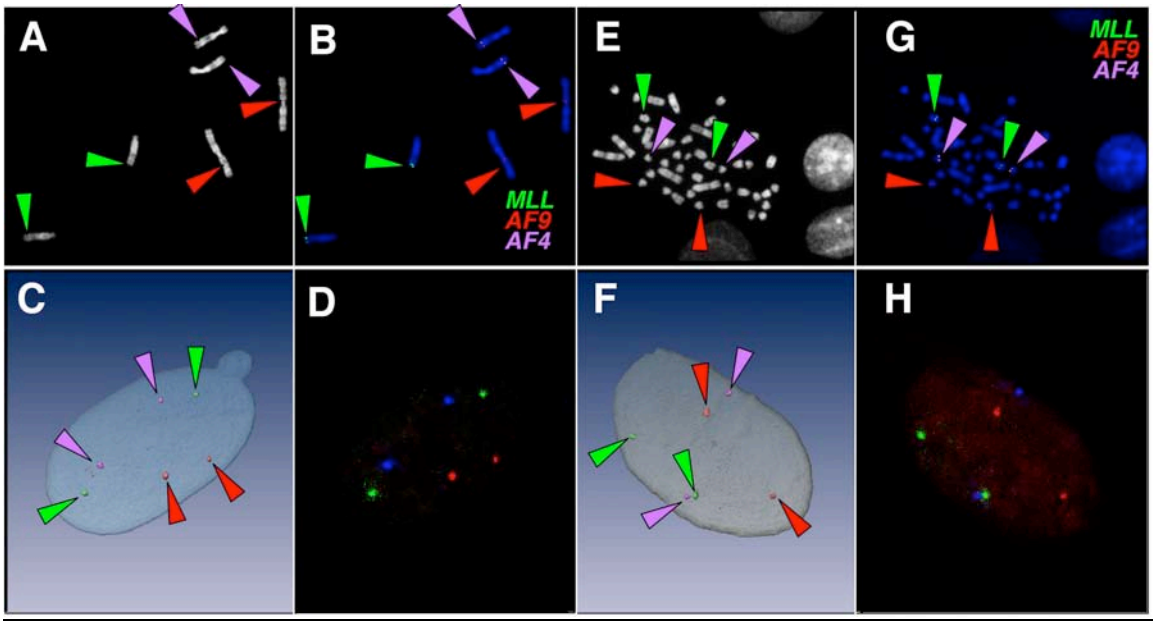

Figure 29: Localization of *MLL*, *AF4* and *AF9* in fibroblasts of 2 different muntjac species.
A-D: Analysis of Indian muntjac.
E-H: Analysis of Chinese muntjac.
A, B, E, G: FISH on MAA fixed metaphase chromosomes,
C, D, F, H: 3D-FISH on PFA fixed material.
C, F: Nucleus volume rendered with the Amira program.
D, H: Total projection of a confocal image stack.
Green arrow heads: *MLL* signals. Purple arrow heads: *AF4* signals. Red arrow heads: *AF9* signals.

5.3.4. Comparison of the position of *MLL*, *AF4* and *AF9* in fibroblasts of human and two muntjac species

The data so far indicated that *MLL* and some of its translocation partners have a defined and predictable 3D localization in the nucleus of multiple hematopoietic cells. It has been described before that conservation of chromatin positions are not limited to hematopoietic cell types or tumor cells. For human fibroblasts conserved positions of chromosome territories have been described (Cremer et al., 2001; Croft et al., 1999). To address the question of whether the genes tested in hematopoietic cells also have a defined 3D localization in other cell types, human dermal fibroblasts were analyzed using the combination of techniques developed for and applied to hematopoietic cells. In addition, this experiment also allowed to address the question of whether there are species specific differences. *MLL*, *AF4*, and *AF9* were stained in *M. muntjak* and *M. reevesi* fibroblasts and compared to data obtained with human fibroblasts. The genes for *MLL*, *AF4* and *AF9* in the muntjac species were detected using the corresponding cattle probes described in Table 4. Typical stainings and 3D analysis are shown in **Figure 29**. *MLL*, *AF4*, and *AF9* are located on 3 different chromosomes in both species. (*M. muntjak*: *MLL* on chromosome 2q36-38, *AF4* on chromosome 1p12-p13, *AF9* on chromosome 3q39; *M. reveesi*: *MLL* on chromosome 10, *AF4* on chromosome 21, *AF9* on chromosome 19). The distribution of all 3 genes was analyzed in fibroblasts of the three species (**Figure 30)**. As mentioned earlier, the shell analysis methods used for hematopoietic cells could not be applied to fibroblasts, due to the difference in geometry of the fibroblast nuclei. Therefore the distances of the genes to the center of gravity of the nucleus were compared. Triggs cells were analyzed in the same way for comparison. The distribution pattern in fibroblasts of the three species was different from the pattern found in Triggs cells. In all fibroblasts, *MLL* had the largest median distance to the nuclear center, whereas *AF4* and *AF9* shared a similar but shorter distance. In contrast and consistent with the 3D analysis of all hematopoietic cells, the distance of *MLL* to the nuclear center in Triggs cells was on average the shortest. This points at an interesting difference in localization of certain genes between hematopoietic cells and other tissues such as fibroblasts.

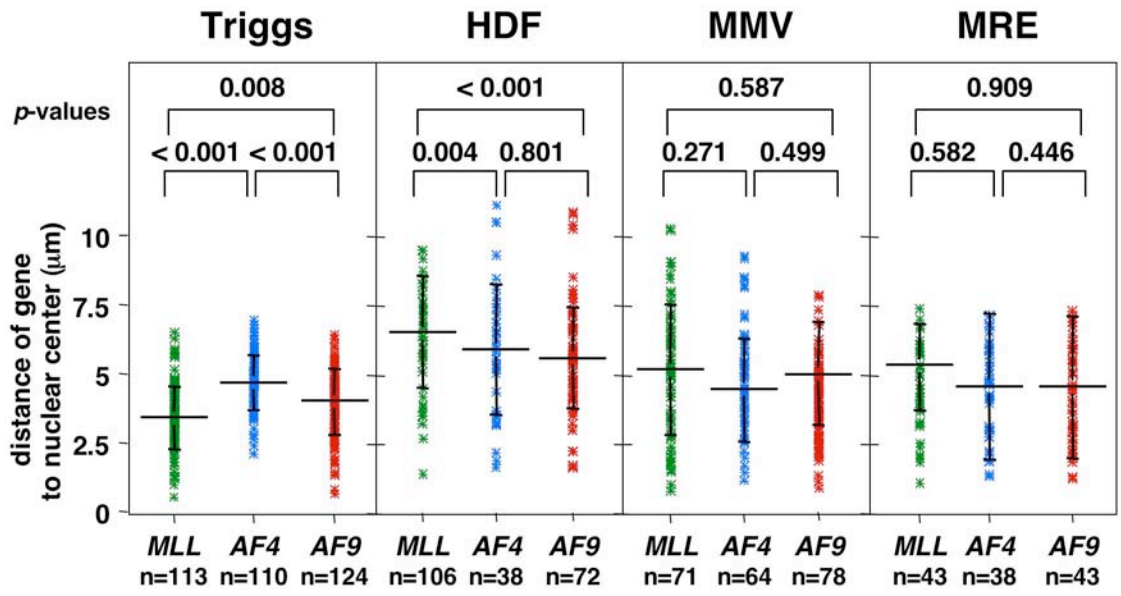

Figure 30: Comparison of the 3D positions of *MLL*, *AF4* and *AF9* relative to the nuclear center in fibroblast nuclei from different species.
Distance measurements of *MLL* to nuclear center in Triggs (B-lymphoblastoid cells), HDF (human dermal fibroblasts), MMV (Indian muntjac fibroblasts), MRE (Chinese muntjac fibroblasts). Values in µm. n = number of measurements. Values for standard deviation and significance (*p*-value, student t-test). Green = *MLL*, blue = *AF4*, red = *AF9*.

5.3.5. Distances between *MLL* and other genes in hematopoietic cells

The composite data clearly indicate that *MLL* and its translocation partners have specific and defined localizations in hematopoietic cell nuclei. These localizations were described as distances from the nuclear surface raising the question, whether the distances between *MLL* and its translocation partners were also defined. The results of this analysis are shown in **Figure 31**. Measurements of gene distances between different genes have been published by others, but their analyses were generally done using 2D FISH (Roix et al., 2003; Taslerova et al., 2003; Volpi et al., 2000) and *MLL* has not been studied yet. In contrast, the analysis of the distances of *MLL* to other gene locations in this work was

performed in 3D. The data were plotted in 1 µm steps (**Figure 31**). The distance that chromatin moves during interphase is 2 µm (Chubb et al., 2002) and was therefore considered for this thesis to be a critical distance, for a translocation to occur (Roix et al., 2003). A polynomial curve fit of second order was applied to better visualize the differences. The data reveal that a distance of 2 µm or less between *MLL* and a translocation partner was a rare event. The closest distance measured in this analysis was between *MLL* and *ENL* in both cell lines tested (Triggs in **Figure 31A** and KG-1 in **Figure 31B**). In conclusion, it appears that the distance of two genes is a function of the relative distribution pattern of a gene in the nucleus.

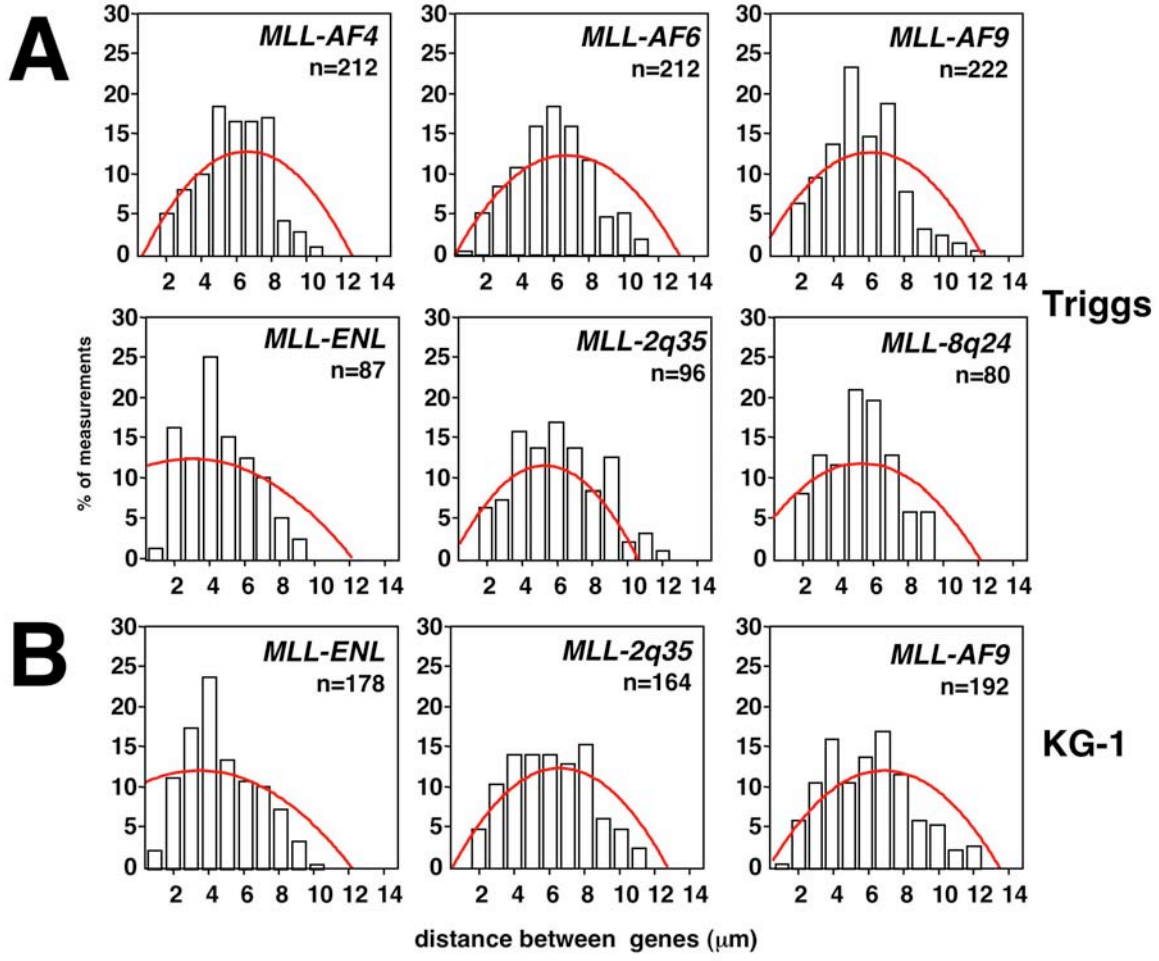

Figure 31: Distances of *MLL* to some of its translocation partner genes.
A: In Triggs cells.
B: In KG-1 cells.
Red line: Curve fit (polinome 2nd order).

As another parameter to describe the distance between different genes or the two alleles of one gene in the same nucleus, the angle differences between genes was determined. Angles were defined as the angle between two genes/alleles with the nuclear center as the angle origin. A predicted angle of two genes, which are distributed independently of each other in the nucleus, should be 90° and this was the result of the analysis (**Figure 32A)**. Individually measured angles between the two *MLL* alleles, between *MLL* and *AF9* and between the two *AF9* alleles are shown in **Figure 32B-D**. These data demonstrate that while genes that are located on different chromosomes are not linked and do not have a predictable position in the nucleus (i.e. are polarized to one side of the nucleus), they have certain probabilities to be found in the different shells defined above.

5.3.6. DNA damage does not affect the 3D positions of *MLL* and *AF9* relative to the nuclear surface

If genes do not have predictable neighborhood relationship (i.e. are adjacent to each other) according to the data presented, how then could one explain, that under certain circumstances genes such as *MLL* are involved in translocations with one group of genes and not with others? This is especially puzzling, because the data suggest that *AF9* and *MLL* clearly have a high probability to be localized in different shells.

For instance *AF9* is closer to the nuclear surface, *MLL* is closer to the nuclear center. However, translocation events may occur as a result of cellular stresses such as DNA damage or induction of apoptosis, which can cause changes in chromatin structure as well as DSBs (Graeves, 2003). The prediction therefore would be that the localization of translocation partners such as *MLL* and *AF9* might change in response to such stress. To test this hypothesis, the 3D localization of *MLL* and *AF9* in Triggs cells after induction of DNA damage was determined (**Figure 33).** As an inducer of DNA DSB/apoptosis, the topoisomerase II inhibitor, VP16, was used. As in other cell types, in untreated Triggs cells *AF9* was found to be closer to the nuclear surface than *MLL*.

A

	n	AVERAGE	MEDIAN	STDEV	SEM
MLL_NC_MLL	43	85	89	48	7
AF9_NC_AF9	43	88	94	48	7
MLL_NC_AF9	172	90	90	45	3

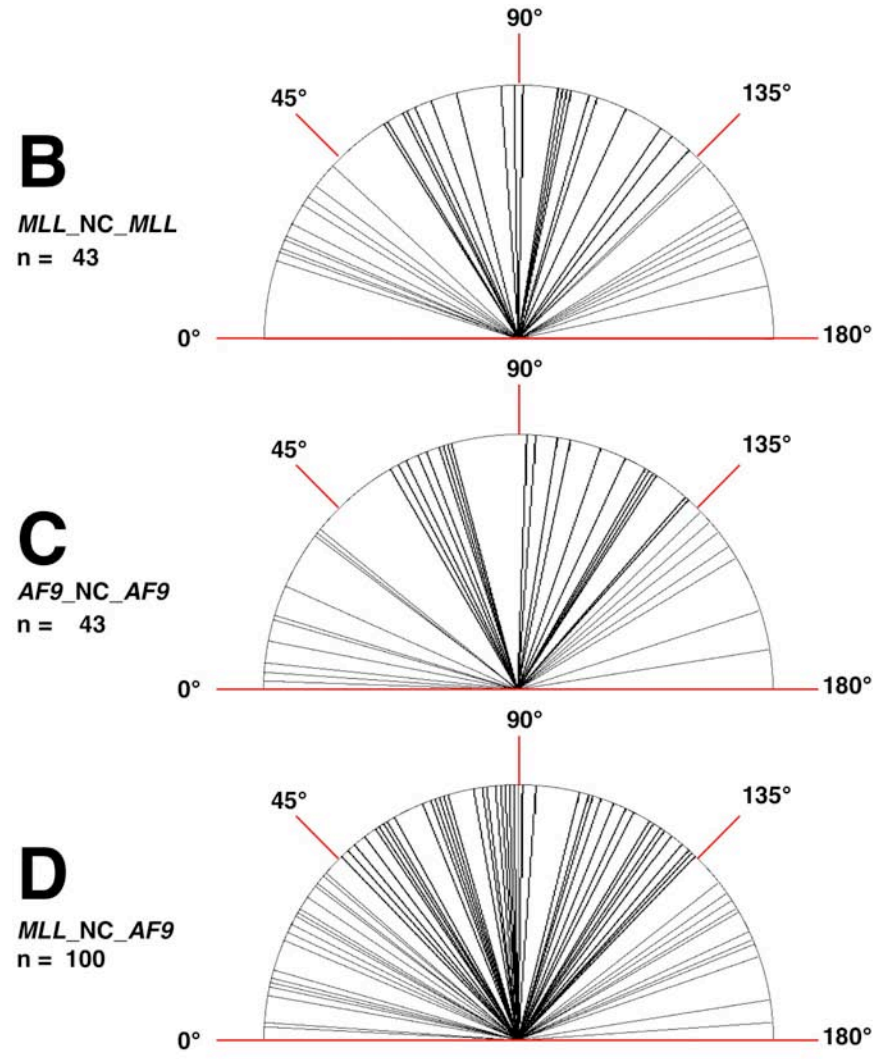

Figure 32: Angle widths between *MLL*/*AF9* alleles using the nuclear center as the angle origin.

A: Summary of the measurements of the nuclear angles between the two *MLL* alleles (*MLL*_NC_*MLL*), the two *AF9* alleles (*AF9*_NC_*AF9*), and between all *MLL* and *AF9* alleles (*MLL*_NC_*AF9*) in interphase nuclei with the nuclear center (NC) as turning point of the angle.

B: Graphical representation of all calculated *MLL*_NC_*MLL* angles.

C: Graphical representation of all calculated *AF9*_NC_*AF9* angles.

D: Graphical representation of all calculated *MLL*_NC_*AF9* angles.

NC = nuclear center, STDEV = standard deviation, SEM = standard error of the mean.

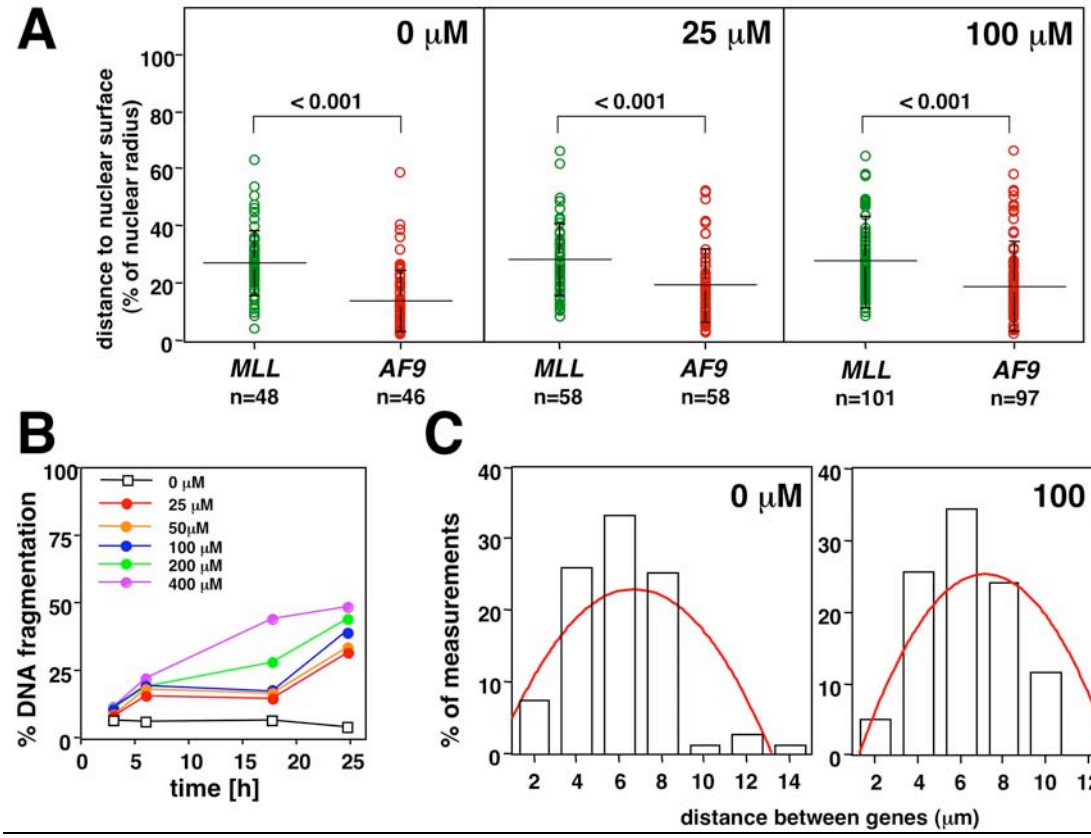

Figure 33: DNA damage does not cause a change in the 3D position of *MLL* and *AF9*.
A: Distances of the *MLL* and *AF9* genes from the nuclear surface in Triggs cells after treatment with the topoisomerase II inhibitor VP16.
B: Quantification of apoptosis induced in Triggs cells by different concentrations of VP16.
C: VP16 does not induce a significant change in the distance between *MLL* and *AF9*. Red line: Curve fit (polinome 2nd order).

Cells were treated with 25 μM or 100 μM VP16 for 6 h (**Figure 33A**), a time point at which some DNA fragmentation was already detectable (**Figure 33B**). The analysis revealed that DNA damage does not significantly affect the localization of the two genes. Both the relative position in the nucleus as well as the relative distance of both genes remained the same. (**Figure 33C**). It is quite remarkable that the overall nuclear architecture, as measured by these parameters, seems to be unaffected by the induction of DSBs.

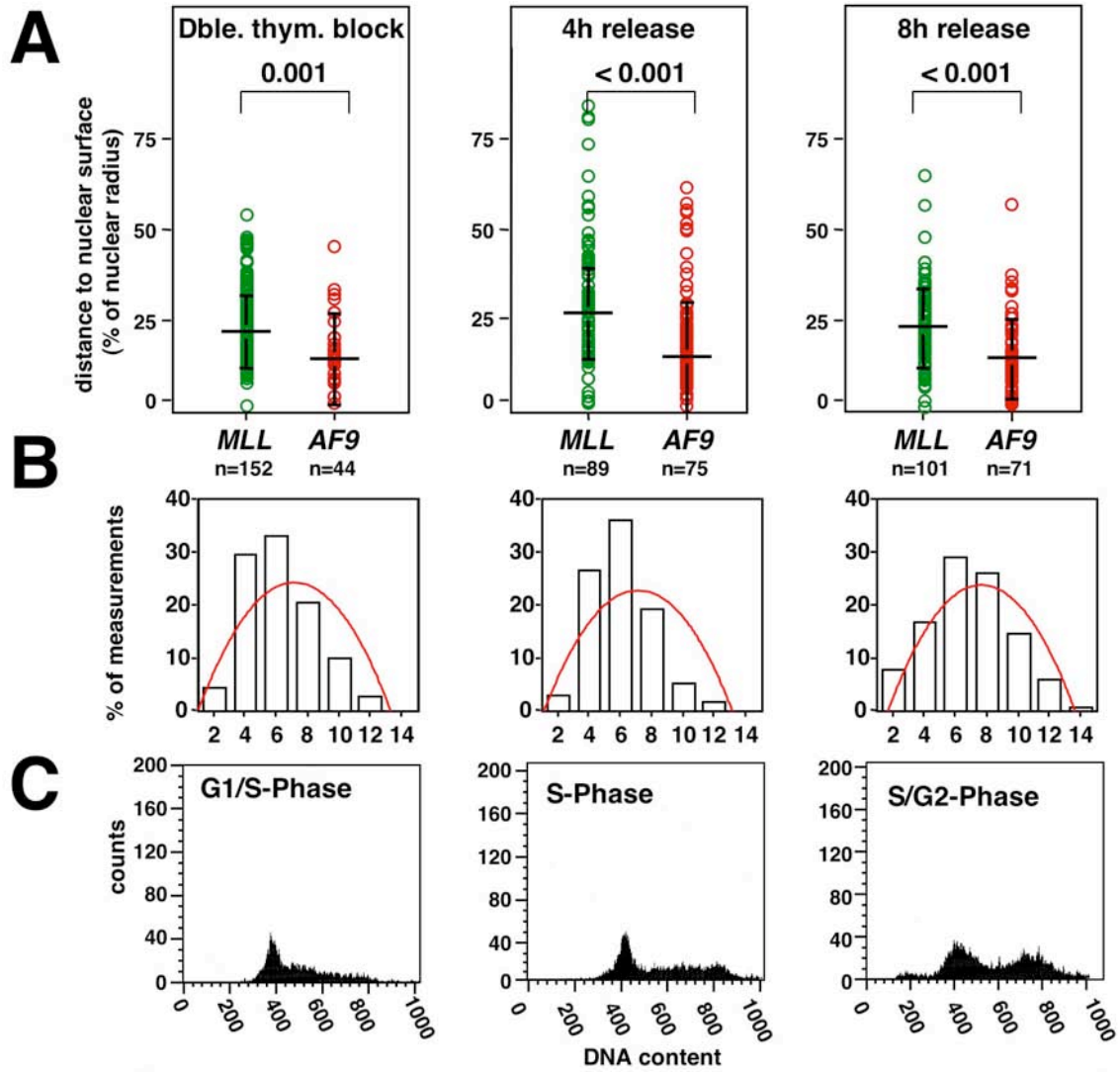

D

Cell cycle phase	n (measurements of R)	Median R	Stdev (+/-)	Cell volume [µm3] (4/3 π*(R)3)
S-phase	145	4.8	1.2	474
late S-phase	166	5.2	1.2	605
S/G2 border	117	5.2	1.4	581
unsynchronized	498	4.9	1.3	501

Figure 34: Position of the *MLL* and *AF9* genes do not change during the cell cycle in Triggs cells, synchronized with double thymidine block.

A: Scatter blot analysis of the 3D localization of *MLL* and *AF9*.

B: Distance measurements between *MLL* and *AF9*. Red line: Curve fit (polinome 2nd order).

C: Cell cycle analysis using flow cytometry.

D: Results of cell cycle analysis. Shown is percentage of cells in G1, S, G2/M of double thymidine arrested Triggs cell line and the mean radius (R) of the cells.

5.3.7. Comparison of the position of *MLL* and *AF9* in cell cycle synchronized cells

DNA synthesis could potentially affect the localization of genes. To test this, Triggs cells were synchronized using a double thymidine block and subsequent release. An analysis of the localization of *MLL* and *AF9* showed no significant differences in their localization in cells at different times after release from the G1/S cell cycle block. Although the median value of the measurements was not significantly different (**Figure 34),** the measurements seemed to be more scattered in cells released for 4 h from the double thymidine block.

5.3.8. Translocation events can change the 3D localization of genes

The data so far demonstrate that *MLL* and some of its translocation partners have defined localizations with respect to the nuclear surface, meaning they reside in different shells. This could be a property of the specific gene or the entire chromosome on which it resides. In addition to the potential relevance of the data for translocation events, in which *MLL* is involved, the results more generally suggest that genes have certain localization probabilities (reside in specific nuclear shells). A question therefore arises: What determines the position of a gene in the nucleus? Is it the gene itself or is it the chromosomal environment on which it resides? Because I could not possibly swap chromosomal domains to address this question experimentally, I made use of the various cell lines that already carry well defined translocation events involving *MLL* and various translocation partners. The question addressed was: In a translocation, in which small parts of chromosome 11 (*MLL*) and chromosome 9 (*AF9*) are exchanged, will the localization of the part of *MLL* that remains on 11, be the same as *MLL* in a normal chromosome 11 or will it acquire the localization of the *AF9* gene? The same question applies to the *AF9* gene on the chromosome 9 in the event of a balanced translocation. Hence, is it the property of a specific chromosomal territory environment, which determines the position of a gene, or is it the gene itself or the subdomain in which it resides? In order to address these questions the following tools were utilized: Probes that allowed the detection and distinguishing of the genes on normal and translocated chromosomes, and cell lines, that carried well defined

translocations involving *MLL*. Five such cell lines representing three different translocations were analyzed and are described in the following sections.

i. MonoMac6

The first cells analyzed were MonoMac6 cells representing a system with normal and derivative chromosomes in the same nucleus. These cells carry a balanced translocation involving *MLL* and *AF9* (Drexler and MacLeod, 2003; MacLeod et al., 1993). First the karyotype was confirmed for chromosome 9 and 11 using whole chromosome paints and gene specific FISH probes (**Figure 35**). As seen in **Figure 35A** and **C**, Monomac6 cells contain 2 normal chromosomes 9, 2 normal chromosomes 11, one derivative der(9) and one der(11).

Figure 35: Characterization of the monocytic cell line MonoMac6 carrying a t(9;11) translocation involving *MLL* and *AF9*.
A-F: Verification of karyotype of MonoMac6 on MAA fixed material.
A: Metaphase spread of MonoMac6 stained with whole chromosome painting probes for chr 9 (green) and chr 11 (red). Green arrow head: chr 9; red arrow head: chr 11; pink arrow head: der(9); aqua arrow head: der(11).
B: Same metaphase spread as seen in A. Inverted DAPI stain. For arrow head color code see A.
C: Selected cut-out of chr 9, chr 11, der(9) and der(11); staining as in A.
D: Metaphase spread of MonoMac-6 stained with gene specific probes for 5'*MLL* and 3'*MLL* (Dual color split probe, spectrum green for 5'*MLL* and spectrum red for 3'*MLL*, location is equivalent to position of clones RP1-217A21 and RP1-167K13), and *AF9* (clones CTD-21K4 and CTD-300E18 labeled with digoxigenin, detected with mouse anti-digoxigenin-Cy5 antibody). Blue arrow head: *AF9* on chr 9; yellow arrow head: 5'*MLL* and 3'*MLL* on chr 11; pink arrow head: 5'*AF9* and 3'*MLL* on der(9); aqua arrow head: 5' *MLL* on der(11).
E: Same metaphase spread as seen in D. Inverted DAPI stain. For arrow head color code see D.
F: Selected cut-out of chr 9, chr 11, der(9) and der(11) with *MLL* and *AF9* signals; staining as in D, but here, due to the RGB-overlay, signals for *AF9* appear green on chr 9 and der(9), 5'*MLL* green on chr 11 and der(11), 3'*MLL* red on chr 11 and der(9). On der(11) there was no signals observed for 3'*AF9*.
chr = normal chromosome. der = derivative chromosome.

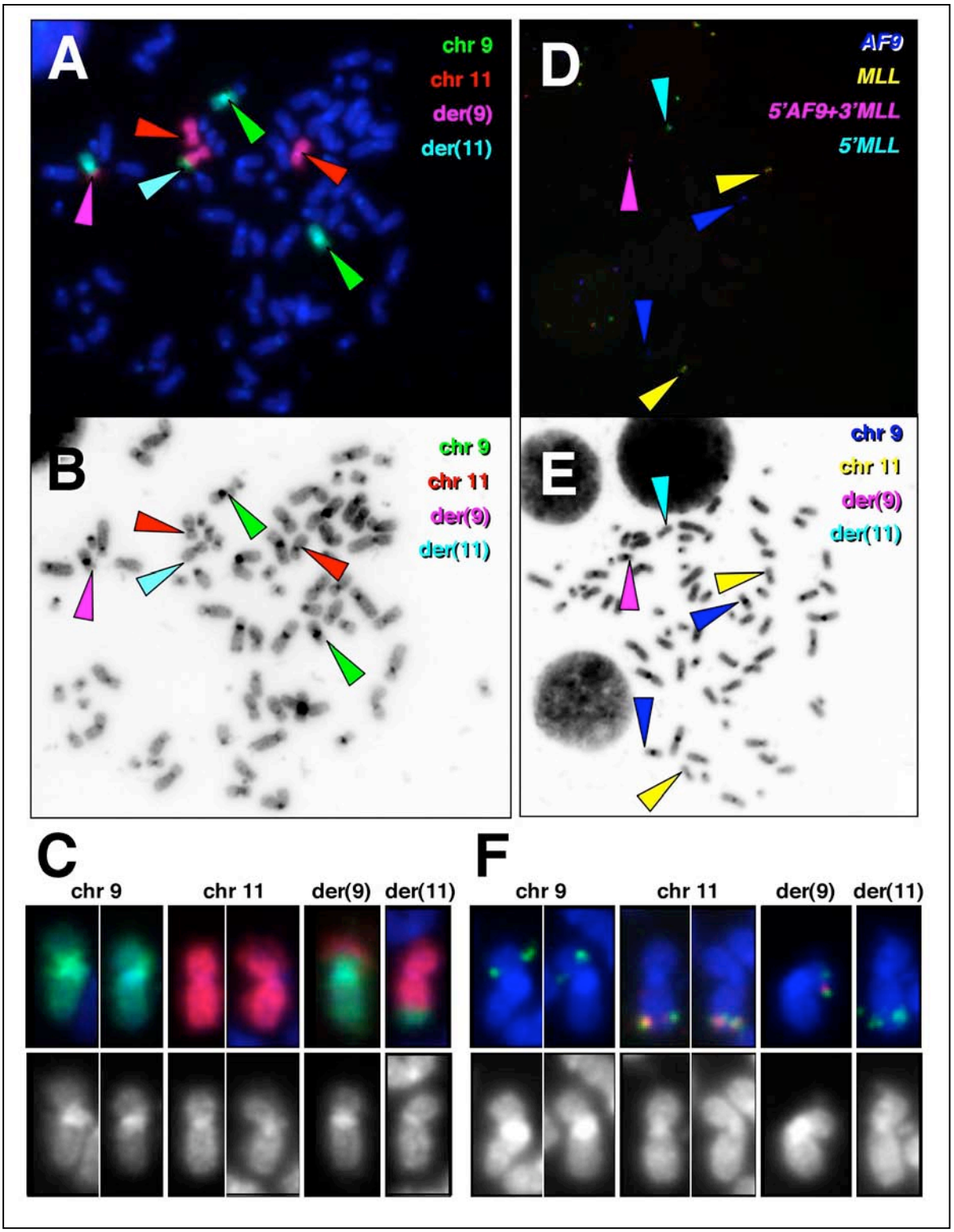
A
chr 9
chr 11
der(9)
der(11)
D
AF9
MLL
5'AF9+3'MLL
5'MLL
B
chr 9
chr 11
der(9)
der(11)
E
chr 9
chr 11
der(9)
der(11)
C
chr 9
chr 11
der(9)
der(11)
F
chr 9
chr 11
der(9)
der(11)

The analysis shown in **Figure 35D** and **F** confirms the good quality of the gene specific probes, and that the normal and the fusion genes could be identified. In **Figure 36A** a total projection of a multi colored confocal image stack is displayed to give an overview of all available signals in one nucleus using the same set of probes as in **Figure 35F**. **Figure 36B** shows an example of two nuclei with all detected signals based on a set of confocal staining as seen in **Figure 36A**. The analysis of the signals in **Figure 36C** again demonstrates that the gene *AF9* (blue data set) had a higher probability to be closer to the nuclear surface than the *MLL* gene (green and red data sets). As expected, the 5' (green) as well as the 3' (red) *MLL* probes on the normal chromosomes 11 gave a similar result. Interestingly, the staining using the 3'*MLL* probe, which detects the translocated part of *MLL* found on der(9) still maintained the localization of that found for *MLL* on chromosome 11.

However, for the 5'*AF9* probe, which detects the part of *AF9* that remains on the der(9), now has a location similar to 3'*MLL* on der(9), suggesting that the small translocated piece of chromosome 11 altered the position of the area of chromosome 9 on which *AF9* is located. At the same time, the 5'*MLL* probe, which detects that part of *MLL* that remains on the der(11), changed localization to that usually found for *AF9* on chromosome 9. Although a probe that allowed detection of the 3' region of *AF9*, which is translocated to 5'*MLL* on der(11) was not available, it is expected, that also this staining would have been similar to the position of the 5' *MLL* on der(11). In summary, the data suggest that it is not the majority of the chromosome that determines a 3D position of a gene within the nucleus, since even a small piece of translocated DNA can influence the localization of the fused gene and very likely its immediate vicinity (chromosomal subdomain). To determine, if this unexpected finding is limited to this particular cell line or whether it is of a more general nature, this kind of analysis was extended to four other cell lines with known translocation events involving *MLL*.

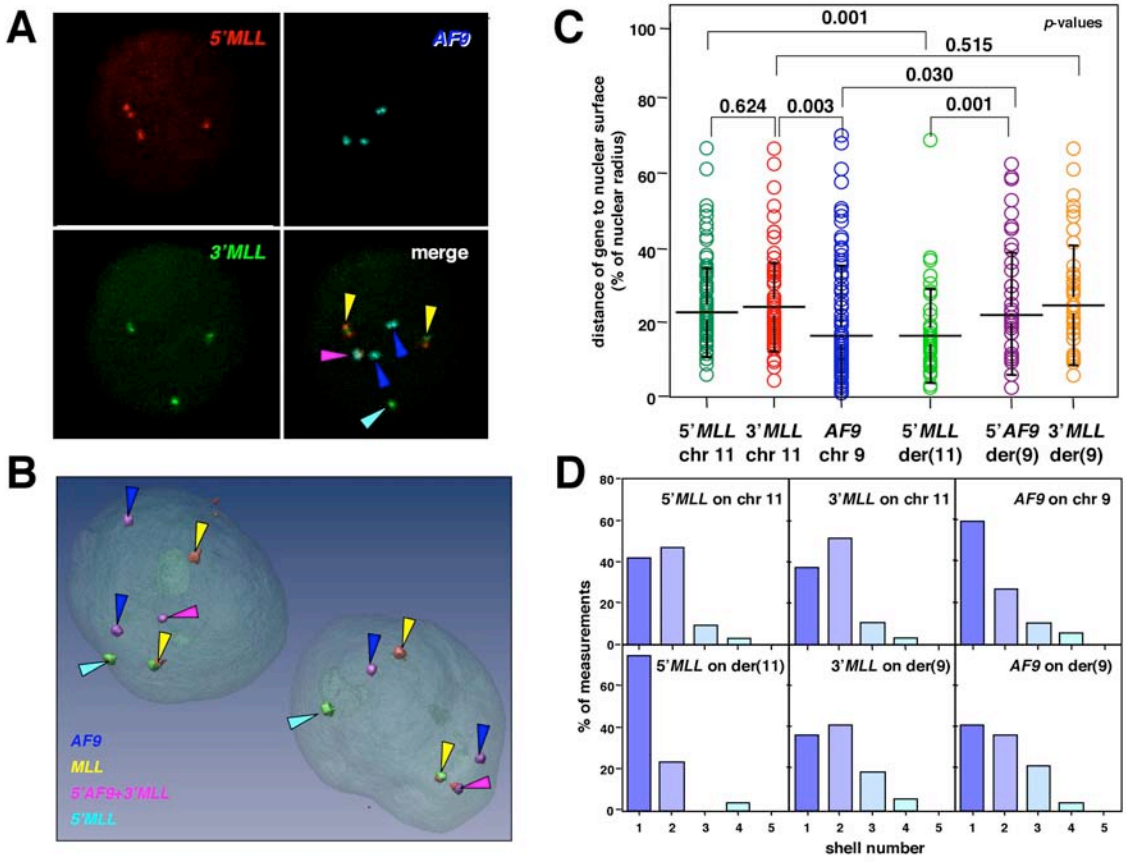

Figure 36: After translocation the 5'*MLL* and 5'*AF9* regions acquire the 3D positions of each other prior to the translocation in MonoMac6 cells.

A and B: 3D-FISH on PFA-fixed interphase cells. Same probe combination was used as in Figure 35D.

A: Total projections of confocal image stacks for the red, green, and Cy5 channel to visualize all signals in one single nucleus. Blue arrow head: *AF9* on chr 9; yellow arrow head: 5'*MLL* and 3'*MLL* on chr 11; pink arrow head: 5'*AF9* and 3'*MLL* on der(9); aqua arrow head: 5' *MLL* on der(11).

B: 3D reconstruction of 2 nuclei from confocal image stacks of PFA-fixed interphase nuclei using the Amira 3.1 computer program. For arrow head color code see A.

C: Positions of the 5'*MLL*, 3'*MLL* and 5'*AF9* signals relative to the nuclear surface. chr = normal chromosome; der = derivative chromosome.

D: Positions of 5'*MLL*, 3'*MLL*, and *AF9*, relative to nuclear surface. Upper panels: positions of genes on normal chromosomes. Lower panels: positions of genes in derivative chromosomes. Positions were analyzed using method I as described in Figure 18A. n = 40 cells were evaluated.

ii. THP-1

The monocytic cell line THP-1 is another cell line that carries a t(9;11) translocation involving *AF9* and *MLL* (**Figure 37A**). Its der(11) is comparable to the der(11) in MonoMac6 cells. The der(9) chromosome in the THP-1 cell line, however, contains an additional inversion, not found in MonoMac6. Thus, der(9) can not be compared in these two cell lines. Interestingly, der(11) in this cell line behaved similarly to der(11) in MonoMac6 cells. The 5'*MLL* signal in der(11) shifted to a more peripheral position characteristic for *AF9* (**Figure 37B**, light green data set). In conclusion, the genes in the two cell lines harboring a similar chromosomal translocation behaved in a similar way, not only confirming the analyses but also indicating the existence of a common underlying principle that determine 3D localization.

iii. RS4;11

RS4;11 is a pro B-cell line that harbors a t(4;11) translocation leading to *MLL-AF4* fusion gene. Firstly, the karyotype was confirmed for chromosome 4 and 11 using whole chromosome paints and gene specific FISH probes (**Figure 38**). As expected, one copy of each, normal chromosome 4, normal chromosome 11, der(4), and der(11) was detected (**Figure 38A** and **C**). **Figure 38D** and **F** confirm the quality of the gene specific probes. The normal and the fusion genes could be identified. **Figure 39A** shows an example of three reconstructed nuclei with the different signals based on a set of confocal staining as seen in **Figure 38D** and **F**. The analysis of the signals in **Figure 39B** demonstrates that the gene *AF4* (blue data set) has a higher probability to be closer to the nuclear surface than the *MLL* gene (green and red data sets). Similar to the situation in MonoMac6 and THP-1 cells, the position of the *MLL* signal on der(11) in the RS4;11 cells changed to a more peripheral localization (**Figure 39B**, light green data set). However, the translocated part of chromosome 4 with *AF4* did not affect chromosome 11 in the same way as the translocating part of chromosome 9: the position of the signal of *AF4* on der(4) did not completely assume the position of *MLL* on the normal chromosome 11.

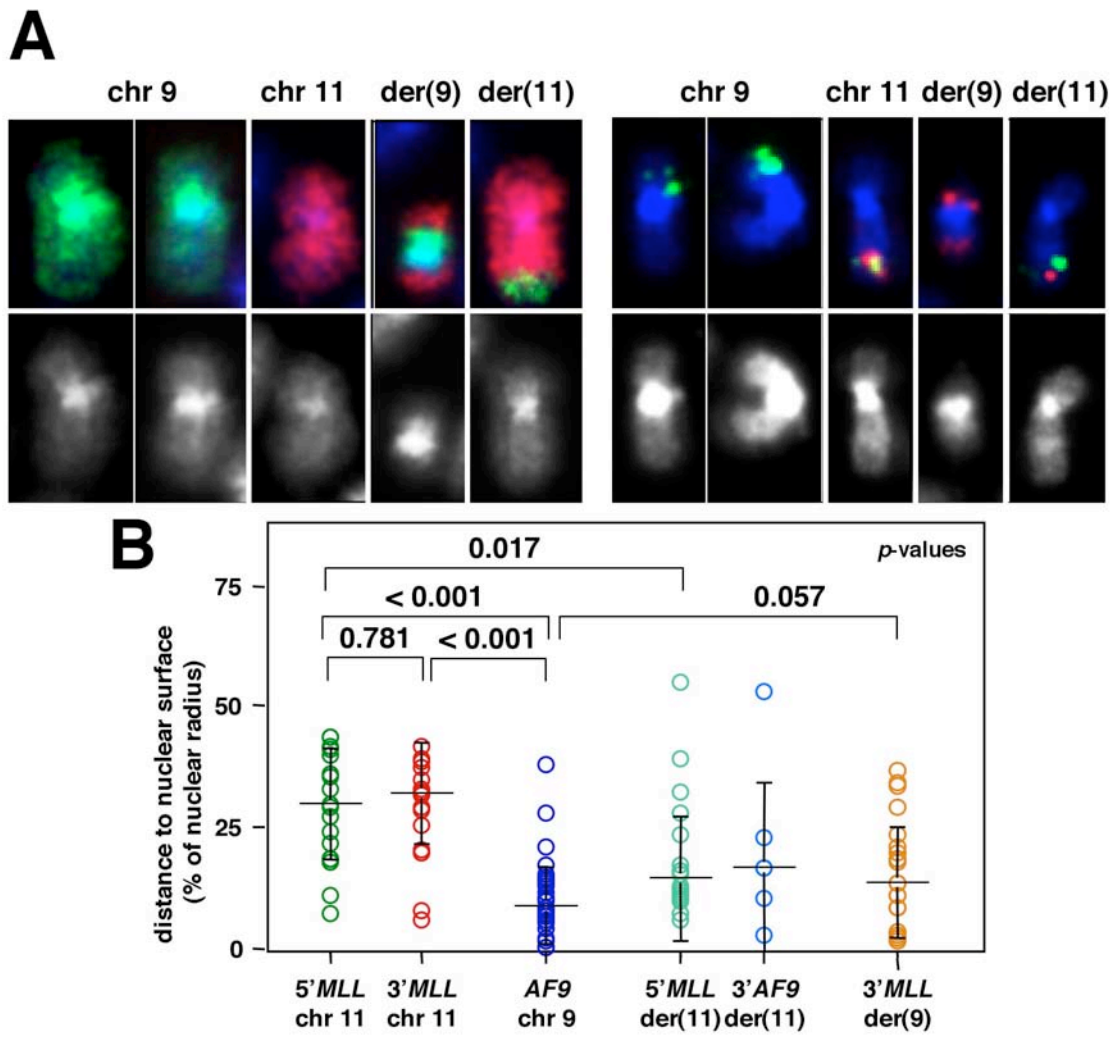

Figure 37: After translocation the 5'*MLL* and 5'*AF9* regions acquire the 3D positions of each other prior to the translocation in THP-1 cells.

A: Selected cut-out of normal and derivative chromosomes 9 and 11, on the left stained with whole chromosome painting probes for chromosomes 9 (green) and 11 (red), and on the right with gene probes specific for *MLL* and *AF9* as described in Figure 35D. Due to the RGB-overlay, signals for *AF9* appear green on chr 9 but red in der(9), 5'*MLL* is green on chr 11 and der(11), 3'*MLL* is red on chr 11 and der(9). The karyotype in this cell line differs from that of cell line MonoMac6 (compare Figure 35). The der(9) of THP-1 carries the 3'*AF9* fusion gene plus an inversion, and therefore signals for 3'AF9 of der(9) could be observed on either end, no signal for 5'*MLL* on der(9) could be observed .

B: Positions of the 5'*MLL*, 3'*MLL*, 5'*AF9* and 3'*AF9* signals relative to the nuclear surface. 18 cells were analyzed. Some signals for the derivative chromosomes could not clearly be identified, resulting in fewer measurements.

chr = normal chromosome; der = derivative chromosome.

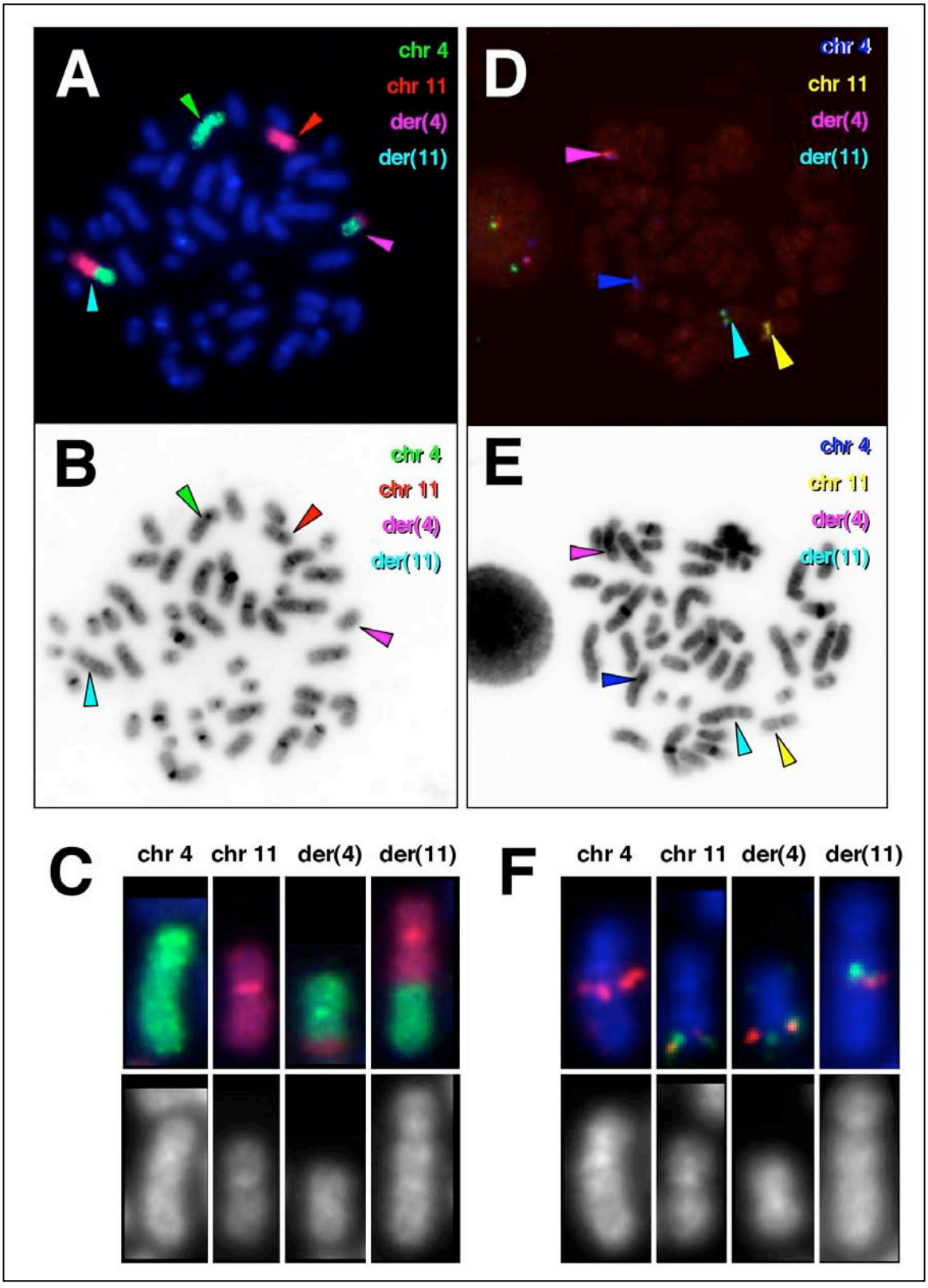
A
chr 4
chr 11
der(4)
der(11)
D
chr 4
chr 11
der(4)
der(11)
B
chr 4
chr 11
der(4)
der(11)
E
chr 4
chr 11
der(4)
der(11)
C
chr 4
chr 11
der(4)
der(11)
F
chr 4
chr 11
der(4)
der(11)

Figure 38: Characterization of the B-cell line RS4;11 carrying a t(4;11) translocation involving *MLL* and *AF4*.

A: Metaphase spread of RS4;11 cells stained with whole chromosome painting probes for chromosomes 4 (red) and 11 (green). Green arrow head: chr 4; red arrow head: chr 11; pink arrow head: der(4); aqua arrow head: der(11).

B: Same metaphase spread as seen in A. Inverted DAPI stain. For arrow head color code see A.

C: Selected cut-out of normal and derivative chromosomes 4 and 11; staining as in A.

D: Metaphase spread of RS4;11 cells were stained with gene specific probes for 5'*MLL* and 3'*MLL*, and *AF4*. Blue arrow head: *AF*4 on chr 4; yellow arrow head: 5'*MLL* and 3'*MLL* on chr 11; pink arrow head: 5'*AF4* and 3'*MLL* on der(4); aqua arrow head: 5'*MLL* on der(11).

E: Same metaphase spread as seen in D. Inverted DAPI stain. For arrow head color code see D.

F: Selected cut-out of normal and derivative chromosomes 4 and 11 with *MLL* and *AF4*; staining as in D.

Due to the RGB-overlay signals for *AF4* are blue in D, but red on chr 4 or der(4), and green on der(4) in F. chr = normal chromosome; der = derivative chromosome.

iv. MV4-11

The result obtained with the RS4;11 cells could be completely confirmed with the MV4-11 cells, which were analyzed in the same way (**Figures 40** and **41**). This reproducibility is remarkable and suggests that independent of the cell type (MV4-11 cells are monocytic cells, whereas RS4;11 cells are B-cells), translocations involving the same chromosomal parts affect the localization of genes in the same way.

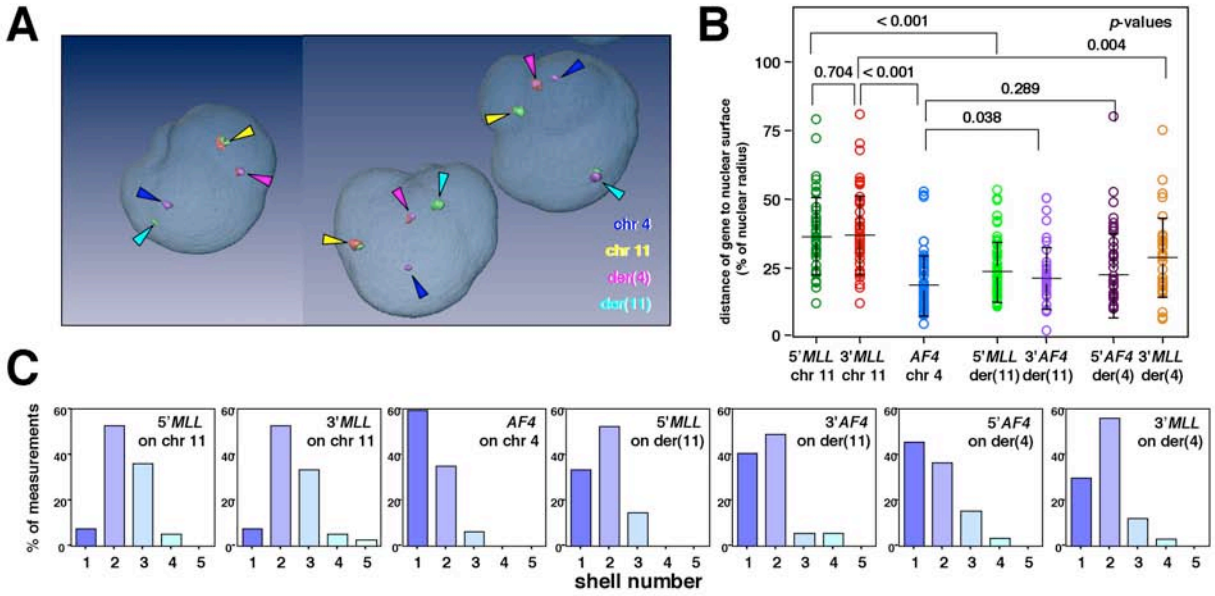

Figure 39: After translocation both the 5'*MLL* and 5'*AF4* regions acquire the 3D position and distance to the nuclear surface that lies between the location of *MLL* on chromosomes 11 and *AF4* on chromosome 4 in the B-cell line RS4;11.

A: 3D reconstruction of three nuclei from confocal image stacks of PFA-fixed interphase cells generated with the Amira 3.1 computer program. Blue arrow head: *AF*4 on chr 4; yellow arrow head: 5'*MLL* and 3'*MLL* on chr 11; pink arrow head: 5'*AF4* and 3'*MLL* on der(4); aqua arrow head: 5'*MLL* on der(11).

B: Positions of the 3'*MLL*, 5'*MLL*, 3'*AF4* and 5'*AF4* signals relative to the nuclear surface. *p*-values were calculated with the computer program Excel.

C: Position of 5'*MLL*, 3'*MLL*, 3'*AF4* and 5'*AF4*, relative to nuclear surface. n = 49 cells were analyzed. In 10 nuclei a second signal for *AF4* on chr 4 was observed. In 14 nuclei, not all signals for the derivative chromosomes were clearly identifiable, resulting in fewer measurements.

chr = normal chromosome; der = derivative chromosome.

Figure 40: Characterization of the monocytic cell line MV4-11 carrying a t(4;11) translocation involving *MLL* and *AF4*. Verification of the karyotype of MV4-11 cells on MAA fixed material.

A: Metaphase spread of MV4-11 cells stained with whole chromosome painting probes for chromosomes 4 (green, spectrum green) and 11 (red, spectrum red). Green arrow head: chr 4; red arrow head: chr 11; pink arrow head: der(4); aqua arrow head: der(11).

B: Same metaphase spread as seen in A. Inverted DAPI stain. For arrow head color code see D.

C: Selected cut-out of normal and derivative chromosomes 4 and 11; staining as in A. Blue: *AF4*.

D: Metaphase spread of MV4-11 cells stained with gene specific probes for 5'*MLL* and 3'*MLL* (dual color split probe, 5'*MLL* spectrum green, 3'*MLL* spectrum red) and *AF4* (CTD-2505N20 or CTD-2574C18, digoxigenin labeled, detected with mouse anti-digoxigenin-cy5 antibody). Blue arrow head: *AF*4 on chr 4; yellow arrow head: 5'*MLL* and 3'*MLL* on chr 11; pink arrow head: 5'*AF4* and 3'*MLL* on der(4); aqua arrow head: 5'*MLL* on der(11).

E: Same metaphase spread as seen in D. Inverted DAPI stain. For arrow head color code see D.

F: Selected cut-out of normal and derivative chromosomes 4 and 11 with *MLL* and *AF4*; staining as in D.

G: Total projections of confocal image stacks for the red, green, and Cy5 channel to visualize all signals in one single nucleus. DAPI staining of the same nucleus is shown below. For arrow head color code see D.

Due to the RGB-overlay signals for *AF4* appear blue in D and G, but green on chr 4 and red on der(4) in F.

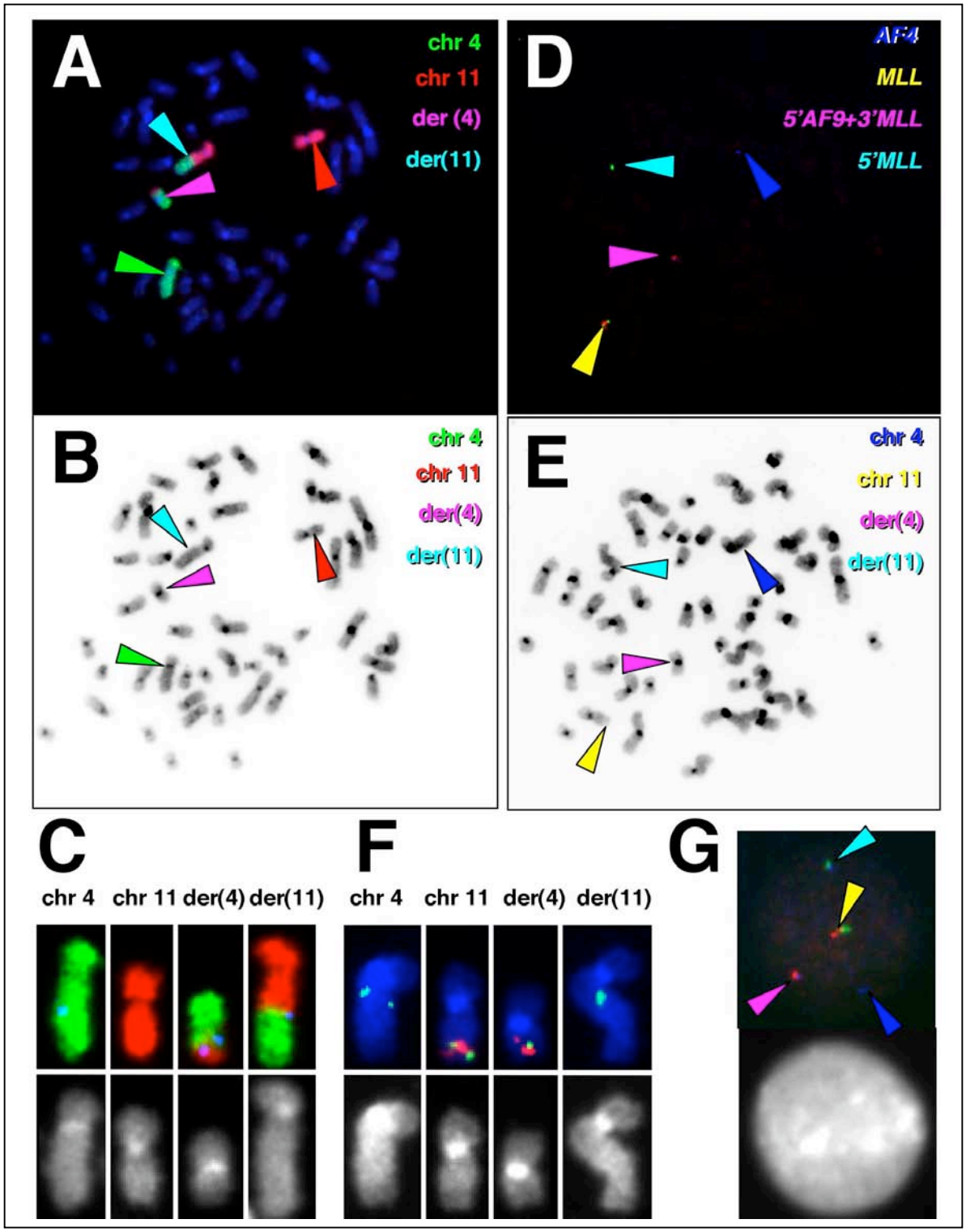
A
chr 4
chr 11
der (4)
der(11)
D
AF4
MLL
5'AF9+3'MLL
5'MLL
B
chr 4
chr 11
der(4)
der(11)
E
chr 4
chr 11
der(4)
der(11)
C
chr 4
chr 11
der(4)
der(11)
F
chr 4
chr 11
der(4)
der(11)
G

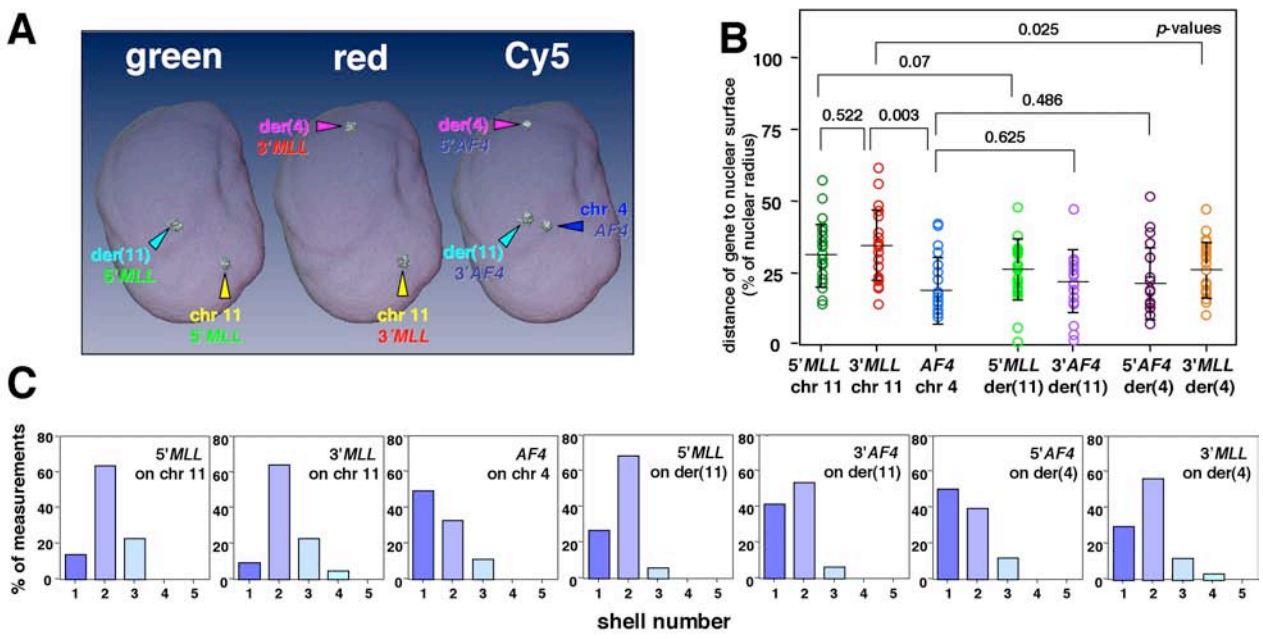

Figure 41: After translocation both the 5'*MLL* and 5'*AF4* regions acquire the 3D position of *AF4* in the monocytic cell line MV4-11.

A: 3D reconstruction of one nucleus from confocal image stacks of PFA-fixed interphase cells with the Amira 3.1 computer program. Signals visualized in each channel are shown in 3 images of the same nucleus. Blue arrow head: *AF*4 on chr 4; yellow arrow head: 5'*MLL* and 3'*MLL* on chr 11; pink arrow head: 5'*AF4* and 3'*MLL* on der(4); aqua arrow head: 5'*MLL* on der(11).

B: Positions of the 3'*MLL*, 5'*MLL*, 3'*AF4* and 5'*AF4* signals relative to the nuclear surface.

C: Position of 5'*MLL*, 3'*MLL*, 3'*AF4* and 5'*AF4*, relative to nuclear surface. n = 25 cells were evaluated. In 10 nuclei not all the signals for the der chromosomes were identifiable.

chr = normal chromosome; der = derivative chromosome.

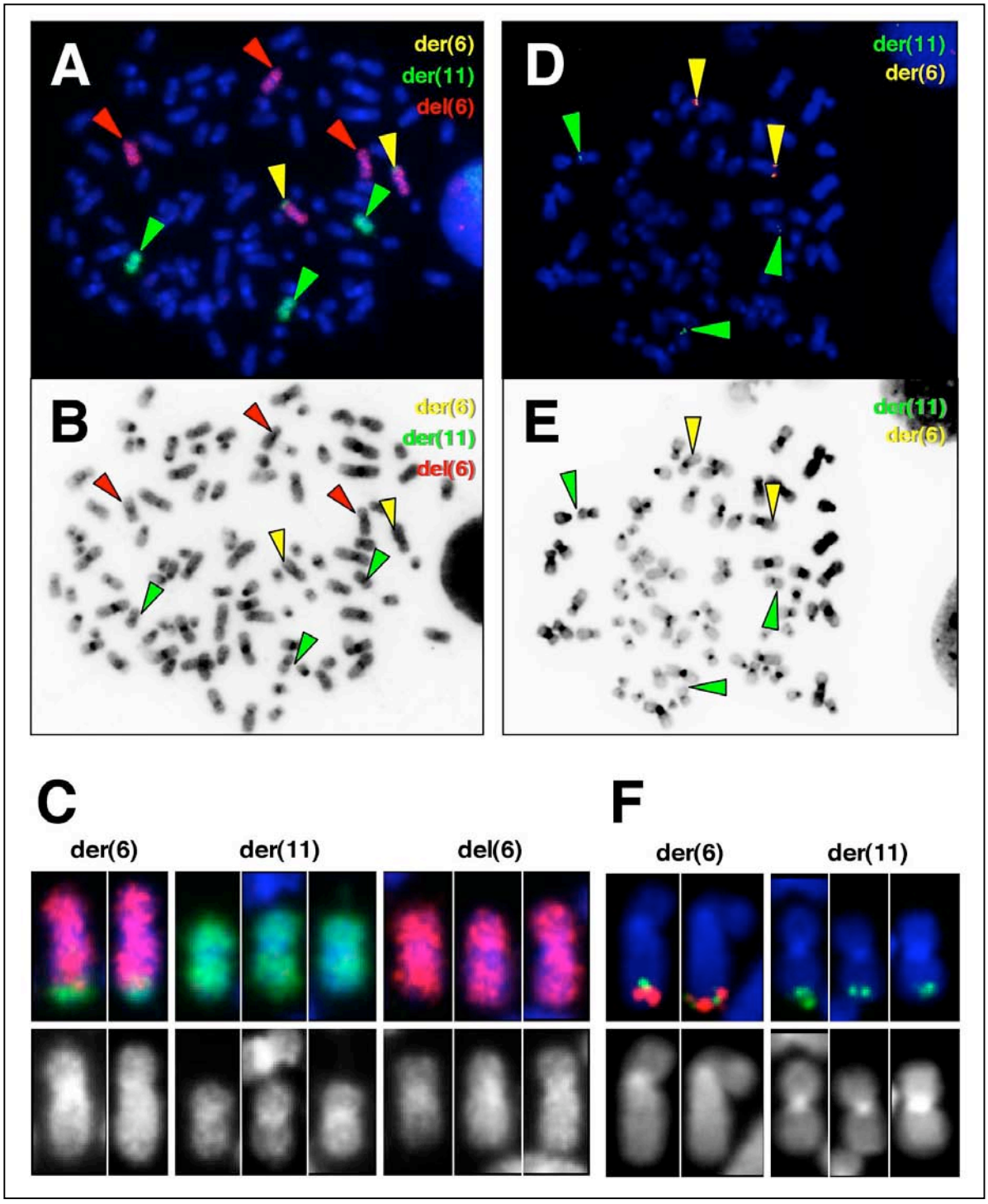
A
der(6)
der(11)
del(6)
D
der(11)
der(6)
B
der(6)
der(11)
del(6)
E
der(11)
der(6)
C
der(6)
der(11)
del(6)
F
der(6)
der(11)

Figure 42: Characterization of the myelomonocytic cell line ML-2 carrying a t(6;11) translocation involving *MLL* and *AF6*.

A: Metaphase spread of ML-2 cells stained with whole chromosome painting probes for chromosomes 6 (red) and 11 (green). Yellow arrow head: der(6); red arrow head: del 6; green arrow head: der(11).

B: Same metaphase spread as seen in A. Inverted DAPI stain. For arrow head color code see A.

C: Selected cut-out of derivative chromosomes 6 and 11; staining as in A.

D: Metaphase spread of ML-2 cells stained with gene specific probes for 5' (green) and 3'*MLL* (red), and *AF6* (orange). Yellow arrow head: der(6); green arrow head: der(11).

E: Same metaphase spread as seen in D. Inverted DAPI stain. For arrow head color code see D.

F: Selected cut-out of derivative chromosomes 6 and 11 with *MLL* and *AF6*; staining as in D.

chr = normal chromosome; der = derivative chromosome; del = deleted chromosome.

Figure 43: Translocated 5'*MLL* and 5'*AF6* regions have 3D positions similar to *AF6* on normal chromosomes in the myelomonocytic cell line ML-2.

A: 3D reconstruction of two nuclei from confocal image stacks of PFA-fixed interphase cells generated with the Amira 3.1 computer program. Red signals: 3'*MLL* on der(6); green signals: 5'*MLL* on der(11); purple signals: *AF6* signals on der(6) and der(11); yellow arrow head: der(6); green arrow head: der(11).

B: Positions of the 3'*MLL*, 5'*MLL*, 3'*AF6* and 5'*AF6* signals relative to the nuclear surface.

C: Position of 5'*MLL*, 3'*MLL*, 3'*AF6* and 5'*AF6*, relative to nuclear surface. n = 51 cells were evaluated. In 11 nuclei only 2 der(11) or 1 der(6) were identifiable.

chr = normal chromosome; der = derivative chromosome; del = deleted chromosome.

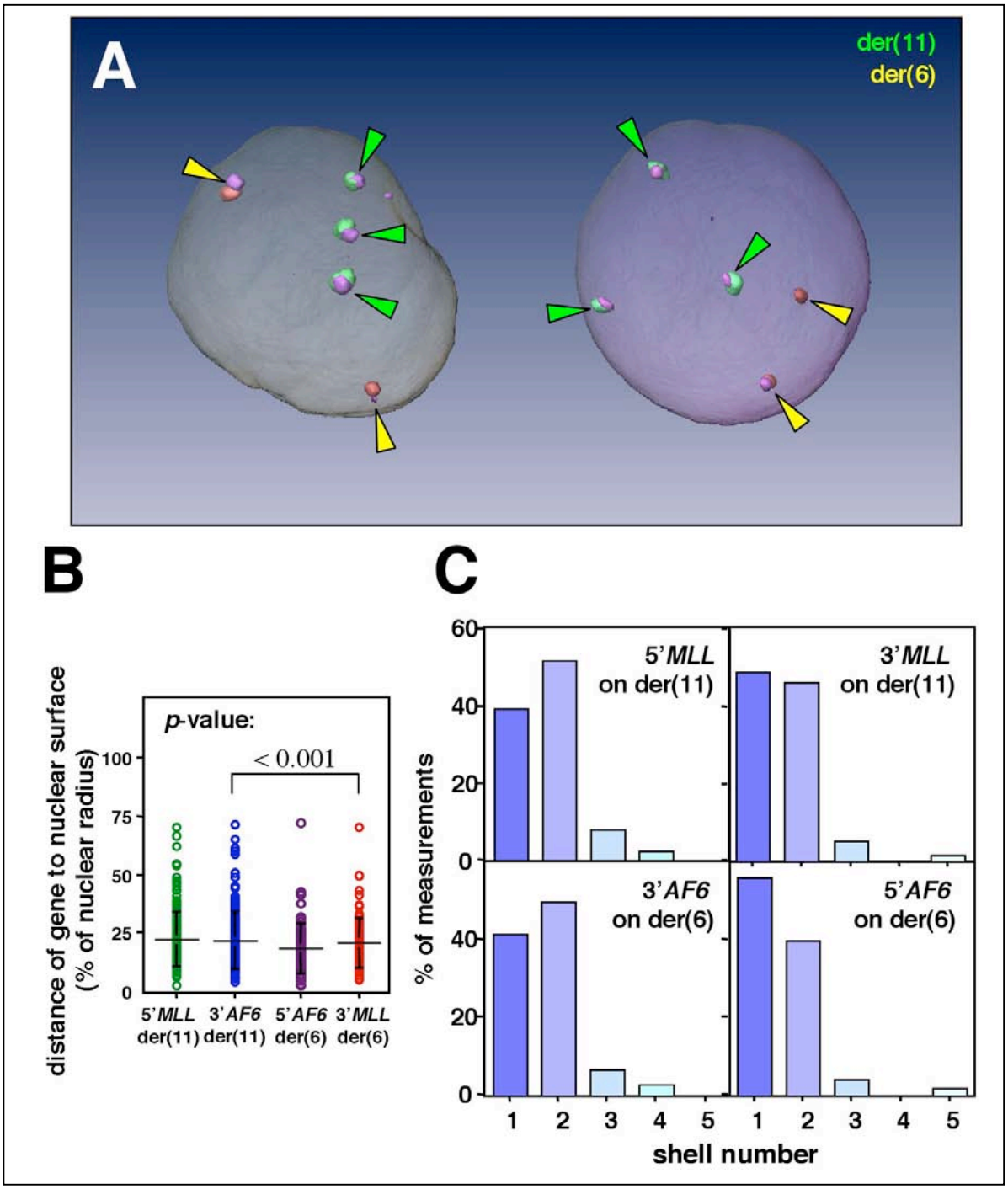
A
der(11)
der(6)
B
C
distance of gene to nuclear surface (% of nuclear radius)
p-value:
< 0.001
100
75
50
25
0
5'MLL der(11)
3'AF6 der(11)
5'AF6 der(6)
3'MLL der(6)
% of measurements
60
40
20
0
5'MLL on der(11)
3'MLL on der(11)
3'AF6 on der(6)
5'AF6 on der(6)
1 2 3 4 5
shell number

v. ML-2

To complete the analysis of the localization of *MLL* and its major translocation partners *AF4*, *AF6* and *AF9*, it was desirable to find a cell line with a translocation involving *MLL* and *AF6*. Unfortunately, a cell line with such a translocation event that still has a set of normal chromosomes was unavailable. For this reason ML-2 cells were analyzed, which which is a monocytic cell line that carries a t(6;11) translocation leading to a *MLL-AF6* fusion gene. In **Figure 42A** and **C** again the karyotype was confirmed. As expected, 2 copies of der(6) and 3 copies for der(11) were found. **Figure 42D** and **F** confirm the quality of the gene specific probes, and that the two derivative genes could be distinguished. **Figure 43A** shows an example of two reconstructed nuclei with the rendered signals for the fusion genes. The analysis of the signals in **Figure 43B** demonstrates that the position of 5'*AF6* and 3'*MLL* (red and purple datasets) on der(6) had a slightly higher probability to be closer to the nuclear surface than 5'*MLL* and 3'*AF6* (green and blue dataset) on der(11). The analysis in **Figure 43** demonstrated that the genes had a very similar localization. Although in this case normal chromosomes were not present to be mapped, it is likely that *MLL* would have had a more central localization than *AF6*, because *MLL* in all other tested hematopoietic cells with a normal chromosome 11 was located much more in the center of the nucleus than the *MLL* signal detected in this cell line. In summary, the analysis of all cell lines that carry defined translocations involving *MLL* and its translocation partners revealed that translocations, which cause a relocalization of a part of a gene, can cause a profound change in its position which seems to depend either on the translocation partner or its immediate chromosomal environment.

6. DISCUSSION

MLL is a gene involved in chromosomal translocations found in certain human leukemia. The mechanism underlying chromosomal translocations are poorly understood. In this work the 3D position of *MLL* and some of its translocation partners was analyzed in various human hematopoietic cell lines and primary cells in an attempt to find principles that determine the 3D localization of genes. To perform this study, methods were established, using confocal image stacks that allowed the precise description of positions of gene loci in the 3D volume of the interphase nucleus and in relationship to other genes. *MLL* was found to be relatively weakly transcribed but frequently found in a "looped out" position relative to the stainable territory of human chromosome 11. In the 3D space of the nucleus, *MLL* had a preferred radial localization characteristically different from other genes including some of its most frequent translocation partners, such as *AF4*, *AF6*, *AF9*, *ENL* and *ELL*. The 3D positions of all these genes were generally conserved among hematopoietic cells but were different when compared to fibroblasts. The position of *MLL* and *AF9* in hematopoietic cells was also constant during the S phase of the cell cycle and was not altered by DNA damage induced by treating cells with etoposide.

To determine whether localization of genes differ between species fibroblasts from two closely related species of deer, *M. muntjak* and *M. reevesi*, with similar DNA content, but vastly different chromosomes numbers, were compared to human fibroblasts after generation of a number of muntjac specific tools such as whole chromosome paints and gene specific probes. Although different from hematopoietic cells, the positions of *MLL*, *AF4* and *AF*9 among fibroblasts from human and the two muntjac species were conserved suggesting different cell types have characteristic 3D positions of genes and these characteristics are conserved among different mammalian species.

Translocations were found to affect the 3D positions of genes. Analysis of the gene density of whole chromosomes and sections of chromosomes revealed new insights into the underlying rules of chromatin location in hematopoietic cells. The position of a gene was found to be dependent on the local environment (gene density) of its chromosomes, rather

than the entire chromosome. The gene density in an area of 2 Mbp surrounding a gene locus was found to best predict its localization in the 3D space of interphase nuclei.

6.1. Synteny between Chinese muntjac, Indian muntjac, human and cattle

The genome of mammalian species contains tens of thousands of genes arranged in linear order along individual packaging units, the chromosomes. The number of chromosomes can widely vary, but it is believed that the arrangement of genes in certain clusters are conserved among species (Carver and Stubbs, 1997; Oeltjen et al., 1997; Pennacchio, 2003). Gene maps have been constructed in human, mouse, and about 30 other mammal species for two general reasons: first, as a resource for locating the genetic determinants of heritable characteristics, i.e. phenotypes including behaviors; and second, as a template for resolving and interpreting patterns of evolving genome organization in their ancestry. *M. muntjak* is of particular interest, because the female muntjac contains only three chromosomes. Syntenic regions have been described between muntjac and other species in an overview by using whole chromosome paints in Zoo-FISH experiments, also known as cross-species chromosome painting, to precisely define chromosomal segments that are homologous between species (Chowdhary et al., 1998; Fronicke et al., 1997; Yang et al., 1995; Yang et al., 1997a). This analysis made it possible to identify a set of chromosome segments (based on human chromosome equivalents) that made up the karyotype of the hypothetical common ancestor. Segments in the genome derived from the common ancestor are identified through their conservation over several million years of evolution (Andersson et al., 1996; Wienberg et al., 1997). This branch of genome analysis is referred to as comparative genome analysis. The human genome was the first completely sequenced mammalian species (Venter et al., 2001), and therefore its map serves as a master mammalian genome. Zoo-FISH studies predominantly used human chromosome-specific plasmid or PCR-generated library DNA probes, because these were the first available (e.g. (Collins et al., 1991; Vooijs et al., 1993). Most comparative analyses were done based on human chromosome equivalents (human chromosomes were used as the reference point), because most of the species studied by Zoo-FISH were probed with human chromosome

specific libraries, and not because the human genome represents the ancestral mammalian karyotype. Three distinct classes of synteny conservation have been designated: (1) conservation of whole chromosome synteny, (2) conservation of large chromosomal blocks, and (3) conservation of neighboring segment combinations (Chowdhary et al., 1998).

Which part of the chromosomes or in what orientation they fused with other chromosomes during evolution can only be determined by the localization of small segments. In addition, it was demonstrated that the resolution limit of Zoo-FISH by painting probes is around 7 Mbp (Scherthan et al., 1994), which will leave small conserved syntenic segments undetected.

The study of the muntjac species in this thesis served two purposes: firstly it allowed the development of some of the principles of 3D localization of genes between two remotely related species with the same number of chromosomes (human and *M. reevesi*) and secondly, it allowed a comparison of the 3D localization of genes, within syntenic regions between two highly related species with drastically different numbers of chromosomes (*M. reevesi* vs. *M. muntjak*). However, a direct comparison of human and *M. muntjak* was not possible, because none of the human gene probes tested gave reliable signals in *M. muntjak*. More than 10 human probes were tested (data not shown). Therefore probes from cattle, a well characterized species, more closely related to *M. muntjak* than human and for which a number of genes with known orthologs in humans were used. A set of 51 cattle clones most of them previously described (Gautier et al., 2001) and 3 other cattle clones (provided by Dr. Buitkamp) were used. This allowed the mapping of 40 genes on *M. muntjak*, distributed over all 3 chromosomes. Furthermore, 23 genes were mapped on *M. reevesi*. The 18S rDNA was assigned to two 2 loci on different chromosomes in both species. The location of each gene on *M. muntjak* could generally be predicted, based on the location of homologous genes between cattle and human (http://www.ncbi.nlm.nih.gov/entrez/ query.fcgi? db=unigene& cmd, and http://locus.jouy.inra.fr/cgi-bin/lgbc/mapping/common/ gene.operl? BASE=cattle) and the Zoo-FISH results obtained with human whole chromosome paints used to stain Indian muntjac (Chowdhary et al., 1998; Fronicke and Scherthan, 1997). Before the start of this work, only a few genes had been assigned to chromosomes with methods other than

FISH (Levy et al., 1992; Zhang et al., 2001). 5 cattle clones had been mapped in both muntjac species, but the gene composition of these clones had not been determined (Fronicke et al., 1997). They were all located on *M. muntjak* chromosome 1, no genes had been localized on chromosomes 2 and 3. The same clones were localized on *M. reevesi* chromosomes 1, 3, 7 and 17. This thesis work, therefore, represents the first mapping of genes located on all three chromosomes of *M. muntjak* and the first identification of a set of clones that allows the characterization of almost all chromosomes in *M. reevesi*. A direct prediction of synteny between cattle and muntjac was not possible because only extremely limited information on the synteny between these two species was available, and only "assumed" regions of synteny were published (Yang et al., 1997a).

All predictions of syntenic regions between human and *M. muntjak* with the help of cattle clones were met with three exceptions.

1. Cattle clone 406B01 described to contain the gene locus *VIL1MS* located on cattle chromosome 2q43 (Hayes et al., 2000), homolog to human chromosome 2q25-q26, hybridized at an unexpected location on *M. muntjak* chromosome 2q12. The expected location according to the analysis of syntenic regions for human chromosome 2 (Fronicke and Scherthan, 1997; Yang et al., 1997a) was on *M. muntjak* chromosome 1.
2. Cattle clone 0963H01 containing *CYP19* on cattle chromosome 10q26, (Hayes et al., 2000) is syntenic to human chromosome 15q21.1. (http://www.ncbi.nlm.nih.gov/entrez/query.fcgi?CMD=search&DB=unigene). The location of hybridization signal *M. muntjak* chromosome 2q32-33 was unexpected. For this region synteny to human chromosomes 16 and 7 was predicted.
3. The gene *RASAI* on cattle chromosome 7q24- 7q-ter was localized with two different clones 143F11 and 982C11. Both showed hybridization on 2 different *M. muntjak* chromosomes, 2q38-q39 and 1q34. Both clones were verified to contain the gene by PCR but only clone 982C11 matches the prediction.

The discrepancy between the described localization of these three genes and my analysis could be due the resolution of Zoo-FISH of 7Mb (Scherthan et al., 1994) which could be lower than the resolution achieved by using gene specific probes used in this study.

For 2 cattle genes (gene *LGB* (clone 286F8) on cattle chromosome 11q28 and *BOLA-DYA* (clones 712H8 and 531B11) on cattle chromosome 23q12-q13) no human homologous genes were known (Gautier et al., 2001). However the gene *LGB* was assumed to meet the prediction, since the previous published location of clone 911 with the similar assignment (cattle chromosome 11q23) was located at the same position (*M. muntjak* chromosome 1p43).

The gene *BOLA-DYA* is the cattle equivalent of a major histocompatibility complex class II gene (http://locus.jouy.inra.fr/cgi-bin/lgbc/mapping/common/ gene.operl?BASE=cattle). The human major histocompatibility complex, class I and class II loci are both located on human chromosome 6 (http://www.ncbi.nlm.nih.gov/entrez/query.fcgi?CMD=search&DB=unigene). The signals observed for all 3 clones, cattle20K (MHC I), 712H8 (MHC II) and 531B11 (MHC II), assigned to cattle chromosome 23q22 and cattle chromosome 23q12-q13, respectively, matched the predicted syntenic region between human for chromosome 6 and the region of *M. muntjak* chromosomes 1p23-24. Although neither of these two cattle genes have direct homologs in the human genome (Gautier et al., 2001), 10 such genes were found to reside in the region of cattle chromosome 23q12-23q23 with syntenic genes located at human chromosome 6p21-6p22 (*BTN1A1*, *C4B*, *CYP21A2*, *HSPA1A*, *MEA*, *MOG*, *PRL*, *PSMB8*, *TAP2* and *TNF*) (data for the cattle chromosome or human chromosome location was obtained from (http://locus.jouy.inra.fr/cgi-bin/lgbc/mapping/common/gene.operl?BASE=cattle) and (http://www.ncbi.nlm.nih.gov/entrez/query.fcgi?CMD=search&DB=unigene). This information supported the conclusion that the clones, cattle20K, 712H8 and 531B11, matched the prediction.

Most of the determined gene positions could be verified through the predicted synteny between human and cattle. However, there was a small region on Indian muntjac chromosome 1 for which no synteny was predicted, the locus at 1p17-p21 (Fronicke and

Scherthan, 1997; Yang et al., 1997a). Cattle clone 111B07 containing the gene *FGG* (localization on cattle chromosome 17q12-q13) mapped to this region at 1p15-p17. Because human *FGG* is localized on human chromosome band 4q28, the analysis indicated that this unknown band is syntenic to this part of human chromosome 4 (see Figure 10 and Table 4). This assignment of the gene *FGG* was supported by the hybridization signal obtained with the clone 1457 (see Figure 10), which had been reported to hybridize to cattle chromosome 17q12 (Fronicke and Scherthan, 1997). The mapping of gene *FGG* is an example where Zoo-FISH was insufficient to identify a syntenic region, but the mapping of a gene was successful.

The prediction of syntenic regions between *M. muntjak* and *M. reevesi* was based on a previous study (Yang et al., 1997c). In this thesis 23 genes could be mapped to the *M. reevesi* karyotype. The identified positions were consistent with the assigned syntenic regions between *M. muntjak* and *M. reevesi* according to (Yang et al., 1997c). To identify the *M. reevesi* chromosomes, a combination of DAPI banding and whole chromosome paints (used for the smaller chromosomes due to their banding similarities) was successful. The mapped genes covered 18 of the 23 chromosomes giving an almost complete set of probes to study the *M. reevesi* chromosomes. The new set of probes specific for genes in both muntjac species can now be used to analyze the connection between local gene environment and 3D gene positions in different species and to visualize genes for the study of nuclear architecture.

6.2. The generation of whole chromosome paints

In the context of studying the nuclear architecture, the 3D location of chromosomal territories and their genes, especially the question of the localization of actively transcribed versus silent genes, were the subject of multiple investigations (Dietzel et al., 1999; Kosak et al., 2002; Mahy et al., 2002b). The majority of these studies were performed using human or mouse cells. It is generally assumed, that the nuclear architecture and the principles that govern gene regulation and transcription are conserved in all mammalians (Mahy et al., 2002a; Mahy et al., 2002b; Tanabe et al., 2002). It would therefore be desirable to be able to

visualize each individual territory in the interphase nucleus. With only 3 chromosome pairs in the female muntjac but about the same DNA content and number of genes as humans (Levy et al., 1993), *M. muntjak* seems to be ideally suited for a comparative analysis. However, the very limited number of mapped genes makes it a very difficult task. As part of this work, a number of important tools were generated to study *M. muntjak*. Forty-one genes, the localization of which were known in human or cattle, were mapped in *M. muntjak.* In addition, whole chromosome paints for *M. muntjak* were generated, which specifically stained individual metaphase chromosomes. However, centromeres were labeled by cross-hybridizations, most likely due to the presence of highly repetitive sequences or to the over amplification of repetitive sequences located at these regions during the DOP-PCR procedure (Cheung and Nelson, 1996). This problem has been observed before (Yang et al., 1995). This kind of crossreactivity of paints with centromeric regions has also been observed in studying human chromosomes and it could be blocked by adding Cot-1 fractionated DNA to the FISH-paint. Human Cot-1 DNA contains a lot of the repetitive sequences of the human genome (Strachan and Read, 1999). Unfortunately, during the course of the thesis, it was impossible to obtain enough genomic DNA from *M. muntjak*, to generate Cot-1 DNA. Cot-1 DNA produced using genomic DNA from cattle, roe deer, or even from Chinese muntjac, did not suppress the nonspecific signals sufficiently. Especially problematic was the constricted neck region on chromosome 3X which was described to contain repetitive sequences like interstitial telomeric DNA, satellite I (C5) and satellite II (MMV0.7) sequences (Lee et al., 1993; Li et al., 2000; Yang et al., 1997b). Whole chromosomal paints specific for each muntjac chromosome have been used before to study chromosomal evolution (Yang et al., 1995). However, to study the 3D localization of chromosomal territories in interphase nuclei, the level of crossreactivity would have to be substantially reduced. With adequate *M. muntjak* Cot-1 DNA, this problem could potentially be solved. The availability of specific whole chromosome paints for *M. muntjak* would allow the localization of genes within their chromosomal territories in the context of a 3D nucleus. In the following research, *M. muntjak* cells were used to analyze the localization of genes in the 3D nucleus.

6.3. 3D analysis of mammalian nuclei

The overwhelming majority of the published analyses of the spatial relationship of genes and chromosomal territories to each other and within the nucleus was done using the method of 2D FISH (Roix et al., 2003; Taslerova et al., 2003; Volpi et al., 2000). The general fixation method for 2D FISH involves a hypotonic treatment, methanol-acetic acid dehydrating fixation, and ultimately dropping of the fixed cell material on a slide resulting in flattened nuclei suitable for 2D analysis. This hypotonic treatment causes an enlargement of cells and their nuclei and the chromatin to be more loosely packed (Yokota et al., 1997; Yokota et al., 1995) making distance measurements between genes inaccurate. Another disadvantage of the 2D analysis is the possibility of misinterpretation of images. Genes that would be located on top of each other in a spherical nucleus (e.g. of a hematopoietic cell) can appear to be in close proximity. To compensate for these problems, Roix et al. analyzed several thousand cells using a semi-automated high-throughput image acquisition system to find significant differences in gene positions (Roix et al., 2003). Kozubek and coworkers developed a prediction model to interpret 2D images with the calculation of the theoretical distribution (Kozubek et al., 2001). However, these analyses can still only provide an approximation of the real 3D organization in a spherical nucleus.

In contrast to most studies, which performed the bulk of their analyses in 2D fixed cells with only a few 3D experiments to confirm the data (Mahy et al., 2002a; Volpi et al., 2000), almost all analyses in this thesis were performed on 3D fixed nuclei. To achieve a more accurate representation of a cell's 3D structure, 4% paraformaldehyde fixation was used in the present study. This established method (Kurz et al., 1996) with few a modifications to optimize analysis in different cell lines, was the method that gave the most reproducible and accurate results. It is the fixation method that has repeatedly been shown to conserve the chromatin architecture during FISH best (Kurz et al., 1996; Solovei et al., 2002). Performing all analyses of hematopoietic cells in 3D presented a number of challenges. For the nearly spherical morphology of these cell, an analytic method had to be found to interpret 3D confocal image stacks. This was accomplished with the help of the Amira 3.1 software and the computational tools developed by Juntao Gao. This form of

analysis allowed the accurate determination of the position genes in the 3D volume of interphase nuclei.

Most analyses expressed the location of genes (Bartova et al., 2002) or chromosomes (Cremer et al., 2003) as a percent of the nuclear radius. To describe positions of various genes in 3D fixed nuclei more accurately, I analyzed data as a percent of nuclear radius and in addition, used two different methods to assign genes to concentric shells. A similar system for the analysis of 2D images was published earlier (Bridger et al., 2000; Croft et al., 1999). The 2D area of the nucleus was divided into 5 concentric shells of equal area, and was used to describe positions of chromosome territories in 2D fixed nuclei. For the analyses in this thesis, the 3D volume of the nuclei was divided into 5 concentric shells, to describe the preferred location of a gene in 3D fixed nuclei. In one system (see Figure 18A) the nucleus was divided into 5 concentric shells of equal volume and in another (see Figure 18B) into 5 equidistant shells (with equal fractions of the nuclear radius). The results obtained with the method of rendering confocal image stacks followed by analysis of gene distances using the mathematical tools developed by Juntao Gao proved to be highly reproducible in determining the 3D position of genes in nuclei of hematopoietic cells. For instance, in all 10 tested cells and cell lines, the order of the localization of all genes and loci tested was preserved.

The improved accuracy of the methods used in this study came at the cost of the time consuming analysis involved to produce the IV-files required to evaluate the data. Proposed improvements for the future would therefore include various automated steps of the rendering process involved in generating "clean" IV-files. Even a small background surface located far outside the signal of interest to be rendered can affect its center of gravity calculation required for distance measurements. Furthermore, in many of the reports describing localization of chromosomes using 2D analysis the location of the chromosomes was expressed as the distance of its intensity weight center to the surface of the nucleus (Boyle et al., 2001; Croft et al., 1999; Taslerova et al., 2003). Calculation of the intensity weight center of rendered objects is not yet possible in 3D with the method developed in this thesis. They will have to be developed to make the method even more accurate.

6.4. The 3D position of *MLL* is conserved in different hematopoietic cells

MLL is the gene with the most known translocation partners (Drexler et al., 2004; Futreal et al., 2004; Huret, 2003). It has been assumed that a correlation exists between the intranuclear localization and the propensity of a gene to be involved in translocations (Roix et al., 2003); this work represents the first 3D localization of *MLL* and some of its most frequent translocation partners. The order of the localization of *MLL*, *AF4*, *AF6*, *AF9*, *ELL* and *ENL* were the same in all hematopoietic cells. *ELL* and *ENL* where found most closely to the nuclear center, and *AF4*, *AF6* and *AF9* were much closer to the nuclear surface. *MLL* was found at an intermediate position. Interestingly *AF4*, *AF6*, and *AF9*, the three most common translocation partners (Gu et al., 1992a; McCabe et al., 1992; Mitelman et al., 2003), had very similar localization probabilities. This result was found for all tumor cell lines as well as in hematopoietic progenitor cells. Originally a difference in the localization of these genes between cells of different stages of hematopoietic development was expected, because it was thought that translocations occur at a stage of development, that precedes the differentiation of progenitor cells into the lymphoid and myeloid cell lineage (Graeves, 2003). This assumption is based on the occurrence of leukemia involving translocations of *MLL* in both the B-cells and myeloid cells, but rarely in other tissues (Baffa et al., 1995). Interestingly, despite the reproducible localization in lymphoid cells, the localization of the 3 genes *MLL*, *AF4*, and *AF9* in fibroblasts was very different. In these cells, *AF4* and *AF9* were located closer to the nuclear center than *MLL*, and this finding was true in human fibroblasts as well as in fibroblasts of the two muntjac species. It is unknown at present how the observation of tissue specific localization of genes relates to the translocations involving *MLL*. However, these reproducible differences between hematopoietic cells and fibroblasts point to a difference in regulation of 3D localization that could be involved in causing these translocation events.

6.5. The distances between *MLL* and its translocation partners

It could be conceivable that genes that frequently participate in translocation events are located close to each other. For instance, translocations between *BCR* and *ABL1* lead to

CML and are more frequently observed than translocation between *EWSR1* and *FLI1* leading to Ewing sarcoma. The different spatial localization of critical genes might be one of the factors responsible for the much lower incidence of Ewing sarcoma than of CML (Taslerova et al., 2003). However, it has been recently demonstrated that most chromosomes do not have a preferred localization relative to each other in interphase nuclei (Cornforth et al., 2002) with the exceptions of chromosomes 1, 16, 17, 19 and 22, a grouping earlier suggested by (Boyle et al., 2001) to be close to the nuclear center. Consistent with this finding, the average distance of *MLL* to most tested genes was very similar with the exception of *ENL*, which was closer to *MLL* then *AF4*, *AF6* and *AF9*. Although *MLL* and its translocation partners were found to have a preferred distance to the nuclear surface, the position of these genes within their predicted shells was random. Using angle measurements, no evidence was found for a clustered or polarized organization of genes. This concurs with the assumption that chromosome positioning patterns are probabilistic rather than absolute (Parada et al., 2003).

There are a number of theories to explain preferred involvement of genes in chromosomal translocations. One model suggests that physical closeness of chromosomes to each other can explain this phenomenon (Croft et al., 1999). This analysis found that genes located on the gene dense chromosome 19 and the gene poor chromosome 18 are rarely involved in translocations with each other. The analysis of this thesis work, however, determining the 3D localization of multiple genes in various cells, did not provide evidence generally to support this hypothesis. Another model states that sizes of chromosomes could be an important factor to explain their involvement in translocations. According to this model larger chromosomes are more likely subject to translocations than smaller ones due to their higher DNA content (Bickmore and Teague, 2002). However, this does not explain the existence of the breakpoint cluster regions that exist in many of the involved genes (Gu et al., 1992a; Reichel et al., 2001; Strissel et al., 2000).

Because the determination of the 3D localization of *MLL* and its translocation partners did not provide a direct clue with respect to the involvement of these genes in translocation events, I assessed the gene size of *MLL* and 38 of its translocation partners (**Figure 44**). The average size of a human gene was determined to be about 28,000 bp (Venter et al., 2001). Of the 39 genes analyzed in this thesis, 32 were larger than the average gene. Many of them were significantly larger. The average size of all these genes was 154,635 bp. Gene size

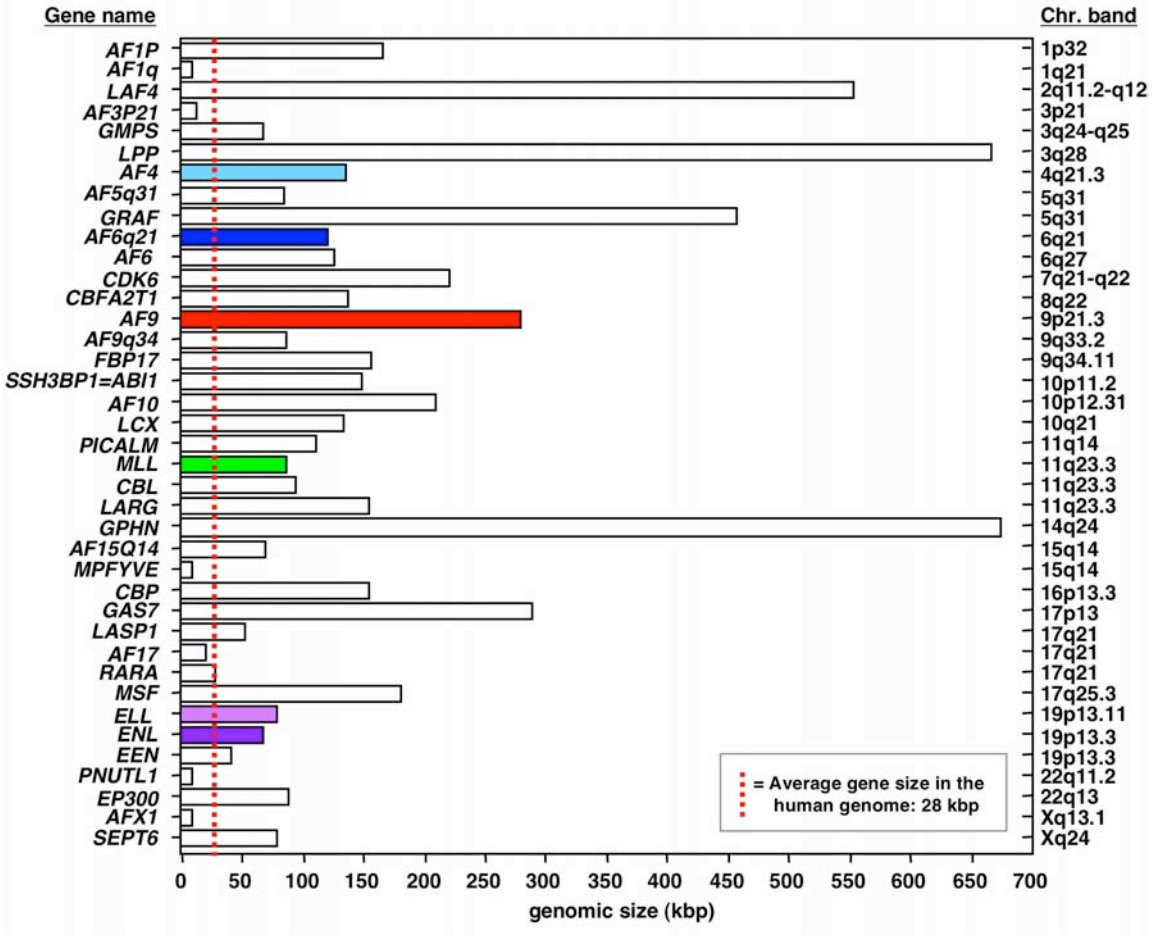

Figure 44: The majority of *MLL* translocation partners are very large genes. The genomic size of *MLL* and its translocation partners is shown. Information about gene size: http://www.ncbi.nlm.nih.gov/entrez/query.fcgi?CMD=search&DB=unigene or http://genome.ucsc.edu//. The average size for a "typical" gene in human DNA is 27,894 bp (see red dotted line) (Venter et al., 2001). 82% of the genes involved in translocation with *MLL* are larger than the average gene size in the human genome. The genes investigated more closely in these work are highlighted with solid colored bars.

could, therefore, be a factor that determines the propensity of genes to participate in translocations.

As part of this work, *MLL* was found to be preferentially located at the surface or even outside the territory of chromosome 11 using both 2D and 3D analysis techniques. This "looping out" effect has been reported for other genes and correlated with the rate of transcription of these genes (Mahy et al., 2002a; Mahy et al., 2002b; Volpi et al., 2000; Williams et al., 2002). This could not be confirmed for *MLL*, which was found to be a weakly transcribed gene according to the analysis of SAGE libraries of various tissues. Many other genes were shown to preferentially localize to the surface of chromosome territories, sometimes even to loop out from the surface and this localization has been frequently thought to reflect the transcriptional activity of a gene. Both, active and inactive genes (*DMD*, *HBB* and *MYH7*), were found to localize preferentially at the periphery of chromosome territories in myoblasts, myotubes, fibroblasts and HeLa cells, whereas a non-transcribed genomic sequence was found randomly distributed in myoblasts, myotubes, fibroblasts or preferentially interior in HeLa cells (Kurz et al., 1996).

A predominantly peripheral position of the major histocompatibility complex (MHCII) locus was observed with a specific looping out from the chromosome 6 surface upon activation of gene transcription with INFγ (Volpi et al., 2000). The position seems to correlate with the transcription of many genes in this region. EDC (epidermal differentiation complex at 1q21 (Williams et al., 2002) was found in keratinocyte nuclei to be frequently positioned external to the chromosome 1 territory compared to lymphoblasts, where the EDC more often adopts a peripheral or internal location.

Some reports support a model, in which the transcriptional activity of genes determines its localization within chromosomal territories (Mahy et al., 2002b). In addition, by studying a larger chromosomal region (11p15.5 region and the syntenic mouse chromosome 7, Bickmore and coworkers suggested that local gene density and transcription, rather than activity of individual genes influence the organization of chromatin outside of the chromosome territory detectable by FISH (Mahy et al., 2002a). This could provide an

explanation for the finding in the present study, that a weakly expressed gene, such as *MLL*, is often found to be "looped out" of its chromosome territory. An analysis of the expression of genes in the vicinity of the *MLL* gene could provide information on whether the transcriptional activity of genes in this region might be responsible for the "exposed" location. An experiment was performed in which transcription was inhibited by actinomycin D (Mahy et al., 2002a). They observed a decrease of signals outside of chromosome territories in treated cells. However, even in treated cells most signals were still outside of territories suggesting that other factors such as chromatin structure could contribute to maintaining the positions of genes.

6.6. Effect of DNA damage and cell cycle on nuclear organization

DSBs have been reported to contribute to translocation events (Richardson and Jasin, 2000). As a first attempt to test this notion, DSBs were introduced experimentally into the DNA of Triggs cells by treatment with etoposide. Etoposide is an inhibitor of topoisomerase II and its use in cancer treatment is associated with translocations that can lead to therapy related leukemia, involving the bcr of *MLL* and *AF9* (Strissel et al., 2000). DNA damage induced by etoposide was shown to have an effect on the global nuclear organization (Bartova et al., 2003; Marchetti et al., 2001). Etoposide had been used to directly induce a translocation involving *MLL* and *AF9* (Betti et al., 2001; Betti et al., 2003). This form of DNA damage did not significantly affect the 3D position of *MLL* or its translocation partners (see Figure 33).

It is unknown, whether translocations preferentially occur at specific stages of the cell cycle. It is known that the chromatin moves during the cell cycle (Chubb et al., 2002; Vazquez et al., 2001). The chromosome order changes during mitosis and early G1 but is relatively stable during the subsequent S and G2 stages (Ferguson and Ward, 1992; Walter et al., 2003). The position of *MLL* and *AF9* was found to be constant in the analyzed phases (see Figure 34). Because a closer proximity of chromosomes could occur either at mitosis or early G1, which might slightly increase the possibility of a translocation event, the 3D

localization of genes will have to be studied at these cell cycle stages using different methods.

Integrate: Ionizing radiation can also induce rearrangements of the genome (Hlatky et al., 2002; Johnson et al., 1998). When irradiation occurs during the G0/G1 phase of the cell cycle, large scale of rearrangements appear as exchange-type chromosome aberrations at the next mitosis (Hlatky et al., 2002).

Leukemia causing translocations can be induced by chemotherapy. Topoisomerase II is an important enzyme during replication. It relaxes stressed supercoiled DNA and unknots tangled chromosome strands (for review see (Wang, 2002)). Etoposide is a widely used chemotherapeutic drug that is closely associated with therapy related leukemia presumably by its inhibition of topoisomerase II (Rowley and Olney, 2002; Whitmarsh et al., 2003).

6.7. Translocation events change the nuclear positions of genes

In this thesis it was demonstrated that translocation events can result in a change in the 3D localization of genes. It was found that translocation events involving the same gene but different translocation partners caused significantly different changes. The same translocation event in different cell lines resulted in similar changes validating the form of analysis and suggesting general principles that underline the 3D localization of genes in hematopoietic cells.

It is now well established that translocation events can change the positions of chromosomal domains. This has been shown repeatedly for chromosome rearrangements between human chromosomes 18 and 19 (Cremer et al., 2003; Croft et al., 1999). It has been argued that differences in the overall composition of bulk chromosome 18 and 19 DNA sequences may play a direct role in the nuclear destiny of these two chromosomes and the genes they contain (Croft et al., 1999), and that the gene density of chromosomes is responsible for their position within the nucleus (Cremer et al., 2003; Croft et al., 1999). The der 18 was shown to be slightly less peripheral than the normal chromosome 18 suggesting that the chromatin composition of a given segment, by itself, is important for its nuclear location (Croft et al., 1999). In general, estimated gene density of each chromosome was

correlated with its average position within the nucleus. Chromosomes with fewer genes are often associated with the nuclear periphery, while gene rich chromosomes reside in a more internal nuclear position. In 7 out of 8 tested tumor cell lines some of which had imbalances or rearrangements of these two chromosomes, this localization was less pronounced suggesting that chromosome aberrations can change the localization of chromosome territories (Cremer et al., 2003). However, translocations do not always change the localization of chromosomal territories. Parada and coworkers (2002) reported that chromosome territories #12, 14, and 15 clustered in nuclei of normal mouse splenocytes as well as in a mouse lymphoma cell line, in which these three chromosomes were involved in two translocation events (Parada et al., 2002). The translocation in this example did not alter the relative arrangement of the territories to each other.

The potential position effect was not only observed for whole chromosomes but also for single genes involved in translocations. A distinct change in the position of genes (*EWSR1* on chromosome 11 and *FLI1* on chromosome 20) was observed after their reciprocal translocation (Taslerova et al., 2003). Normal *EWSR1* had a more central, *FLI1* a more peripheral position. Both fusion genes took a position intermediate for both normal genes. This finding was interpreted to be caused by the changed gene density of the translocated chromosomes. Consistent with this model, it was found that the two genes *ABL1* (on chromosome 9) and *BCR* (on chromosome 22) did not significantly change their position after translocation (formation of the Philadelphia chromosome), because the position of these genes on the normal chromosomes was very similar. It was proposed that the radial location of the fusion gene does not depend on the location of the translocation event, but that it might be determined by the final structure of the chimeric chromosomes (Taslerova et al., 2003).

It is generally believed that the interaction between two ends from different DNA double-strand breaks can produce a tumorigenic chromosome translocation (Elliott and Jasin, 2002), but until recently it was unknown to what extent DSB-containing chromosome domains are mobile and can interact. Two theories were proposed involving different requirements for the mobility of the chromosomal ends generated by a DSB: the static

"contact-first" or dynamic "breakage-first" theory. Independent of the resulting factor of a double strand break, the "contact-first" theory proposes that interaction between unrelated chromosome breaks can take place only when the breaks are created in chromatin fibers, which colocalize at the time of DNA damage induction. The "breakage-first" theory assumes that breaks formed at distant locations can subsequently be brought together to produce translocations. These theories were first developed in the first half of the 20th century (reviewed by (Belyaev, 2004)). Aten at al. (2004) were able to observe double strand breaks in living cells, and noted that DSBs are motile and can interact (Aten et al., 2004), giving support to the "breakage-first" theory and possibly explaining the origin of chromosomal translocations. Aten et al. (2004) analyzed the dynamics of DNA double strand breaks in HeLa cells. DSBs were induce by irradiation (alpha-particles) and visualized by immunodetection of histone H2AX phosphorylation. The observed tracks of the moving breaks points changed within minutes. The results support the breakage-first theory by showing that DSB-containing chromosome domains are mobile and can cluster.

It has been shown that two DSBs (Richardson and Jasin, 2000) or even only one (Ludwikow et al., 2002) are sufficient to cause a translocation event involving chromosomes that are not necessarily directly adjacent. Together with the finding described above (loose ends of chromosomes produced by DSBs can move in the nucleus) it is conceivable that fixed positions of genes in the 3D nucleus can cause preferred translocations, explaining why the analysis in this thesis did not find a general close proximity of translocation partners, but revealed their preferred and now predictable localizations in lymphoid cells. In support of this hypothesis are the data that demonstrate that the localizations of these genes in fibroblasts were very different. In conclusion, the analysis presented here supports the "breakage first" theory. In summary, the available information suggests that a direct co-localization of DSBs is not a pre-requirement for a translocation event. Close proximity chromosomal ends that have resulted from DSBs, however, might favor a translocation event.

6.8. Rules that govern organization of genomes in interphase

It is likely that the principles that helped to shape the structure of genomes are applicable to both higher as well as lower organisms. A high level of organization is found not only in mammalian nuclei, but also in organisms with simple circular genomes such as prokaryotes (eubacteria and archaebacteria). It has been shown that conserved genes in bacteria, which cluster together, might be functionally linked (Martin et al., 2003). By applying comparative genomics, it was postulated that the different phenotypes of bacteria are not only caused by differences in gene composition, but also by the manner genes are distributed in the genome. Specific gene clusters were identified, which distinguished gram positive from gram negative bacteria (Martin et al., 2003). Furthermore, in a comprehensive comparison of archaeal and bacterial genomes, it was observed, that a statistically significant number of orthologs maintained their relative locations over the entire genome (Horimoto et al., 2001). A relationship between genome architecture and gene function was therefore suggested even in bacteria. This seems to indicate that genome architecture is an early concept in the development of living organism.

Nonrandom positions of chromosomes and subchromosomal domains are observed in all eukaryotes, and the functional implications for the long-range organization of the genome in the interphase nucleus for gene function is a subject of current research (Taddei et al., 2004).

While analyzing the human genome as part of this work, it was striking to find chromosomes with very different gene densities ranging from about 4 to 24 genes per 1 million base pairs (all gene density analyses were performed utilizing the online database at http://www.ncbi.nlm.nih.gov/mapview/). Gene poor chromosomes are Y, 13, 18 and gene rich chromosomes were 17, 19, 22. When chromosome arms were compared, many chromosomes showed a similar density for both arms (less than 1 gene/Mbp difference for chromosomes 2, 3, 4, 9, 12, 19, X and the largest differences for chromosomes 6 (8.4 genes/Mbp) and 16 (6.0 genes/Mbp)). This leads me to speculate that a uniform gene density throughout the chromosome might be beneficial to uniformly orient the chromosomes in the 3D volume of the nucleus while avoiding physical strains.

I therefore postulate that in order for a germline translocation to manifest itself in a living organism and survive evolution, it must (among other requirements) not disrupt or compromise the functional organization of the genome. It may therefore not be sufficient for a translocation not to cause a disadvantage on the molecular level (e.g. lethal effect of a translocation, or loss of an important protein function), but it also has to comply with the existing nuclear architectural requirements of the organism. This maintenance-requirement might lead to a drastic reduction of successful translocation events in evolution. This requirement may also contribute to the rareness of successful translocation events in higher organisms. The increased complexity of the genome might make it more difficult for a translocation to survive. Given the uniformity of gene density among chromosomes, as analyzed in detail for humans and chicken (Habermann et al., 2001; Saccone and Bernardi, 2001; Saccone et al., 2002; Saccone et al., 1999), it seems to have been beneficial that chromosomal rearrangements or exchanges involve chromatin of similar gene density.

This makes the analysis of the two muntjac species with their drastically different numbers of chromosomes but same number of genes very attractive. Unfortunately, due to the lack of detailed information on the gene composition in the two muntjac species the distribution of genes within the syntenic regions could not be evaluated. However, using cattle probes and the knowledge of syntenic regions between cattle and human, a predicted gene density map of the *M. muntjak* genome could be generated (**Figure 45**). Although gene dense and gene poor clusters were found on each chromosome, in general the three chromosomes could not be clearly grouped into gene dense and gene poor chromosomes. This indicates that rules that govern positions of genes on human chromosomes may not be directly applicable to the unique situation of the *M. muntjak* genome. The three muntjac chromosomes are so large that their territories could easily span the entire nucleus. The analysis supports a model that local gene densities determining localization of genes and loci rather than of the entire chromosome. This is most obvious in the extreme case of the *M. muntjak* chromosomes.

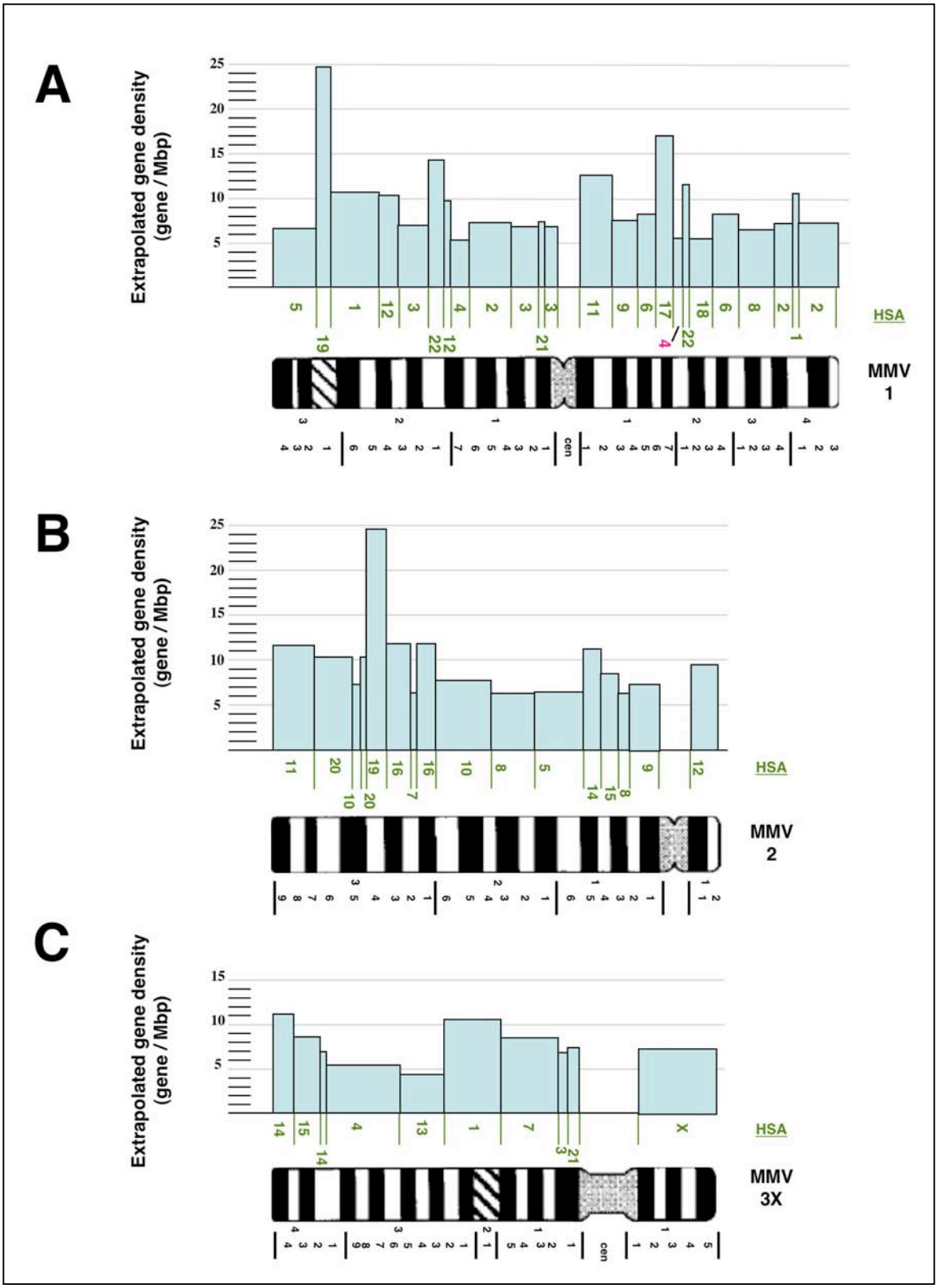
A
Extrapolated gene density (gene / Mbp)
HSA
MMV 1
B
Extrapolated gene density (gene / Mbp)
HSA
MMV 2
C
Extrapolated gene density (gene / Mbp)
HSA
MMV 3X

Figure 45: Gene density of Indian muntjac chromosomes extrapolated from the average human whole chromosome density at the sites of designated synteny between both species (Ideogram was adapted from Yang et al., 1997).
A: Extrapolated gene density of Indian muntjac chromosome 1.
B: Extrapolated gene density of Indian muntjac chromosome 2.
C: Extrapolated gene density of Indian muntjac chromosome 3X.
Light green: Summary of syntenic regions between *M. muntjak* and *Homo sapiens* as published by Yang et al. (Yang et al., 1997a) and Fronicke and Scherthan (Fronicke and Scherthan, 1997).
Pink: Assignment of the previously unassigned small region located at 1q17-q21 to be syntenic to human chromosome 4 (for detailed explanation see Figure 9).
HSA = chromosomes from *Homo sapiens.*
MMV = chromosomes from *M. muntjak.*

Gene density information for the human chromosomes was obtained from the website http://www.ncbi.nlm.nih.gov/mapview/maps.cgi.

6.9. Gene densities in the immediate proximity of genes serves as a predictor of their 3D localization

One of the main findings is that genes have specific 3D-localizations in the interphase nucleus. This could be demonstrated for 10 different genes, and it was highly reproducible in various different hematopoietic cell types. Interestingly the localization of the fusion genes after translocation events changed in a very specific and reproducible fashion. The same type of translocation event showed very similar behavior in different cells (e.g. the t(9;11) in MonoMac6 and THP-1 cells and the t(4;11) in RS4;11 and MV4-11 cells). The question therefore arose as to what determines the position of a gene within the nucleus prior to and after a translocation event. Or more generally, what determines the 3D localization of a DNA sequence relative to the nuclear surface? Do parts of the chromosomes, such as the centromere or telomeres play a role in the positioning of a gene or is the chromosome as a whole responsible for gene localization? It was speculated that centromeres might be important for the chromosome position. After centromeric heterochromatin was disrupted with a DNA interchelator, positioning patterns of chromosomes were lost (Gerlich et al., 2003). It was therefore assumed that chromosome specific timing of sister chromatid

separation transmits the position of a chromosome from one cell generation to the next. If the centromere of chromosome 11 would be the determining factor of its position, 5'*MLL* in the der(11) should have maintained the same position as in the normal chromosome 11, which is clearly not the case. If the telomeres played a significant role in the position, 3'*MLL* should have the same position in der(4) and in normal chromosome 11, and that is not the case either. Another model to explain the behavior of genes is based on analyses of the location of chromosomal territories. It was proposed that gene density of chromosomes determine their position (Cremer et al., 2003; Mahy et al., 2002a; Tanabe et al., 2002). Chromosomes with higher gene density are closer positioned to the nuclear center, whereas

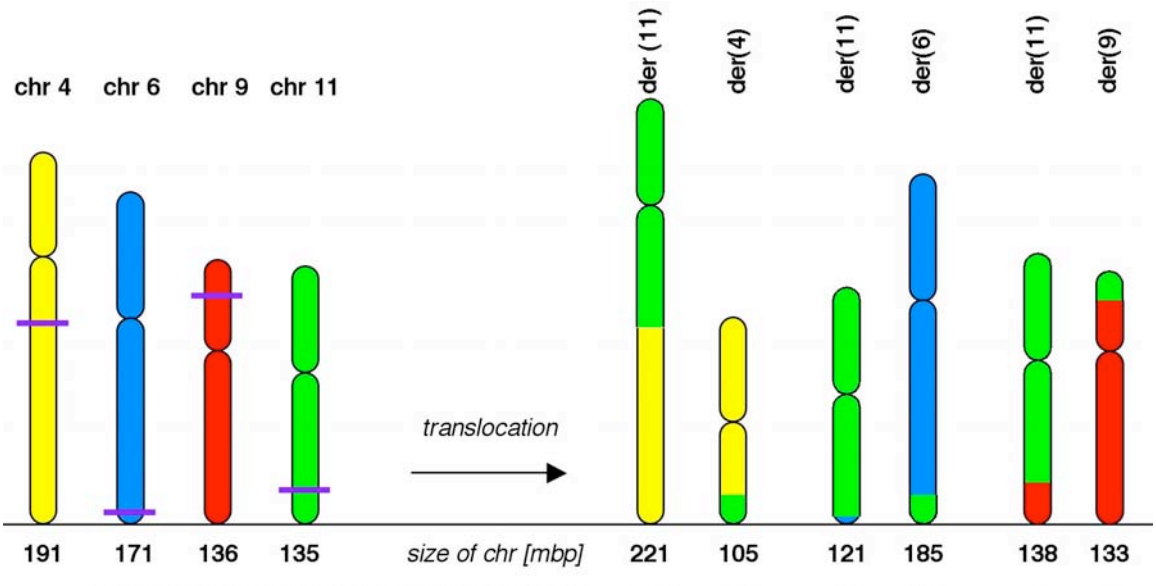

191	171	136	135	*size of chr [mbp]*	221	105	121	185	138	133
				size change from normal chr to der(chr) (mbp)	+86	-86	-14	+14	-4	+4
				size change from normal chr to der(chr) (%)	+63	-45	-10	+8	+3	-3
				part of chr 11 in der(chr) (mbp)	118	17	118	17	118	17
				part of other chr in der(chr) (mbp)	103	88	3	168	20	116
				part of chr 11 in der(chr) (%)	53	16	98	9	86	13
				part of other chr. in der(chr) (%)	47	84	2	91	14	87

Figure 46: Overview of the transfer of chromosomal material during the translocations involving *MLL* and some of its major translocation partner genes.
Left: normal chromosomes are drawn approximately to scale. Purple bars indicate location of MLL or its translocation partners. Information about chromosome size was retrieved from the NCBI-websites. chr = normal chromosome, der = derivative chromosome.

chromosomes with low gene density are located more at the nuclear periphery (Boyle et al., 2001; Croft et al., 1999). A preliminary analysis obtained as part of this thesis suggested, that this model cannot be completely correct. For instance, the t(9;11) translocation resulted in only a small balanced exchange between chromosome 11 and 9 (**Figure 46**). It seemed unlikely that the overall gene density of the der(11) could be changed that dramatically compared to normal chromosome 11 in order to explain the shift in the position of the 5'*MLL* signal from a more central to a more peripheral localization, which was almost identical to the position of *AF9*. The same was true for the *AF9* locus on chromosome 9 and its change of position after translocation (see Figure 36). To explain the discrepancy, I hypothesized that the gene density not of the entire chromosome or chromosomal arms, but

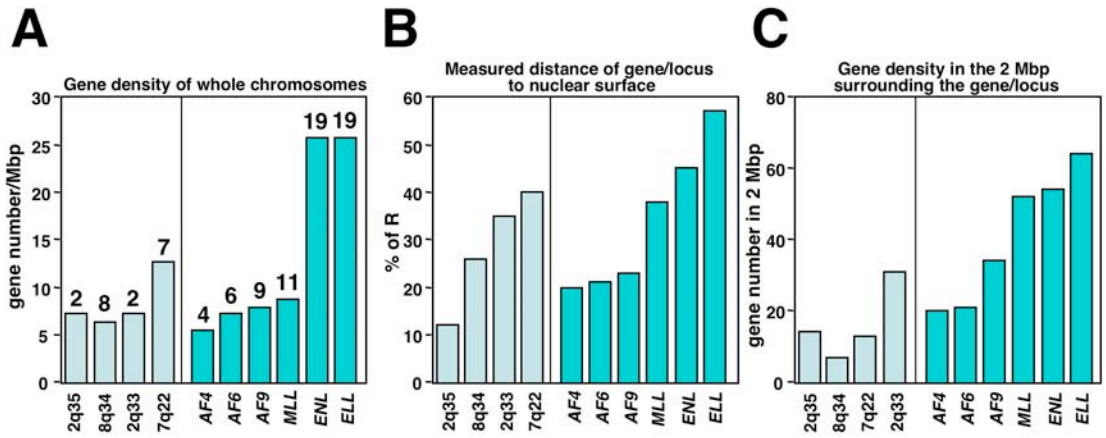

Figure 47: Comparison of the gene density of entire chromosomes with the local gene density within 2 Mbp of genes/loci for being predictors for the 3D nuclear position of genes.

Light blue bars are relevant for the control loci, dark green bars for *MLL* and 5 translocation partners.

A: Gene density of entire chromosomes.

B: Measured distances of genes/loci to nuclear surface. Values are the normalized median values as seen in Figure 25.

C: Gene density in the 2 Mbp windows surrounding the genes/loci.

HSA = chromosomes from *H. sapiens.*

MMV = chromosomes from *M. muntjak.*

Gene density information for the human chromosomes was obtained from the website http://www.ncbi.nlm.nih.gov/mapview/maps.cgi.

rather of a specific region surrounding the locus, may determine the 3D position of that locus.

To test this hypothesis and, if correct, to determine the size of the region, that determines nuclear location, the gene density of whole chromosomes, chromosomal arms, and different areas of 0.2, 2, 5, 10, 20, and when possible 30 and 40 Mbp surrounding all the tested loci on normal and derivative chromosomes was assessed (data not shown). This analysis revealed that the gene density of a region of 1 Mbp upstream and downstream (2 Mbp total) of a locus was the best predictor for the intranuclear localization of that locus. The result of the analysis of 4 control loci (light green), and of *MLL* and 5 of its translocation partners (dark green) is shown in **Figure 47**. **Figure 47A** shows the gene density of entire chromosomes of the tested loci expressed as number of genes per Mbp. It is obvious that the tested loci were on chromosomes with similar gene density except for *ENL* and *ELL*, which are both on the highly gene dense chr19. According to the current model, the gene density of the chromosome should determine the localization of its genes. Thus, *AF4*, *AF6*, *AF9* and *MLL* should have a position similar to *ENL* and *ELL*. However, the result of the analysis, which is shown in **Figure 47B**, is not consistent with that prediction. *MLL* clearly has a position more central than *AF4*, *AF6* and *AF9*, and so does *ELL* when compared to *ENL*. **Figure 47C** illustrates that local gene density (2 Mbp surrounding the locus), predicts more correctly the localization of *MLL* and its translocation partners.

The situation becomes even more obvious, when translocation events are evaluated using the 2 Mbp window. **Figure 48A** shows the analysis of the t(9;11) translocation found in MonoMac6 cells, **Figure 48B** of the t(4;11) translocation in RS4;11 cells, and **Figure 48C** of the t(6;11) translocation in ML-2 cells. In all three cases, the analysis of the gene density of whole chromosomes (**Figure 48**, left panels) did not predict a major change of the localization of loci prior or after translocation. In contrast, the analysis of the gene density using the 2 Mbp window predicted major changes (**Figure 48**, center panels). These predicted changes were more in agreement with the actually measured distances of loci to the nuclear surface (**Figure 48**, right panels). For instance using the 2 Mbp method, this gene density of the loci on der(9), der(4), and der(6) was much higher than on der(11).

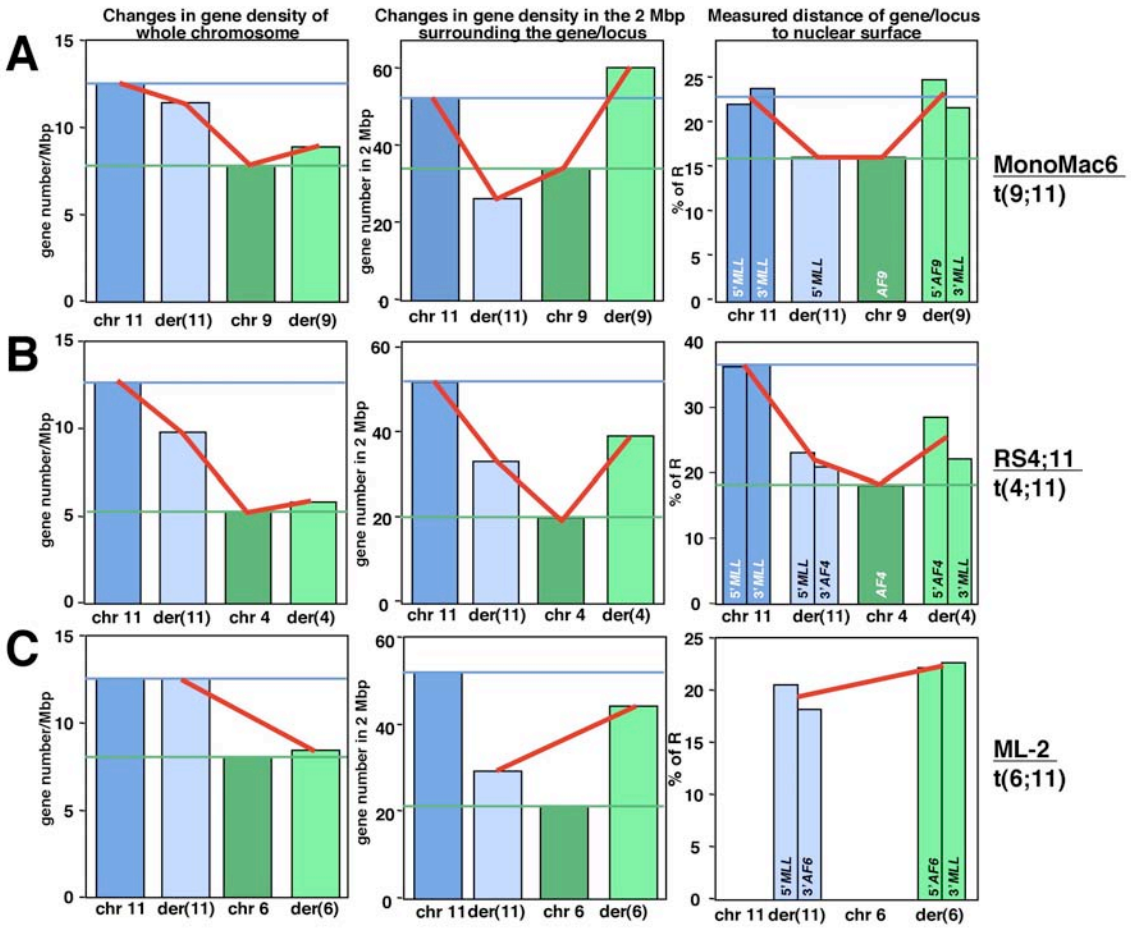

Figure 48: Comparison of gene density of entire chromosomes with the local gene density in a 2 Mbp window surrounding the gene as a predictor for changes of 3D localization after translocation events.

Dark blue column: chr 11; light blue column: der(11); dark green column: other normal chromosome; light green column: other derivative chromosome. Red line indicates the general pattern of change between the normal and derivative chromosomes.

Left panels: Gene density of whole chromosomes.

Center panels: Gene density in the 2 Mbp window surrounding the gene.

Right panels: Measured distances of genes to nuclear surface. Median values as calculated for Figures 36, 39, 43.

A: Values relevant for the cell line MonoMac6 with t(9;11) involving *AF9* and *MLL*.

B: Values relevant for the cell line RS4;11 with t(4;11) involving *AF4* and *MLL*.

C: Values relevant for the cell line ML-2 with t(6;11) involving *AF6* and *MLL*.

Gene density information was obtained from the website http://www.ncbi.nlm.nih.gov/mapview/maps.cgi, and calculated for the derivative chromosomes.

In contrast, the whole chromosome showed a lower gene density in all 3 cases. The analysis of the three translocations was much more consistent with the 2 Mbp model than with the conventional model (note: since ML-2 cells do not have normal chromosomes 6 and 11, only derivative chromosomes could be analyzed). Similar data were also found for THP-1 cells, another t(9;11), and MV4-11 cells, another t(4;11) cells (data not shown). As mentioned above, all translocations in all cells were also analyzed with the 0.2, 5, 10, 20, 30, and 40 Mbp window (data not shown). The 2 Mbp window gave the best fit between gene density and measured distances of loci to nuclear surface. The data therefore suggest that the gene density in the immediate vicinity of a gene (a region as small as 2 Mbp) is the best predictor of its 3D localization in the interphase nucleus.

6.10. Putting the "2 Mbp method" to the test

Most of the published data suggest that changes in the position of genes and chromosomal territories after a translocation event depend on the gene density of the whole chromosomes or large chromosomal regions. However, none of these models were able to predict the dramatic changes detected in some of the analyzed translocations in this work. Using the 2 Mbp window allowed me to more accurately predict the 3D positions of genes in all cells with normal and rearranged loci.

To determine whether this novel method can be applied more generally to predict the localization of genes and subchromosomal domains, I re-analyzed some of published data:

Example #1: In a 2D image analysis of cells with a t(11;22) translocation involving the genes *EWSR1* on chromosome 22q12 and *FLI1* on chromosome 11q24, a positional shift of the derivative genes was observed (Taslerova et al., 2003). The authors measured the distance of the normal genes and the genes on the derivative chromosomes to the nuclear center as of % of the nuclear radius. *EWSR1* was more centrally located than *FLI1*. To analyze these published data by analogy to the data produced in this thesis (see Figure 46), the median distance of genes to the nuclear center were converted to the distance to the nuclear periphery. Both derivatives took an intermediate position compared to the genes on the normal chromosomes (**Figure 49C**). The authors concluded that the transfer of a part of

chromosomes 22 with high gene density to chromosome 11 caused the relocation of the chimeric der(11) to a more central position, but as seen in **Figure 49A**, the analysis of the gene density of the whole chromosomes would only have predicted this change in localization for der(11) but not for der(22). The gene density for the der(22) was dramatically reduced (a value below that of normal chromosome 11, **Figure 49A**). Using the 2 Mbp window (**Figure 49B**) allows me to correctly predict the change in 3D localization of both derivative chromosomes.

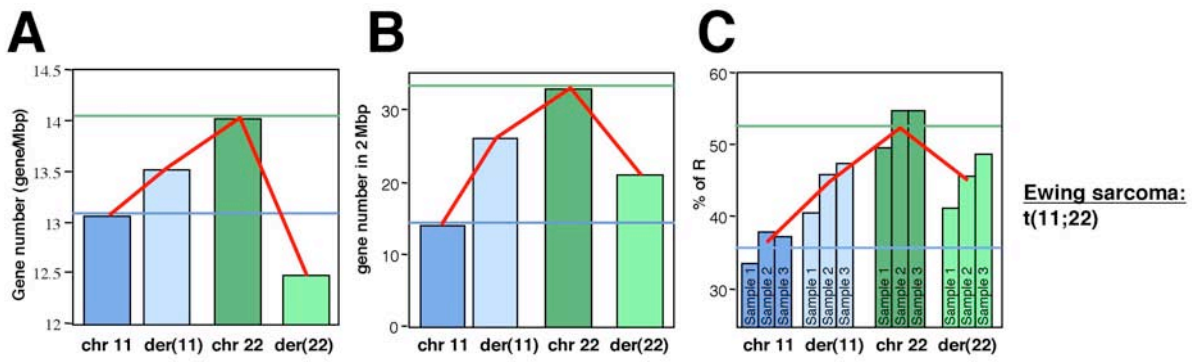

Figure 49: Putting the 2 Mbp-rule to the test: Example #1.
Translocation t(11;22) involving the genes *EWSR1* on chr 22 and *FLI1* on chr 11 of Ewing sarcoma cells. The data were taken from published 2D image analysis (Taslerova et al., 2003). Original data was converted from distances of signals to nuclear center in % of total radius to distances of signals to nuclear periphery. Average distances values are displayed.
Dark blue column: chr 11; light blue column: der(11); dark green column: chr 22; light green column: der(22). Red line should indicate the general pattern of change between the normal and derivative chromosomes.
A: Gene density of the whole chromosomes chr 11 , chr 22, der(11), and der(22).
B: Changes in gene density in the 2 Mbp surrounding the gene.
C: Measured distances of genes to nuclear surface.
chr = normal chromosome. der = derivative chromosome.
Gene density information was obtained from the website http://www.ncbi.nlm.nih.gov/mapview/maps.cgi, and calculated for the derivative chromosomes.

Example #2: Weierich et al. performed a 3D evaluation of radial chromatin distribution in mouse and human lymphocyte nuclei (Weierich et al., 2003). In this analysis

the localization of the telomeres was very different between the two species. Mouse telomeres clustered more in the nuclear periphery than human telomeres (red line in **Figure 50A** and **B**). This result could not have been predicted from the general gene density of the

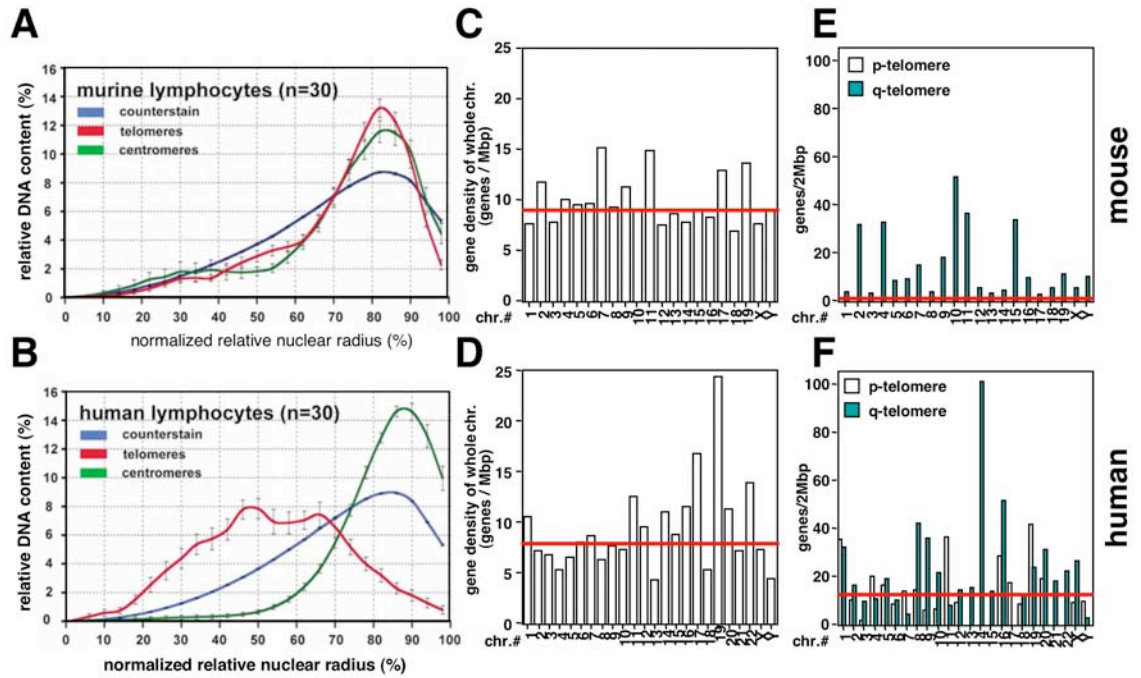

Figure 50: Putting the 2 Mbp-rule to the test: Example #2.
A, B: Quantitative 3D evaluation of radial chromatin distributions in 30 mouse (A) and 30 human (B) lymphocyte nuclei (Figues A and B were taken from Weierich et al.). The presentation of the relative nuclear radius (%) is different from the orientation used throughout this thesis. In these images 0% describes the nuclear center and 100% the nuclear periphery. Telomere signals (red curves), centromere signals (green curves), and TO-PRO-3 stained nuclear DNA (blue curves) were plotted. n = number of evaluated nuclei in each experiment. Distribution of telomere signals differs between the two species: in human, telomere signals are distributed mainly internally, while, in mouse, telomere signals are located mainly peripherally (Weierich et al., 2003).
C, D: Gene density of entire chromosomes of mouse (C) and human (D). Median gene density is 9.0 genes/Mbp for mouse chromosomes and 7.9 for human chromosomes.
E, F: Genes within the terminal 2 Mbp or each telomere in mouse (E) and human (F). The median amount of genes found in this window was 1.5 genes for mouse and 14.3 genes for human.

entire chromosomes from mouse and human since the median densities are quite similar (red lines in **Figure 50C** and **D**). However, when the gene densities of only the last 2Mbp of each telomere were considered the median number of genes present in mouse was much lower (1.5) than in humans (14.25). On average the gene density of the telomeres is much lower in chromosomes of the mouse than in humans, whereas the general gene density of whole chromosomes is similar. One could argue that mouse chromosomes are acrocentric, but even if only q-telomeres are considered, again, much fewer genes are found in the 2 Mbp window of the q telomeres of mouse (18 genes) than human (34.5 genes). The analysis therefore demonstrates that local gene densities can allow a more accurate prediction of 3D localization of not only genes but also chromosomal domains than the total chromosomal gene density.

A number of analyses have found a correlation between the gene density of a locus and its localization not only within the nucleus but also within its chromosomal territory. The MHC cluster on chromosome 6 (Volpi et al., 2000), the EDC on chromosome 1 (Williams et al., 2002) and the *MLL* gene on chromosome 11 (this work) have all been reported to be preferentially localized at the surface or even outside the surface of their territories. By plotting the gene density in 2 Mbp-steps from the p to the q telomere of these chromosomes (data not shown), it appeared that these genes are located in regions of high gene density:

MHC: Chromosome 6 has an average gene density of 16.2 genes per 2 Mbp step. The MHC cluster is localized in the region 6p21.3. This sub-band contains the locus of the highest gene density found in the entire human genome (Volpi et al., 2000). Within this locus a 2 Mbp section (between *HLA-B* in the MHC I gene cluster and *RING1* in the extended MHC II cluster) has a gene density of 105 genes per 2 Mbp. This region was found in lymphoblastoid cells to be predominantly localized outside the chromosome 6 territory and this localization could be induced in fibroblasts by treatment with interferon γ (Volpi et al., 2000).

EDC: The epidermal differentiation complex (EDC) is located at 1q21. It is mostly positioned at the periphery or external of the territory in differentiating keratinocytes (Williams et al., 2002). The gene density in that region is the highest observed in the entire chromosome 1 (72 vs. 21 genes per 2 Mbp).

MLL: The local gene density around *MLL* on chromosome 11, which was determined in this work to often loop out of the territory, is significantly higher than the average gene density of chromosome 11 (54 vs. 25 genes per 2 Mbp). The relative position of a number of other regions within chromosome territory 11 were published and I again analyzed their surrounding local gene density. The following regions were reported to be preferentially positioned outside the territory: 11pter *IGF2*, and RP11-80N22 on 11q13.1. For these 3 locations the local gene density is higher than the average of the entire chromosome (73, 73, 79 genes vs. 25 genes per 2 Mbp). In contrast loci with low gene density were found either at the surface or interior of the territory (on the surface, *WEE1* (28 genes per 2 Mbp), interior, *PAX* (13 genes per 2 Mbp)).

During the course of this thesis a contradiction between the localization of gene dense regions at the surface of chromosomal territories and towards the center of the nucleus became apparent. This contradiction can only be solved if one assumes that actively transcribed and/or gene dense regions loop out of territories preferentially towards the center of the nucleus. In fact close inspection of some published results seems to indicate that this is the case. In the majority of images shown genes loop out of territories towards the center of the nucleus (Mahy et al., 2002a; Mahy et al., 2002b; Volpi et al., 2000; Williams et al., 2002).

What determines the position of a sequence within the nucleus and inside a chromosomal territory and what could be the mechanisms that maintain a gradient of gene density from the nuclear surface to the nuclear center? The local gene density of a 2 Mbp window surrounding a gene seems to be a good predictor for the nuclear position of genes. Although gene density alone cannot be the determining factor, because it has been observed that genes change position after activation or inactivation (Kosak et al., 2002), a process which does not alter the actual gene content. Nevertheless, the gene density that surrounds

MLL and its translocation partners correlates remarkably well with their 3D position in the nucleus. It is likely that the transcriptional activity of loci contributes to their localization. The more genes are present in a local region the higher the potential transcriptional activity could be. This has been demonstrated for the localization of genes within chromosomal territories. Activation of genes can result in a more peripheral location of genes in territories (Volpi et al., 2000). Tissue specific differences that have been reported (Williams et al., 2002) are consistent with these results. The difference in localization of loci could be caused by differences in protein factors bound to these sites. The determinants or regulators of the localization of such proteins within the 3D nucleus are unknown at present. If the position of a gene is independent of the remaining nuclear content of a cell, one could assume that an extra chromosome in a new nuclear environment, e.g. after microinjection, would assume a position characteristic for its gene content. Another experiment one could perform is to incorporate a chromosomal domain of 2 Mbp with known gene content (low or high gene density) into a chromosome and determine the change of the position of this locus within the territory and the nucleus.

This work has already provided a few examples, where the location of a gene was significantly changed as a result of a chromosomal translocation event. The localization of genes correlated well with the change in local gene density at the break point. Since this change of position is very likely to affect genes positioned in close proximity of the breakpoint, the question arises how the change in position of genes in 5' or 3' direction of the translocation point can be affected in their transcriptional activity. The results of this work have the potential to shed a new light on reciprocal translocations. So far the concept of a reciprocal translocation is that two genes get disrupted leading to the loss or gain of function mutations. If these genes are part of a signal transduction cascade, the expression and activity of many other genes can also be influenced. After a change in position, genes in close proximity of the breakpoint, not disrupted by the break itself, could also be affected in their expression. One could speculate, that a shift to the nuclear surface would result in down regulated transcriptional activity, and a shift to the nuclear interior could upregulate the expression of genes. To test this, the expression of specific genes could be compared by

using reverse PCR or northern blot analysis, or by establishing SAGE libraries to quantify the expression of genes. SAGE libraries of patient material or cell lines carrying well defined translocation events (involving *MLL* and *AF9* in t(9;11) or *MLL* and *AF4* in t(4;11)) have been constructed in the laboratories of Dr. Rowley and of Dr. Markus Müschen (University of Düsseldorf, Düsseldorf, Germany). Upon completion of the analysis, genes positioned 5' and 3' of the genes *MLL*, *AF9* and *AF4* will be analyzed in SAGE libraries with derivative and normal chromosomes. The results of this analysis might help to explain some of the findings of this thesis and if significant changes of the expression of the genes in the vicinity of the breakpoint are found, one might have to broaden the assumption of the effect of a translocation not only on the directly effected genes but also on their neighboring genes.

7. REFERENCES

Alberts, B., D. Bray, J. Lewis, M. Raff, K. Roberts, and J.D. Watson. 1994. Molecular Biology of the Cell. Garland Publishing, New York and London.

Algeciras-Schimnich, A., B.C. Barnhart, and M.E. Peter. 2002. Apoptosis-independent functions of killer caspases. *Curr Opin Cell Biol*. 14:721-6.

Andersson, L., A. Archibald, M. Ashburner, S. Audun, W. Barendse, J. Bitgood, C. Bottema, T. Broad, S. Brown, D. Burt, C. Charlier, N. Copeland, S. Davis, M. Davisson, J. Edwards, A. Eggen, G. Elgar, J.T. Eppig, I. Franklin, P. Grewe, T. Gill, 3rd, J.A. Graves, R. Hawken, J. Hetzel, J. Womack, and et al. 1996. Comparative genome organization of vertebrates. The First International Workshop on Comparative Genome Organization. *Mamm Genome*. 7:717-34.

Aplan, P.D., D.S. Chervinsky, M. Stanulla, and W.C. Burhans. 1996. Site-specific DNA cleavage within the MLL breakpoint cluster region induced by topoisomerase II inhibitors. *Blood*. 87:2649-58.

Aten, J.A., J. Stap, P.M. Krawczyk, C.H. van Oven, R.A. Hoebe, J. Essers, and R. Kanaar. 2004. Dynamics of DNA double-strand breaks revealed by clustering of damaged chromosome domains. *Science*. 303:92-5.

Ausubel, F.M., R. Brent, R.E. Kingston, D. Moore, J.G. Seidman, J.A. Smith, and K. Struhl. 1998. Current Protocols in Molecular Biology. unit 2.2.1 - 2.2.3.

Baffa, R., M. Negrini, S.A. Schichman, K. Huebner, and C.M. Croce. 1995. Involvement of the ALL-1 gene in a solid tumor. *Proc Natl Acad Sci U S A*. 92:4922-6.

Bailly, J.D., C. Muller, J.P. Jaffrezou, C. Demur, G. Gassar, C. Bordier, and G. Laurent. 1995. Lack of correlation between expression and function of P-glycoprotein in acute myeloid leukemia cell lines. *Leukemia*. 9:799-807.

Bartova, E., P. Jirsova, M. Fojtova, K. Soucek, and S. Kozubek. 2003. Chromosomal territory segmentation in apoptotic cells. *Cell Mol Life Sci*. 60:979-90.

Bartova, E., S. Kozubek, P. Jirsova, M. Kozubek, H. Gajova, E. Lukasova, M. Skalnikova, A. Ganova, I. Koutna, and M. Hausmann. 2002. Nuclear structure and gene activity in human differentiated cells. *J Struct Biol*. 139:76-89.

Bartova, E., S. Kozubek, M. Kozubek, P. Jirsova, E. Lukasova, M. Skalnikova, and K. Buchnickova. 2000. The influence of the cell cycle, differentiation and irradiation on the nuclear location of the abl, bcr and c-myc genes in human leukemic cells. *Leuk Res*. 24:233-41.

Belyaev, I. 2004. Molecular targets and mechanisms in formation of chromosomal aberrations: contributions of Soviet scientists. *Cytogenet Genome Res*. 104:56-64.

Bernard, O.A., R. Berger, C.M. Clemson, J.A. McNeil, H.F. Willard, and J.B. Lawrence. 1995a. Molecular basis of 11q23 rearrangements in hematopoietic malignant proliferations. *Genes Chromosomes Cancer*. 13:75-85.

Bernard, O.A., R. Berger, S.E. Horning, G.A. Brown, and S.J. Korsmeyer. 1995b. Molecular basis of 11q23 rearrangements in hematopoietic malignant proliferations. *Genes Chromosomes Cancer*. 13:75-85.

Betti, C.J., M.J. Villalobos, M.O. Diaz, and A.T. Vaughan. 2001. Apoptotic triggers initiate translocations within the MLL gene involving the nonhomologous end joining repair system. *Cancer Res*. 61:4550-5.

Betti, C.J., M.J. Villalobos, M.O. Diaz, and A.T. Vaughan. 2003. Apoptotic stimuli initiate MLL-AF9 translocations that are transcribed in cells capable of division. *Cancer Res*. 63:1377-81.

Bickmore, W.A., and P. Teague. 2002. Influences of chromosome size, gene density and nuclear position on the frequency of constitutional translocations in the human population. *Chromosome Res*. 10:707-15.

Boveri, T. 1909. Die Blastomerkerne von Ascaris megalocepha und die Theorie der Chromosomenindividualität. *Arch Zellforschung*. 3:181 ff.

Boyle, S., S. Gilchrist, J.M. Bridger, N.L. Mahy, J.A. Ellis, and W.A. Bickmore. 2001. The spatial organization of human chromosomes within the nuclei of normal and emerin-mutant cells. *Hum Mol Genet*. 10:211-9.

Bradbury, E.M. 1998. Nucleosome and chromatin structures and functions. *J Cell Biochem Suppl*. 30-31:177-84.

Brady, H.J. 2003. Apoptosis and leukaemia. *Br J Haematol*. 123:577-85.

Bridger, J.M., S. Boyle, I.R. Kill, and W.A. Bickmore. 2000. Re-modelling of nuclear architecture in quiescent and senescent human fibroblasts. *Curr Biol*. 10:149-52.

Bridger, J.M., H. Herrmann, C. Munkel, and P. Lichter. 1998. Identification of an interchromosomal compartment by polymerization of nuclear-targeted vimentin. *J Cell Sci*. 111:1241-53.

Brown, K.E., S.S. Guest, S.T. Smale, K. Hahm, M. Merkenschlager, and A.G. Fisher. 1997. Association of transcriptionally silent genes with Ikaros complexes at centromeric heterochromatin. *Cell*. 91:845-54.

Brown, R.L. 1831. Observations on the organs and mode of fecundation in Orchideae and Asclepiadeae. *Transactions of the Linnean Society*. 1829-1832:685-746.

Cafourkova, A., E. Luka ova, S. Kozubek, M. Kozubek, R.D. Govorun, I. Koutna, E. Bartova, M. Skalnikova, P. Jirsova, R. Pasekova, and E.A. Krasavin. 2001. Exchange aberrations among 11 chromosomes of human lymphocytes induced by gamma-rays. *Int J Radiat Biol*. 77:419-29.

Carter, N.P., M.E. Ferguson-Smith, N.A. Affara, H. Briggs, and M.A. Ferguson-Smith. 1990. Study of X chromosome abnormality in XX males using bivariate flow karyotype analysis and flow sorted dot blots. *Cytometry*. 11:202-7.

Carver, E.A., and L. Stubbs. 1997. Zooming in on the human-mouse comparative map: genome conservation re-examined on a high-resolution scale. *Genome Res*. 7:1123-37.

Chai, L.S., A.A. Sandberg, J. Aquiles Sanchez, R.J. Karni, and L.J. Wangh. 1988. Chromosomes and their relationship to nuclear components during the cell cycle in Chinese hamster cells. *Cell Tissue Res*. 251:197-204. models that attempt to explain nuclear morphology in terms of chromosome spatial organization.

Chen, J.J., J.D. Rowley, and S.M. Wang. 2000. Generation of longer cDNA fragments from serial analysis of gene expression tags for gene identification. *Proc Natl Acad Sci U S A*. 97:349-53.

Cheung, V.G., and S.F. Nelson. 1996. Whole genome amplification using a degenerate oligonucleotide primer allows hundreds of genotypes to be performed on less than one nanogram of genomic DNA. *Proc Natl Acad Sci U S A*. 93:14676-9.

Chowdhary, B.P., T. Raudsepp, L. Fronicke, and H. Scherthan. 1998. Emerging patterns of comparative genome organization in some mammalian species as revealed by Zoo-FISH. *Genome Res*. 8:577-89.

Chubb, J.R., S. Boyle, P. Perry, and W.A. Bickmore. 2002. Chromatin motion is constrained by association with nuclear compartments in human cells. *Curr Biol*. 12:439-45.

Clemson, C.M., and J.B. Lawrence. 1996. Multifunctional compartments in the nucleus: insights from DNA and RNA localization. *J Cell Biochem*. 62:181-90.

Clemson, C.M., J.A. McNeil, H.F. Willard, and J.B. Lawrence. 1996. XIST RNA paints the inactive X chromosome at interphase: evidence for a novel RNA involved in nuclear/chromosome structure. *J Cell Biol*. 132:259-75.

Collins, C., W.L. Kuo, R. Segraves, J. Fuscoe, D. Pinkel, and J.W. Gray. 1991. Construction and characterization of plasmid libraries enriched in sequences from single human chromosomes. *Genomics*. 11:997-1006.

Cornforth, M.N., K.M. Greulich-Bode, B.D. Loucas, J. Arsuaga, M. Vazquez, R.K. Sachs, M. Bruckner, M. Molls, P. Hahnfeldt, L. Hlatky, and D.J. Brenner. 2002. Chromosomes are predominantly located randomly with respect to each other in interphase human cells. *J Cell Biol*. 159:237-44.

Corral, J., I. Lavenir, H. Impey, A.J. Warren, A. Forster, T.A. Larson, S. Bell, A.N. McKenzie, G. King, T.H. Rabbitts, M.A. Caligiuri, M.P. Strout, S.A. Schichman, K. Mrozek, D.C. Arthur, G.P. Herzig, M.R. Baer, C.A. Schiffer, K. Heinonen, S. Knuutila, T. Nousiainen, T. Ruutu, A.W. Block, P. Schulman, J. Pedersen-Bjergaard, C.M. Croce, and C.D. Bloomfield. 1996. An Mll-AF9 fusion gene made by homologous recombination causes acute leukemia in chimeric mice: a method to create fusion oncogenes. *Cell*. 85:853-61.

Cremer, M., K. Kupper, B. Wagler, L. Wizelman, J. von Hase, Y. Weiland, L. Kreja, J. Diebold, M.R. Speicher, and T. Cremer. 2003. Inheritance of gene density-related higher order chromatin arrangements in normal and tumor cell nuclei. *J Cell Biol*. 162:809-20.

Cremer, M., J. von Hase, T. Volm, A. Brero, G. Kreth, J. Walter, C. Fischer, I. Solovei, C. Cremer, and T. Cremer. 2001. Non-random radial higher-order chromatin arrangements in nuclei of diploid human cells. *Chromosome Res*. 9:541-67.

Croft, J.A., J.M. Bridger, S. Boyle, P. Perry, P. Teague, and W.A. Bickmore. 1999. Differences in the localization and morphology of chromosomes in the human nucleus. *J Cell Biol*. 145:1119-31.

Davi, F., C. Gocke, S. Smith, and J. Sklar. 1996. Lymphocytic progenitor cell origin and clonal evolution of human B-lineage acute lymphoblastic leukemia. *Blood*. 88:609-21.

de Wynter, E.A., D. Buck, C. Hart, R. Heywood, L.H. Coutinho, A. Clayton, J.A. Rafferty, D. Burt, G. Guenechea, J.A. Bueren, D. Gagen, L.J. Fairbairn, B.I. Lord, and N.G. Testa. 1998. CD34+AC133+ cells isolated from cord blood are highly enriched in long-term culture-initiating cells, NOD/SCID-repopulating cells and dendritic cell progenitors. *Stem Cells*. 16:387-96.

Dietzel, S., K. Schiebel, G. Little, P. Edelmann, G.A. Rappold, R. Eils, C. Cremer, and T. Cremer. 1999. The 3D positioning of ANT2 and ANT3 genes within female X chromosome territories correlates with gene activity. *Exp Cell Res*. 252:363-75.

Dillon, N., and R. Festenstein. 2002. Unravelling heterochromatin: competition between positive and negative factors regulates accessibility. *Trends Genet*. 18:252-8.

Domer, P.H., S.S. Fakharzadeh, C.S. Chen, J. Jockel, L. Johansen, G.A. Silverman, J.H. Kersey, and S.J. Korsmeyer. 1993. Acute mixed-lineage leukemia t(4;11)(q21;q23) generates an MLL-AF4 fusion product. *Proc Natl Acad Sci U S A*. 90:7884-8.

Drexler, H.G. 2003. Leukemia-lymphoma cell line Facts Book. Academic Press, San Diego, San Francisco, New York, Boston, London, Sydney, Tokyo.

Drexler, H.G., and R.A. MacLeod. 2003. Leukemia-lymphoma cell lines as model systems for hematopoietic research. *Ann Med*. 35:404-12.

Drexler, H.G., H. Quentmeier, and R.A. MacLeod. 2004. Malignant hematopoietic cell lines: in vitro models for the study of MLL gene alterations. *Leukemia*. 18:227-32.

Dumont, C., A. Durrbach, N. Bidere, M. Rouleau, G. Kroemer, G. Bernard, F. Hirsch, B. Charpentier, S.A. Susin, and A. Senik. 2000. Caspase-independent commitment phase to apoptosis in activated blood T lymphocytes: reversibility at low apoptotic insult. *Blood*. 96:1030-8.

Dundr, M., and T. Misteli. 2001. Functional architecture in the cell nucleus. *Biochem J*. 356:297-310.

Earnshaw, W.C., L.M. Martins, and S.H. Kaufmann. 1999. Mammalian caspases: structure, activation, substrates, and functions during apoptosis. *Annu Rev Biochem*. 68:383-424.

Elliott, B., and M. Jasin. 2002. Double-strand breaks and translocations in cancer. *Cell Mol Life Sci*. 59:373-85.

Fawcett, J.J., J.L. Longmire, J.C. Martin, L.L. Deaven, and L.S. Cram. 1994. Large-scale chromosome sorting. *Methods Cell Biol*. 42 Pt B:319-30.

Ferguson, M., and D.C. Ward. 1992. Cell cycle dependent chromosomal movement in pre-mitotic human T-lymphocyte nuclei. *Chromosoma*. 101:557-65.

Fontana, F., and M. Rubini. 1990. Chromosomal evolution in Cervidae. *Biosystems*. 24:157-74.

Fred M. Ausubel, R.B., Robert E. Kingston, David D. Moore, J.G. Seidman, John A. Smith, Kevin Struhl. 1998. Current Protocols in Molecular Biology. John Wiley & Sons.

Fronicke, L., B.P. Chowdhary, and H. Scherthan. 1997. Segmental homology among cattle (Bos taurus), Indian muntjac (Muntiacus muntjak vaginalis), and Chinese muntjac (M. reevesi) karyotypes. *Cytogenet Cell Genet.* 77:223-7.

Fronicke, L., and H. Scherthan. 1997. Zoo-fluorescence in situ hybridization analysis of human and Indian muntjac karyotypes (Muntiacus muntjak vaginalis) reveals satellite DNA clusters at the margins of conserved syntenic segments. *Chromosome Res.* 5:254-61.

Futreal, P.A., L. Coin, M. Marshall, T. Down, T. Hubbard, R. Wooster, N. Rahman, and M.R. Stratton. 2004. A census of human cancer genes. *Nat Rev Cancer.* 4:177-83.

Gautier, M., P. Laurent, H. Hayes, and A. Eggen. 2001. Development and assignment of bovine-specific PCR systems for the Texas nomenclature marker genes and isolation of homologous BAC probes. *Genet Sel Evol.* 33:191-200.

Gerlich, D., J. Beaudouin, B. Kalbfuss, N. Daigle, R. Eils, and J. Ellenberg. 2003. Global chromosome positions are transmitted through mitosis in mammalian cells. *Cell.* 112:751-64.

Geske, F.J., R. Lieberman, R. Strange, and L.E. Gerschenson. 2001. Early stages of p53-induced apoptosis are reversible. *Cell Death Differ.* 8:182-91.

Geske, F.J., A.C. Nelson, R. Lieberman, R. Strange, T. Sun, and L.E. Gerschenson. 2000. DNA repair is activated in early stages of p53-induced apoptosis. *Cell Death Differ.* 7:393-401.

Gibbs, R.A., G.M. Weinstock, M.L. Metzker, D.M. Muzny, E.J. Sodergren, S. Scherer, G. Scott, D. Steffen, K.C. Worley, P.E. Burch, G. Okwuonu, S. Hines, L. Lewis, C. DeRamo, O. Delgado, S. Dugan-Rocha, G. Miner, M. Morgan, A. Hawes, R. Gill, Celera, R.A. Holt, M.D. Adams, P.G. Amanatides, H. Baden-Tillson, M. Barnstead, S. Chin, C.A. Evans, S. Ferriera, C. Fosler, A. Glodek, Z. Gu, D. Jennings, C.L. Kraft, T. Nguyen, C.M. Pfannkoch, C. Sitter, G.G. Sutton, J.C. Venter, T. Woodage, D. Smith, H.M. Lee, E. Gustafson, P. Cahill, A. Kana, L. Doucette-Stamm, K. Weinstock, K. Fechtel, R.B. Weiss, D.M. Dunn, E.D. Green, R.W. Blakesley, G.G. Bouffard, P.J. De Jong, K. Osoegawa, B. Zhu, M. Marra, J. Schein, I. Bosdet, C. Fjell, S. Jones, M. Krzywinski, C. Mathewson, A. Siddiqui, N. Wye, J. McPherson, S. Zhao, C.M. Fraser, J. Shetty, S. Shatsman, K. Geer, Y. Chen, S. Abramzon, W.C. Nierman, P.H. Havlak, R. Chen, K.J. Durbin, A. Egan, Y. Ren, X.Z. Song, B. Li, Y. Liu, X. Qin, S. Cawley, A.J. Cooney, L.M. D'Souza, K. Martin, J.Q. Wu, M.L. Gonzalez-Garay, A.R. Jackson, K.J. Kalafus, M.P. McLeod, A. Milosavljevic, D. Virk, A. Volkov, D.A. Wheeler, Z. Zhang, J.A. Bailey, E.E. Eichler, E. Tuzun, et al. 2004. Genome sequence of the Brown Norway rat yields insights into mammalian evolution. *Nature.* 428:493-521.

Graeves, M. 2003. Pre-natal origins of childhood leukemia. *Rev Clin Exp Hematol.* 7:233-45.

Greaves, M.F., and J. Wiemels. 2003. Origins of chromosome translocations in childhood leukaemia. *Nat Rev Cancer.* 3:639-49.

Green, D., and G. Kroemer. 1998. The central executioners of apoptosis: caspases or mitochondria? *Trends Cell Biol*. 8:267-71.

Green, D.R., and G. Kroemer. 2004. The pathophysiology of mitochondrial cell death. *Science*. 305:626-9.

Green, R.J., and G.F. Bahr. 1975. Comparison of G-, Q- and EM-banding patterns exhibited by the chromosome complement of the Indian muntjac, Muntiacus muntjak, with reference to nuclear DNA content and chromatin ultrastructure. *Chromosoma*. 50:53-67.

Groffen, J., J.R. Stephenson, N. Heisterkamp, A. de Klein, C.R. Bartram, and G. Grosveld. 1984. Philadelphia chromosomal breakpoints are clustered within a limited region, bcr, on chromosome 22. *Cell*. 36:93-9.

Grosschedl, R., K. Giese, J. Pagel, M. Reichenzeller, A. Burzlaff, P. Lichter, H. Herrmann, H. Bornfleth, P. Edelmann, D. Zink, T. Cremer, and C. Cremer. 1994. HMG domain proteins: architectural elements in the assembly of nucleoprotein structures. *Trends Genet*. 10:94-100.

Grummt, I., C. Soellner, and I. Scholz. 1979. Characterization of a cloned ribosomal fragment from mouse which contains the 18S coding region and adjacent spacer sequences. *Nucleic Acids Res*. 6:1351-69.

Gu, Y., G. Cimino, H. Alder, T. Nakamura, R. Prasad, O. Canaani, D.T. Moir, C. Jones, P.C. Nowell, C.M. Croce, and et al. 1992a. The (4;11)(q21;q23) chromosome translocations in acute leukemias involve the VDJ recombinase. *Proc Natl Acad Sci U S A*. 89:10464-8.

Gu, Y., T. Nakamura, H. Alder, R. Prasad, O. Canaani, G. Cimino, C.M. Croce, and E. Canaani. 1992b. The t(4;11) chromosome translocation of human acute leukemias fuses the ALL-1 gene, related to Drosophila trithorax, to the AF-4 gene. *Cell*. 71:701-8.

Habermann, F.A., M. Cremer, J. Walter, G. Kreth, J. von Hase, K. Bauer, J. Wienberg, C. Cremer, T. Cremer, and I. Solovei. 2001. Arrangements of macro- and microchromosomes in chicken cells. *Chromosome Res*. 9:569-84.

Hamkalo, B.A., and J.B. Rattner. 1980. Folding up genes and chromosomes. *Q Rev Biol*. 55:409-17.

Hayes, H., G.P. Di Meo, M. Gautier, P. Laurent, A. Eggen, and L. Iannuzzi. 2000. Localization by FISH of the 31 Texas nomenclature type I markers to both Q- and R-banded bovine chromosomes. *Cytogenet Cell Genet*. 90:315-20.

Hedges, S.B., P.H. Parker, C.G. Sibley, and S. Kumar. 1996. Continental breakup and the ordinal diversification of birds and mammals. *Nature*. 381:226-9.

Hediger, F., and S.M. Gasser. 2002. Nuclear organization and silencing: putting things in their place. *Nat Cell Biol*. 4:E53-5.

Hengartner, M.O. 2000. The biochemistry of apoptosis. *Nature*. 407:770-6.

Herrmann, H., A. Eckelt, M. Brettel, C. Grund, and W.W. Franke. 1993. Temperature-sensitive intermediate filament assembly. Alternative structures of Xenopus laevis vimentin in vitro and in vivo. *J Mol Biol*. 234:99-113.

Hiwatari, M., T. Taki, T. Taketani, M. Taniwaki, K. Sugita, M. Okuya, M. Eguchi, K. Ida, and Y. Hayashi. 2003. Fusion of an AF4-related gene, LAF4, to MLL in childhood acute lymphoblastic leukemia with t(2;11)(q11;q23). *Oncogene*. 22:2851-5.

Hlatky, L., R.K. Sachs, M. Vazquez, and M.N. Cornforth. 2002. Radiation-induced chromosome aberrations: insights gained from biophysical modeling. *Bioessays*. 24:714-23.

Horimoto, K., S. Fukuchi, and K. Mori. 2001. Comprehensive comparison between locations of orthologous genes on archaeal and bacterial genomes. *Bioinformatics*. 17:791-802.

Huret, J. 2003. 11q23 rearrangements in leukaemia. Atlas Genet Cytogenet Oncol Haematol. August 2003 .

Iida, S., M. Seto, K. Yamamoto, H. Komatsu, Y. Akao, S. Nakazawa, Y. Ariyoshi, T. Takahashi, R. Ueda, C.H. Pui, L.S. Frankel, A.J. Carroll, S.C. Raimondi, J.J. Shuster, D.R. Head, W.M. Crist, V.J. Land, D.J. Pullen, C.P. Steuber, et al., O.A. Bernard, S.P. Romana, S.A. Schichman, M. Mauchauffe, P. Jonveaux, and R. Berger. 1993a. Molecular cloning of 19p13 breakpoint region in infantile leukemia with t(11;19)(q23;p13) translocation. *Jpn J Cancer Res*. 84:532-7. suggest that the t(4;11) is an adverse prognostic feature in these two age groups.

Iida, S., M. Seto, K. Yamamoto, H. Komatsu, A. Tojo, S. Asano, N. Kamada, Y. Ariyoshi, T. Takahashi, and R. Ueda. 1993b. MLLT3 gene on 9p22 involved in t(9;11) leukemia encodes a serine/proline rich protein homologous to MLLT1 on 19p13. *Oncogene*. 8:3085-92.

Inohara, N., T. Koseki, Y. Hu, S. Chen, and G. Nunez. 1997. CLARP, a death effector domain-containing protein interacts with caspase-8 and regulates apoptosis. *Proc Natl Acad Sci U S A*. 94:10717-22.

Joh, T., Y. Kagami, K. Yamamoto, T. Segawa, J. Takizawa, T. Takahashi, R. Ueda, and M. Seto. 1996. Identification of MLL and chimeric MLL gene products involved in 11q23 translocation and possible mechanisms of leukemogenesis by MLL truncation. *Oncogene*. 13:1945-53.

Joh, T., K. Yamamoto, Y. Kagami, H. Kakuda, T. Sato, T. Yamamoto, T. Takahashi, R. Ueda, K. Kaibuchi, and M. Seto. 1997. Chimeric MLL products with a Ras binding cytoplasmic protein AF6 involved in t(6;11) (q27;q23) leukemia localize in the nucleus. *Oncogene*. 15:1681-7.

Johansson, B., A.V. Moorman, and L.M. Secker-Walker. 1998. Derivative chromosomes of 11q23-translocations in hematologic malignancies. European 11q23 Workshop participants. *Leukemia*. 12:828-33.

Johnson, K.L., J.D. Tucker, and J. Nath. 1998. Frequency, distribution and clonality of chromosome damage in human lymphocytes by multi-color FISH. *Mutagenesis*. 13:217-27.

Johnston, F.P., R.B. Church, and C.C. Lin. 1982. Chromosome rearrangement between the Indian muntjac and Chinese muntjac is accompanied by a delection of middle repetitive DNA. *Can J Biochem*. 60:497-506.

Kaneko, Y., N. Maseki, N. Takasaki, M. Sakurai, Y. Hayashi, S. Nakazawa, T. Mori, T. Takeda, T. Shikano, and et al. 1986. Clinical and hematologic characteristics in acute leukemia with 11q23 translocations. *Blood*. 67:484-91.

Kennison, J.A., A.M. Mazo, D.H. Huang, B.A. Mozer, I.B. Dawid, M. Reichenzeller, A. Burzlaff, P. Lichter, H. Herrmann, H. Bornfleth, P. Edelmann, D. Zink, T. Cremer, and C. Cremer. 1993. Transcriptional activation of Drosophila homeotic genes from distant regulatory elements. *Trends Genet*. 9:75-9. exhibits other function(s) besides those involved in the regulation of Ubx expression in the ventral nerve cord of the embryo.

Kerr, J.F., A.H. Wyllie, and A.R. Currie. 1972. Apoptosis: a basic biological phenomenon with wide-ranging implications in tissue kinetics. *Br J Cancer*. 26:239-57.

Khodarev, N.N., I.A. Sokolova, and A.T. Vaughan. 1999. Abortive apoptosis as an initiator of chromosomal translocations. *Med Hypotheses*. 52:373-6.

Koeffler, H.P., R. Billing, A.J. Lusis, R. Sparkes, and D.W. Golde. 1980. An undifferentiated variant derived from the human acute myelogenous leukemia cell line (KG-1). *Blood*. 56:265-73.

Kosak, S.T., J.A. Skok, K.L. Medina, R. Riblet, M.M. Le Beau, A.G. Fisher, and H. Singh. 2002. Subnuclear compartmentalization of immunoglobulin loci during lymphocyte development. *Science*. 296:158-62.

Kozubek, S., E. Bartova, M. Kozubek, E. Lukasova, A. Cafourkova, I. Koutna, and M. Skalnikova. 2001. Spatial distribution of selected genetic loci in nuclei of human leukemia cells after irradiation. *Radiat Res*. 155:311-9.

Krawetz, S.A., M.H. Herfort, and G.H. Dixon. 1990. In situ localization of a mammalian protamine gene: parameters affecting specificity of hybridization. *Genome*. 33:459-63.

Kurz, A., S. Lampel, J.E. Nickolenko, J. Bradl, A. Benner, R.M. Zirbel, T. Cremer, and P. Lichter. 1996. Active and inactive genes localize preferentially in the periphery of chromosome territories. *J Cell Biol*. 135:1195-205.

Lamond, A.I., and W.C. Earnshaw. 1998. Structure and function in the nucleus. *Science*. 280:547-53.

Lampel, S., J.M. Bridger, R.M. Zirbel, U.R. Mathieu, and P. Lichter. 1997. Nuclear RNA accumulations contain released transcripts and exhibit specific distributions with respect to Sm antigen foci. *DNA Cell Biol*. 16:1133-42.

Lavau, C., C. Du, M. Thirman, and N. Zeleznik-Le. 2000a. Chromatin-related properties of CBP fused to MLL generate a myelodysplastic-like syndrome that evolves into myeloid leukemia. *Embo J*. 19:4655-64.

Lavau, C., R.T. Luo, C. Du, and M.J. Thirman. 2000b. Retrovirus-mediated gene transfer of MLL-ELL transforms primary myeloid progenitors and causes acute myeloid leukemias in mice. *Proc Natl Acad Sci U S A*. 97:10984-9.

Lee, C., R. Sasi, and C.C. Lin. 1993. Interstitial localization of telomeric DNA sequences in the Indian muntjac chromosomes: further evidence for tandem chromosome fusions in the karyotypic evolution of the Asian muntjacs. *Cytogenet Cell Genet*. 63:156-9.

Levy, H.P., R.A. Schultz, and M.M. Cohen. 1992. Comparative gene mapping in the species Muntiacus muntjac. *Cytogenet Cell Genet*. 61:276-81.

Levy, H.P., R.A. Schultz, J.V. Ordonez, and M.M. Cohen. 1991. Anti-kinetochore staining for single laser, bivariate flow sorting of Indian muntjac chromosomes. *Cytometry*. 12:695-700.

Levy, H.P., R.A. Schultz, J.V. Ordonez, and M.M. Cohen. 1993. DNA content measurements and an improved idiogram for the Indian muntjac. *Cytometry*. 14:362-8.

Li, G., G. Sudlow, and A.S. Belmont. 1998. Interphase cell cycle dynamics of a late-replicating, heterochromatic homogeneously staining region: precise choreography of condensation/decondensation and nuclear positioning. *J Cell Biol*. 140:975-89.

Li, Y.C., C. Lee, D. Sanoudou, T.H. Hseu, S.Y. Li, C.C. Lin, and T.H. Hsu. 2000. Interstitial colocalization of two cervid satellite DNAs involved in the genesis of the Indian muntjac karyotype. *Chromosome Res*. 8:363-73.

Lichter, P., T. Cremer, J. Borden, L. Manuelidis, D.C. Ward, and G. Cabot. 1988. Delineation of individual human chromosomes in metaphase and interphase cells by in situ suppression hybridization using recombinant DNA libraries. *Hum Genet*. 80:224-34.

Liming, S., and S. Pathak. 1981. Gametogenesis in a male Indian muntjac x Chinese muntjac hybrid. *Cytogenet Cell Genet*. 30:152-6.

Liming, S., Y. Yingying, and D. Xingsheng. 1980. Comparative cytogenetic studies on the red muntjac, Chinese muntjac, and their F1 hybrids. *Cytogenet Cell Genet*. 26:22-7.

Lin, C.C., R. Sasi, Y.S. Fan, and Z.Q. Chen. 1991. New evidence for tandem chromosome fusions in the karyotypic evolution of Asian muntjacs. *Chromosoma*. 101:19-24.

Ludwikow, G., Y. Xiao, R.A. Hoebe, N.A. Franken, F. Darroudi, J. Stap, C.H. Van Oven, C.J. Van Noorden, and J.A. Aten. 2002. Induction of chromosome aberrations in unirradiated chromatin after partial irradiation of a cell nucleus. *Int J Radiat Biol*. 78:239-47.

Luger, K., A.W. Mader, R.K. Richmond, D.F. Sargent, and T.J. Richmond. 1997. Crystal structure of the nucleosome core particle at 2.8 A resolution. *Nature*. 389:251-60.

Lugo, T.G., A.M. Pendergast, A.J. Muller, and O.N. Witte. 1990. Tyrosine kinase activity and transformation potency of bcr-abl oncogene products. *Science*. 247:1079-82.

Macaya, G., J.P. Thiery, and G. Bernardi. 1976. An approach to the organization of eukaryotic genomes at a macromolecular level. *J Mol Biol*. 108:237-54.

MacLeod, R.A., M. Voges, and H.G. Drexler. 1993. Mono Mac 6: a mature monoblastic leukemia cell line with t(9;11)(p21;q23). *Blood*. 82:3221-2.

Mahy, N.L., P.E. Perry, and W.A. Bickmore. 2002a. Gene density and transcription influence the localization of chromatin outside of chromosome territories detectable by FISH. *J Cell Biol*. 159:753-63.

Mahy, N.L., P.E. Perry, S. Gilchrist, R.A. Baldock, and W.A. Bickmore. 2002b. Spatial organization of active and inactive genes and noncoding DNA within chromosome territories. *J Cell Biol*. 157:579-89.

Manuelidis, L. 1984. Different central nervous system cell types display distinct and nonrandom arrangements of satellite DNA sequences. *Proc Natl Acad Sci U S A*. 81:3123-7.

Marchetti, F., J.B. Bishop, X. Lowe, W.M. Generoso, J. Hozier, and A.J. Wyrobek. 2001. Etoposide induces heritable chromosomal aberrations and aneuploidy during male meiosis in the mouse. *Proc Natl Acad Sci U S A*. 98:3952-7.

Marschalek, R., I. Nilson, K. Lochner, R. Greim, G. Siegler, J. Greil, J.D. Beck, and G.H. Fey. 1997. The structure of the human ALL-1/MLL/HRX gene. *Leuk Lymphoma*. 27:417-28.

Marshall, W.F., A. Straight, J.F. Marko, J. Swedlow, A. Dernburg, A. Belmont, A.W. Murray, D.A. Agard, and J.W. Sedat. 1997. Interphase chromosomes undergo constrained diffusional motion in living cells. *Curr Biol*. 7:930-9.

Martin, M.J., J. Herrero, A. Mateos, and J. Dopazo. 2003. Comparing bacterial genomes through conservation profiles. *Genome Res*. 13:991-8.

Martinez-Lopez, W., E.M. Boccardo, G.A. Folle, V. Porro, and G. Obe. 1998. Intrachromosomal localization of aberration breakpoints induced by neutrons and gamma rays in Chinese hamster ovary cells. *Radiat Res*. 150:585-92.

Mazo, A.M., D.H. Huang, B.A. Mozer, I.B. Dawid, M. Reichenzeller, A. Burzlaff, P. Lichter, H. Herrmann, H. Bornfleth, P. Edelmann, D. Zink, T. Cremer, and C. Cremer. 1990. The trithorax gene, a trans-acting regulator of the bithorax complex in Drosophila, encodes a protein with zinc-binding domains. *Proc Natl Acad Sci U S A*. 87:2112-6. Im Neuenheimer Feld 280, Heidelberg, D-69120, Germany.

McCabe, N.R., R.C. Burnett, H.J. Gill, M.J. Thirman, D. Mbangkollo, M. Kipiniak, E. van Melle, S. Ziemin-van der Poel, J.D. Rowley, and M.O. Diaz. 1992. Cloning of cDNAs of the MLL gene that detect DNA rearrangements and altered RNA transcripts in human leukemic cells with 11q23 translocations. *Proc Natl Acad Sci U S A*. 89:11794-8.

Mitelman, F. 1991. Catalog of chromosome aberration in cancer.

Mitelman, F., B. Johansson, and F.E. Mertens. 2001. Mitelman Database of Chromosome Aberrations in Cancer.

Mitelman, F., B. Johansson, and F.e. Mertens. 2003. Mitelman Database of Chromosome Aberrations in Cancer.

Mitterbauer, G., C. Zimmer, H. Pirc-Danoewinata, O.A. Haas, S. Hojas, I. Schwarzinger, H. Greinix, U. Jager, K. Lechner, and C. Mannhalter. 2000. Monitoring of minimal residual disease in patients with MLL-AF6-positive acute myeloid leukaemia by reverse transcriptase polymerase chain reaction. *Br J Haematol*. 109:622-8.

Mrozek, K., S.M. Tanner, K. Heinonen, and C.D. Bloomfield. 2003. Molecular cytogenetic characterization of the KG-1 and KG-1a acute myeloid leukemia cell lines by use of spectral karyotyping and fluorescence in situ hybridization. *Genes Chromosomes Cancer*. 38:249-52.

Nakamura, T., H. Alder, Y. Gu, R. Prasad, O. Canaani, N. Kamada, R.P. Gale, B. Lange, W.M. Crist, P.C. Nowell, and et al. 1993. Genes on chromosomes 4, 9, and 19

involved in 11q23 abnormalities in acute leukemia share sequence homology and/or common motifs. *Proc Natl Acad Sci U S A*. 90:4631-5.

Nicoletti, I., G. Migliorati, M.C. Pagliacci, F. Grignani, and C. Riccardi. 1991. A rapid and simple method for measuring thymocyte apoptosis by propidium iodide staining and flow cytometry. *J Immunol Methods*. 139:271-9.

O'Brien, S.J. 1991. Mammalian genome mapping: lessons and prospects. *Curr Opin Genet Dev*. 1:105-11.

O'Brien, S.J., M. Menotti-Raymond, W.J. Murphy, W.G. Nash, J. Wienberg, R. Stanyon, N.G. Copeland, N.A. Jenkins, J.E. Womack, and J.A. Marshall Graves. 1999. The promise of comparative genomics in mammals. *Science*. 286:458-62, 479-81.

Odero, M.D., J.L. Vizmanos, J.P. Roman, I. Lahortiga, C. Panizo, M.J. Calasanz, N.J. Zeleznik-Le, J.D. Rowley, and F.J. Novo. 2002. A novel gene, MDS2, is fused to ETV6/TEL in a t(1;12)(p36.1;p13) in a patient with myelodysplastic syndrome. *Genes Chromosomes Cancer*. 35:11-9.

Oeltjen, J.C., T.M. Malley, D.M. Muzny, W. Miller, R.A. Gibbs, and J.W. Belmont. 1997. Large-scale comparative sequence analysis of the human and murine Bruton's tyrosine kinase loci reveals conserved regulatory domains. *Genome Res*. 7:315-29.

Ohno, S. 1973. Ancient linkage groups and frozen accidents. *Nature*. 244:259-62.

Olins, A.L., and D.E. Olins. 1974. Spheroid chromatin units (v bodies). *Science*. 183:330-2.

Olins, D.E., and A.L. Olins. 2003. Chromatin history: our view from the bridge. *Nat Rev Mol Cell Biol*. 4:809-14.

Parada, L., and T. Misteli. 2002. Chromosome positioning in the interphase nucleus. *Trends Cell Biol*. 12:425-32.

Parada, L.A., P.G. McQueen, P.J. Munson, and T. Misteli. 2002. Conservation of relative chromosome positioning in normal and cancer cells. *Curr Biol*. 12:1692-7.

Parada, L.A., J.J. Roix, and T. Misteli. 2003. An uncertainty principle in chromosome positioning. *Trends Cell Biol*. 13:393-6.

Pardue, M.L., and T.C. Hsu. 1975. Locations of 18S and 28S ribosomal genes on the chromosomes of the Indian muntjac. *J Cell Biol*. 64:251-4.

Park, J.P., S.L. Ladd, P. Ely, N.J. Weiner, S.A. Wojiski, A.B. Hawk, W.W. Noll, and T.K. Mohandas. 2000. Amplification of the MLL region in acute myeloid leukemia. *Cancer Genet Cytogenet*. 121:198-205.

Parry, P., M. Djabali, M. Bower, J. Khristich, M. Waterman, B. Gibbons, B.D. Young, and G. Evans. 1993. Structure and expression of the human trithorax-like gene 1 involved in acute leukemias. *Proc Natl Acad Sci U S A*. 90:4738-42.

Passegue, E., C.H. Jamieson, L.E. Ailles, and I.L. Weissman. 2003. Normal and leukemic hematopoiesis: are leukemias a stem cell disorder or a reacquisition of stem cell characteristics? *Proc Natl Acad Sci U S A*. 100 Suppl 1:11842-9.

Pedersen-Bjergaard, J., and J.D. Rowley. 1994. The balanced and the unbalanced chromosome aberrations of acute myeloid leukemia may develop in different ways and may contribute differently to malignant transformation. *Blood*. 83:2780-6.

Pennacchio, L.A. 2003. Insights from human/mouse genome comparisons. *Mamm Genome*. 14:429-36.

Pinkel, D., J.W. Gray, B. Trask, G. van den Engh, J. Fuscoe, and H. van Dekken. 1986. Cytogenetic analysis by in situ hybridization with fluorescently labeled nucleic acid probes. *Cold Spring Harb Symp Quant Biol*. 51 Pt 1:151-7.

Pinkel, D., J. Landegent, C. Collins, J. Fuscoe, R. Segraves, J. Lucas, and J. Gray. 1988. Fluorescence in situ hybridization with human chromosome-specific libraries: detection of trisomy 21 and translocations of chromosome 4. *Proc Natl Acad Sci U S A*. 85:9138-42.

Pirruccello, S.J., J.D. Jackson, and J.G. Sharp. 1994. The leukemic myeloid cell line OMA-AML-1: an in vitro model of hematopoietic cell differentiation. *Leuk Lymphoma*. 13:169-78.

Pui, C.H., L.S. Frankel, A.J. Carroll, S.C. Raimondi, J.J. Shuster, D.R. Head, W.M. Crist, V.J. Land, D.J. Pullen, C.P. Steuber, et al., O.A. Bernard, S.P. Romana, S.A. Schichman, M. Mauchauffe, P. Jonveaux, and R. Berger. 1991a. Clinical characteristics and treatment outcome of childhood acute lymphoblastic leukemia with the t(4;11)(q21;q23): a collaborative study of 40 cases. *Blood*. 77:440-7. (INSERM), Paris, France.

Pui, C.H., R.C. Ribeiro, M.L. Hancock, G.K. Rivera, W.E. Evans, S.C. Raimondi, D.R. Head, F.G. Behm, M.H. Mahmoud, J.T. Sandlund, and et al. 1991b. Acute myeloid leukemia in children treated with epipodophyllotoxins for acute lymphoblastic leukemia. *N Engl J Med*. 325:1682-7.

Qumsiyeh, M.B. 1995. Impact of rearrangements on function and position of chromosomes in the interphase nucleus and on human genetic disorders. *Chromosome Res*. 3:455-65.

Rabl. 1885. Über Zellteilung. *Morphologisches Jahrbuch*. 10:214-330.

Reeves, R., M.S. Nissen, R.M. Burian, and S.F. Gilbert. 1990. The A.T-DNA-binding domain of mammalian high mobility group I chromosomal proteins. A novel peptide motif for recognizing DNA structure. *J Biol Chem*. 265:8573-82. rmburian@vt.edu.

Reichel, M., E. Gillert, S. Angermuller, J.P. Hensel, F. Heidel, M. Lode, T. Leis, A. Biondi, O.A. Haas, S. Strehl, E.R. Panzer-Grumayer, F. Griesinger, J.D. Beck, J. Greil, G.H. Fey, F.M. Uckun, and R. Marschalek. 2001. Biased distribution of chromosomal breakpoints involving the MLL gene in infants versus children and adults with t(4;11) ALL. *Oncogene*. 20:2900-7.

Richardson, C., and M. Jasin. 2000. Frequent chromosomal translocations induced by DNA double-strand breaks. *Nature*. 405:697-700.

Richardson, C., M.E. Moynahan, and M. Jasin. 1998. Double-strand break repair by interchromosomal recombination: suppression of chromosomal translocations. *Genes Dev*. 12:3831-42.

Richkind, K., R. Hromas, C. Lytle, D. Crenshaw, J. Velasco, S. Roherty, J. Srinivasiah, and M. Varella-Garcia. 2000. Identification of two new translocations that disrupt the AML1 gene. *Cancer Genet Cytogenet*. 122:141-3.

Robinett, C.C., A. Straight, G. Li, C. Willhelm, G. Sudlow, A. Murray, and A.S. Belmont. 1996. In vivo localization of DNA sequences and visualization of large-scale chromatin organization using lac operator/repressor recognition. *J Cell Biol*. 135:1685-700.

Roix, J.J., P.G. McQueen, P.J. Munson, L.A. Parada, and T. Misteli. 2003. Spatial proximity of translocation-prone gene loci in human lymphomas. *Nat Genet*. 34:287-91.

Ross, J.A. 2000. Dietary flavonoids and the MLL gene: A pathway to infant leukemia? *Proc Natl Acad Sci U S A*. 97:4411-3.

Roth, D.B., and J.H. Wilson. 1986. Nonhomologous recombination in mammalian cells: role for short sequence homologies in the joining reaction. *Mol Cell Biol*. 6:4295-304.

Rowley, J.D. 1990. Recurring chromosome abnormalities in leukemia and lymphoma. *Semin Hematol*. 27:122-36.

Rowley, J.D. 1998a. The critical role of chromosome translocations in human leukemias. *Annu Rev Genet*. 32:495-519.

Rowley, J.D. 1998b. Seminars from the University of Minnesota. Chromosome translocations: dangerous liaisons. *J Lab Clin Med*. 132:244-50.

Rowley, J.D., and H.J. Olney. 2002. International workshop on the relationship of prior therapy to balanced chromosome aberrations in therapy-related myelodysplastic syndromes and acute leukemia: overview report. *Genes Chromosomes Cancer*. 33:331-45.

Saccone, S., and G. Bernardi. 2001. Human chromosomal banding by in situ hybridization of isochores. *Methods Cell Sci*. 23:7-15.

Saccone, S., C. Federico, and G. Bernardi. 2002. Localization of the gene-richest and the gene-poorest isochores in the interphase nuclei of mammals and birds. *Gene*. 300:169-78.

Saccone, S., C. Federico, I. Solovei, M.F. Croquette, G. Della Valle, and G. Bernardi. 1999. Identification of the gene-richest bands in human prometaphase chromosomes. *Chromosome Res*. 7:379-86.

Saito, S., M. Matsushima, S. Shirahama, T. Minaguchi, Y. Kanamori, M. Minami, and Y. Nakamura. 1998. Complete genomic structure DNA polymorphisms, and alternative splicing of the human AF-6 gene. *DNA Res*. 5:115-20.

Scherthan, H., T. Cremer, U. Arnason, H.U. Weier, A. Lima-de-Faria, and L. Fronicke. 1994. Comparative chromosome painting discloses homologous segments in distantly related mammals. *Nat Genet*. 6:342-7.

Scheuermann, M. 2004. Characterization of nuclear subcompartments by analysis of the topology of genes and non-transcribed sequences as well as ectopically expressed proteins in mammalian cells with different karyotypes. *Dissertation, submitted to the Combined Faculties for the Natural Sciences and for Mathematics of the Ruperto-Carola University of Heidelberg, Germany for the degree of Doctor of Natural Sciences*.

Schliephacke, T., A. Meinl, M. Kratzmeier, D. Doenecke, and W. Albig. 2004. The telomeric region is excluded from nucleosomal fragmentation during apoptosis, but the bulk nuclear chromatin is randomly degraded. *Cell Death Differ*. 11:693-703.

Schmidtke, J., H. Brennecke, M. Schmid, H. Neitzel, and K. Sperling. 1981. Evolution of muntjac DNA. *Chromosoma*. 84:187-93.

Shannon, M.F. 2003. A nuclear address with influence. *Nat Genet*. 34:4-6.

Shows, T.B., J.A. Brown, and V.M. Chapman. 1976. Comparative gene mapping of HPRT, G6PD, and PGK in man, mouse, and muntjac deer. *Cytogenet Cell Genet*. 16:436-9.

Shtivelman, E., B. Lifshitz, R.P. Gale, and E. Canaani. 1985. Fused transcript of abl and bcr genes in chronic myelogenous leukaemia. *Nature*. 315:550-4.

Siebert, R., P. Matthiesen, S. Harder, Y. Zhang, A. Borowski, R. Zuhlke-Jenisch, S. Metzke, S. Joos, K. Weber-Matthiesen, W. Grote, and B. Schlegelberger. 1998. Application of interphase fluorescence in situ Hybridization for the detection of the Burkitt translocation t(8;14)(q24;q32) in B-cell lymphomas. *Blood*. 91:984-90.

So, C.W., C. Caldas, M.M. Liu, S.J. Chen, Q.H. Huang, L.J. Gu, M.H. Sham, L.M. Wiedemann, and L.C. Chan. 1997a. EEN encodes for a member of a new family of proteins containing an Src homology 3 domain and is the third gene located on chromosome 19p13 that fuses to MLL in human leukemia. *Proc Natl Acad Sci U S A*. 94:2563-8.

So, C.W., Z.G. Ma, C.M. Price, S. Dong, S.J. Chen, L.J. Gu, C.K. So, L.M. Wiedemann, and L.C. Chan. 1997b. MLL self fusion mediated by Alu repeat homologous recombination and prognosis of AML-M4/M5 subtypes. *Cancer Res*. 57:117-22.

Solovei, I., A. Cavallo, L. Schermelleh, F. Jaunin, C. Scasselati, D. Cmarko, C. Cremer, S. Fakan, and T. Cremer. 2002. Spatial preservation of nuclear chromatin architecture during three-dimensional fluorescence in situ hybridization (3D-FISH). *Exp Cell Res*. 276:10-23.

Solovei, I., L. Schermelleh, K. During, A. Engelhardt, S. Stein, C. Cremer, and T. Cremer. 2004. Differences in centromere positioning of cycling and postmitotic human cell types. *Chromosoma*. 112:410-23.

Spector, D.L., R.D. Goldman, and L.A. Leinwand. 1998. Cells: a laboratory manual. Cold Spring Harbor Laboratory Press, 10 Skyline Drive, Plainview, New York 11803-2500, Phone 1-800-843-4388, cshpress@cshl.org, http://cshl.org.

Stanulla, M., P. Chhalliyil, J. Wang, S.N. Jani-Sait, and P.D. Aplan. 2001. Mechanisms of MLL gene rearrangement: site-specific DNA cleavage within the breakpoint cluster region is independent of chromosomal context. *Hum Mol Genet*. 10:2481-91.

Stanulla, M., J. Wang, D.S. Chervinsky, S. Thandla, and P.D. Aplan. 1997. DNA cleavage within the MLL breakpoint cluster region is a specific event which occurs as part of higher-order chromatin fragmentation during the initial stages of apoptosis. *Mol Cell Biol*. 17:4070-9.

Strachan, T., and A.P. Read. 1999. Human Molecular Genetics 2. John Wiley & Sons Inc.,, 605 Third Avenue, New York, NY 10158–0012, USA.

Strick, R., P.L. Strissel, S. Borgers, S.L. Smith, and J.D. Rowley. 2000. Dietary bioflavonoids induce cleavage in the MLL gene and may contribute to infant leukemia. *Proc Natl Acad Sci U S A*. 97:4790-5.

Strissel, P.L., R. Strick, J.D. Rowley, and N.J. Zeleznik-Le. 1998. An in vivo topoisomerase II cleavage site and a DNase I hypersensitive site colocalize near exon 9 in the MLL breakpoint cluster region. *Blood*. 92:3793-803.

Strissel, P.L., R. Strick, R.J. Tomek, B.A. Roe, J.D. Rowley, and N.J. Zeleznik-Le. 2000. DNA structural properties of AF9 are similar to MLL and could act as recombination hot spots resulting in MLL/AF9 translocations and leukemogenesis. *Hum Mol Genet*. 9:1671-9.

Strout, M.P., G. Marcucci, C.D. Bloomfield, and M.A. Caligiuri. 1998. The partial tandem duplication of ALL1 (MLL) is consistently generated by Alu-mediated homologous recombination in acute myeloid leukemia. *Proc Natl Acad Sci U S A*. 95:2390-5.

Sturtevant, A.H. 1925. The Effects of Unequal Crossing Over at the Bar Locus in Drosophila. *Genetics*. 10:117-147.

Sugimoto, K., R. Fukuda, and M. Himeno. 2000. Centromere/kinetochore localization of human centromere protein A (CENP-A) exogenously expressed as a fusion to green fluorescent protein. *Cell Struct Funct*. 25:253-61.

Sullivan, G.J., J.M. Bridger, A.P. Cuthbert, R.F. Newbold, W.A. Bickmore, and B. McStay. 2001. Human acrocentric chromosomes with transcriptionally silent nucleolar organizer regions associate with nucleoli. *Embo J*. 20:2867-74.

Sullivan, K.F., and R.D. Shelby. 1999. Using time-lapse confocal microscopy for analysis of centromere dynamics in human cells. *Methods Cell Biol*. 58:183-202.

Super, H.G., P.L. Strissel, O.M. Sobulo, D. Burian, S.C. Reshmi, B. Roe, N.J. Zeleznik-Le, M.O. Diaz, and J.D. Rowley. 1997. Identification of complex genomic breakpoint junctions in the t(9;11) MLL-AF9 fusion gene in acute leukemia. *Genes Chromosomes Cancer*. 20:185-95.

Super, H.J., N.R. McCabe, M.J. Thirman, R.A. Larson, M.M. Le Beau, J. Pedersen-Bjergaard, P. Philip, M.O. Diaz, and J.D. Rowley. 1993. Rearrangements of the MLL gene in therapy-related acute myeloid leukemia in patients previously treated with agents targeting DNA-topoisomerase II. *Blood*. 82:3705-11.

Taddei, A., F. Hediger, F.R. Neumann, and S.M. Gasser. 2004. The Function of Nuclear Architecture: A Genetic Approach. *Annu Rev Genet*.

Tajbakhsh, J., H. Luz, H. Bornfleth, S. Lampel, C. Cremer, and P. Lichter. 2000. Spatial distribution of GC- and AT-rich DNA sequences within human chromosome territories. *Exp Cell Res*. 255:229-37.

Tanabe, H., S. Muller, M. Neusser, J. von Hase, E. Calcagno, M. Cremer, I. Solovei, C. Cremer, and T. Cremer. 2002. Evolutionary conservation of chromosome territory arrangements in cell nuclei from higher primates. *Proc Natl Acad Sci U S A*. 99:4424-9.

Taslerova, R., S. Kozubek, E. Lukasova, P. Jirsova, E. Bartova, and M. Kozubek. 2003. Arrangement of chromosome 11 and 22 territories, EWSR1 and FLI1 genes, and

other genetic elements of these chromosomes in human lymphocytes and Ewing sarcoma cells. *Hum Genet*. 112:143-55.

Telenius, H., A.H. Pelmear, A. Tunnacliffe, N.P. Carter, A. Behmel, M.A. Ferguson-Smith, M. Nordenskjold, R. Pfragner, and B.A. Ponder. 1992. Cytogenetic analysis by chromosome painting using DOP-PCR amplified flow-sorted chromosomes. *Genes Chromosomes Cancer*. 4:257-63.

Thirman, M.J., D.A. Levitan, H. Kobayashi, M.C. Simon, and J.D. Rowley. 1994. Cloning of ELL, a gene that fuses to MLL in a t(11;19)(q23;p13.1) in acute myeloid leukemia. *Proc Natl Acad Sci U S A*. 91:12110-4.

Thompson, L.H., and D. Schild. 2001. Homologous recombinational repair of DNA ensures mammalian chromosome stability. *Mutat Res*. 477:131-53.

Tkachuk, D.C., S. Kohler, and M.L. Cleary. 1992. Involvement of a homolog of Drosophila trithorax by 11q23 chromosomal translocations in acute leukemias. *Cell*. 71:691-700.

Tsukamoto, Y., and H. Ikeda. 1998. Double-strand break repair mediated by DNA end-joining. *Genes Cells*. 3:135-44.

Tyler, J.K. 2002. Chromatin assembly. Cooperation between histone chaperones and ATP-dependent nucleosome remodeling machines. *Eur J Biochem*. 269:2268-74.

van der Feltz, M.J., M.K. Shivji, P.B. Allen, N. Heisterkamp, J. Groffen, and L.M. Wiedemann. 1989. Nucleotide sequence of both reciprocal translocation junction regions in a patient with Ph positive acute lymphoblastic leukaemia, with a breakpoint within the first intron of the BCR gene. *Nucleic Acids Res*. 17:1-10.

Vazquez, J., A.S. Belmont, and J.W. Sedat. 2001. Multiple regimes of constrained chromosome motion are regulated in the interphase Drosophila nucleus. *Curr Biol*. 11:1227-39.

Venter, J.C., M.D. Adams, E.W. Myers, P.W. Li, R.J. Mural, G.G. Sutton, H.O. Smith, M. Yandell, C.A. Evans, R.A. Holt, J.D. Gocayne, P. Amanatides, R.M. Ballew, D.H. Huson, J.R. Wortman, Q. Zhang, C.D. Kodira, X.H. Zheng, L. Chen, M. Skupski, G. Subramanian, P.D. Thomas, J. Zhang, G.L. Gabor Miklos, C. Nelson, S. Broder, A.G. Clark, J. Nadeau, V.A. McKusick, N. Zinder, A.J. Levine, R.J. Roberts, M. Simon, C. Slayman, M. Hunkapiller, R. Bolanos, A. Delcher, I. Dew, D. Fasulo, M. Flanigan, L. Florea, A. Halpern, S. Hannenhalli, S. Kravitz, S. Levy, C. Mobarry, K. Reinert, K. Remington, J. Abu-Threideh, E. Beasley, K. Biddick, V. Bonazzi, R. Brandon, M. Cargill, I. Chandramouliswaran, R. Charlab, K. Chaturvedi, Z. Deng, V. Di Francesco, P. Dunn, K. Eilbeck, C. Evangelista, A.E. Gabrielian, W. Gan, W. Ge, F. Gong, Z. Gu, P. Guan, T.J. Heiman, M.E. Higgins, R.R. Ji, Z. Ke, K.A. Ketchum, Z. Lai, Y. Lei, Z. Li, J. Li, Y. Liang, X. Lin, F. Lu, G.V. Merkulov, N. Milshina, H.M. Moore, A.K. Naik, V.A. Narayan, B. Neelam, D. Nusskern, D.B. Rusch, S. Salzberg, W. Shao, B. Shue, J. Sun, Z. Wang, A. Wang, X. Wang, J. Wang, M. Wei, R. Wides, C. Xiao, C. Yan, et al. 2001. The sequence of the human genome. *Science*. 291:1304-51.

Volpi, E.V., E. Chevret, T. Jones, R. Vatcheva, J. Williamson, S. Beck, R.D. Campbell, M. Goldsworthy, S.H. Powis, J. Ragoussis, J. Trowsdale, and D. Sheer. 2000. Large-

scale chromatin organization of the major histocompatibility complex and other regions of human chromosome 6 and its response to interferon in interphase nuclei. *J Cell Sci*. 113:1565-76.

von Bergh, A., P. Gargallo, B. De Prijck, H. Vranckx, R. Marschalek, I. Larripa, P. Kluin, E. Schuuring, and A. Hagemeijer. 2001. Cryptic t(4;11) encoding MLL-AF4 due to insertion of 5' MLL sequences in chromosome 4. *Leukemia*. 15:595-600.

Vooijs, M., L.C. Yu, D. Tkachuk, D. Pinkel, D. Johnson, and J.W. Gray. 1993. Libraries for each human chromosome, constructed from sorter-enriched chromosomes by using linker-adaptor PCR. *Am J Hum Genet*. 52:586-97.

Waller, C.F., U.M. Martens, and W. Lange. 1999. Philadelphia chromosome-positive cells are equally distributed in AC133+ and AC133- fractions of CD34+ peripheral blood progenitor cells from patients with CML. *Leukemia*. 13:1466-7.

Walter, J., L. Schermelleh, M. Cremer, S. Tashiro, and T. Cremer. 2003. Chromosome order in HeLa cells changes during mitosis and early G1, but is stably maintained during subsequent interphase stages. *J Cell Biol*. 160:685-97.

Wang, J.C. 2002. Cellular roles of DNA topoisomerases: a molecular perspective. *Nat Rev Mol Cell Biol*. 3:430-40.

Waterston, R.H., K. Lindblad-Toh, E. Birney, J. Rogers, J.F. Abril, P. Agarwal, R. Agarwala, R. Ainscough, M. Alexandersson, P. An, S.E. Antonarakis, J. Attwood, R. Baertsch, J. Bailey, K. Barlow, S. Beck, E. Berry, B. Birren, T. Bloom, P. Bork, M. Botcherby, N. Bray, M.R. Brent, D.G. Brown, S.D. Brown, C. Bult, J. Burton, J. Butler, R.D. Campbell, P. Carninci, S. Cawley, F. Chiaromonte, A.T. Chinwalla, D.M. Church, M. Clamp, C. Clee, F.S. Collins, L.L. Cook, R.R. Copley, A. Coulson, O. Couronne, J. Cuff, V. Curwen, T. Cutts, M. Daly, R. David, J. Davies, K.D. Delehaunty, J. Deri, E.T. Dermitzakis, C. Dewey, N.J. Dickens, M. Diekhans, S. Dodge, I. Dubchak, D.M. Dunn, S.R. Eddy, L. Elnitski, R.D. Emes, P. Eswara, E. Eyras, A. Felsenfeld, G.A. Fewell, P. Flicek, K. Foley, W.N. Frankel, L.A. Fulton, R.S. Fulton, T.S. Furey, D. Gage, R.A. Gibbs, G. Glusman, S. Gnerre, N. Goldman, L. Goodstadt, D. Grafham, T.A. Graves, E.D. Green, S. Gregory, R. Guigo, M. Guyer, R.C. Hardison, D. Haussler, Y. Hayashizaki, L.W. Hillier, A. Hinrichs, W. Hlavina, T. Holzer, F. Hsu, A. Hua, T. Hubbard, A. Hunt, I. Jackson, D.B. Jaffe, L.S. Johnson, M. Jones, T.A. Jones, A. Joy, M. Kamal, E.K. Karlsson, et al. 2002. Initial sequencing and comparative analysis of the mouse genome. *Nature*. 420:520-62.

Weierich, C., A. Brero, S. Stein, J. von Hase, C. Cremer, T. Cremer, and I. Solovei. 2003. Three-dimensional arrangements of centromeres and telomeres in nuclei of human and murine lymphocytes. *Chromosome Res*. 11:485-502.

White, C.L., R.K. Suto, and K. Luger. 2001. Structure of the yeast nucleosome core particle reveals fundamental changes in internucleosome interactions. *Embo J*. 20:5207-18.

Whitmarsh, R.J., C. Saginario, Y. Zhuo, E. Hilgenfeld, E.F. Rappaport, M.D. Megonigal, M. Carroll, M. Liu, N. Osheroff, N.K. Cheung, D.J. Slater, T. Ried, T. Knutsen, I.A. Blair, and C.A. Felix. 2003. Reciprocal DNA topoisomerase II cleavage events at 5'-TATTA-3' sequences in MLL and AF-9 create homologous single-stranded

overhangs that anneal to form der(11) and der(9) genomic breakpoint junctions in treatment-related AML without further processing. *Oncogene*. 22:8448-59.

Wienberg, J., R. Stanyon, W.G. Nash, P.C. O'Brien, F. Yang, S.J. O'Brien, and M.A. Ferguson-Smith. 1997. Conservation of human vs. feline genome organization revealed by reciprocal chromosome painting. *Cytogenet Cell Genet*. 77:211-7.

Williams, R.R., S. Broad, D. Sheer, and J. Ragoussis. 2002. Subchromosomal positioning of the epidermal differentiation complex (EDC) in keratinocyte and lymphoblast interphase nuclei. *Exp Cell Res*. 272:163-75.

Wischnitzer, S. 1973. The submicroscopic morphology of the interphase nucleus. *Int Rev Cytol*. 34:1-48.

Wurster, D.H., and N.B. Atkin. 1972. Muntjac chromosomes: a new karyotype of Muntiacus muntjak. *Experientia*. 28:972-973.

Wurster, D.H., and K. Benirschke. 1967. Chromosome studies in some deer, the springbok, and the pronghorn, with notes on placentation in deer. *Cytologia (Tokyo)*. 32:273-85.

Wurster, D.H., and K. Benirschke. 1970. Indian muntjac, Muntiacus muntjak: a deer with a low diploid chromosome number. *Science*. 168:1364-6.

Wyllie, A.H., J.F. Kerr, and A.R. Currie. 1980. Cell death: the significance of apoptosis. *International Review of Cytology*. 68:251-306.

Yamamoto, K., H. Hamaguchi, K. Nagata, and M. Taniwaki. 1998. A variant Burkitt-type translocation (8;22)(q24;q11) in multiple myeloma. Report of a new case and review of the literature. *Cancer Genet Cytogenet*. 104:98-103.

Yamamoto, K., M. Seto, S. Iida, H. Komatsu, N. Kamada, S. Kojima, Y. Kodera, S. Nakazawa, H. Saito, T. Takahashi, and et al. 1994. A reverse transcriptase-polymerase chain reaction detects heterogeneous chimeric mRNAs in leukemias with 11q23 abnormalities. *Blood*. 83:2912-21.

Yang, F., N.P. Carter, L. Shi, and M.A. Ferguson-Smith. 1995. A comparative study of karyotypes of muntjacs by chromosome painting. *Chromosoma*. 103:642-52.

Yang, F., S. Muller, R. Just, M.A. Ferguson-Smith, and J. Wienberg. 1997a. Comparative chromosome painting in mammals: human and the Indian muntjac (Muntiacus muntjak vaginalis). *Genomics*. 39:396-401.

Yang, F., P.C. O'Brien, J. Wienberg, and M.A. Ferguson-Smith. 1997b. A reappraisal of the tandem fusion theory of karyotype evolution in Indian muntjac using chromosome painting. *Chromosome Res*. 5:109-17.

Yang, F., P.C. O'Brien, J. Wienberg, H. Neitzel, C.C. Lin, and M.A. Ferguson-Smith. 1997c. Chromosomal evolution of the Chinese muntjac (Muntiacus reevesi). *Chromosoma*. 106:37-43.

Yokota, H., M.J. Singer, G.J. van den Engh, and B.J. Trask. 1997. Regional differences in the compaction of chromatin in human G0/G1 interphase nuclei. *Chromosome Res*. 5:157-66.

Yokota, H., G. van den Engh, J.E. Hearst, R.K. Sachs, and B.J. Trask. 1995. Evidence for the organization of chromatin in megabase pair-sized loops arranged along a random walk path in the human G0/G1 interphase nucleus. *In* J Cell Biol. Vol. 130. 1239-49.

Yu, B.D., J.L. Hess, S.E. Horning, G.A. Brown, and S.J. Korsmeyer. 1995. Altered Hox expression and segmental identity in Mll-mutant mice. *Nature*. 378:505-8.

Zeleznik-Le, N.J., A.M. Harden, and J.D. Rowley. 1994. 11q23 translocations split the "AT-hook" cruciform DNA-binding region and the transcriptional repression domain from the activation domain of the mixed-lineage leukemia (MLL) gene. *Proc Natl Acad Sci U S A*. 91:10610-4.

Zhang, Y., X.N. Shan, X.X. Lu, N.S. Liu, and D.W. Yu. 2001. [Cloning, sequencing and chromosome location of Sry gene of Muntjak munticus vaginalis by DOP-PCR and microdissection]. *Yi Chuan Xue Bao*. 28:322-6.

Zhang, Y., N. Zeleznik-Le, N. Emmanuel, N. Jayathilaka, J. Chen, P. Strissel, R. Strick, L. Li, M.B. Neilly, T. Taki, Y. Hayashi, Y. Kaneko, B. Schlegelberger, and J.D. Rowley. 2004. Characterization of genomic breakpoints in MLL and CBP in leukemia patients with t(11;16). *Genes Chromosomes Cancer*. 41:257-65.

Ziemin-van der Poel, S., N.R. McCabe, H.J. Gill, R. Espinosa, III, Y. Patel, A. Harden, P. Rubinelli, S.D. Smith, M.M. LeBeau, J.D. Rowley, and et al. 1991. Identification of a gene, MLL, that spans the breakpoint in 11q23 translocations associated with human leukemias. *Proc Natl Acad Sci U S A*. 88:10735-9.

Zirbel, R.M., U.R. Mathieu, A. Kurz, T. Cremer, and P. Lichter. 1993. Evidence for a nuclear compartment of transcription and splicing located at chromosome domain boundaries. *Chromosome Res*. 1:93-106.

8. SUMMARY

Chromosomal translocations are the cause of many forms of leukemia. The mechanisms of how they occur are poorly understood. After a double strand break event, chromosomes are fused generating derivative chromosomes. During the fusion, a chimeric gene can be created and a fusion protein with new functions may be expressed which might cause malignant transformation. One such gene is *MLL,* which can be fused to a large number of other genes in different types of leukemias. It is believed that the 3D localization of genes, involved in chromosomal translocations in the interphase nucleus of certain hematopoietic tissues, could be a determining factor for a translocation event. This work has analyzed the 3D localization of *MLL* and some of its major translocation partners in the interphase nucleus of various cells cultured under different conditions, as well as in cell lines carrying translocation involving these genes.

An analysis procedure was developed to precisely determine gene positions in the 3D space of the spherical interphase nucleus of hematopoietic cells. The nuclear localization of a gene relative to the nuclear center and the nuclear periphery was determined. To provide a general understanding of the distribution pattern of a given locus within the nucleus, the nuclear volume was divided into five concentric shells in two different ways: 1. shells, of same thickness, which permitted detection of large differences in the position of genes, and 2. shells, whose volume were identical, which permitted a high resolution for genes that were close to the nuclear periphery. Using these tools, the positions of *MLL*, five of its translocation partners, (*AF4*, *AF6*, *AF9*, *ENL* and *ELL*) and four control loci (2q33, 2q35, 7q22 and 8q34) were analyzed in different human cell lines of hematopoietic origin and in primary hematopoietic stem cells. Despite the cell materials' differences in maturation state, cell lineage, and chromosome number, the localization of each gene and chromosomal locus showed a characteristic distribution pattern in the interphase nucleus in all studied hematopoietic cells, with the extremes being 2q35 having the most peripheral position, and the genes *ENL* and *ELL* on 19p13 sharing the most interior nuclear position. The three most common translocation partners of *MLL* (*AF4*, *AF6* and *AF9*) were found to be remarkably similar in their localization, which was more peripheral than that of *MLL*. The position of

MLL and AF9 relative to the nuclear surface was independent of the cell cycle and the induction of DSB/apoptosis. Interestingly, despite the differences in distances to the nuclear surface that were characteristic, distance analyses and angle measurements among genes revealed, that their relative positioning to each other is random.

To determine whether differences in either chromosome number, tissue type or species would affect the localization of genes, the distribution of *MLL* and its translocation partners *AF4* and *AF9* were analyzed in fibroblasts of three different species: human and two closely related species of the genus Muntiacus, *Muntiacus muntjak* and *Muntiacus reevesi*, with a large difference in chromosome number (2n = 6/7 vs. 2n = 46). For the cytogenetic analysis of both muntjac species genomic reagents had to be developed. Syntenic regions between human and muntjac were identified using gene specific cattle probes. Genes were localized and whole chromosome paints were generated. In fibroblasts of the three different species, the distribution of *MLL*, *AF4* and *AF9* was similar, but showed a different order in nuclear distribution, from that observed in hematopoietic cells. The results suggest, that tissue specific differences in the nuclear distribution of genes is maintained beyond the borders of species.

The effect of translocations on gene position was also studied in various cell lines carrying well defined translocations involving *MLL* and its translocation partners *AF4*, *AF6* or *AF9*. For this study, a designed set of locus specific probes allowed the simultaneous detection of the genes on the normal and the derivative chromosomes. The positions for the normal genes were notably different from the positions of the fusion genes depending on the type of translocation. The analysis of gene density of whole chromosomes and local gene density, within a 2 Mbp window surrounding the locus, revealed a strong correlation between the nuclear position of a locus and its local gene density. In general, genes in areas of high local gene density were found towards the nuclear center, whereas genes in regions of low gene density were detected near the nuclear periphery. The gene density within a 2 Mbp window was determined to be a good predictor for the relative positioning of a locus within the nucleus and could explain the change of position observed after translocation events. Furthermore a correlation between the position of a locus and its position relative to

its chromosomal territory seemed to be linked to the gene density. The "2 Mbp prediction" was successfully applied to various examples of nuclear positional studies published in the literature. This work revealed therefore new insight into the nuclear architecture of mammalian cells and has identified principles that determine the 3D position of genes in the nucleus. The results of this work that could help us to better understand the basis for chromosomal translocations that cause leukemia.

9. ZUSAMMENFASSUNG

Viele Formen von Leukämie sind durch chromosomale Translokationen charakterisiert. Die Mechanismen, die zu Translokationen führen sind wenig verstanden. Der Fusion von Chromosomen gehen Doppelstrangbrüche voraus. Dies führt häufig zur Bildung von derivaten Chromosomen und der Expression von chimären Genen und Genprodukten mit neuen Funktionen, welche zelluläre Transformation verursachen können. Eines der Gene, die häufig an Translokationen beteiligt sind, ist *MLL*, welches in verschiedenen Leukämiearten mit einer Reihe von anderen Genen fusionieren kann. Man nimmt an, dass die Position von Genen im Interphasezellkern bestimmter hämatopoietischer Gewebe eine wichtige Rolle bei der Entstehung von Translokationen spielen kann. In dieser Arbeit wurde die Lage von *MLL* und einiger seiner wichtigsten Translokationspartner im 3 dimensionalen Raum des Interphasezellkerns in verschiedenen Zellen unter verschiedenen Bedingungen untersucht, sowie die Lage dieser Gene auf derivaten Chromosomen.

Zuerst wurde eine Analysemethode entwickelt, mit deren Hilfe die akkurate Position von Genen im 3D Volumen des sphärischen Interphasenukleus hämatopoietischer Zellen ermittelt werden kann. Um einen generellen Überblick über das Verteilungsmuster eines Gens innerhalb des Zellkerns zu gewinnen, wurde der nukleare Raum in 5 konzentrische Schalen auf zweierlei Art unterteilt: 1. In Schalen gleicher Dicke, und 2. in Schalen gleichen Volumens. Der Einsatz dieser Methoden erlaubte zum einen die Darstellung großer Positionsunterschiede genomischer Loci im Nukleus und zum anderen eine hohe Auflösung von Genen nahe der nuklearen Oberfläche. Mit Hilfe dieser Methoden wurden die Positionen von *MLL*, fünf seiner Translokationspartner (*AF4*, *AF6*, *AF9*, *ENL* und *ELL*) und 4 Kontroll-Loci (2q33, 2q35, 7q22 und 8q34) in verschiedenen menschlichen Zellinien hämatopoietischen Ursprungs sowie primären hämatopoietischen Stammzellen bestimmt. Die Position der analysierten Loci erschien generell unabhängig vom Reifungsgrad, von der Differenzierung oder von der Anzahl der Chromosomen der analysierten Zellen zu sein. Alle Loci zeigten ein charakteristisches Verteilungsmuster im Interphasekern aller untersuchten Zellen. 2q35 nahm eine extrem randständige Position ein, wohingegen die Gene *ENL* und *ELL* auf 19p13 die zentralste Position einnahmen. Die drei häufigsten Translokationspartner

von *MLL* (*AF4*, *AF6* und *AF9*) zeigten eine auffällige Ähnlichkeit in ihrer 3D Position, die randständiger war als die von *MLL*. Die Lage von *MLL* und *AF9* relativ zur Kernoberfläche war unabhängig von Zellzyklus und Induktion von Doppelstrangbrüchen/Apoptose. Obwohl die Abstände der Gene zur nukleären Oberfläche für jedes Gen charakteristisch waren, zeigte die Analyse von Abständen und Winkeln der Gene zueinander eine zufällige Verteilung.

Um festzustellen ob Unterschiede in der spezifischen Lokalisierung von Genen in Zellen unterschiedlicher Chromosomenzahl oder in Zellen anderer Gewebe oder Spezies bestehen, wurde die Verteilung von *MLL* und seiner Translokationspartner *AF4* und AF9 in Fibroblasten dreier verschiedenen Spezies analysiert: Im Menschen, und in zwei nahe verwandten Spezies des Genus Muntiacus, *Muntiacus muntjak* und *Muntiacus reevesi*, die große Unterschiede in ihrer Chromosomenzahl aufweisen (2n = 6/7 gegenüber 2n= 46). Es mußten eine Reihe genomischer Reagenzien entwickelt werden, um die beiden Muntjak-Spezies zytogenetisch analysieren zu können. Es wurden syntene Regionen zwischen Mensch und Muntjak mittels Gen-spezifischer Proben aus dem Rind bestimmt. Zusätzlich wurden Gene lokalisiert und Chromosomen-Paints hergestellt. In Fibroblasten der drei verschiedenen Spezies war die Verteilung von *MLL*, *AF4* und *AF9* ähnlich, zeigte aber eine andere Verteilung als die, die in hämatopoietischen Zellen gefunden wurde. Die Daten deuten auf eine gewebespezifische Verteilung von Genen im Kern hin, die über Spezies-Grenzen hinweg besteht.

Schließlich wurde der Effekt chromosomaler Translokationen auf die Genposition in verschiedenen Zellinien untersucht, die gut charakterisierte Translokationen aufwiesen, an denen *MLL* und jeweils einer der Translokationspartner *AF4*, *AF6* oder *AF9* beteiligt waren. Dafür wurden Gen-spezifische Proben hergestellt, mit denen gleichzeitig die Gene auf normalen und derivaten Chromosomen gefärbt werden konnten. Die Positionen der Gene auf normalen und derivaten Chromosomen war deutlich unterschiedlich und abhängig davon, welche Translokation vorlag.

Der Vergleich der Gendichte ganzer Chromosomen mit der eines Bereiches von 2 Mbp um einen Gen-Locus herum zeigte eine starke Korrelation zwischen der nuklearen

Position des Locus und der lokalen Gendichte. Generell wurden Loci mit hoher Gendichte im Kerninneren gefunden, Loci mit niedriger Gendichte hingegen in der Kernperipherie. Die Bestimmung der Gendichte im 2 Mbp Fenster erlaubte eine gute Vorhersage der Veränderung der Position eines Locus nach einer Translokation. Dies konnte auch erfolgreich für verschiedene veröffentlichte Befunde zur nuklearen Positionierung von Genen demonstriert werden. Die vorliegende Arbeit liefert neue Einblicke in die nukleare Architektur von Säugetierzellen und hat Prinzipien aufgedeckt, die die 3D Position eines Gens im Nukleus bestimmen. Die Ergebnisse dieser Arbeit könnten helfen, die Mechanismen, die der Entstehung chromosomaler Translokationen zu Grunde liegen und zu Leukämie führen, besser zu verstehen.

Appendices:

Appendix I: Adresses of Companies

AAPER Alcohol and Chemical Co.
P.O. Box 339, Shelbyville, KY 40066-0339
Telephone: (800) 456-1017, Fax: (502) 633-0685
Web site: www.aaper.com
Email: contact@aaper.com

AllCells, LLC.
2001 Dwight Way, Ste. 1360, Berkeley, California 94704, Berkeley, CA94704
Telephone: (888) 535-3444, (510) 548-8908, Fax: 510-548-8327
Web site: www.allcells.com/ordering/index.htm
Email: Info@AllCells.Com

American Laboratory Technologies, Inc. = ALTechnologies
2611 Jefferson Davis hwy, Suite 12000, Arlington, Virginia 22202
Telephone: (703) 418-0640
Web site: www.altechnologies.com/default.htm

American Laboratory Technologies,
2611 Jefferson Davis Hwy, suite 12000, Arlington, Virginia 22202, USA
Telephone: (703) 418-0640 or (800) 558-2880
Web site: www.altechnologies.com/default.htm

American Type Culture Collection (ATCC)
P.O. Box 1549, Manassas, VA 20108, USA
Telephone: (703) 365-2700, or (800) 638-6597
Web site: www.atcc.org

Amersham Biosciences (Formerly Amersham Pharmacia Biotech, Inc. (APBiotech))
800 Centennial Avenue, Piscataway, New Jersey, NJ 08855 U.S.A.
Telephone: (732) 457-8000, Fax: 877-295-8102

Applied Biosystems
850 Lincoln Centre Drive, Foster City, CA 94404 USA
Telephone: (800) 327-3002, (650) 638-5800, Fax: 650.638.5884
Web site: www.appliedbiosystems.com

Applied Genetics Laboratories, Inc.

1335 Gateway Drive, Suite 2001, Melbourne, FL 32901, USA
Telephone: (800) 235-5529 or (321) 768-2048, Fax: (321) 727-2643
Web site: www.appliedgenetics.com/

Bacharach Inc.
625 Alpha Drive, Pittsburgh, PA, 15238-2878, USA
Telephone: (724) 334-5000, (800) 736-4666, Fax: (724) 334-5001
Web site: www.bacharach-inc.com
Email: help@bacharach-inc.com

Baker Company Inc.
Web site: www.bakerco.com/
Ordering for their products through:

DAI Scientific Equipment, Inc.
1840 Industrial Drive, Suite 200, Libertyville, IL 60084, USA
Telephone: (800) 816-8388 Ext. 12, Fax: (847) 816-8420
Web site: www.daiscientific.com
E-mail: info@daiscientific.com

Barnstead/Thermolyne
2555 Kerper Boulevard, Dubuque, Iowa 52001, USA
Web site: www.barnsteadthermolyne.com/

B. Brown Biotech, Inc
999 Postal Road, Allentown, PA 18103
Telephone: (610) 266-6262, (800) 258-9000

Beckman Coulter, Inc.
4300 N. Harbor Boulevard, P.O. Box 3100, Fullerton, CA 92834-3100
Telephone: (714) 871-4848, Fax: (714) 773-8283
Web site: www.beckman.com

Beckton Dickinson
2350 Qume Drive, San Jose, CA 95131-1807, USA
Telephone: (877) 232-8995, (800) 448-2347, Fax: (408) 954-2347
Web site: www.bdbiosciences.com/

Biofluids Inc.
1146 Taft Street, Rockville MD 20850, USA
Telephone: (301) 424-4140, (800) 972-5200, Fax: (301) 424-3619
Website: www.biosource.com
E-mail: davidan@biosource.com

Bio-Rad Laboratories
Life Science Research, 2000 Alfred Nobel Drive, Hercules, CA 94547, USA
Telephone: (800) 4-BIORAD, (800) 424-6723, Fax: (510) 741-5800
Website: www.bio-rad.com

BOC Group Inc.
Murray Hill, NJ 07974, USA
Website: www.boc.com

Boekel industries
through Fisher scientific
Website: www.boekelsci.com/new_optima_series.htm

Boehringer/Roche
Roche Diagnostics Corporation, Roche Applied Science
P.O. Box 50414, 9115 Hague Road, Indianapolis, IN 46250-0414, USA
Telephone: (800) 428-5433, (800) 262-1640, Fax: (800) 428-2883
Website: www.roche-applied-science.com

Brinkmann Instruments Inc., an Eppendorf company
One Cantiague Road, P.O. Box 1019, Westbury, NY 11590-0207
Telephone : (800) 645-3050, (516) 334-7500, Fax: (516) 334-7506
Website: www.brinkmann.com,
E-mail: info@brinkmann.com

Behring Diagnostics Inc. (formerly Calbiochem Behring Corporation)
P O Box 49013, 3403 Yerba Buena Road, San Jose CA 95161-9013, USA
Website: www.dadebehring.com

Clay Adams Inc.
New York, NY, USA
Not more information found

C&M Scale Company
7142 Roosevelt Road, Forest Park, IL 60130, USA
Telephone: (800) 243-3721

Continental Laboratory Products = CLP
5648 Copley Drive, San Diego, CA. 92111 USA
Telephone: (858) 279-5000, (858) 279-5465, (800) 456-7741
Website: www.clpdirect.com/go/
Email: service@clpdirect.com

Cornelius commercial ice system (Vivian Ice Machines)
1735 Larkin Williams Rd., Fenton, MO 63026, USA
Telephone: (877) 325-9517
Website: www.vivian-ice-machines.com
Email: sales@vivianinternational.com

Corning Incorporated Life Sciences
45 Nagog Park, Acton, MA 01720
Telephone: (978) 635-2200, (800) 492-1110, Fax: (978) 635-2476
Website: www.corning.com/lifesciences/
Email: clswebmail@corning.com

Denver Instrument company
1855 Blake St. Suite 201, Denver, Colorado 80202
Telefone: (800) 321-1135, (303) 431-7255, Fax: (303) 423-4831
Web site: www.denverinstrumentusa.com

Deutsche Sammlung von Mikroorganismen und Zellkulturen GmbH = DSMZ
Mascheroder Weg 1b, 38124 Braunschweig, Germany
Telefone: (0 531) 2616-0, Fax: (0531)-2616-418
Web site: www.dsmz.de

Drummond Scientific Company
500 Parkway, Box 700, Broomall, PA 19008, USA
Telephone: (800) 523-7480, (610) 353-0200, Fax: (610) 353-6204
Web site: www.drummondsci.com
Email: info@drummondsci.com

Fermentas Inc.
7520 Connelley Drive, Unit A, Hanover, MD 21076, USA
Telephone: (800) 340-9026, Fax: (800) 472-8322
Web site: www.fermentas.com

Fisher Scientific
4500 Turnberry Dr., Hanover Park, IL 60103
Telephone: (630) 259-1200, Fax: (630) 259-4444
Web site: www1.fishersci.com/index.jsp

Forma Scientific, Inc.
P.O. Box 649, Marietta, OH 45750
Telephone: (740) 373-4763 / (800) 848-3080
Fax: (740) 374-1817
Web site: www.forma.com

E-mail: fmarketing@forma.com

Gibco see Invitrogen Corporation

Gilson Inc.
3000 W Beltine Hwy, P.O. Box 620027, Middleton, WI 53562-0027 USA
Web site: www.gilson.com
E-mail: sales@gilson.com

Integrated DNA technologies Inc. = IDT
8930 Gross Point Road Suite 700, Skokie, IL 60077, USA
Telephone: (847) 745-1700, (800) 328-2661, Fax: (847) 745-1710
Web site: www.idtdna.com/Home/Home.aspx

Invitrogen Corporation (also Gibco)
1600 Faraday Avenue, PO Box 6482, Carlsbad, CA 92008, USA
Telephone: (760) 603-7200, Fax: (760) 602-6500
Web site: www.invitrogen.com

Jackson ImmunoResearch Laboratories, Inc. (Jackson laboratories)
P.O. Box 9, 872 West Baltimore Pike, West Grove, PA 19390, USA
Telephone: (800) FOR-JAXN (367-5296), 610-869-4024, Fax: 610-869-0171
Web site: www.jacksonimmuno.com/home.htm

Kimberly-Clark Corporation
Dept. INT, P.O. Box 2020, Neenah, WI 54957-2020
Telephone: (888) 525-8388
Web site: www.kimberly-clark.com

Kodak Digital Sciences
through NEN™ Life Science Products, Inc.
549 Albany Street, Boston, MA 02118-2512 USA
Telephone: (800) 446-0035 (800) 551-2121, Fax: (617) 482-1380

Lab-Line Instruments Inc.
15th and Bloomingdale Avenues, Melrose Park IL 60160-1491, USA
Web site: www.labline.com

Lab Safety Corporation
Chicago, IL 60646

Lindberg/Blue M, a General Signal Company
308 Ridgefield Ct, Asheville, NC 28806

Telephone: (828) 658-2711, (800) 252-7100, Fax: 828-645-3368
Web site: www.lindbergbluem.com/home.shtml
Email: service@lindbergbluem.com , or info@kendro.spx.com.

Marsh Biomedical Products Inc.
565 Blossom Road, Rochester, NY 14610
Telephone: (716) 654-4800, Fax: (716) 654-4810
Web site: www.marshbio.com

Marabuwerke GmbH & Co.
D-71732 Tamm
Web site: www.marabu.de

Mettler Instrument Corp
Princeton Road Hightstown, Hightstown, NJ 08520, USA
Telephone: (609) 448-3000, (800) 638-8537

Merz Optical Instrument
(microscope)
not found

Midwest Scientific
280 Vance Road, St. Louis, MO 63088, USA
Telephone: (800) 227-9997; (636) 225-9997, Fax: (800) 610-4488 or (800) 227-9911
Web site: www.midsci.com

Miltenyi Biotec Inc.
12740 Earhart Avenue, Auburn, CA 95602, USA
Telephone: (530) 888-8871, (800) FOR MACS, Fax: (530) 888-8925,
Web site: www.miltenyibiotec.com

Molecular Probes, Inc.
29851 Willow Creek Road, Eugene, OR 97402, USA
Phone: (541) 335-0338, Fax: (541) 335-0305
Web site: www.probes.com
E-mail: order@probes.com

Nalge Nunc International
75 Panorama Creek Drive, Rochester, NY 14625. U.S.A.
Telephone: (800) 625-4327, Fax: (585) 586-8987
Web site: www.nalgenunc.com/
E-mail: nnics@nalgenunc.com

NAPCO
170 Marcel Dr., Winchester, VA 22602, USA
Telephone: (800) 621-8820
Web site: www.napco2.com/lab/contact
E-mail: info.btd.winchester@thermo.com

NEN = PerkinElmer Life Science = PerkinElmer = Lifescience Products Inc.
45 William Street, Wellesley, MA 02481-4078, USA
Telephone: (781) 237-5100, (800) 245-5774, (800) 762-4000
Web site: las.perkinelmer.com/content/corporate/about/nenlifescience.html

New England Biolabs
32 Tozer Road, Beverly, MA 01915-5599, USA
Telephone: (800) 632-5227, (800) NEB-LABS, Fax: (800) 632-7440
Web site: www.neb.com/nebecomm/default.asp

Oncor
does not exist anymore, was in part purchases by Vysis

PerkinElmer
549 Albany Street, Boston, MA 02118, USA
Telephone: (617) 482-9595, (800) 762-4000
Web site: www.perkinelmer.com
E-mail: ProductInfo@perkinelmer.com

PGC Scientific
7311 Governors Way Frederick, MD 21704 USA
Telephone: (301) 620-7777, :(800) 424-3300, Fax: (800) 662-1112

Pierce Equipment Company
9685 West 55th Street, Countryside, IL 60525, USA
Telephone: (708) 354-1265, Fax: (708) 354-1361
http://www.pierceequipment.com/
E-mail: chefmart@aol.com

Photometrics LTD
3440 East Britannia Drive, Tucson, AZ 85706, USA
Telephone: (520) 889-9933, FAX: (602) 573-1944
Web site: www.photomet.com/

Qiagen Inc.
27220 Turnberry Lane, Valencia, CA 91355, USA
Telephone: (800) 426-8157, (800) DNA-PREP, Fax: 800-718-2056

Web site: www1.qiagen.com

Roche see Boehringer

Savant Instruments
100 Colin Drive, Holbrook, NY, 11741, USA
Telephone: (516)244-2929, (800) 634-8886, Fax: (516) 244-0606

Sigma (or Sigma-Aldrich)
3050 Spruce St., St. Louis, MO 63103
Telephone: (800) 521-8956
Web site: www.sigma-aldrich.com.

Stratagene
11011 N. Torrey Pines Road, La Jolla, CA 92037, USA
Telephone: (800) 894-1304
Web site: www.stratagene.com/contacts/

Sorvall see under VWR International

Sullivan and Kelly
7900 S. Cass Avenue, Darien, IL 60561
Fax: 630-969-8506

Taylor-Wharton-Cryogenics
4075 Hamilton Boulevard, Theodore, AL 36582, USA
Telephone: (251) 443-8680, (800) 898-2657, Fax: (251) 443-2250
Web site: www.taylor-wharton.com/
E-mail: twsales@harsco.com

UVP, Inc.
2066 W. 11th Street, Upland, CA 91786
Telephone: (800) 452-6788, (909) 946-3197, Fax: (909) 946-3597
Web site: www.uvp.com/new
E-Mail: info@uvp.com

Vector laboratory
30 Ingold Road, Burlingame, CA 94010
Telephone: (800) 227-6666
Web site: www.vectorlabs.com

VWR
Chicago Regional Distribution Center, 800 East Fabyan Parkway, Batavia, IL 60510

Telephone: (800) 932-5000, (630) 879-0600, Fax: (630) 879-6718
Web site: www.vwrsp.com

VWR International
2360 Argentia Road
Mississauga, ON L5N 5Z7
Telephone: (800) 932-5000, Fax: (800) 668-6348
www.vwr.com
Web site: www.sorvall.com
E-mail: solutions@vwr.com

Vysis
3100 Woodcreek Drive, Downers Grove IL 60515-5400, USA
Telephone: (800) 553-7042
Web site: www.vysis.com

Zeiss
Carl Zeiss MicroImaging, Inc.
One Zeiss Drive, Thornwood, NY 10594
Phone: (800) 233-2343, Fax: (914) 681-7446
Web site: www.zeiss.com/micro
E-mail: micro@zeiss.com

Appendix II: Adresses of collaborators

Dr. J. Buitkamp
Lehrstuhl fuer Tierzucht, Technische Universitaet Muenchen,
85350 Freising-Weihnestephan
E-mail: buitkamp@pollux.edv.agrar.TU-Muenchen.de

Dr. Janis Burkhardt
Children's Hospital of Philadelphia, 816D Abramson Research Center
3615 Civic Center Boulevard, Philadelphia, PA 19104
Office phone: (267) 426-5410, Lab phone: (267) 426-5523, FAX: (267) 426-5165
E-mail: Jburkhar@mail.med.upenn.edu

Dr. Nigel Carter
Wellcome Trust Sanger Institute,
Molecular Genetics, Cambridge, UK
E-mail: npc@sanger.ac.uk

Dr. Peter Domer

Department of Medicine
University of Chicago

Dr. Roland Eils and Juntao Gao
DKFZ Heidelberg
Im Neuenheimer Feld 580, 69120 Heidelberg
E-mail: R.Eils@Dkfz-Heidelberg.de ; J.Gao@Dkfz-Heidelberg.de

Dr. Jens Eilbracht
Abteilung fuer Zellbiologie / A010
Deutsches Krebsforschungszentrum
Im Neuenheimer Feld 280, 69120 Heidelberg
Telephone: (06221) 423419, Fax: (06221) 423404
E-mail: j.eilbracht@dkfz-heidelberg.de

Drs. André Eggen and Mathieu Gautier
Institut National de la Recherche Agronomique (INRA
E-mail: gautier@jouy.inra.fr

Dr. Antje Fischer
University of Bielefeld, Department of Animal Behaviour.
E-mail: info@zoo-schule-gruenfuchs.de

Dr. Stefan Lampel
Ingenium Pharmaceuticals
Fraunhoferstrasse 13, 2152 Munich/Martinsried
E-mail: Stefan.Lampel@Ingenium-AG.com

Dr. Peter Lichter
DKFZ Heidelberg
Im Neuenheimer Feld 580, 69120 Heidelberg
E-mail: Peter.Lichter@dkfz-heidelberg.de

Dr. Michelle LeBeau
Department of Medicine
University of Chicago
E-mail: mlebeau@medicine.bsd.uchicago.edu

Jill M. Lahti, PhD
St Judes-Hospital, Memphis, TE
Department of Genetics and Tumor Cell Biology
St. Jude Children's Research Hospital
332 N. Lauderdale, Memphis, TN 38105-2794, USA

Phone: (901) 495-3501, FAX: (901) 495-2381
E-mail: jill.lahti@stjude.org

Dr. Marcus Peter
Ben May Institute for Cancer Research
University of Chicago
E-mail: MPeter@uchicago.edu

Dr. Janet D. Rowley
Department of Medicine
University of Chicago
E-mail: jrowley@medicine.bsd.uchicago.edu

Dr. Roger A. Schultz
UT Southwestern Medical Center at Dallas
5323 Harry Hines Blvd, Dallas, Texas 75390-9072;
Phone: (214) 645-7008
E-mail: roger.schultz@utsouthwestern.edu

Dr. Ed Schuuring
University Hospital Groningen, The Netherlands

Dr. Mike Thirman, Associate Professor of Medicine
University of Chicago, Department of Medicine
Section of Hematology / Oncology
E-mail: mthirman@medicine.bsd.uchicago.edu

Dr. Fengtang Yang
Department of Clinical Veterinary Medicine
Molecular Cytogenetics Laboratory, Centre for Veterinary Science, University of Cambridge, Madingley Road, CAMBRIDGE, CB3 0ES, United Kingdom,
Tel: +44-(0)-1223-766498, Fax: +44-(0)-1223-337610
E-mail: cytogenetics@vet.cam.ac.uk

Appendix III: Adresses of Core facilities at the University of Chicago

Confocal Laser Scanning Microscope
BSD Light Microscopy Core Facility
Director Dr. Vytas Bindokas
The University of Chicago, Dept Neurobiol Pharmacol Physiol MC0926
947 E 58th Street, Chicago IL 60637

telephone: 773-834-9040, fax 773-702-5903
email vytas@drugs.bsd.uchicago.edu
http://digital.bsd.uchicago.edu/index.html

Cytogenetics Laboratory
Department Medicine, Section Hematology / Oncology
University of Chicago

Fluorescence Microscopy
Integrated Microscopy Resource Facility
Technical Director Shirley Bond, MA
E-mail: sbond@mort.bsd.uchicago.edu
University of Chicago

Flow Cytometry
Immunology Applications Facility
Technical Director: Bart Eisfelder, PhD
Marjorie B. Kovler Building, 910 E. 58th St., Chicago, IL 60637.
Kovler Room 037, University of Chicago,
E-mail: beisfeld@midway.uchicago.edu
Web page: http://iacf.bsd.uchicago.edu/Flow_Cytometry_Facility/ flowcytometryhome.htm.